

THEORETICAL AND EXPERIMENTAL INVESTIGATION ON THE MULTIPLE SHAPE
MEMORY IONIC POLYMER-METAL COMPOSITE ACTUATOR

By

Qi Shen

Bachelor of Science – Mechanical Engineering
Beihang University, China
2010

A dissertation submitted in partial fulfillment
of the requirements for the

Doctor of Philosophy – Mechanical Engineering

Department of Mechanical Engineering
Howard R. Hughes College of Engineering
The Graduate College

University of Nevada, Las Vegas
December 2017

ProQuest Number: 10686309

All rights reserved

INFORMATION TO ALL USERS

The quality of this reproduction is dependent upon the quality of the copy submitted.

In the unlikely event that the author did not send a complete manuscript and there are missing pages, these will be noted. Also, if material had to be removed, a note will indicate the deletion.



ProQuest 10686309

Published by ProQuest LLC (2018). Copyright of the Dissertation is held by the Author.

All rights reserved.

This work is protected against unauthorized copying under Title 17, United States Code
Microform Edition © ProQuest LLC.

ProQuest LLC.
789 East Eisenhower Parkway
P.O. Box 1346
Ann Arbor, MI 48106 – 1346

November 8, 2017

This dissertation prepared by

Qi Shen

entitled

THEORETICAL AND EXPERIMENTAL INVESTIGATION ON THE MULTIPLE
SHAPE MEMORY IONIC POLYMER-METAL COMPOSITE ACTUATOR

is approved in partial fulfillment of the requirements for the degree of

Doctor of Philosophy – Mechanical Engineering
Department of Mechanical Engineering

Kwang J. Kim, Ph.D.
Examination Committee Chair

Kathryn Hausbeck Korgan, Ph.D.
Graduate College Interim Dean

Woosoon Yim, Ph.D.
Examination Committee Member

Hui Zhao, Ph.D.
Examination Committee Member

David Lee, Ph.D.
Examination Committee Member

Daniel Gerrity, Ph.D.
Graduate College Faculty Representative

Abstract

Shen, Qi, Ph.D., Mechanical Engineering, University of Nevada, Las Vegas, October 2017.
Theoretical and Experimental Investigation on the Multiple Shape Memory Ionic Polymer-Metal Composite Actuator

Major Professor: Kwang J. Kim.

Development of biomimetic actuators has been an essential motivation in the study of smart materials. However, few materials are capable of controlling complex twisting and bending deformations simultaneously or separately using a dynamic control system. The ionic polymer-metal composite (IPMC) is an emerging smart material in actuation and sensing applications, such as biomimetic robotics, advanced medical devices and human affinity applications. Here, we report a Multiple Shape Memory Ionic Polymer-Metal Composite (MSM-IPMC) actuator having multiple-shape memory effect, and is able to perform complex motion by two external inputs, electrical and thermal. Prior to the development of this type of actuator, this capability only could be realized with existing actuator technologies by using multiple actuators or another robotic system. Theoretical and experimental investigation on the MSM-IPMC actuator were performed.

To date, the effect of the surface electrode properties change on the actuating of IPMC have not been well studied. To address this problem, we theoretically predict and experimentally investigate the dynamic electro-mechanical response of the IPMC thin-strip actuator. A model of the IPMC actuator is proposed based on the Poisson-Nernst-Planck equations for ion transport and charge dynamics in the polymer membrane, while a physical model for the change of surface resistance of the electrodes of the IPMC due to deformation is also incorporated. By

incorporating these two models, a complete, dynamic, physics-based model for IPMC actuators is presented. To verify the model, IPMC samples were prepared and experiments were conducted. The results show that the theoretical model can accurately predict the actuating performance of IPMC actuators over a range of dynamic conditions. Additionally, the charge dynamics inside the polymer during the oscillation of the IPMC are presented. It is also shown that the charge at the boundary mainly affects the induced stress of the IPMC. This study is beneficial for the comprehensive understanding of the surface electrode effect on the performance of IPMC actuators.

In our study, we introduce a soft MSM-IPMC actuator having multiple degrees-of-freedom that demonstrates high maneuverability when controlled by two external inputs, electrical and thermal. These multiple inputs allow for complex motions that are routine in nature, but that would be otherwise difficult to obtain with a single actuator. To the best of our knowledge, this MSM-IPMC actuator is the first solitary actuator capable of multiple-input control and the resulting deformability and maneuverability.

The shape memory properties of MSM-IPMC were theoretically and experimentally studied. We presented the multiple shape memory properties of Nafion cylinder. A physics based model of the IPMC was proposed. The free energy density theory was utilized to analyze the shape properties of the IPMC. To verify the model, IPMC samples with the Nafion as the base membrane were prepared and experiments were conducted. Simulation of the model was performed and the results were compared with the experimental data. It was successfully demonstrated that the theoretical model can well explain the shape memory properties of the IPMC. The results showed that the reheat glass transition temperature of the IPMC is lower than

the programming temperature. It was also found that the back-relaxation of the IPMC decreases as the programming temperature increases. This study may be useful for the better understanding of the shape memory effect of IPMC.

Furthermore, we theoretically modeled and experimentally investigated the multiple shape memory effect of MSM-IPMC. We proposed a new physical principle to explain the shape memory behavior. A theoretical model of the multiple shape memory effect of MSM-IPMC was developed. Based on our previous study on the electro-mechanical actuation effect of IPMC, we proposed a comprehensive physics-based model of MSM-IPMC which couples the actuation effect and the multiple shape memory effect. It is the first model that includes these two actuation effect and multiple shape memory effect. Simulation of the model was performed using finite element method. To verify the model, an MSM-IPMC sample was prepared. Experimental tests of MSM-IPMC were conducted. By comparing the simulation results and the experimental results, both results have a good agreement. The multiple shape memory effect and reversibility of three different polymers, namely the Nafion, Aquivion and GEFC with three different ions, which are the hydrogen, lithium and sodium, were also quantitatively tested respectively. Based on the results, it is shown that all the polymers have good multiple shape memory effect and reversibility. The ions have an influence on the broad glass transition range of the polymers. The current study is beneficial for the better understanding of the underlying physics of MSM-IPMC.

A biomimetic underwater robot, that was actuated by the MSM-IPMC, was developed. The design of the robot was inspired by the pectoral fish swimming modes, such as stingrays, knifefish and cuttefish. The robot was actuated by two soft fins which were consisted of multiple IPMC samples. Through actuating the IPMCs separately, traveling wave was generated on the

soft fin. Experiments were performed for the test of the robot. The deformation and the blocking force of the IPMCs on the fin were measured. A force measurement system in a flow channel was implemented. The thrust force of the robot under different frequencies and travelling wave numbers were recorded. Multiple shape memory effect was performed on the robot. The robot was capable of changing its swimming modes from Gymnotiform to Mobuliform, which has high deformability, maneuverability and agility.

Acknowledgements

First of all, I would like to extend my deepest gratitude to my academic advisor and committee chair Professor Kwang J. Kim, for his instructive advice and useful suggestions on my research, study, dissertation and many other things. Without his guidance and persistent help, this dissertation would not have been possible.

I would like to thank my committee members, Professor Woosoon Yim, Professor Hui Zhao, Professor Daniel Gerrity and Professor David Lee for their valuable suggestions on my research work. I also would like to thank the research members in my lab, Dr. Viljar Palmre, Dr. Tyler Stalbaum, Dr. David Pugal, Dr. Haeseon Hwang, Sarah Trabia, Robert Hunt, Zakai Olsen, Blake Naccarato, Kevin Yim, Jameson Lee, Choonghan Lee, Dr. Junwoo Park, Dr. Md Bhuiya, Shelby Nelson, Jiyeon Park, Dr. Dongseob Kim and Dr. Anupam Kumar. Thanks to all of your kind help on my research. Special thanks to Dr. Viljar Palmre for his help on the IPMC fabrication, and experiments. I also want to thank Joan Conway of the UNLV Department of Mechanical Engineering for her kind help to me during my stay in UNLV. Thanks to Jeffery Markle, Liu Yang, and Jean Chagas Vaz for their help to my teaching assistant work. I am grateful for the teaching of many professors throughout my study in UNLV as well.

I would like to extend my sincere appreciation to Professor Tianmiao Wang, who is my advisor from Beihang University, China, for his guidance and support all these years. I also would like to thank Professor Li Wen and Lei Bao from Beihang University who helped me with their professional expertise. Special thanks should also go to my friends who gave me their help in my work and life.

Finally, I am indebted to my parents for their continuous support and encouragement.
Additional thanks to partial financial support from the U.S. National Science Foundation (No. 1545857), U.S. Office of Naval (N00014-16-1-2356).

Table of Contents

Abstract.....	iii
Acknowledgements.....	vii
List of Tables	xiv
List of Figures.....	xv
Nomenclature.....	xx
Chapter 1. Introduction	1
1.1. Background and objectives	2
1.1.1. The actuation effect of ionic polymer-metal composites (IPMCs).....	2
1.1.2. Multiple shape memory effect of Nafion.....	5
1.2. Rationale, Objectives and Significance of Research Activities.....	6
1.2.1. Rationale	6
1.2.2. Objectives	7
1.3. The specific technical objectives for this project.....	9
1.3.1. A physical model of the IPMC actuator	9
1.3.2. Underlying physics of multiple shape memory effect	10
1.3.3. A multiphysics model of MSM-IPMC	12
1.3.4. A robotic system based on the MSM-IPMC actuator.....	15
1.4. Broader Impact.....	17
Chapter 2. A Physics-Based Model Encompassing Variable Surface Resistance and Underlying Physics of Ionic Polymer-Metal Composite Actuators.....	18
2.1. Introduction.....	18

2.2. Mathematical model.....	22
2.2.1. The electrode model.....	22
2.2.2. The polymer membrane model.....	24
2.3. Experimental method.....	28
2.3.1. Sample preparation.....	28
2.3.2. Surface resistance.....	29
2.3.3. Actuation performance.....	33
2.4. Simulations and experimental results.....	34
2.4.1. Resistance model verification.....	34
2.4.2. Actuation model verification.....	38
2.5. Discussions.....	43
2.5.1. Mathematical model.....	43
2.5.2. Simulation results.....	46
2.6. CONCLUSIONS.....	51
Chapter 3. A multiple-shape memory polymer-metal composite actuator capable of programmable control, creating complex 3D motion of bending, twisting, and oscillation	52
3.1. Introduction.....	52
3.2. Results.....	60
3.2.1. Shape programming of MSM-IPMC.....	60
3.2.2. Deformation analysis of MSM-IPMC.....	61
3.2.3. Electrical analysis of MSM-IPMC.....	65
3.3. Discussion.....	68

3.4. Methods.....	71
3.4.1. Sample preparation.	71
3.4.2. Experiments.	72
3.4.3. Image analysis.....	73
Chapter 4. Theoretical and experimental investigation of shape memory properties of ionic polymer-metal composite.....	76
4.1.1. Introduction.....	76
4.2. Results.....	78
4.2.1. Multiple shape memory properties of cylindrical Nafion.....	78
4.2.2. Modeling of the IPMC	82
4.2.3. Experimental verification.....	86
4.3. Discussion	92
4.3.1. Application of thermo-mechanical transaction.....	92
4.3.2. Model of the shape memory properties	93
4.4. Methods.....	94
4.4.1. Sample preparation	94
4.4.2. Parameter identification	94
Chapter 5. Multiphysics modeling and experimental investigation of a soft multiple-shape-memory ionic polymer-metal composite actuator	96
5.1. Introduction.....	96
5.2. Mathematic model	100
5.2.1. Modeling of the multiple shape memory effect.....	100

5.2.2. Modeling of the MSM-IPMC	102
5.3. Experimental investigation	104
5.3.1. Multiple shape memory effect model validations.....	104
5.3.2. Validation of the MSM-IPMC model.....	108
5.3.3. Glass transition.....	115
5.3.4. Shape recovery.....	117
5.3.5. Reversibility	121
5.4. Discussion	124
5.4.1. Ionic effects on the membrane.....	124
5.4.2. Shape memory distribution.....	126
5.5. Conclusion	127
Chapter 6. Development of a robotic fish actuated by MSM-IPMC	129
6.1. Introduction.....	129
6.2. Materials and Methods.....	132
6.2.1. Fabrication of MSM-IPMCs.....	132
6.2.2. Biomimetic underwater robot prototype.....	133
6.2.3. Displacement and blocking force.....	135
6.2.4. Thrust	136
6.2.5. Multiple shape memory effect	139
6.3. Results.....	141
6.4. Conclusion	151
Chapter 7. Conclusion.....	153

Chapter 8. Future work	154
Appendix A: Derivation of charge density	156
Appendix B: Derivation of deformation	157
Appendix C: LabVIEW set up	158
Appendix D: Modeling of the IPMC in COSMOL	162
Appendix E: Robotic fish control code.....	166
Appendix F: Copyright Permission Approvals.....	180
Bibliography	207
Curriculum Vitae	219

List of Tables

Table 2.1 Value of the resistance model constant.....	37
Table 2.2 Dimensions of the IPMC samples.	40
Table 2.3 Value of IPMC actuator model constants [58].	41
Table 4.1 Dimensions of the IPMC samples.	88
Table 5.1 Parameters of the multiple shape memory model.....	107
Table 5.2 Properties of Nafion, Aquivion and GEFC membranes.	108
Table 5.3 Dimensions of the MSM-IPMC membrane samples.....	109
Table 5.4 The ion exchange capacity of each membrane.	113
Table 6.1 Parameters of the towing experiment.	146

List of Figures

Figure 1.1 Energy density for various smart materials and systems.....	3
Figure 1.2 Illustration of consecutive deformation of multiple degrees of freedom actuator.	8
Figure 1.3 Research flow of the IPMC physical model.....	10
Figure 1.4 Physical principle of the multiple shape memory behavior.	12
Figure 1.5 Molecular mechanism of shape memory effect.....	13
Figure 1.6 Research flow of the MSM-IPMC multiphysics model.....	15
Figure 2.1 Schematic of IPMC beam.....	25
Figure 2.2 Cross-section SEM images of the IPMC.....	30
Figure 2.3 Illustration of the experimental set up for the surface resistance test.....	31
Figure 2.4 Snapshot of the experimental set up: (a) general set up; (b) close-up of the IPMC surface resistance measurement.....	32
Figure 2.5 Illustration of the experimental set up for the actuation test.	34
Figure 2.6 Snapshot of the experimental set up; (a) general set up; (b) close-up of the IPMC actuation measurement.....	35
Figure 2.7 Comparison between the simulation results and experimental results of the electrode resistance at the oscillation amplitude of 10 mm and frequency of 2 Hz.	37
Figure 2.8 Comparison between the simulation results and experimental results of the electrode resistance change.	38
Figure 2.9 Comparison of experimental results of IPMC strain with model predictions, with and without consideration of surface resistance change.....	42

Figure 2.10 Meshes used in finite element simulations: (a) mesh sparsely mapped along length; (b) triangulated mesh.	45
Figure 2.11 IPMC strip displacement for one cycle during steady-state response for a sinusoidal voltage input of 4 V peak-to-peak amplitude and 1 Hz frequency.	48
Figure 2.12 Simulation result of the IPMC tip displacement.	48
Figure 2.13 Simulation result of the IPMC cation concentration: (a) near top electrode, (b) near bottom electrode.	49
Figure 2.14 Simulation results of cation concentration along the thickness of IPMC.	50
Figure 3.1 Properties of an IPMC made with Nafion™ membrane.	56
Figure 3.2 Nafion™ fiber demonstrating quadruple shape memory cycles with a 1-g weight on the tip.	59
Figure 3.3 Programming of MSM-IPMC.	61
Figure 3.4 A MSM-IPMC actuator with multiple degree-of-freedom deformation.	61
Figure 3.5 MSM-IPMC 3D motion trajectory.	64
Figure 3.6 Deformation of MSM-IPMC.	65
Figure 3.7 Impedance response of MSM-IPMC.	67
Figure 3.8 Experimental setup. The experimental setup used for measuring thermal and electromechanical responses of the MSM-IPMC actuator.	72
Figure 4.1 Multiple shape memory properties of Nafion cylinder.	80
Figure 4.2 Shape memory cycle of Nafion cylinder.	81
Figure 4.3 Recovering ratio of Nafion cylinder at different programming temperatures.	81
Figure 4.4 Schematic illustration of IPMC beam.	86

Figure 4.5 Experimental set up for the shape memory properties.	87
Figure 4.6 Thermo-mechanically shape of IPMC at different temperatures.	89
Figure 4.7 Comparison of the simulation and experimental results of the IPMC shape recovery at different programming temperatures: (a) IPMC 1; (b) IPMC 2; (c) IPMC 3.	91
Figure 4.8 Back-relaxation deformation of the IPMC at different programming temperatures. ..	92
Figure 5.1 Illustration of the multiple shape memory effect.	97
Figure 5.2 Quadruple shape memory properties of the MSM-IPMC.	105
Figure 5.3 Comparison between the simulation and experimental results of the multiple shape memory effect.	107
Figure 5.4 Polymer structures of different membranes: (a) Nafion and GEFC; (b) Aquivion. ..	109
Figure 5.5 Experimental set up of the MSM-IPMC test.	111
Figure 5.6 Measured displacement, temperature, current and voltage of GEFC sample.	112
Figure 5.7 Comparison of theoretical and experimental results of different membrane based IPMCs: (a) Nafion; (b) Aquivion; (c) GEFC.	115
Figure 5.8 First and second glass transition ranges of membranes with different cations.	116
Figure 5.9 Quintuple shape memory process of the Na ⁺ -form GEFC.	118
Figure 5.10 Shape recovery of different samples: (a) H ⁺ -form membrane based IPMCs; (b) Li ⁺ -form membrane based IPMCs; (c) Na ⁺ -form membrane based IPMCs.	120
Figure 5.11 Multiple shape memory reverse process of Na ⁺ -form Aquivion.	121
Figure 5.12 Reversibility of different samples: (a) H ⁺ -form membrane based IPMCs; (b) Li ⁺ -form membrane based IPMCs; (c) Na ⁺ -form membrane based IPMCs.	123
Figure 5.13 Enthalpy and free energy of different ions.	126

Figure 6.1 Prototype of the biomimetic robot.....	133
Figure 6.2 Schematic of the control circuit.....	134
Figure 6.3 Snapshot of the thrust measurement system.....	138
Figure 6.4 Illustration of the robot force measurement at static state.....	139
Figure 6.5 Illustration of the robot force measurement at prescribed speed.....	139
Figure 6.6 Biomimetic underwater robot with different pectoral swimming modes: (a) Mobuliform; (b) Gymnotiform.	140
Figure 6.7 Twisting fins of the biomimetic underwater robot with different pectoral swimming modes: (a) Mobuliform; (b) Gymnotiform.	141
Figure 6.8 Deformation of the MSM-IPMCs in the soft fin at different frequencies: (a) 1 Hz; (b) 0.5 Hz; (c) 0.25 Hz.....	143
Figure 6.9 Blocking force of the MSM-IPMCs in the soft fin: (a) IPMC 1; (b) IPMC 3; (c) IPMC 6.....	145
Figure 6.10 Experimental and theoretical results of the towing experiments.....	146
Figure 6.11 Experimental results of thrust force at static state.....	147
Figure 6.12 Experimental results of thrust force at prescribed towing velocity.....	148
Figure 6.13 Twisting deformation of the soft fin.....	149
Figure 6.14 Displacement of the MSM-IPMCs during the twisting deformation.	149
Figure 6.15 Programmed biomimetic underwater robot with different swimming modes: (a) Mobuliform; (b) Gymnotiform.	151
Figure 8.1 Screen printing process of MSM-IPMC.....	155
Figure C.1 LabVIEW set up for the actuator test: (a) Block diagram; (b) Front panel.	159

Figure C.2 LabVIEW set up for the sensor test: (a) Block diagram; (b) Front panel.....	161
Figure D.1 Parameters of the model.	162
Figure D.2 Geometry of the model.	163
Figure D.3 The Model Builder of the model.	164
Figure D.4 Displacement of the IPMC actuator.	165

Nomenclature

C	Cation concentration (mol/m ³)
μ	Cation mobility (mol·s/kg)
D	Diffusion coefficient (m ² /s)
F	Faraday's constant (C/mol)
z	Charge number
ϕ	Electric potential in the polymer (V)
R	Gas constant (J/mol·K)
T	Absolute temperature (°C)
ρ	Charge density (C/m ³)
ε	Absolute dielectric permittivity (F/m)
C_0	Initial ionic concentration (mol/m ³)
s	Laplace variable
t	Time (s)
γ	Angle of curved IPMC (rad)
r	Radius of IPMC midline (m)
ρ_p	Resistivity of the particle of the electrode ($\Omega\cdot m$)
ρ_v	Resistivity of the void of the electrode ($\Omega\cdot m$)
a	Side length of the unit cell of the electrode (m)
s_v	Side length of the void cube of the electrode (m)
P_x, P_y, P_z	Percentages of the defective cube of the electrode in the x, y, z direction
\bar{E}	Strength of the electric field (V/m)
σ	Induced stress (Pa)
α	Coefficient relates the charge density at the boundary of polymer membrane to the induced stress (J/C)
V	Applied voltage (V)
M	Moment (N·m)
I	Moment of inertia (kg·m ²)
W	Width of the actuator (m)
L	Length of the actuator (m)
h	Half thickness of the actuator (m)
Y	Young's modulus (Pa)
w	Displacement of the actuator (m)
D_p	Diameter of the metal particle of the electrode (m)
h_e	Thickness of the electrode (m)
W_e	Width of the surface electrode (m)
R_e	Resistance of the surface electrode (Ω)
V_p	Voltage on the circuit (V)

V_r	Voltage across the resistor (V)
R_r	Resistance of the resistor (Ω)
V_e	Voltage on the electrode (V)
I_e	Current on the electrode (A)
P_v	Percentage of the vacancy of the electrode
ρ_r	Radius of the curvature (m)
δ	End deflection of the actuator (m)
ρ_m	Material density (kg/m^3)
ν	Poisson's ratio
ε_f	Strain of fixed shape of the actuator
ε_p	Strain of programmed shape of the actuator
ε_r	Strain of recovered shape of the actuator
$\lambda_l, \lambda_w, \lambda_h$	Strain along the length, width and thickness direction of the actuator
$\sigma_l, \sigma_w, \sigma_h$	Actual stress along the length, width and thickness direction of the actuator (Pa)
F_l, F_w, F_h	Nominal force along the length, width and thickness direction of the actuator (N)
E_s	Stretching free-energy (J)
E_m	Mix free-energy (J)
E_p	Polarizing free-energy (J)
E_{ion}	Ions transporting free-energy (J)
N	Number of polymer chains divided by the volume of the polymer element
k	Boltzmann constant (J/K)
χ	Enthalpy constant (J)
D	Ratio between the strain in the z direction and the strain in the x and y direction
G	Free energy density (J/m^3)
i	Refers to each individual shape memory process
ρ_n	Density of the polymer (kg/m^3)
M_C	Molecule weight of the actuator (kg/mol)
α_i	Extension ratio
Y^{eq}	Equilibrium Young's modulus (Pa)
Y_i^{neg}	Nonequilibrium Young's modulus (Pa)
a	Shape memory coefficient
T_i	Reference temperature corresponds to the programming temperature (T)
w_s	Deformation induced by the multiple shape memory effect (m)
w_a	Deformation induced by the actuation effect (m)
w_t	Total deformation of MSM-IPMC (m)
ΔL	Relative deformation of the actuator (m)
$R_{f,x}$	Shape recover ratio of shape x
A	Amplitude of the input voltage (V)
ω	Angular frequency (rad/s)
f	Operating frequency (Hz)

m	Number of waves of the travelling wave
A_c	Cross-section reference area of the robot (m^2)
C_d	Form force coefficient
F_a	Resultant force on the robot (N)
F_t	Thrust force on the robot (N)
F_d	Drag force on the robot (N)

Chapter 1. Introduction

The smart material is one of the key foundations supporting the development of new biomimetic based technologies. Many actuators and sensors have been developed and applied in various fields with the attributions of smart materials [1]–[6]. Ionic polymer-metal composite (IPMC) is one of the promising smart materials to be used as underwater actuators applied in biomimetic robotics, biomedical devices and micro/nanomanipulation [7]–[9]. The IPMC is based on a polymer material Nafion or Flemion. A layer of noble metal such as platinum or gold is chemically plated on both sides of the IPMC as electrodes [10]. If an electric field is applied across the thickness of the IPMC, the ions redistribute within the polymer, causing the IPMC to deform. Meanwhile, a detectable voltage can be generated by the IPMC material if subjected to a mechanical deformation as the result of the mobile ions distribution. It has the characteristics of inherent softness, resilience, and biocompatibility, which makes the IPMC suitable for a useful underwater actuator [11]–[14]. The microfabrication of IPMCs has also been reported, which enable scientists and engineers develop micro underwater actuators and sensors based on IPMCs [15].

Shape memory polymers are materials that can memorize a permanent shape, and then later return to their original shape under specific conditions of external thermal, electrical, or other stimulation [16], [17]. They have the advantages of high deformation, low cost, low density, and potential biocompatibility and biodegradability. Recently, it was found that Nafion, which is the intermediate layer of an IPMC, exhibits the multiple shape memory effect [18]. By programming a shape of the Nafion in one temperature and fixing the shape at a lower temperature, this shape is ‘memorized’ within the temperature range. This process can be

repeated multiple times with different shapes. As the result, multiple shapes are programmed in the polymer. The programmed shapes are recovered, respectively, in response to subsequent heating to each corresponding temperature. These recoveries result from the glass transitions at each recovery temperature. However, the underlying physics of this multiple shape memory effect is not well studied.

A new actuator is introduced that takes advantage of both the multiple shape memory effect and the electrical actuation effect. This actuator, the multiple-shape-memory ionic-polymer-metal composite (MSM-IPMC), has multiple degrees of freedom. In this project, we have investigated the underlying physics of the multiple shape memory effect, and model the MSM-IPMC which couples the multiple shape memory effect and the electrical actuation effect. This will enable ones to better understand the mechanism of MSM-IPMC. Furthermore, multiple degrees of freedom actuator was developed using MSM-IPMC, which can be applied on biomimetic robotic systems.

1.1. Background and objectives

1.1.1. The actuation effect of ionic polymer-metal composites (IPMCs)

The IPMC is an of Electroactive Polymer (EAP), which is promising for biomimetic underwater propulsion and sensing [19]–[24]. The IPMC consists of an electrode on both sides and a polymer membrane between them. In aqueous environments, under an applied voltage across the thickness direction, the ions and water molecules within the polymer transmit towards the cathode. As a result, cations and water molecules accumulate on the cathode side. This along with the associated electrostatic interactions causes the cathode side to expand while the opposite side shrinks. This volume change leads to a bending deformation, which is the electro-

mechanical actuation effect [25]. The electro-mechanical actuation effect has the capabilities of resilience, inherent softness, and biocompatibility. Figure 1.1 shows the energy density (dotted diagonal lines) for various smart materials and systems [26]. The energy density of IPMC is between 10^3 J/m^3 to 10^5 J/m^3 . Compared with other smart materials, the IPMC has a relatively high actuation strain and relatively low blocking stress.

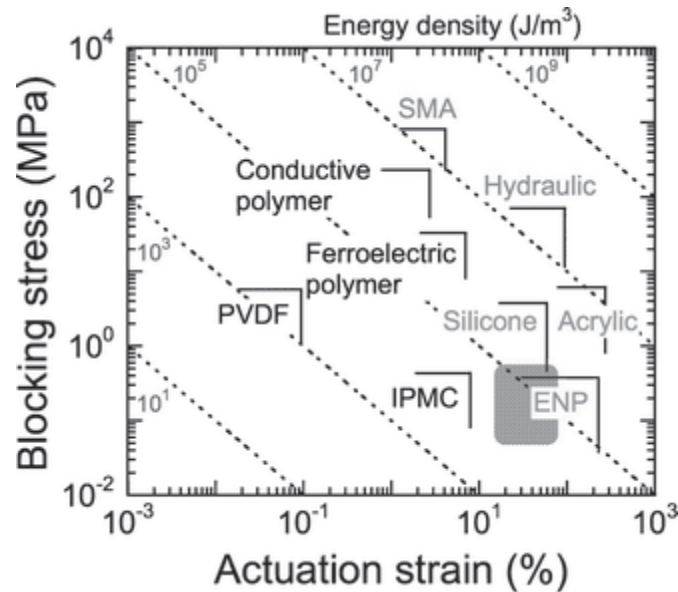


Figure 1.1 Energy density for various smart materials and systems.

During electromechanical actuation of an IPMC by a supplied voltage input to its electrodes, the main contribution to the deformation is assumed to be the cation migration and corresponding swelling effects. The contribution from the concentration gradient and electric potential are much larger than the contribution of the pressure gradient. Therefore the pressure gradient term was omitted. The Nernst-Planck equation can be expressed as [27]

$$\frac{\partial C}{\partial t} + \nabla \cdot (-D\nabla C - z\mu FC\nabla\phi) = 0 \quad (1.1)$$

where C is cation concentration, μ is cation mobility, D is the diffusion coefficient, F is the Faraday's constant, z is the charge number, and ϕ is the electric potential in the polymer. The mobility can be described as $\mu=D/(RT)$, where R is the gas constant and T is the absolute temperature. The gradient of electric potential in the polymer, $\nabla\phi$, is described by Poisson's equation. Poisson's equation is used in the model as follows

$$-\nabla \cdot \nabla\phi = \frac{\rho_c}{\varepsilon} \quad (1.2)$$

where ρ_c is the charge density and ε is the effective absolute dielectric permittivity. Equations (1.1) and (1.2) provide the Poisson-Nernst-Planck equations for ionic concentration and electric potential within the polymer. The anions of the IPMC are fixed to the polymer backbone. Thus the anion concentration only varies based on the deformation. Meanwhile the cations can migrate freely within the polymer under the applied electric field. As a result, when the IPMC was actuated under the input voltage, the change of anion concentration is relatively small compared with the change of cation concentration. It was assumed that the charge density is a function of cation concentration as

$$\rho_c = F(C - C_0) \quad (1.3)$$

where C_0 is the initial ionic concentration. A number of theoretical models of the IPMC have been developed [28]–[30]. Nevertheless, the reported models consider the electrode as a bulk metal, and its electrical properties do not change during the deformation.

1.1.2. Multiple shape memory effect of Nafion

The ability of shape memory polymers to remember multiple shapes has attracted significant attention from scientists and engineers for the application of actuators, sensors and smart devices [31].

The shape memory properties of Nafion has recently been studied [32]. Xie reported that annealed dry Nafion can be programmed to memorize four different shapes [18]. Even more complex locomotion is possible if a Nafion cylinder is used instead of a rectangular strip, due to its two-dimensional cross-section. A given shape is set at one temperature and fixed at a lower temperature. This shape may be later recovered by returning to that temperature. With the broad glass transition range, the Nafion can be potentially programmed at plenty of unique shapes, which can be recovered at different temperatures respectively. Rossiter et al. presented the shape memory properties of Nafion-based IPMC [33]. Deformations were induced by external force and electrical actuation to program the IPMC. Slow decay was also observed along with the shape memory effect. Xiao et. al applied a finite deformation, nonlinear viscoelastic model with a discrete spectrum of relaxation times to describe the shape memory behavior of Nafion [34].

A theory was proposed to explain this behavior [1]. The critical point for this theory is that a single broad thermal transition can be regarded as the collective contribution of numerous infinitely sharp transitions continuously distributed in the broad temperature range. Each of these sharp transitions has its infinitely sharp transition temperature T_d . Each infinitely sharp transition temperature corresponds to an elemental memory unit (EMU). Based on this theory, at any T_d , only the EMUs with their T_{trans} below this particular T_d are activated for the shape memory function. For a single broad transition, the distribution of the EMUs is continuous. Thus, any T_d

within this broad transition would correspond to a particular group of activated EMUs.

Performing a triple-shape programming at any two deformation temperatures would always activate two different groups of EMUs for fixing. More importantly, these two EMU groups can be distinctively activated during reheating for two recovery events. Overall, this led to a tunable triple-shape memory effect. The same principle could be extended to a multi-shape memory effect with more than three modes.

To date, while some experimental investigations on the shape memory properties of Nafion have been done, little work has been done concerning the theoretical investigation of the multiple shape memory effect of Nafion. Poor understanding exists on the physics of the shape memory properties of Nafion. A faithful model is desirable to explain the thermo-mechanical transaction phenomenon.

1.2. Rationale, Objectives and Significance of Research Activities

1.2.1. Rationale

The MSM-IPMC consists of Nafion and platinum electrodes chemically plated on both sides. The actuation effect and shape memory effect are the two key characteristics of MSM-IPMC. Based on these two effects, which are electro-mechanical actuation effect and thermo-mechanical multiple shape memory effect, the MSM-IPMC can perform deformation with multiple degrees of freedom. Several shapes can be programmed into MSM-IPMC material memory at various temperatures, which enables the thermo-mechanical actuation effect. Meanwhile, the MSM-IPMC can bend under an applied voltage, which results from the electro-mechanical effect.

I am interested in investigating the fundamental physical principle of the shape memory behavior of the MSM-IPMC. Through coupling with our previous study of the actuation effect of IPMC, a comprehensive model of MSM-IPMC was developed. Furthermore, I am interested in studying the application of MSM-IPMC in soft robotic systems. This type of actuator can demonstrate high maneuverability by controlling two external inputs – electrical input and thermal input, allowing the complex twisting, bending, and oscillating motions that are frequently observed in nature-made systems.

1.2.2. Objectives

Development of biomimetic actuators has been an essential motivation in the study of smart materials. However, few materials are capable of controlling complex twisting and bending deformations simultaneously or separately using a dynamic control system. An example of the deformation of a multiple degrees of freedom actuator was shown in Figure 1.2. The actuator has a rectangular shape. It can perform a stable bending and twisting deformation. Meanwhile, it can also have a high frequency oscillation.

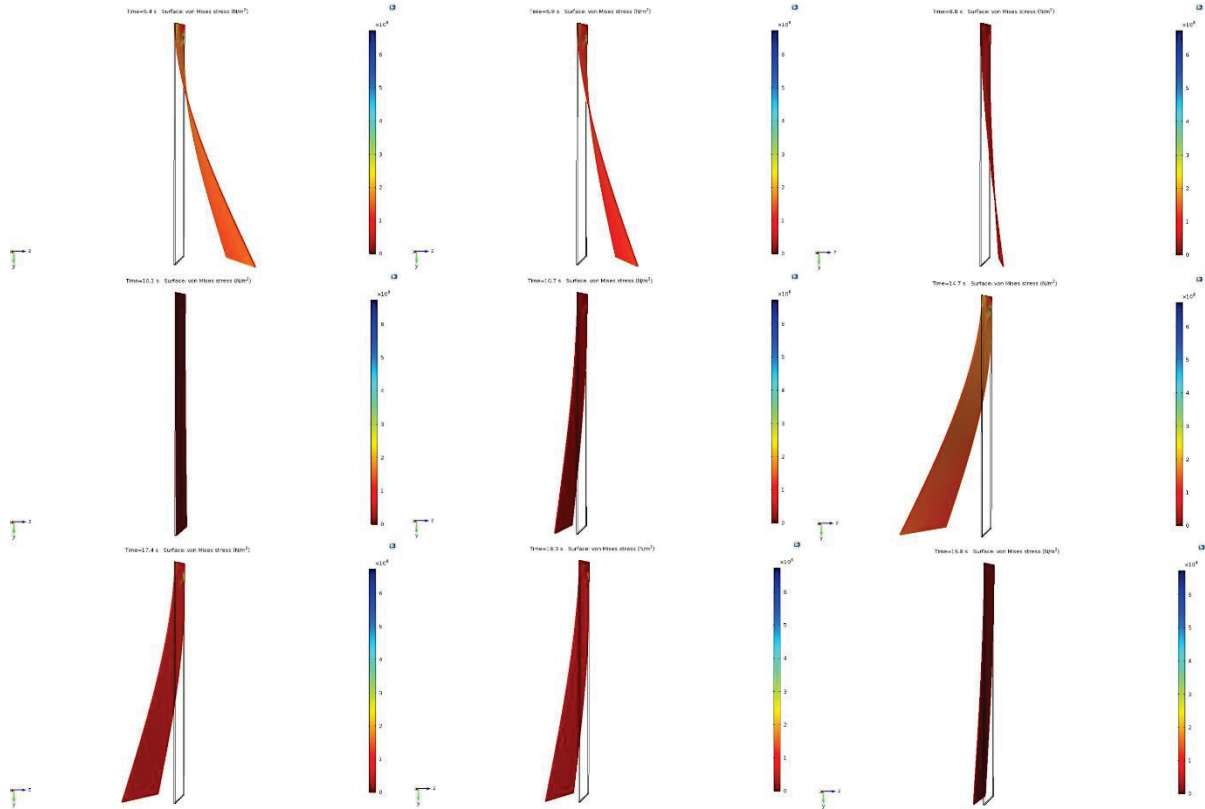


Figure 1.2 Illustration of consecutive deformation of multiple degrees of freedom actuator.

Herein, I plan to investigate an IPMC actuator having a multiple shape memory effect. MSM-IPMC is able to perform complex motion by two external inputs, electrical and thermal. Prior to the development of this type of actuator, this capability only could be realized with existing actuator technologies by using multiple actuators or another robotic system.

In this study, I introduce a soft MSM-IPMC actuator having multiple degrees-of-freedom that demonstrates high maneuverability when controlled by two external inputs, electrical and thermal. These multiple inputs allow for complex motions that are routine in nature, but that would be otherwise difficult to obtain with a single actuator. To the best of our knowledge, this

MSM-IPMC actuator is the first solitary actuator capable of multiple-input control and the resulting deformability and maneuverability.

I focus on the theoretical modeling and experimental investigation of MSM-IPMC. The underlying physics of the multiple shape memory behavior was explored. Based on our preliminary study on the electro-mechanical transaction of MSM-IPMC, I proposed a comprehensive model which couple the actuation effect and the multiple shape memory effect of MSM-IPMC. Furthermore, the application of MSM-IPMC on the soft biomimetic robotic system was studied.

1.3. The specific technical objectives for this project

1.3.1. A physical model of the IPMC actuator

Objective 1 is to develop a physical model of the IPMC actuator. Many physical models of IPMC actuator have been developed [28]–[30], [35]. However, some of the models previously developed mainly focused on the ionic exchange membrane and did not take the surface electrodes into consideration. In some other models, the electrodes were considered as a bulk metal. Its electrical properties such as resistance, and capacitance do not change during actuation.

Based on my previous study, it was found that when the IPMC actuator was deformed, the resistance and capacitance changes accordingly [10]. Therefore, a physical model which includes the surface electrodes properties change and ions migration within the polymer is desirable for the understanding of the physics of the IPMC actuating.

This current study proposed a physics-based model of the IPMC actuator that combines the effect of the electrode resistance change and the charge dynamics of the ionic polymer. The model of the surface electrodes microstructure and the model of the polymer membrane were

developed separately. Then these two models were coupled together at the boundaries of the polymer and the IPMC model was developed. Experiments were performed and the model was validated. A finite element method was also used to simulate the model. Figure 1.3 shows the research flow of the IPMC physical model.

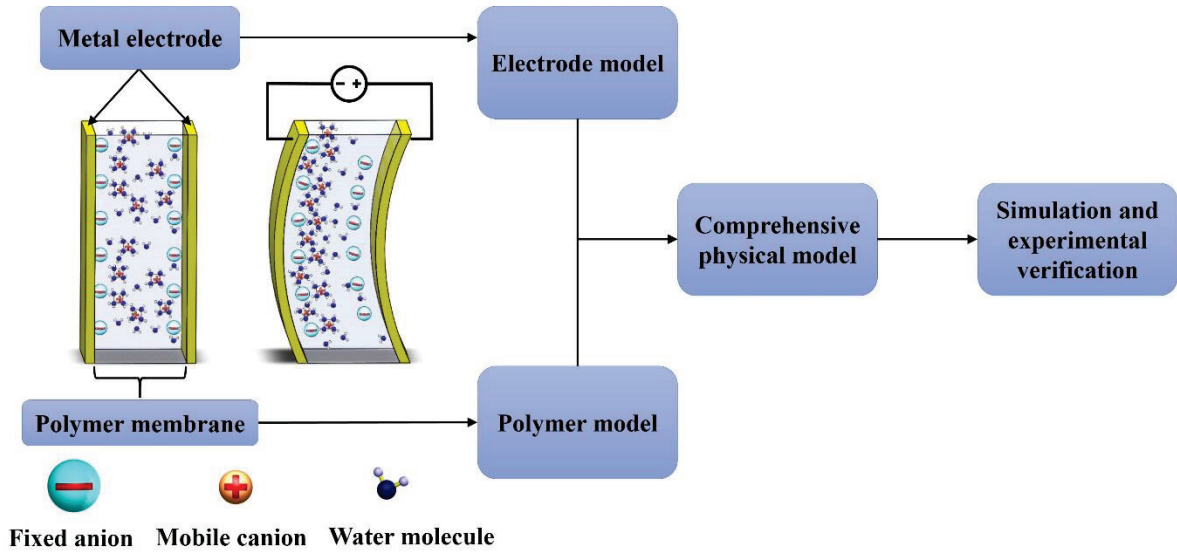


Figure 1.3 Research flow of the IPMC physical model.

1.3.2. Underlying physics of multiple shape memory effect

Objective 2 is to explore the underlying physics of multiple shape memory effect. So far, limited theoretical work has been attempted to describe the multiple shape memory effect of MSM-IPMC. Unique physical principles was proposed to explain the multiple shape memory effect of MSM-IPMC. A theoretical model of the MSM-IPMC, based upon thermal stress analysis, was developed. Experiments of the MSM-IPMC was conducted. The simulation results and experimental results were compared. This work may shed some light on the underlying physics of multiple shape memory effect.

Several works have been done on the modeling of the shape memory behavior of Nafion. One theory is that by modeling the glass transition, the shape memory process was modeled [34]. A temperature-dependent relaxation time or viscosity was assumed in the model. During the glass transition, the relaxation time changes significantly. This allows the materials to store a temporary shape and recover a permanent shape.

In our study, I proposed a new physical principle to explain the multiple shape memory behavior. The fundamental concept is that the glass transition is independent of each other. Based on previous work, the Nafion has multiple shape-memory properties and can be programmed into multiple shapes and then programmed by thermal or electric inputs [18]. We assumed that the broad glass transition temperature could be regarded as the consecutive distribution of a series of glass transitions. Within the range of the broad glass transition temperature of inherent, $\sim 55^{\circ}\text{C}$ to $\sim 130^{\circ}\text{C}$, the Nafion could be programmed with multiple unique shapes, and recovered under different temperatures. A theoretical model of the multiple shape memory effect of Nafion was developed. It is based on the assumption that the multiple shape memory effect is caused by the internal stress and each individual Young's modulus is 'memorized' during the previous programming process. As the MSM-IPMC was reheated to each temperature T_i , the internal stress σ_i was released on the MSM-IPMC, and nonequilibrium Young's modulus E^{neq}_i was recovered, which results in the shape recovery of the MSM-IPMC. Figure 1.4 shows the illustration of the multiple shape memory process induced by the internal stress and Young's modulus.

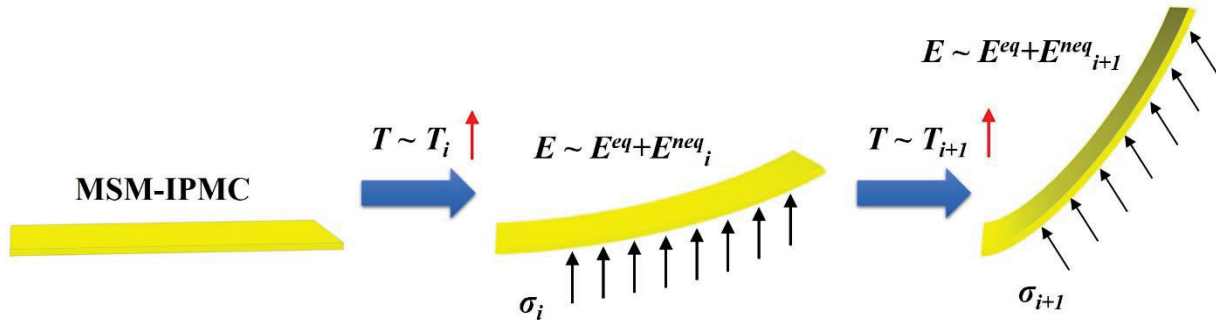


Figure 1.4 Physical principle of the multiple shape memory behavior.

1.3.3. A multiphysics model of MSM-IPMC

Objective 3 is to develop a multiphysics model of MSM-IPMC. Based on the actuation model of IPMC developed in Objective 2 and the multiple shape memory model obtained in Objective 1, a comprehensive multiphysics model of MSM-IPMC which couples the aforementioned two effects was developed. This will be the first model that includes this two actuation effect and multiple shape memory effect, simultaneously. Simulation of the model was performed for an appropriate range of temperature. The MSM-IPMC sample was also experimentally tested to verify the model. This work is beneficial for the understanding of the physics underneath this two effect working together on a single actuator.

The MSM-IPMC actuator can demonstrate complex 3D deformation. The MSM-IPMC has two characteristics, which are the electromechanical actuation effect and the shape memory effect. The bending, twisting, and oscillating motions of the actuator could be controlled simultaneously or separately by means of thermal-mechanical and electro-mechanical transactions. These two separate transactions are significant properties of the presented actuator.

Numerous works on the electromechanical actuation effect of MSM-IPMC have been studied previously. Under an applied electrical field, the migration of ions along with the water molecule, and the electrostatic force lead to the deformation of the actuator, which is the main actuation effect. The physical principle of multiple shape memory behavior has not been well studied. According to the previous study [1], the destabilization of electrostatic interactions between ions and the crystalline segments which are used as physical crosslinks to hold the temporary shape is the main contribution to the multiple shape memory behavior. Figure 1.5 shows the molecular mechanism of shape memory effect [36]. The black dots represents the netpoints. The blue lines represents the molecular chains of low mobility below the glass transition temperature. The red lines represents the molecular chains of high mobility above the glass transition temperature.

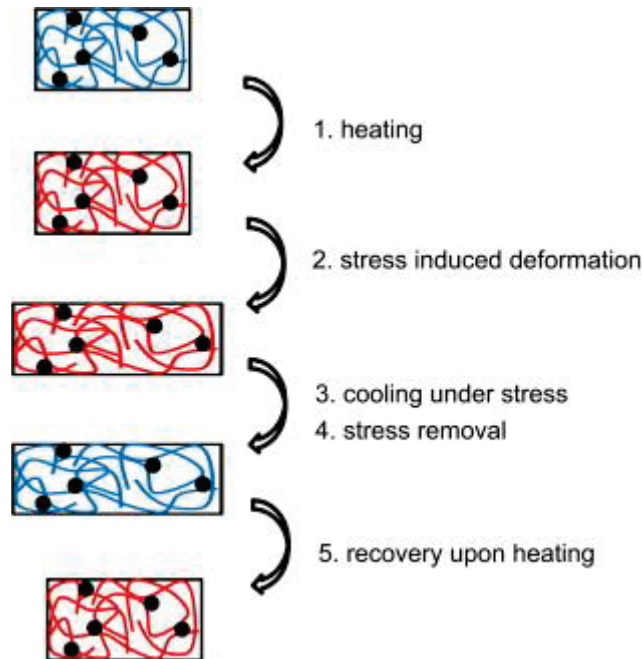


Figure 1.5 Molecular mechanism of shape memory effect.

Based on the results of Objective 1, we proposed a comprehensive model which couple the actuation effect and the multiple shape memory effect for MSM-IPMC. It is the first model that includes this two actuation effect and multiple shape memory effect. Simulation of the model was performed and experiments were conducted to verify the model. Furthermore, the shape recovery and reversibility of MSM-IPMCs with different membranes and ions were tested and the results were compared. Figure 1.6 shows the research flow of the MSM-IPMC multiphysics model.

By programming the actuator, complex shape change of the actuator could be achieved with thermal control, and the thermo-mechanical actuation could be used for overall structural deformation. Meanwhile, the MSM-IPMC could perform an oscillation motion by applying a voltage to the electrodes. The actuation amplitude and frequency of the oscillation could be adjusted by changing the amplitude and frequency of input voltage. Thus, the electro-mechanical actuation of the MSM-IPMC could be utilized for locomotion.

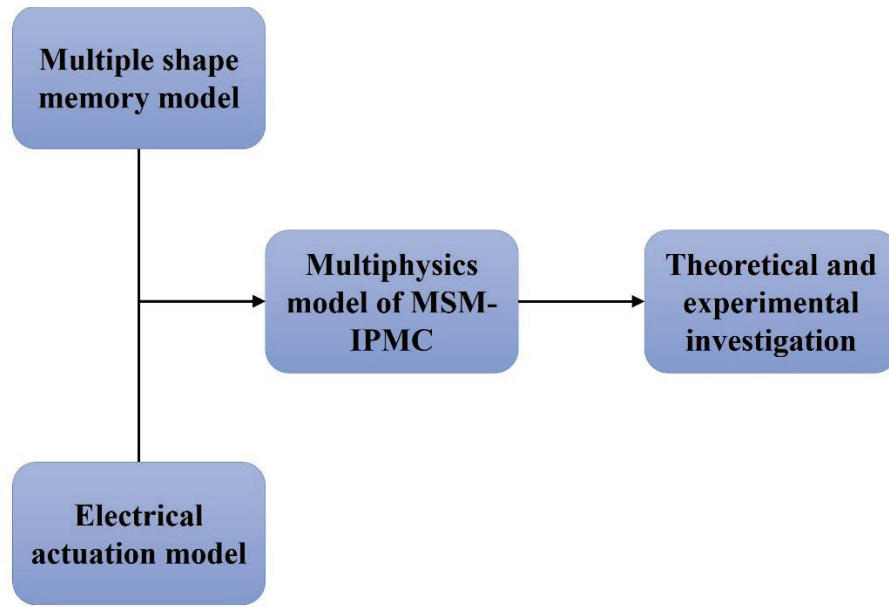


Figure 1.6 Research flow of the MSM-IPMC multiphysics model.

1.3.4. A robotic system based on the MSM-IPMC actuator

Objective 4 is to demonstrate a robotic system that is based on the multiple degrees of freedom MSM-IPMC actuator. Through the electro-mechanical actuation effect, the actuator is able to perform (high-frequency) bending motions under external electrical input. With the thermo-mechanical multiple shape memory effect, the actuator can obtain stable, complex (low-frequency) motion under external thermal inputs. Compared with the electro-mechanical actuation effect, the thermo-mechanical multiple shape memory effect occurs over a much longer timescale. The ability to control MSM-IPMC actuators by two external inputs, electrical and thermal, enables these devices to be used to perform highly complex motions, twisting, bending and oscillating simultaneously or separately. The twisting and bending motions are induced thermally and the oscillating motion is induced electrically. The bending motion and oscillating

motion take place with the same rotation axis; previously, this could be realized only with existing actuator technologies by using multiple actuators or another complicated robotic system. Moreover, to the best of my knowledge, the MSM-IPMC actuator presented in this paper is the first solitary actuator capable of multiple-input control and the resulting deformability and maneuverability. This work with the capacitance of MSM-IPMC brings inspiration to researchers and engineers to designing new soft robotic systems.

The MSM-IPMC could be controlled separately by means of thermal and electrical inputs. It has the advantages of resilience and inherent softness; moreover, the electrical characteristics of the MSM-IPMC change as the temperature change. Potentially, it could be applied to medical devices and biomimetic robotics.

We developed a multiple degrees of freedom MSM-IPMC actuator and apply it in biomimetic robotic systems. One potential application of MSM-IPMC is in underwater biomimetics, which has been studied for many years. Fish (or whale or dolphin) fins undergo considerable deformation, which enables the fish to generate propulsive forces and control body position. Robotic flapping foil devices were developed in order to understand the significance of flexible propulsive surfaces for locomotor performance [37]. A biomimetic fin was developed based on the monolithic fabrication of IPMC actuators [15]. Complex deformation modes can be produced. However, most of the devices contain complicated systems. MSM-IPMC can be used as a single actuator that performs similar deformations as does a fish fin. By programming MSM-IPMC to different desired shapes, and by controlling the thermal and electrical inputs, multiple degrees of freedom deformation of the actuator can be performed.

1.4. Broader Impact

The research results of our study will have a significant impact not only in the areas of material physics and soft actuator which can potentially apply in the field of soft robotics, but also in the related educational activities. The MSM-IPMC, which is developed in my work, will be useful in soft biomimetic robotic systems and bio-medical systems. Meanwhile, the MSM-IPMC provide a reliable, easily scalable and omnidirectional solution to the field of soft actuators, which has a substantial market potentially.

Meanwhile, the project also provided an excellent opportunity for myself. Through the training in the Active Materials and Smart Living Laboratory, I was able to learn cutting-edge research technologies and the training also helped me to maintain the global leadership in science and engineering in connection with IPMC.

Chapter 2. A Physics-Based Model Encompassing Variable Surface Resistance and Underlying Physics of Ionic Polymer-Metal Composite Actuators

In this chapter, a research paper published in Journal of Applied Physics is included. The authors are Qi Shen, Viljar Palmre, Tyler Stalbaum, and Kwang J. Kim in order of appearance on the article. This article provides a coupled model encompassing change in electrode material properties during deformation and the associated influence on actuation performance. This chapter was reprinted from Journal of Applied Physics, Shen, Q., Palmre, V., Stalbaum, T., and Kim, K. J., “A comprehensive physics-based model encompassing variable surface resistance and underlying physics of ionic polymer-metal composite actuators,”118(12), 124904, (2015), with the permission of AIP Publishing.

KJK conceived the idea and designed the project. The primary contributions to the mathematical modeling of the electrodes and analytical physics based modeling are from QS. The primary contributions to the finite element modeling are from TS and QS. The experimental work was conducted by QS and VP. The data analysis, simulations, conclusions, and discussion were a combined effort from the whole research team.

2.1. Introduction

Smart materials are the foundation supporting the development of new biomimetic based technologies. Many actuators and sensors have been developed and applied in various fields with the attributions of smart materials [38]–[45]. Ionic polymer-metal composite (IPMC) is one of the promising smart materials to be used as underwater actuators applied in biomimetic robotics, biomedical devices and micro/nanomanipulation [46]. The IPMC is based on a polymer material Nafion or Flemion [47], [48]. A layer of noble metal such as platinum or gold are chemically

plated on both sides of the IPMC as electrodes. If an electric field is applied across the thickness of the IPMC, the ions inside the polymer will begin to redistribute, causing the IPMC to deform. Meanwhile, a detectable voltage can be generated by the IPMC material if subjected to a mechanical deformation as a result of the mobile ions distribution. It has the characteristics of inherent softness, resilience and biocompatibility, which makes the IPMC suitable for the underwater actuator [11], [13], [21], [49]. The microfabrication of IPMCs has also been reported, which enable scientists and engineers develop micro underwater actuators and sensors based on IPMCs [50]–[53].

Several works concerning the modeling of IPMC have been reported [28], [29]. Kanno et al. modeled the electrical characteristics of the IPMC actuator [54]. De Gennes et al. describes the effect of an applied electric field on the spontaneous curvature and an imposed curvature on the electric field [55]. Shahinpoor and Kim investigated the influence of the electrode conductivity on the transduction behavior of IPMC [56]. Nemat-Nasser and Li proposed a model that describes electromechanical transduction in relation to the electrostatic interaction within the polymer [27]. Farinholt derived the impedance response for a cantilevered IPMC beam under step and harmonic voltage excitations [57]. The underlying cause of the actuation is explained by the internal stress induced by the interaction between the ion pairs inside a cluster. Newbury and Leo developed a model which is based on an equivalent circuit representation that is related to the mechanical, electrical, and electromechanical properties of the material [58]. Bonomo et al. developed a nonlinear dynamic model of IPMC actuator that results from the cascade of both the electrical and the electromechanical stages [59]. Brunetto et al. introduced a model that describes the interaction between the beam and the water [60]. However, the models presented above only

consider the charge dynamics inside the polymer membrane and do not consider the surface electrode. Chen and Tan investigated the electrical dynamics of the IPMC based on Nemat-Nasser's work [61]. They expanded the model and added the effect of surface resistance. Porfiri showed that the electrodes do significantly affect the charge dynamics and hence the actuation performance of IPMC [62]. Pugal et al. developed a physics based model that couples the currents in the polymer to the electric current in the continuous electrodes of IPMC [63]. Nevertheless, the above models consider the electrode as a bulk metal, and its electrical properties do not change during the deformation.

An electrode model for IPMCs was proposed by Kim et al. [64]. In this work it was shown that the properties of electrode such as the resistance and capacitance do change during the deformation. Our previous work showed that when the IPMC is subjected to a mechanical deformation, the change of surface electrode properties have effect on the sensing of IPMC. The underlying physics of the electrode properties change during the deformation is that the coagulation of the platinum atoms is generated through the electroless plating process [25], [48]. The incipient particles, with diameters less than 10 nm, coagulate during the reduction process and eventually grow to 50-100 nm. As the IPMC oscillates, the surface electrode are compressed and stretched periodically, and since the size of the particle do not change, the voids between the particles vary accordingly. Thus, it can be predicted that the surface electrode resistance varies when the IPMC is actuated and have effects on the actuating performance. However, to date, few works consider the effect of the surface resistance change on the actuating performance of the IPMC.

In current paper, to address the above problem, a physics-based model that combines the effect of the electrode resistance change and the charge dynamics of the ionic polymer was proposed. Firstly, a microstructure model of the surface electrode was proposed. The arrangement of particles used in this model was inspired by the primary metallic crystal structures. Based on the volume change of the electrode caused by the IPMC beam bending, the variation of the resistance of the IPMC was obtained. Secondly, a physics based model of the polymer membrane was developed. The model is based on the Poisson-Nernst-Planck equations. The Ramo-Shockley theorem was used to calculate the current in the continuous electrodes of the IPMC [65], [66]. The finite element approach is used to describe the dynamics of the segmented IPMC strip, which considers as composition of finite elements that can be used to represent a mechanical deflection of the IPMC. By combining the model of the surface electrode and the polymer membrane, the actuation model of the IPMC was obtained. To the best knowledge of the authors, the proposed actuation model is the most complete physics-based IPMC model presented to date including the effect of surface electrode.

Experiments were also conducted to validate the model. The IPMC samples were prepared. The scanning electron microscope (SEM) was used to study the microstructure of the IPMC. Experimental apparatuses were implemented to measure the surface resistance and the deformation of the IPMC strip. The parameters of the model were identified based on the experimental results. The simulation results were compared with the experimental results to verify the model. The model of the IPMC was simulated using the finite element implementation. The charge dynamics inside the polymer was presented and discussed.

The rest of this paper is organized as follows. The physical model is presented in Section II. Experimental validation and results are shown in Section III and IV, respectively. A discussion with the finite element implementation of the IPMC model is presented in Section V. Section VI is the conclusion.

2.2. Mathematical model

2.2.1. The electrode model

The model of the electrode resistance is developed in this section. It is assumed that the IPMC satisfies the following restrictions: 1) compared with the IPMC's length, the oscillation of the IPMC is far small. The IPMC is assumed to bend vertically at the tip denoted by $w(L, t)$; 2) During the oscillation of the electrode, the relative position of the metal particles changes accordingly as well as the size of the unit cell ; 3) The electrode of the IPMC is composed of the metal particles and the voids between the particles; The microstructure of the electrodes can be described in terms of its unit cell; 4) The metal particle arrangement-microstructure is based on the Face Center Cubic (FCC) [67]–[71]; 5) It is assumed that the particle on each side of the defective unit cell is missing [10]. By integrating the unit cell in the three dimensions along with the defective cell, the impedance of the electrode can be obtained. The vacancy defect was also included in the model. The length and width of the IPMC beam is L and W . The thickness of the polymer membrane and electrode are $2h$ and h_e . The unit length of the curved IPMC midline is assumed as dz . The unit cell length of the stretched electrode can be expressed as [10]

$$dL(\hat{h}, w(L, t)) = d\gamma(w(L, t))(r(w(L, t)) + h + \hat{h}) \quad (2.1)$$

where $\gamma(t)$ is the angle of the curved beam, $r(w(L, t))$ is the radius of the midline and \hat{h} is the position of the unit cell along the thickness direction of the electrode. The expressions of $\gamma(t)$

and $r(w(L,t))$ are defined in Ref. [10]. Two kinds of cubes are considered: the normal cube and the cube with a vacancy defect. The resistance of the normal cube and defective cube can be expressed as

$$\Delta R_n(w(L,t)) = \frac{\rho_p(a-2s_v)}{a^2} \frac{r(w(L,t))+h+\hat{h}}{r(w(L,t))} + \frac{2\rho_p\rho_v s_v}{2\rho_p s_v^2 + \rho_v(a^2-2s_v^2)} \frac{r(w(L,t))+h+\hat{h}}{r(w(L,t))} \quad (2.2)$$

$$\Delta R_d(w(L,t)) = \frac{\rho_p(a-s_v)}{a^2} \frac{r(w(L,t))+h+\hat{h}}{r(w(L,t))} + \frac{\rho_p\rho_v s_v}{2\rho_p s_v^2 + \rho_v(a^2-2s_v^2)} \frac{r(w(L,t))+h+\hat{h}}{r(w(L,t))} \quad (2.3)$$

where ρ_p and ρ_v are the resistivity of the particle and void, a and s_v are the side length of the unit cell and void cube, which were defined in Ref. [10]. In the current study, the IPMC is hydrated and the void is water. Then we integrate the resistance of the cube (see Eqs. (2.2) and (2.3)) in the z, y, x direction to obtain the resistance of the electrode. One can obtain the expression of the electrode resistance as follows

$$R_e(w(L,t)) = \frac{1}{\left[J_e \frac{1-P_x}{a} + \frac{P_x W r(w(L,t))}{G_e a L} \right] \ln \left(\frac{r(w(L,t))+h+h_e}{r(w(L,t))+h} \right)} \quad (2.4)$$

with

$$J_e = \frac{(1-P_y)W}{E_e L} + \frac{P_y W r(w(L,t))}{G_e L}, \quad E_e = F_e \frac{(1-P_y)}{r(w(L,t))} + G_e \frac{P_z}{r(w(L,t))},$$

$$F_e = \frac{\rho_p(a-2s_v)}{a^2} + \frac{2\rho_p\rho_v s_v}{2\rho_p s_v^2 + \rho_v(a^2-2s_v^2)}, \quad G_e = \frac{\rho_v(a-s_v)}{a^2} + \frac{\rho_p\rho_v s_v}{2\rho_p s_v^2 + \rho_v(a^2-2s_v^2)},$$

where P_x , P_y , P_z are the percentages of the defective cube in the x , y , z direction. The percent of the vacancy can be expressed as

$$P_v = \frac{1}{2} \left(1 - (1 - P_x)(1 - P_y)(1 - P_z) \right). \quad (2.5)$$

2.2.2. The polymer membrane model

Analytical solutions are available for several special cases of geometric nonlinearity in a cantilever beam [72]. Herein, the finite element approach is used to describe the dynamics of the IPMC strip. The IPMC actuator was assumed to be divided by a series of elements, where the voltage on each element is constant, as shown in Fig. 2.1. The IPMC was assumed in the fully hydrated condition. The Nernst-Planck equation, which describes the cation migration and diffusion in the polymer element backbone, and the Poisson's equation, which describes the concentrating of local charges at the boundary between the polymer and surface electrodes resulting in an electric field increase in the opposite direction, are expressed as [27], [73]

$$\frac{\partial C}{\partial t} + \nabla \cdot (-D\nabla C - \hat{z}\mu FC\nabla\phi) = 0 \quad (2.6)$$

$$\nabla \cdot \vec{E} = -\nabla^2\phi = \frac{\rho_c}{\varepsilon} \quad (2.7)$$

$$\rho_c = F(C - C_0) \quad (2.8)$$

where C , t , μ , D , F , \hat{z} , ϕ , ε , \vec{E} , ρ_c and C_0 are the cation concentration, time, mobility of cations, diffusion constant, Faraday constant, charge number, electric potential in the polymer element, absolute dielectric constant, strength of the electric field, charge density and constant anion concentration respectively. To solve for the actuation of IPMC, Eqs (2.1), (2.2) and (2.3)

were transformed to the Laplace form. The following variables were also converted to the frequency domain. Nemat-Nasser and Li presented a theory that the charge density at the boundary of polymer is proportional to the induced stress σ and is expressed as [27]

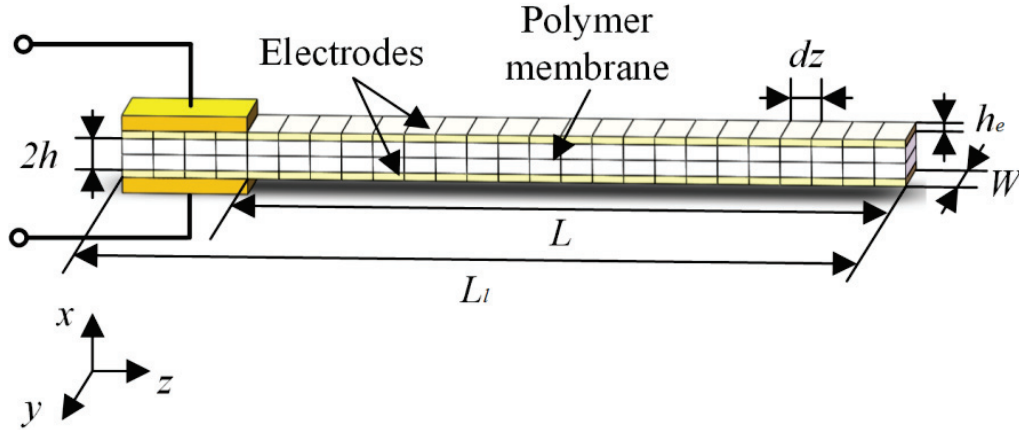


Figure 2.1 Schematic of IPMC beam.

$$\sigma(\pm h, z, s) = \alpha \rho_c(\pm h, z, s) . \quad (2.9)$$

The boundary condition of Eq. (2.9) is $\rho(h, z, s) + \rho(-h, z, s) = 0$. By combining Eqs. (2.6), (2.7), (2.8) and (2.9), the expression of ionic flux in the x direction within the polymer can be obtained as [74]

$$f(x, z, s) = -2DC(z, s) \left(\cosh(A(s)x) + \cosh(A(s)h) \right) \left(\frac{A(s)}{F} - \frac{FC_0}{RT\hat{\epsilon}A(s)} \right) \quad (2.10)$$

where

$$A(s) = \sqrt{\frac{B+s}{D}} , \quad B = \frac{\hat{z}\mu F^2 C_0}{\hat{\epsilon}} .$$

and R is the gas constant, and T is the absolute temperature. Based on Ramo-Shockley theorem [75], which describes a relationship between the instantaneous induced current on an electrode and the charge motion in the vicinity, the local current density at an electrode boundary is expressed as

$$j(z, s) = \frac{1}{h} \int_{-h/2}^{h/2} f(x, z, s) dx . \quad (2.11)$$

The electric potential on the surface of the IPMC element can be expressed as

$$\phi(\pm h, z, s) = \pm \frac{V(s)}{2} \mp \int_0^z j(\tilde{z}, s) W_e h_e R_e (w(L, s)) \frac{d\tilde{z}}{L} \quad (2.12)$$

where $V(s)$ is the voltage applied to the clamp. Through combing (2.11) and (2.12), the $\rho(x, z, s)$ can be obtained as

$$\rho(x, z, s) = -G(z, s) \sinh(A(s)x) V(s) \quad (2.13)$$

with

$$G(z, s) = -\frac{\exp(J(s, w(L, s))z / L)}{K(s)}$$

$$J(s, w(L, s)) = -\frac{\frac{D}{h} \left(\frac{2 \sinh(A(s)h)}{A(s)} + 2h \cosh(A(s)h) \right) \left(\frac{A(s)}{F} - \frac{FC_0}{RT \hat{\epsilon} A(s)} \right) W_e h_e R_e (w(L, s))}{2 \frac{\sinh(A(s)h)}{\hat{\epsilon} A^2(s)} + 2 \cosh(A(s)h) \left(\frac{RTA(s)}{F^2 C_0} - \frac{1}{\hat{\epsilon} A(s)} \right) h}$$

$$K(s) = 2 \frac{\sinh(A(s)h)}{\hat{\varepsilon}A^2(s)} + 2 \cosh(A(s)h) \left(\frac{RTA(s)}{F^2C_0} - \frac{1}{\hat{\varepsilon}A(s)} \right) h$$

The detailed derivation can be seen in Appendix A. By relating the induced stress $\sigma(\pm h, z, s)$ to the bending moment, one can obtain

$$\sigma(\pm h, z, s) = \frac{\pm hM(z, s)}{I} \quad (2.14)$$

where I is the moment of inertia of the IPMC element and $I = \frac{2}{3}Wh^3$. With Eqs. (2.9), (2.13) and (2.14), the bending moment can be obtained as

$$M(z, s) = -\frac{\alpha l}{h} G(z, s) \sinh(A(s)h) V(s) \quad (2.15)$$

Through relating the moment to the displacement of the IPMC elements and integrating the displacements, one can obtain

$$w(L, s) = -\frac{\alpha L}{hY} \frac{(-\exp(J(s, w(L, s))) + J(s, w(L, s)) + 2)}{J(s, w(L, s))K(s)} \sinh(A(s)h) V(s) \left(1 + \frac{1}{J(s, w(L, s))} \right) \quad (2.16)$$

where Y is the Young's modulus. See Appendix B for the detailed derivation of $w(L, s)$. By solving Eq. (2.16), the deformation of the IPMC $w(L, s)$ under the voltage $V(s)$ can be obtained. The equation was converted to the time domain. Since Eq. (2.16) have no analytical solution, the Matlab was used to obtain the numerical solution for $w(L, s)$. In current study, the actuation bandwidth of an IPMC actuator is relatively low (under 10 Hz) [61]. To accommodate

the vibration dynamics of the beam, we project $w(L, s)$ on the first mode of vibration expressed as

$$X_1(z) = ch\beta_1 z - \cos \beta_1 z - \frac{ch\beta_1 L + \cos \beta_1 L}{sh\beta_1 L + \sin \beta_1 L} (sh\beta_1 z - \sin \beta_1 z) \quad (2.17)$$

where β_1 is the constant in relative with the natural frequency and the damping ratio [76]. The actual tip displacement of the IPMC beam can be expressed as

$$w_1(z) = w(L, t)X_1(L) . \quad (2.18)$$

2.3. Experimental method

2.3.1. Sample preparation

IPMC samples were prepared for the experimental validation. Firstly, the NafionTM-117 membrane was pretreated. The surface of the membrane was polished. The membrane was immersed in 3% hydrogen peroxide (H₂O₂) to eliminate organic impurities and in 1 M sulphuric acid (H₂SO₄) to remove the metallic impurities. The deionized (D.I) water was used to clean the membrane. Secondly, the platinum metal particles were plated on the polymer membrane. The membrane was immersed in a platinum complex solution (Pt(NH₃)₄Cl₂·H₂O) for the primary plating process. This procedure impregnates the membrane with Pt salt. After the Pt impregnation, a sodium borohydride solution (NaBH₄) was prepared and the Pt impregnated sheet was placed in the solution. This is a reduction reaction to reduce the Pt salt from the membrane to the surface of the polymer. After reduction process, the membrane was cleaned in multiple baths of D.I water and a sulphuric acid solution. Secondary plating was conducted to lower the surface resistance of the membrane. The membrane were suspended in the solution

while hydrazine ($\text{NH}_2\text{NH}_2 \cdot \text{H}_2\text{O}$) and hydroxylamine hydrochloride ($\text{H}_2\text{NOH} \cdot \text{HCl}$) were added to the solution. Finally, the membrane was cleaned in multiple baths of D.I water and a sulphuric acid solution. After the plating process, the hydrogen ion is present in the membrane. In order for a better transport of ions through the membrane, an ion exchange was conducted. To improve the ion transportation through the membrane, the hydrogen ions were replaced with lithium ions. This exchange was completed by soaking the membrane in a solution of lithium chloride. After the exchange has completed, the sample was rinsed and stored in D.I water.

2.3.2. Surface resistance

The SEM was used to study the structure of the IPMC sample. Figure 2.2 shows the cross-sectional image of the IPMC, which indicates the platinum content distribution in the electrode and vicinity. Based on the image, the IPMC was composed of the electrode and the polymer membrane. In the surface resistance model above, the electrodes are considered a bulk metal. However, in reality from the SEM images it can be seen that the structure is more complicated. The thickness of the electrode could vary significantly. The thin electrolessly plated electrodes on a polymer do not result in a uniform conductivity in each direction at each location, so the defective factor helps to take those effects into account. The parameters of the electrode were measured based on the SEM images.

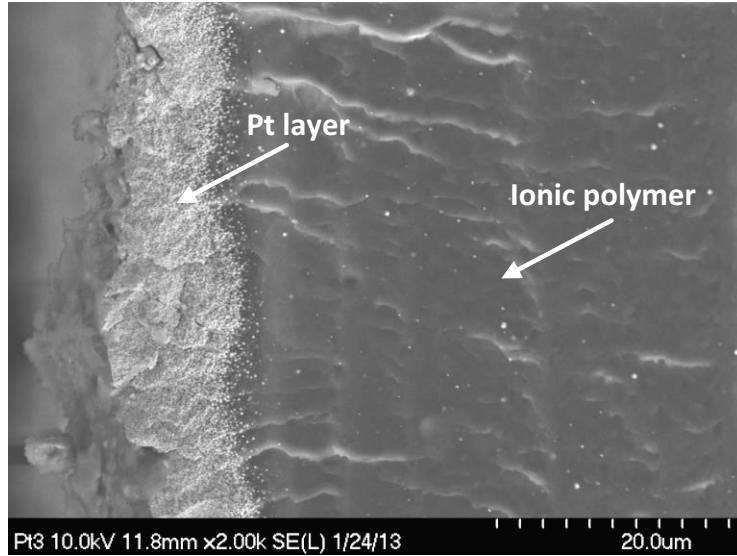


Figure 2.2 Cross-section SEM images of the IPMC.

Figure 2.3 shows the illustration of the experimental apparatus for the surface resistance test. In accordance with the model, during the experiments, the IPMC sample was submerged in the D.I water to achieve a fully hydrated condition. The IPMC was clamped at one end. An electromagnetic shaker (VR-5200, Vibration Research Corp.) was used to provide a linear, oscillatory motion at the free end of the IPMC. A PC was utilized to send the orders to the vibration controller (VR-8500, Vibration Research Corp.). By using an amplifier to amplify the signal from the controller, the sinusoid oscillating frequency and amplitude of the electromagnetic shake were controlled. In current study, the frequency varies from 1 to 5 Hz and the amplitude varies from 5 to 10 mm. Figure 2.4 shows the snapshot of the experimental set up.

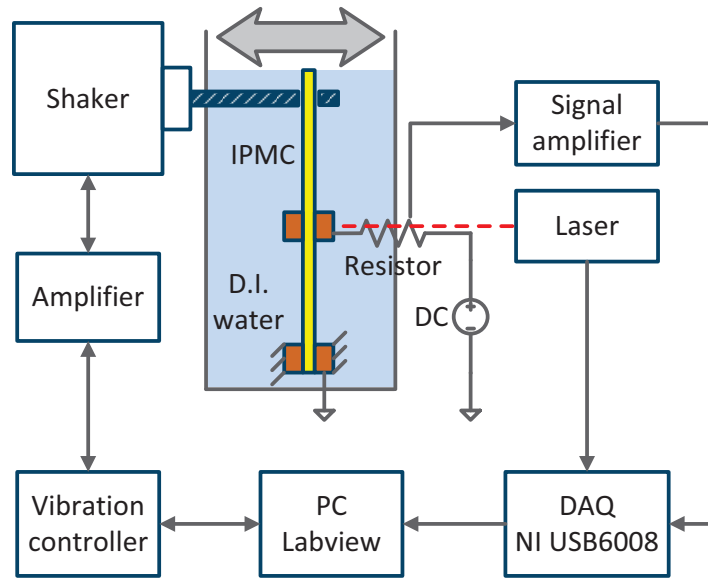
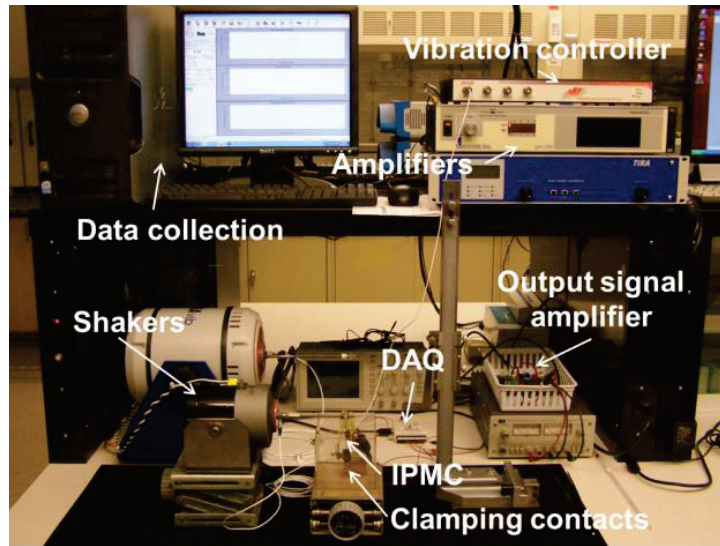
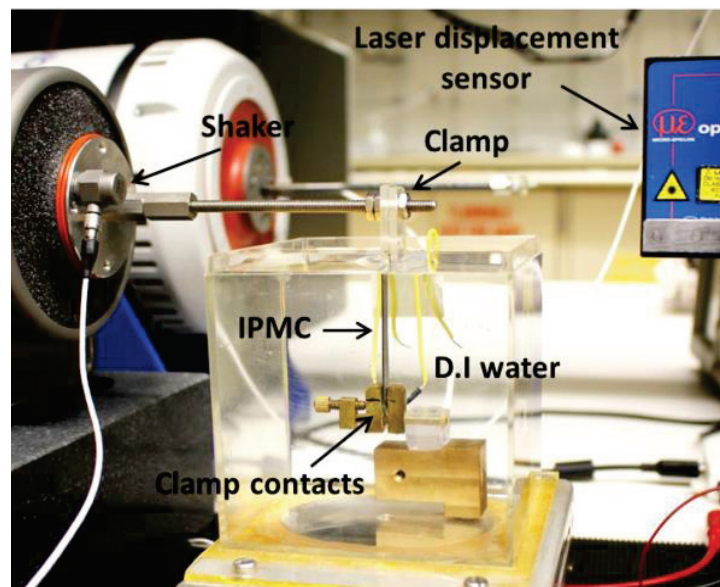


Figure 2.3 Illustration of the experimental set up for the surface resistance test.



(a)



(b)

Figure 2.4 Snapshot of the experimental set up: (a) general set up; (b) close-up of the IPMC surface resistance measurement.

Cha et. al presented an experimental method to test the impedance of IPMC [77]. The IPMC was clamped at one end and the other end was subjected to a periodical stimulus along the length direction. In current study, the curvature of the IPMC surface electrode is assumed to be

circular arc. To obtain a curved IPMC with a radius for the resistance measurement, a clamp was set at the middle of the IPMC, which is 20 mm from the clamp at the end. A circuit which connects the two points of the surface electrode at one side of the IPMC was designed. It consists of a stabilized voltage supply of 0.1 V and a 0.5 Ω resistor in series. The surface resistance of the IPMC was measured under the mechanical stimulus. An amplifier was used to amplify the output signal. A laser sensor (optoNCDT-1401, Micro-Epsilon) was used to measure the displacement of the measured point of the IPMC. A DAQ was used to measure the signals (NI USB-6008, National Instruments). A LabVIEW data acquisition system was used to record the experimental results.

2.3.3. Actuation performance

Experiments were conducted to test the actuation performance of IPMC. Figure 2.5 shows the schematic illustration of the experimental set up. The IPMC was submerged in D.I water and clamped at one end in vertical cantilever position. A signal generator (FG-7002C, EZ digital) was used to provide the sinusoid actuation signals to the IPMC actuator at the clamp through a power amplifier (LVC-608, AE Techron). The frequencies of the signal vary from 0.2 Hz to 10 Hz, and the amplitudes vary from 2 V to 4 V. The oscillation of the IPMC strip was measured by a laser displacement sensor (optoNCDT-1401, Micro-Epsilon). A DAQ (NI SCB-68, National Instruments) was used to measure the signals. The current, voltage and displacement responses were recorded simultaneously using LabView 8 software. Figure 2.6 shows the snapshot of the experimental set up.

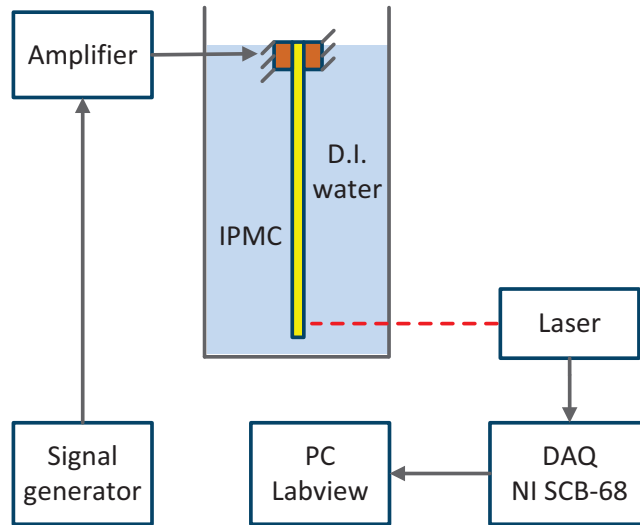


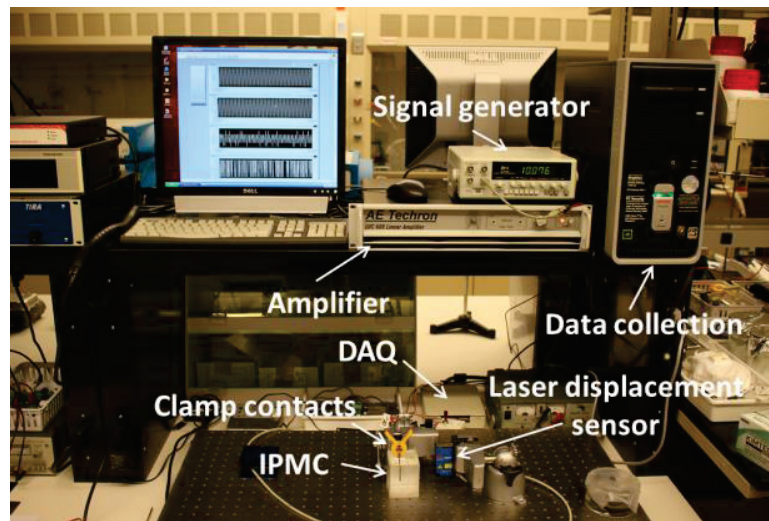
Figure 2.5 Illustration of the experimental set up for the actuation test.

2.4. Simulations and experimental results

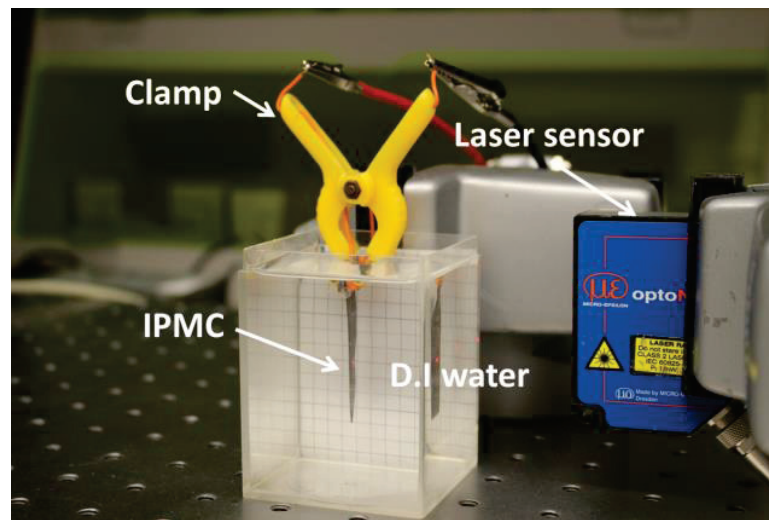
2.4.1. Resistance model verification

An IPMC sample with the size of 51.07 mm in length, 9.94 mm in width, and 0.57 mm in thickness was used for the resistance model verification. To obtain the resistance R_e of the electrode, a DC voltage of 0.1 V, which was provided by a power supply, was applied to the circuit. This voltage value is represented by V_p in the mathematical model. The LabVIEW was used to measure the voltage of the resistor. The voltage value across the resistor is represented in the model by V_r . The resistance of the resistor is given by R_r in the model. The voltage and current of the electrode can be obtained as the electrode is in series with the resistor. These

values are designated as V_e and I_e for voltage and current, respectively. According to Ohm's law, the resistance R_e of the electrode can be expressed as



(a)



(b)

Figure 2.6 Snapshot of the experimental set up; (a) general set up; (b) close-up of the IPMC actuation measurement.

$$R_e = \frac{V_e}{I_e} = \frac{V_p - V_r}{V_r / R_r} = \frac{2(0.1 - V_r)}{V_r}. \quad (2.19)$$

The recorded experimental data was analysed in a computer using MATLAB. To validate the model, the parameters need to be identified. The physical constants are shown in Table 2.1. The diameter of the metal particle is $D_p = 50 \times 10^{-9}$ m (50 nm) [64]. Based on the SEM image, the average thickness of the electrode is measured as $h_e = 6 \times 10^{-6}$ m (6 μ m). The percentage of the vacancy need to be identified through curve-fitting using the least-square method. Based on the least-square error analysis of the experimental results, the percentage of the vacancy P_v of the resistance model were identified as $P_v = 15.6\%$, this result is close to that in our previous work [10]. Figure 2.7 shows the comparison between simulation results and experimental results of the electrode resistance. It is noticed that under the sinusoidal mechanical stimulus, the resistance of the electrode shows a sinusoidal variation. It is also found that the simulation results match well with the experimental results. One of the explanations to this is that some of the parameters of the model were identified based on the experimental results, such as percentage of the vacancy P_v , Shahinpoor presented the radius of the curvature ρ_r of the IPMC beam as [78]

$$\rho_r \cong \frac{L^2 + \delta^2}{2\delta} \quad (2.20)$$

where δ is the end deflection. The radius of the curvature ρ_r is in turn related to the maximum tensile (positive) or compressive (negative) strains, which can be expressed as

$$\varepsilon \cong \frac{h}{\rho_r}. \quad (2.21)$$

In current study, the deformation of the IPMC is converted to the strain for intuitive comparison. Figure 2.8 shows the resistance change of the IPMC electrode versus different strains. The

simulation results were compared with the experimental results. It can be seen that the model can well describe the resistance change of the IPMC electrode. It is also noticed that with the strain increasing, the resistance change of the electrode increased.

Table 2.1 Value of the resistance model constant.

Item	Value
$\rho_p (\Omega \text{ m})$	1.06×10^{-6}
$\rho_v (\Omega \text{ m})$	1×10^3

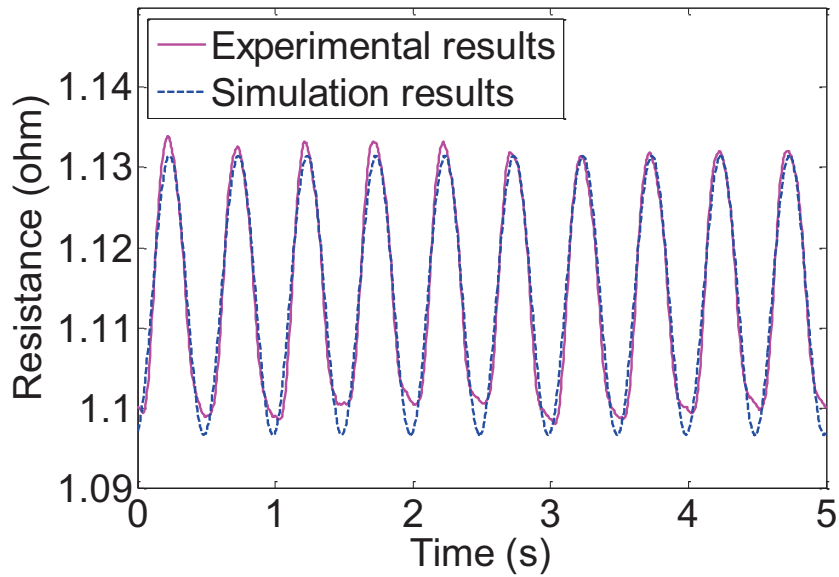


Figure 2.7 Comparison between the simulation results and experimental results of the electrode resistance at the oscillation amplitude of 10 mm and frequency of 2 Hz.

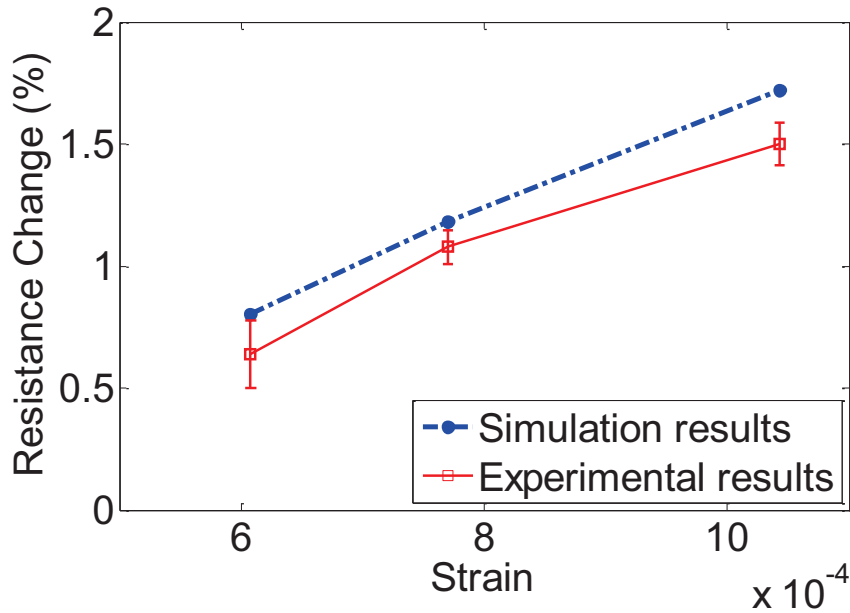


Figure 2.8 Comparison between the simulation results and experimental results of the electrode resistance change.

2.4.2. Actuation model verification

The IPMCs as the actuators were tested to verify the actuation model. Three samples with different length were tested. For the comparison of the strain, the widths of the samples were the same. Table 2.2 shows the dimensions of the IPMC samples. The definition of L_1 , L , W and $2h$ can be found in Figure 2.1. Some parameters of the actuation model were based on previous results of the surface resistance. Some are physical constants. Table 2.3 shows the value of the IPMC actuator model constants [63]. The absolute temperature is $T = 297$ K. The rest need to be identified. In current study, the voltage amplitude applied on the IPMC was constant. By applying varies frequencies to the IPMC, varies deformation as well as strains can be obtained. The deformations of the IPMC actuators were measured. Based on the experimental results of IPMC 1 through the least-square method in MATLAB, the parameters of the model were

identified as $Y = 90.92 \times 10^6$ Pa and $\alpha = 104$ J/C. The Young's module of IPMC varies from 41×10^6 Pa to 571×10^6 Pa based on previous work [61], [63]. The coupling constant α , which relates the charge density at the boundary of polymer membrane to the induced stress, varies from 30 J/C to 148 J/C based on previous work [27]. Thus the values in current paper are reasonable. The parameters were plugged into the actuation model (except geometric dimensions) for predicting the actuating performance of IPMC 2 and IPMC 3. Model with and without surface resistance change were compared. For the model without consideration of the surface resistance change, the surface resistance R in Eq. (2.23) is a constant value and was identified as $R = 1.8 \Omega$ through the non-linear fitting process. The surface resistance per {unit length · unit width} of the IPMC is $7.44 \Omega/\text{m}^2$. Previous work reported the surface resistance per {unit length · unit width} as $22.3 \Omega/\text{m}^2$ [61]. The reasons for the difference are the different electrode plating times and different reduction temperatures during the fabrication process of IPMC. The rest parameters are the same as previous simulations.

The actuation model was verified in experiments by applying sinusoidal actuation signals to the IPMC samples and measuring the deformations. Figure 2.9 shows the comparison of experimental results with theoretical model simulation results with and without consideration of surface resistance change. It is clear that the model considering the effect of surface resistance change shows better agreement than the one ignoring the resistance. This indicates that the model incorporating the surface resistance change is more effective in capturing the actuation dynamics of IPMC. Based on Fig. 2.9, it can be found that for all samples, good agreement between the model prediction and the experimental data is achieved. These figures show that current actuation model can well predict the actuating of IPMCs. It is also noticed that with the

voltage amplitude increasing, the strain of the IPMC increased. As the actuating frequency rose, the strain of the IPMC reduced. It was found that in general when the frequency is approached 6 Hz, the strain of the IPMC increased. This might be caused by the natural frequency of the IPMC beam. Meanwhile, this tendency was not clear for the IPMC beam with the length of 26 mm. One possible explanation is that the experimental test and theoretical simulation of the IPMC model with the consideration of the surface resistance change were discrete, which only tested at several frequencies. The tendency could be more clear if the IPMC sample was tested at more frequencies.

Table 2.2 Dimensions of the IPMC samples.

Item	L_1 (mm)	L (mm)	W (mm)	$2h$ (mm)
IPMC 1	51.07	41.07	9.94	0.57
IPMC 2	37.05	27.05	9.94	0.57
IPMC 3	22.16	12.16	9.94	0.57

Table 2.3 Value of IPMC actuator model constants [63].

Item	Value
D (m ² /s)	7×10^{-10}
C_0 (mol/m ³)	1091
$\hat{\varepsilon}$ (F/m)	0.2×10^{-3}
μ (mol·s/kg)	2.9×10^{-15}
z	1
F (C/mol)	96487
R (J/mol·K)	8.3143

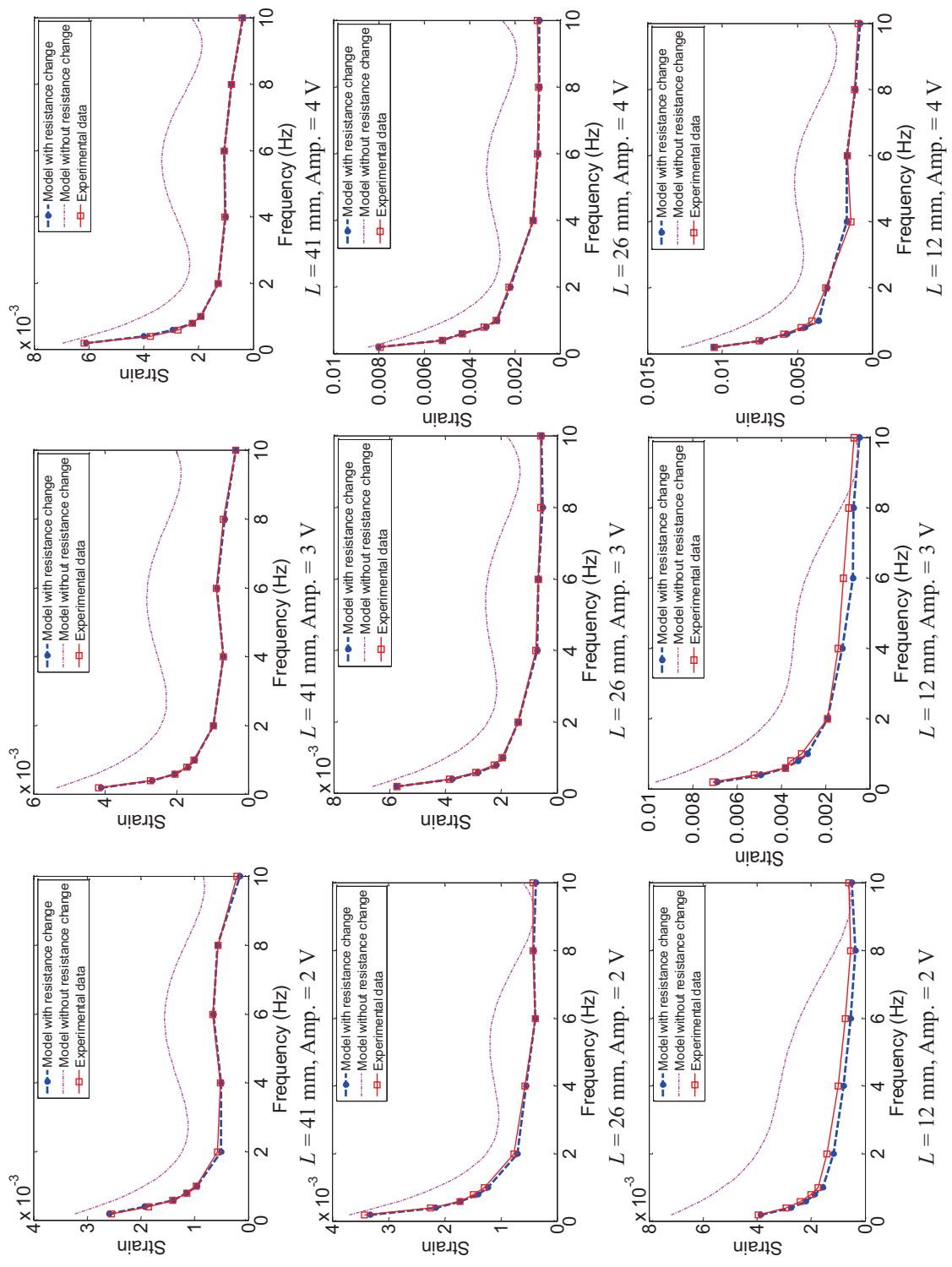


Figure 2.9 Comparison of experimental results of IPMC strain with model predictions, with and without consideration of surface resistance change.

2.5. Discussions

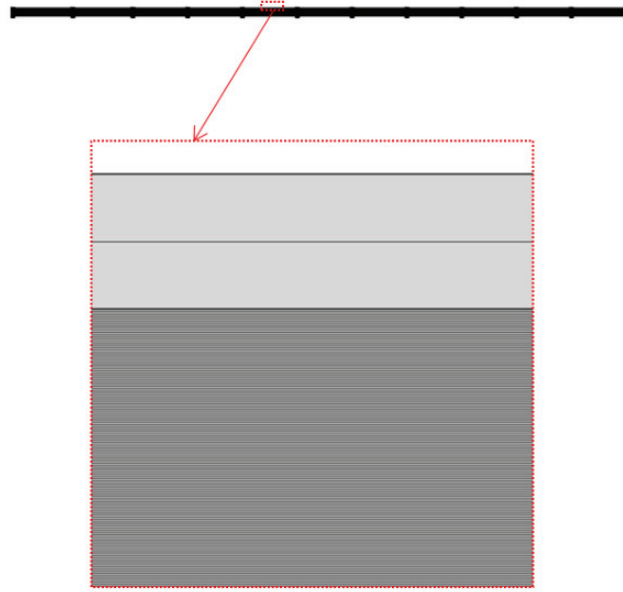
2.5.1. Mathematical model

A physics-based model was used to simulate ion concentration, polymer electric potential, charge density and displacement response to a low voltage input signal to obtain further insight into the underlying physics. A 2-dimensional finite element simulation was performed using COMSOL Multiphysics 4.3b software. Two mesh types were used in simulation: (1) a sparsely mapped mesh along the length with a very large element aspect ratio; (2) a triangular mesh with fine distribution near electrodes and maximum aspect ratio of 1.3:1, as shown in Fig. 2.10. The sparsely mapped mesh was utilized because the changes in the length direction were assumed to be negligible. The sparsely mapped mesh has 55,044 elements, whereas the triangulated mesh has 145,952 elements. Both meshes were refined to within 1% solution change. Additionally, the sparse mesh produced the same solutions as the triangulated mesh and was thus chosen for use in simulations.

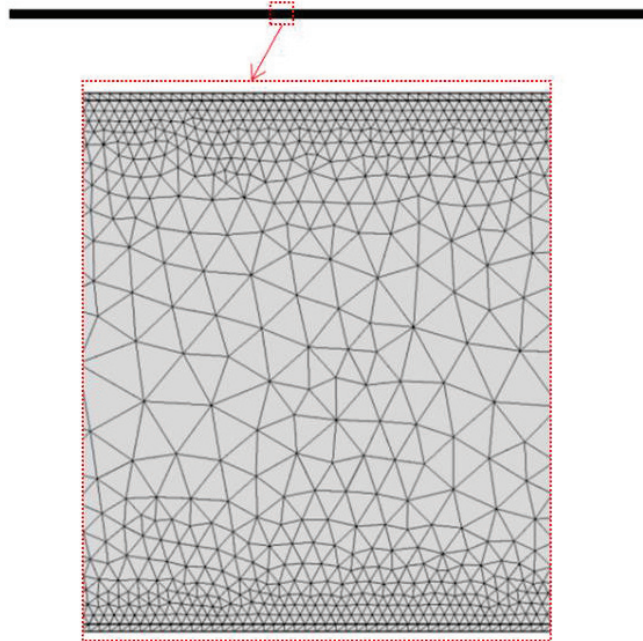
The simulation utilizes the transport of diluted species, general form partial differential equation (PDE), electric currents, and solid mechanics physics modules in COMSOL to achieve the desired governing set of PDEs. The transport of diluted species and general form PDE physics provide the Poisson-Nernst-Planck (PNP) set of coupled PDEs, which are used to describe cation concentration and electric potential within the polymer. A linear elastic material model with infinitesimal strain theory was implemented for the solid mechanics physics. The simulation is divided into two studies: first the electric currents and PNP physics are applied simultaneously to find ion concentration and charge density in the IPMC for a given sinusoidal voltage input, and then the solid mechanics study is performed. The voltage is applied over a

fixed region of 10 mm in length to the electrodes, similar to the experimental setup. The solids model is done with one end of the IPMC fixed. A body load which is assumed proportional to the charge density is applied across the free length of the IPMC strip.

During electromechanical actuation of an IPMC by supplied voltage input to its electrodes, the main contribution to the deformation is assumed to be the cation migration and corresponding swelling effects. In current model, the IPMC is in fully hydrated condition. The contribution from the concentration gradient and electric potential are much larger than the contribution of the pressure gradient, thus this term has been omitted and the Nernst-Planck equation is expressed in Eq. (2.6). Poisson's equation as used in the model is expressed in Eq. (2.7). The anions of the IPMC are fixed to the polymer backbone making the anion concentration variable with deformation only, while the cations are free to migrate based on the electric potential. Thus in actuation of the IPMC by input voltage, the change of anion concentration is very small in comparison with the change in cation concentration and the charge density is assumed to be a function of cation concentration only as expressed in Eq. (2.8). A body force in the bending direction, which is assumed to be proportional to the charge density as $F_y = \alpha\rho_c$, is the input into the solid mechanics model. The solids mechanics describe the stress, strain, and local displacement. The governing solid mechanics equation used is



(a)



(b)

Figure 2.10 Meshes used in finite element simulations: (a) mesh sparsely mapped along length; (b) triangulated mesh.

$$\rho_m \frac{\partial^2 u}{\partial t^2} - \nabla \cdot \sigma_m = F \quad (2.22)$$

where ρ_m is material density and $\rho_m = 874 \text{ kg/m}^3$, $u = \{u, v\}$ is the local displacement vector in x and y directions respectively, and F is the body force vector. Notation σ_m is the material stress tensor written in terms of local displacement using Hooke's Law as

$$\begin{bmatrix} \sigma_{xx} \\ \sigma_{yy} \\ \sigma_{xy} \end{bmatrix} = \frac{E}{(1+\nu)(1-2\nu)} \begin{bmatrix} 1-\nu & \nu & 0 \\ \nu & 1-\nu & 0 \\ 0 & 0 & 1-2\nu \end{bmatrix} \begin{bmatrix} \frac{\partial u}{\partial x} \\ \frac{\partial v}{\partial y} \\ \frac{1}{2} \left(\frac{\partial u}{\partial y} + \frac{\partial v}{\partial x} \right) \end{bmatrix} \quad (2.23)$$

where ν is the Poisson's ratio and $\nu = 0.49$ [63]. As the material is assumed to deform primarily in the bending plane, a plane strain deformation assumption was utilized, hence strains in the x - z , y - z , and z - z planes are assumed to be zero. The model first utilizes Eqs. (2.6), (2.7), and (2.8) to solve for the charge density, ρ_c . Then, Eqs. (B.1) and (B.2) are solved for the deformation. The constant parameters used for COMSOL simulations are shown in Table 2.3. The details of the modeling were presented in Appendix D.

2.5.2. Simulation results

Since an experimental method of measuring the cation migration and charge density within the polymer is not readily available, the COSMOL simulation results were used primarily to gain insight into these phenomena. The simulation of the IPMC actuating was performed under an input voltage with amplitude of 2 V and frequency of 1 Hz. Figure 2.11 illustrates the IPMC oscillation time-series during steady-state response. Within one oscillation cycle, the stress on the IPMC strip varied along the length. The stress on the IPMC increased as the IPMC

curved. At the maximum tip displacement, the stress reached its maximum. Figure 2.12 shows the simulation result of the IPMC tip displacement. As can be seen in the graph, after several cycles of oscillation, the quasi-steady state of the IPMC tip movement appeared to be reached. The amplitude of the oscillation is 2.1×10^{-3} m. The tip displacement result also shows a good agreement with the experimental result.

Figure 2.13 show the cation concentration in the polymer near the top and bottom electrode separately. The location (x, y, z) of the measured points are $(h - 1 \times 10^6 \text{ m}, W/2, L/2)$ and $(-h + 1 \times 10^6 \text{ m}, W/2, L/2)$. A sinusoid variation of the cation concentration was observed during the deformation of the IPMC actuator within a range between $1.44 \times 10^3 \text{ mol/m}^3$ and $0.82 \times 10^3 \text{ mol/m}^3$ for both points. As shown in Fig. 2.13, the cation concentration reached its quasi-steady state after several cycles of oscillation. It was also noticed that the cation concentration near the top and bottom electrode show an opposite variation, as was expected. The initial transient phase of actuation response can be verified experimentally. This can be thought of as the result of the initial cation distribution at the beginning of the first oscillation cycle (at $t = 0$ seconds) being different than at the beginning of following cycles, until the cation distribution at the start of each cycle is nearly constant.

Figure 2.14 shows the cation concentration time series along the thickness direction in accordance with Fig. 2.11. The location of the measured line was $y = W/2$ and $z = L/2$. It can be found that in one cycle, the cation concentration near the upper and bottom electrode changed significantly, and remained the same in the central area. The simulation results indicated that the charge density at the boundary has a main effect on the stress of the IPMC. This result was partly verified the Nemat-Nasser and Li's theory, as shown in Eq. (2.9). However, the relationship

between the charge density and induced stress cannot be verified based on current simulation and experimental results.

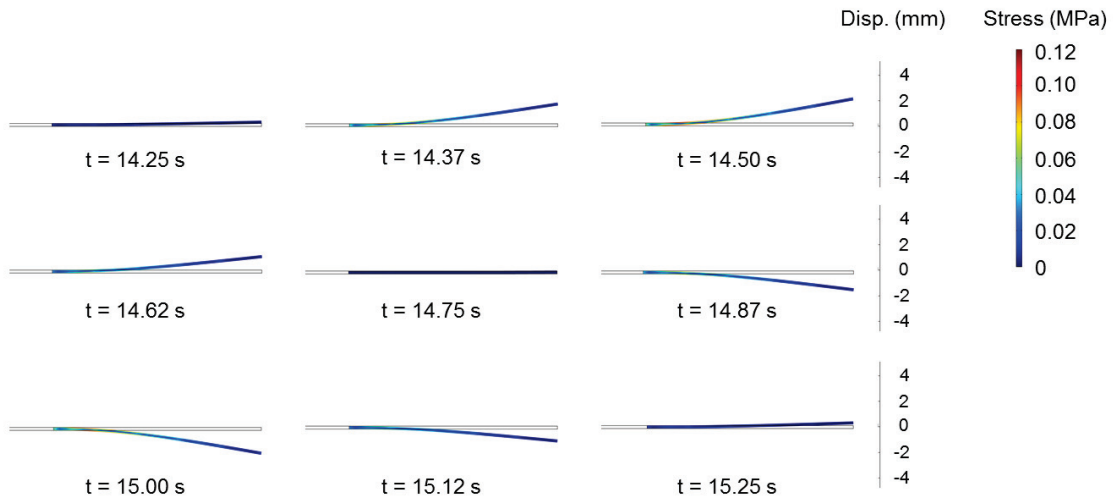


Figure 2.11 IPMC strip displacement for one cycle during steady-state response for a sinusoidal voltage input of 4 V peak-to-peak amplitude and 1 Hz frequency.

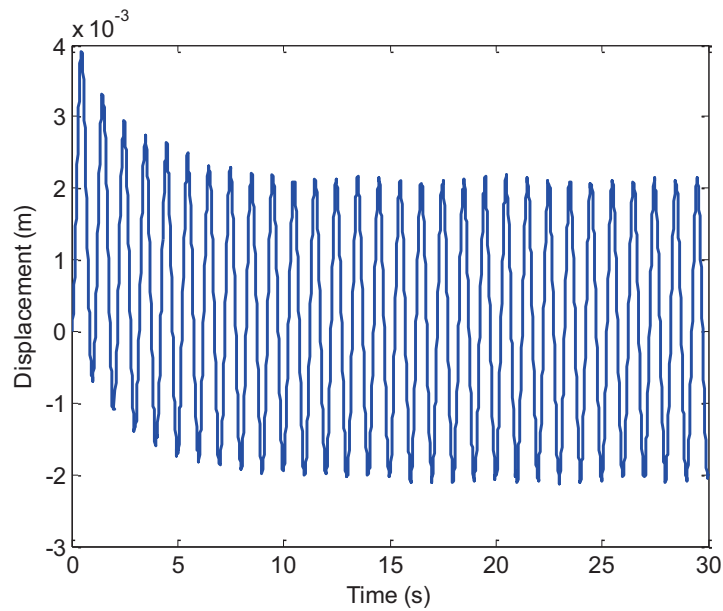
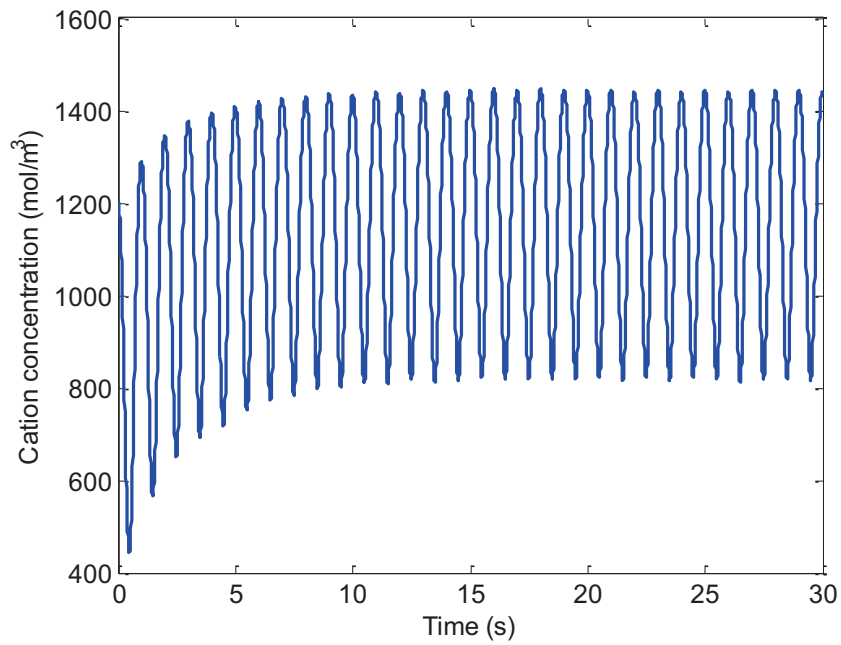
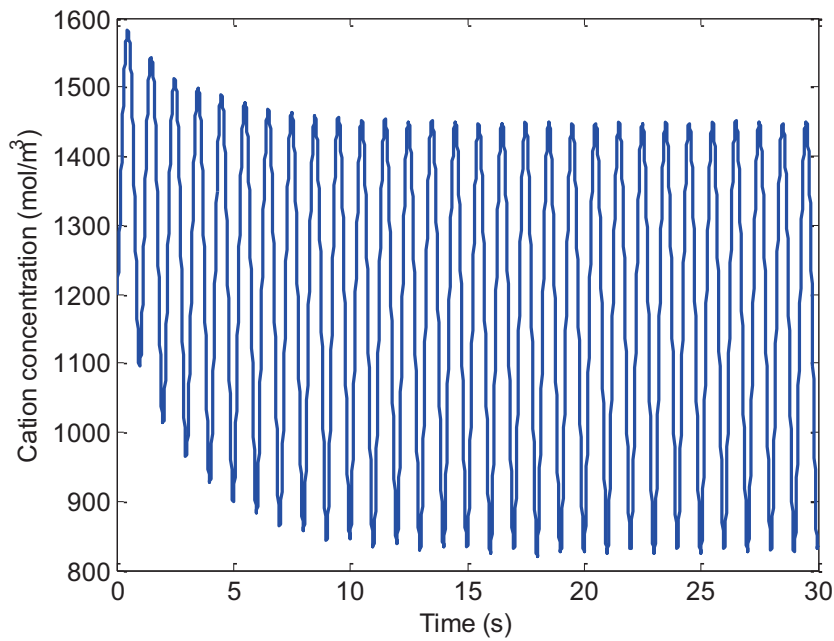


Figure 2.12 Simulation result of the IPMC tip displacement.



(a)



(b)

Figure 2.13 Simulation result of the IPMC cation concentration: (a) near top electrode, (b) near bottom electrode.

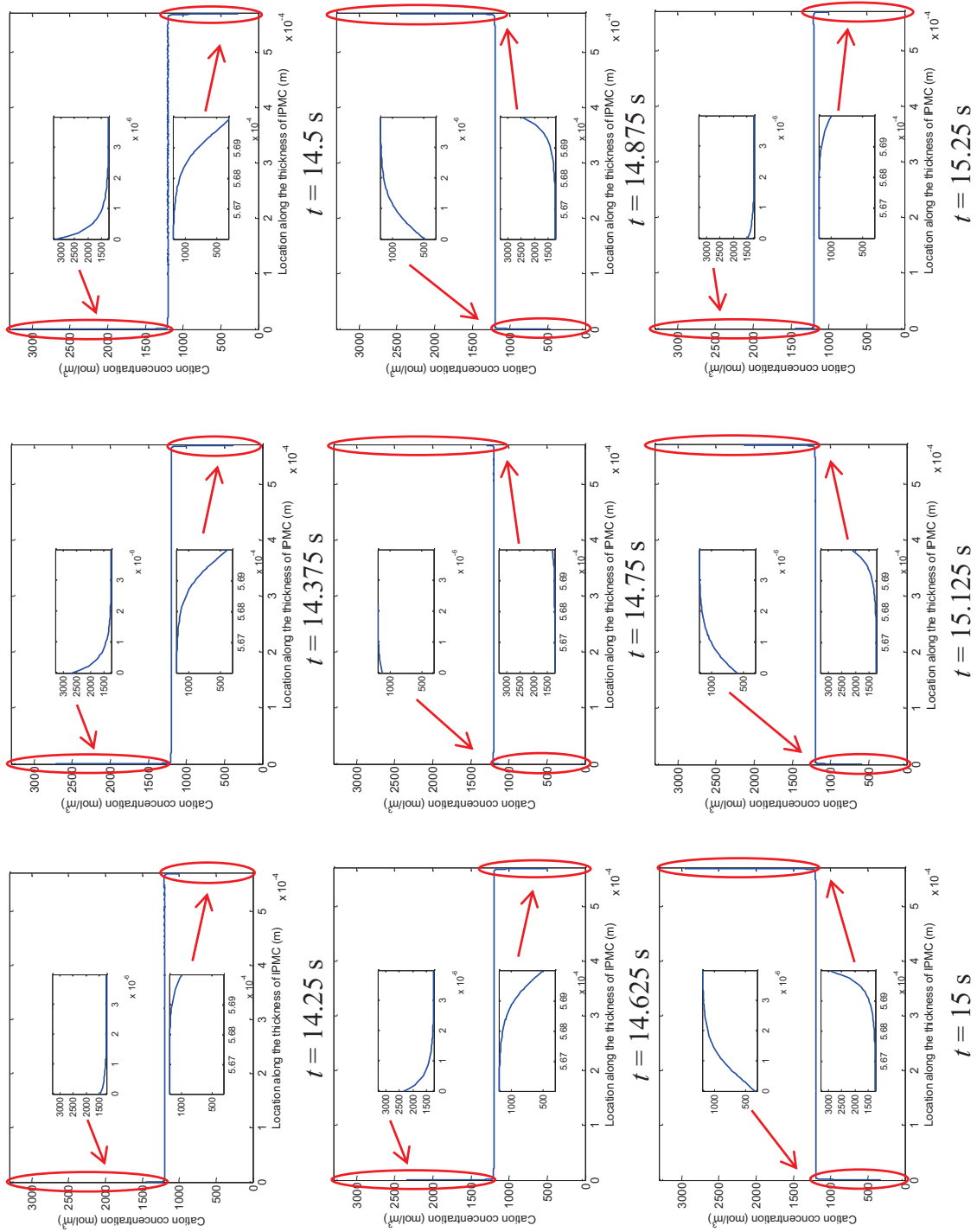


Figure 2.14 Simulation results of cation concentration along the thickness of IPMC.

2.6. Conclusions

In this paper, a physical based model of IPMC was developed. The model is based on the charge dynamics model of the polymer membrane and a microstructure model of the electrode. Experiments were conducted to verify the model. Theoretical results and experimental results were compared and showed a good agreement. The results show that the model that considers the surface resistance change is better in predicting the actuating response of IPMC than the model without considering the surface resistance change. Finite element approach was implemented to study the charge dynamics inside the polymer. It was found that the charge at the boundary of the IPMC has a major effect on the performance of IPMC actuators.

Chapter 3. A multiple-shape memory polymer-metal composite actuator capable of programmable control, creating complex 3D motion of bending, twisting, and oscillation

In this chapter, a research paper published in Scientific Reports is included. The authors are Qi Shen, Sarah Trabia, Tyler Stalbaum, Viljar Palmre, Kwang Kim, and Il-Kwon Oh, in order of appearance on the article. This article reported an ionic polymer-metal composite actuator having multiple-shape memory effect, and is able to perform complex motion by two external inputs, electrical and thermal. This chapter was reprinted from Scientific Reports, Shen, Qi, Sarah Trabia, Tyler Stalbaum, Viljar Palmre, Kwang Kim, and Il-Kwon Oh. "A multiple-shape memory polymer-metal composite actuator capable of programmable control, creating complex 3D motion of bending, twisting, and oscillation." Scientific Reports 6 (2016): 24462.

K.J.K. conceived the idea and designed the project. Q.S., S.T., T.S., V.P. carried out the experiments, analyzed the data and wrote the paper. I.O. helped analyzing the data. All authors discussed the results and commented on the manuscript.

3.1. Introduction

Many life forms have unique organs that exhibit high deformability, maneuverability, and control. For example, most fish have a pectoral fin that can bend and twist in different ways to create various swimming motions, such as hovering and flapping [79]–[81]. Biomimicry has been a great inspiration to scientists and engineers. Materials and robotic systems have been developed over the last 25 years to reproduce the motion and abilities of life forms as best as possible [28], [82]–[88]. Various projects have been able to demonstrate the ability to mimic these natural soft tissue systems, although only to a limited extent in terms of control and simplicity [20], [89], [90].

One common method to develop a multiple degree-of-freedom actuator is to use mechanisms. Recently, robotics has emerged that are driven by hydraulic and pneumatic pressure. Marchese et al. [43] reported a soft-body robotic fish that can swim in three dimensions with its hydraulic actuator, which was driven by a gear pump. Tolley et al. developed a pneumatically powered soft robot with four flexible legs [91]. The robot could move under various conditions of terrain. Inspired by an elephant trunk, an actuator was developed for assistance in object handling [92]. This flexible robot, which was actuated pneumatically, could perform complicated deformations. On the other hand, many robotic systems with motor-driven actuators have been developed. For example, robotic arms with actuation having multiple degrees-of-freedom have been studied for decades; these robotic arms could be driven by cables [93] or directly by motors [94]. Most actuators contain mechanisms that have large size and complex structures. Hence, their application is limited with regard to small-sized robots. Moreover, undesired motor noise could be produced when operating the system.

Major contributions to these studies have been made on smart materials, such as shape memory alloys (SMA), shape memory polymers (SMP), piezoelectric materials, ionic polymer actuators, and other artificial muscle devices and systems [95]–[103]. Another method to achieve complex deformation is to use the shape memory effects of polymers and alloys. SMPs and SMAs can recover their original shapes by means of external stimuli, such as thermal or electrical inputs [17], [104]. Besides shape changing, however, most robotic systems require reciprocating motion, which enables them to propel themselves forward. Most SMPs respond to thermal change. They recover their shape over a relatively long period, and cannot respond instantaneously. This limits SMPs to be applied only for shape change; they cannot be used as

fast dynamic actuators. A recent application example of SMPs involved a crawling robot with an origami structure, developed by Felton et al. [105]. The shape memory composites were utilized only during the folding process. Complex electronics were embedded to achieve the crawling motion, and the overall motion was driven by motors. Shape-memory effects also have been reported in ionic polymer materials, such as Nafion™. Xie presented a highly-tunable method of creating multiple shape-memory effects in an individual Nafion™ sample by fixing different shapes at several temperatures [18]. Rossiter et al. showed that actuators using a Nafion™-based ionic polymer-metal composite (IPMC) have shape-memory effects [33].

Another method involves using electro-mechanical transitions of smart materials, such as piezoelectric actuators or electroactive polymer actuators. Piezoelectric materials have been widely used as actuators on micro-robots, such as swimming and flying robots [95]. Many actuators have been developed using electroactive polymers. In particular, robots have been developed with ionic polymer-metal composites (IPMCs) as actuators and sensors [106]–[112]. For example, Palmre et al. developed a soft bio-inspired fin [113]. Complex deformation can be obtained by integrating IPMC actuators and by selectively actuating. However, most of the actuators perform a bending/oscillating motion near a neutral position. Maintaining a static position other than neutral due to hysteresis and creep in IPMCs²⁴ has been shown to be difficult. To date, no single actuator has been capable of dynamic control of complex twisting and bending deformations, either simultaneously or separately. For example, SMP actuators can exhibit complex deformation by means of electric or thermal inputs, but they cannot achieve multiple-input control simultaneously for independent control of twisting and bending motions [114], [115].

This study introduces a multiple degree-of-freedom soft multiple shape memory ionic polymer-metal composite (MSM-IPMC) actuator. Similar to the structure of IPMC actuators, the MSM-IPMC is composed of two or more electrodes separated by an ion-conductive polymer material (Figs. 3.1a, 3.1b, and 3.1c). Under an applied voltage, the transport of ions and water molecules as well as the associated electrostatic interactions within the polymer result in a bending deformation, which is the electro-mechanical actuation effect (Figs. 3.1d and 3.1e) [116]. The electro-mechanical actuation effect has the capabilities of resilience, inherent softness, and biocompatibility.

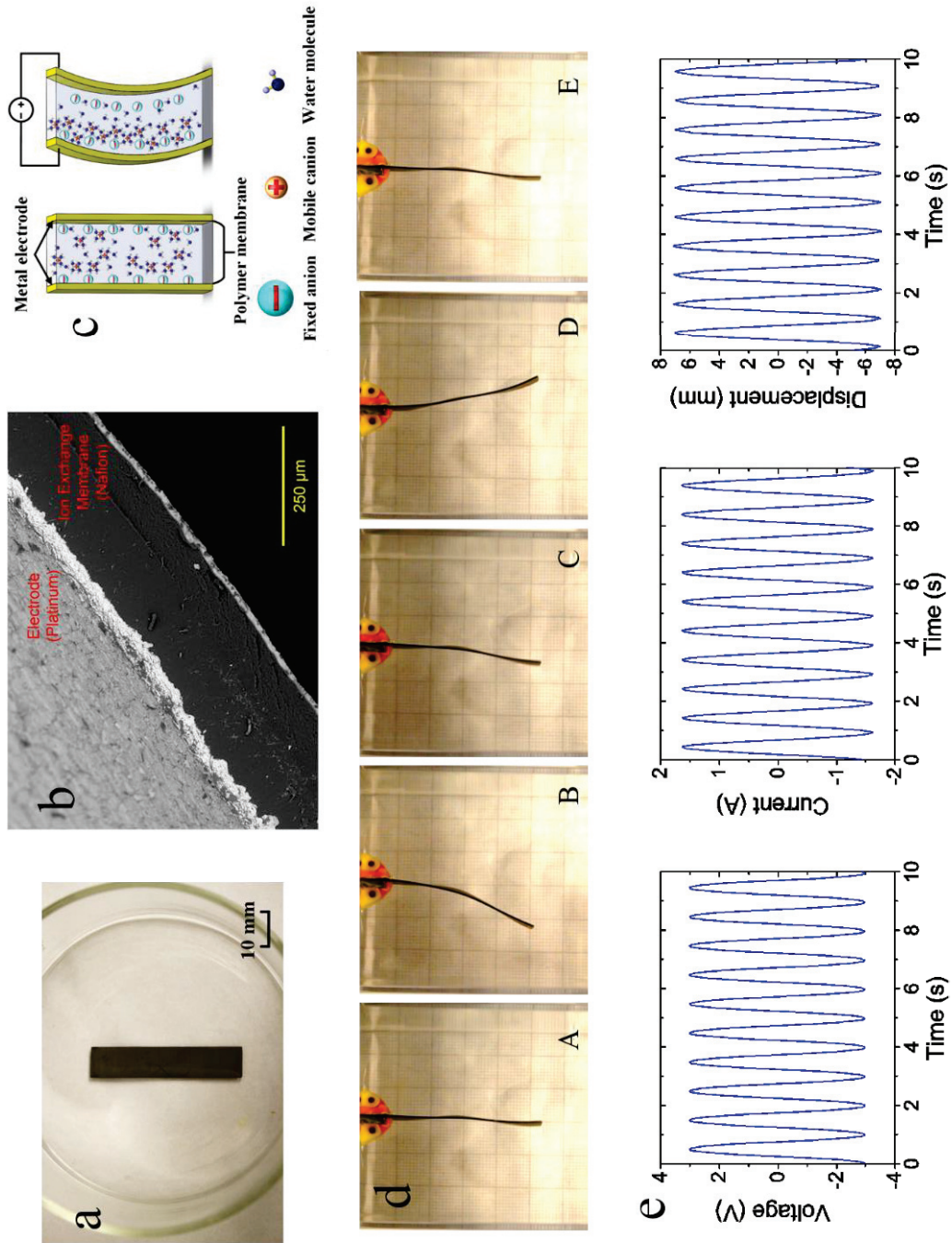


Figure 3.1 Properties of an IPMC made with Nafion™ membrane.

(a) An IPMC sample in the evaporating pan. (b) A scanning electron microscopy (SEM) image of a cross-section of IPMC. The IPMC consists of the electrode on both sides and the polymer membrane between them. (c) An illustration of the IPMC operating principle. Deformation will occur if an electric field is applied across the IPMC, which causes the ions to redistribute along with the water molecule. The size of the IPMC is 50.78 mm in length, 9.82 mm in width and 0.53 mm in thickness. (d) Continuous deformation of IPMC in one cycle under the voltage of 2.6 V amplitude and 1 Hz frequency. (e) Input voltage, output current, and displacement of IPMC versus time under the above voltage input.

Shape memory polymers are materials that can memorize a permanent shape, and then later return to their original shape under specific conditions of external thermal, electrical, or other stimulation [16], [17]. They have the advantages of high elastic deformation, low cost, low density, and potential biocompatibility and biodegradability. Nafion™, perfluorinated alkene with short side-chains terminated by ionic group of sulfonate, was shown to be able to ‘memorize’ multiple shapes under multiple temperature programming, which is the multiple shape-memory effect [18]. The Nafion™ has a broad glass transition temperature, which is from ~ 55 °C to ~ 130 °C. Assuming the original shape of Nafion™ is S0. When the Nafion™ is fixed with an extra load in shape S1, heated to programming temperature T_{p1} for three minutes and cooled to fixing temperature T_{f1} for one minute, the shape S1 is ‘memorized’ within the temperature range from T_{p1} to T_{f1} . Upon reheating the Nafion™ to T_{p1} , the Nafion™ can recover to shape S1. The broad glass transition can be divided into a series of individual glass switching transitions for each programmed shape. Different shapes S1, S2, S3 are heated to programming temperatures T_{p1} , T_{p2} , T_{p3} and cooled to T_{f1} , T_{f2} , T_{f3} respectively, where $T_{p1} > T_{f1} > T_{p2} > T_{f2} > T_{p3} > T_{f3}$. Multiple shapes S1, S2 and S3 are programmed at each individual temperature range $T_{p1} \sim T_{f1}$, $T_{p2} \sim T_{f2}$, $T_{p3} \sim T_{f3}$. When the Nafion™ is reheated from T_{f3} to T_{p1} , multiple shapes recovered at each temperature range through glass transition. The crystalline segments, which

work as physical crosslinks, hold the programmed shapes during each glass transition. This multiple shape memory effect cannot be repeated. The multiple shape memory effect of a Nafion™ fiber is demonstrated in Fig. 3.2. Since it is controlled by the thermal input, the multiple shape memory effect can also be seen as thermo-mechanical actuation effect.

Based on these two effects, which are electro-mechanical and thermo-mechanical actuation effect, the MSM-IPMC can perform deformation with multiple degrees of freedom. Several shapes can be programmed into MSM-IPMC material memory at various temperatures, which enables thermo-mechanical actuation effect. This type of actuator demonstrates high maneuverability by controlling two external inputs – electrical input and thermal input - allowing the complex twisting, bending, and oscillating motions that are frequently observed in nature-made systems.

Through the electro-mechanical actuation effect, the actuator is able to perform high-frequency bending motions under external electrical input. *With the thermo-mechanical actuation effect*, the actuator can obtain stable, complex motion under external thermal inputs. Compared with the electro-mechanical actuation effect, the thermo-mechanical actuation effect occurs over a much longer timescale. The ability to control MSM-IPMC actuators by two external inputs, electrical and thermal, enables these devices to be used to perform highly complex motions, twisting, bending and oscillating simultaneously or separately. The twisting and bending motions are induced thermally and the oscillating motion is induced electrically. The bending motion and oscillating motion take place with the same rotation axis; previously, this could be realized only with existing actuator technologies by using multiple actuators or another complicated robotic system. Moreover, to the best of the authors' knowledge, the MSM-

IPMC actuator presented in this paper is the first solitary actuator capable of multiple-input control and the resulting deformability and maneuverability.

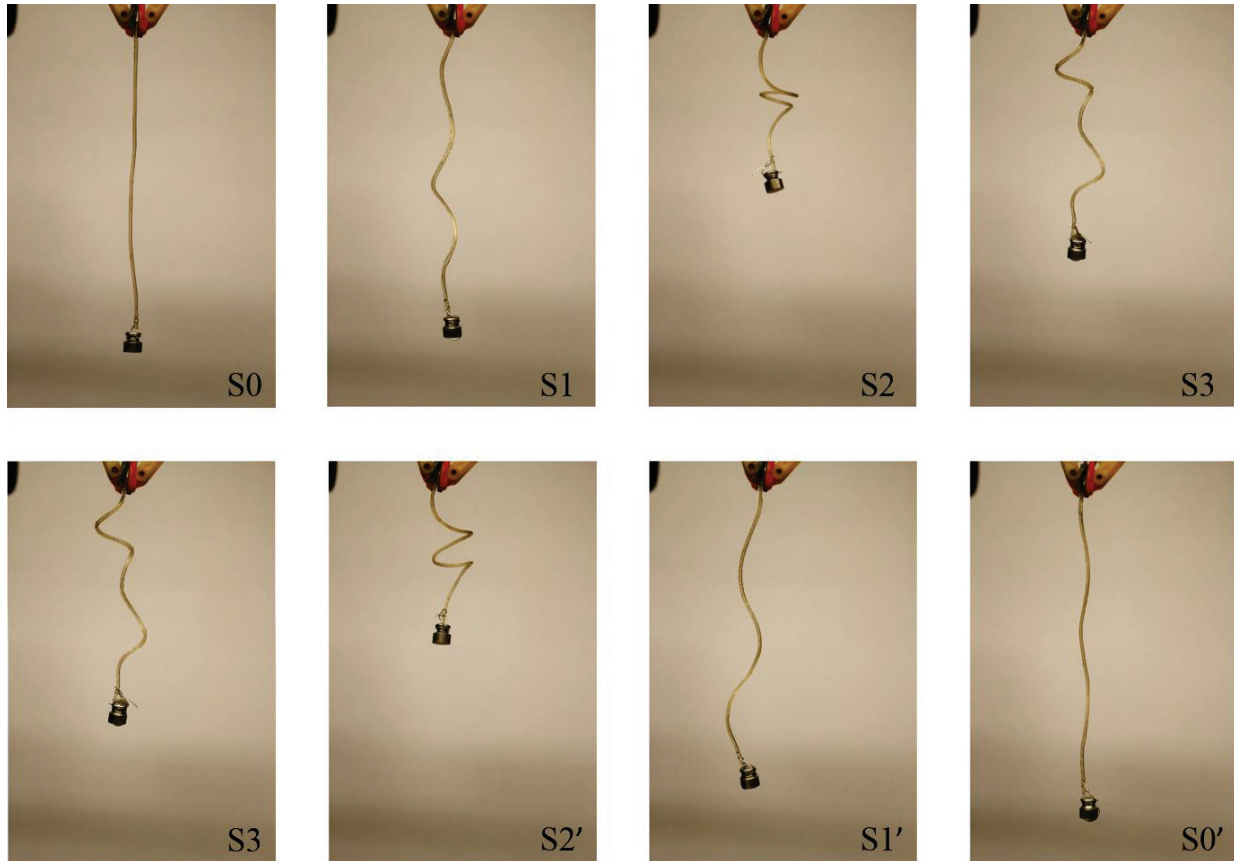


Figure 3.2 Nafion™ fiber demonstrating quadruple shape memory cycles with a 1-g weight on the tip.

Triple shapes of the Nafion™ fiber, 99.87 mm in length and 0.95 mm in diameter, were programmed with loops having different shapes wrapping around a metal rod in the water. The fiber with original shape, S0, was wrapped and programmed at 85°C and fixed at 75°C to achieve the first programmed shape, S1. The second shape, S2, and third shape, S3, was programmed at 70°C, 55°C and fixed at 60°C and 21°C, respectively by wrapping around the rod with different cycles. Then, the Nafion™ fiber was reheated. The Nafion™ fiber recovered to S2', S1', and S0' upon reheating to 55°C, 70°C, and 85°C, respectively.

3.2. Results

3.2.1. Shape programming of MSM-IPMC.

The MSM-IPMC sample is shown in Fig. 3a. The length, width, and thickness of the MSM-IPMC are 51.81 mm, 10.49 mm, and 0.60 mm, respectively. The desired twisted shape of the MSM-IPMC was programmed prior to actuation. The broad glass transition temperature of the Nafion™ is ~ 55 °C to ~ 130 °C. The MSM-IPMC would be programmed and tested in deionized water and the boiling temperature of the water is 100 °C. Thus, the programming temperature of MSM-IPMC would be ~ 55 °C to ~ 100 °C. To program the shapes into the MSM-IPMC, it was wrapped around a metal rod and fixed. By heating to programming temperature T_1 for three minutes and cooling to fixing temperature T_2 for one minute, the shape was ‘memorized’ within the temperature T_1 to T_2 . When the MSM-IPMC was reheated to T_2 , it would recover to the programmed shape through glass transition. Dual shapes were programmed using this process. For distancing the two glass transitions, the programming temperatures were chosen to be 85 °C, 60 °C and the fixing temperatures were chosen to be 70 °C and 22 °C, respectively. To program the first shape, the MSM-IPMC was heated to 85 °C for three minutes and cooled to 70 °C for one minute (Fig. 3.3b) in deionized water. Then, the MSM-IPMC was deformed on the other side further using the same metal rod. To program the second shape, the MSM-IPMC was heated to 60 °C for three minutes and cooled to 22 °C for one minute (Fig. 3.3c) in deionized water.

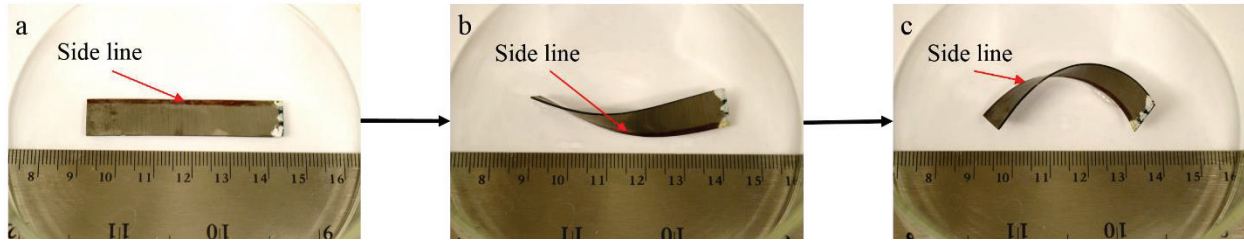


Figure 3.3 Programming of MSM-IPMC.

(a) The original shape of MSM-IPMC. The length, width, and thickness of the MSM-IPMC were 51.81 mm, 10.49 mm, and 0.60 mm, respectively. The tip of the MSM-IPMC was painted white to facilitate image analysis. A side line was painted on the MSM-IPMC to distinguish the deformation. (b) The first shape of the MSM-IPMC was programmed by heating at 85 °C and cooling at 70 °C. The MSM-IPMC was wrapped around a rod during the programming. (c) The second shape of the MSM-IPMC was programmed by heating at 60 °C and cooling at 22 °C.

3.2.2. Deformation analysis of MSM-IPMC.

Figure 3.4 shows the sequential photographs of an MSM-IPMC actuator in deionized water. A sinusoid AC voltage of 3.7 V initial amplitude and 1 Hz frequency was applied to the MSM-IPMC as external electrical input. An immersion heater was used to heat the deionized water as an external thermal input. To cover the programming temperature range, the water was heated from room temperature (22 °C) to 90 °C. As the water temperature increased, the MSM-IPMC gradually recovered to its previously programmed shapes.

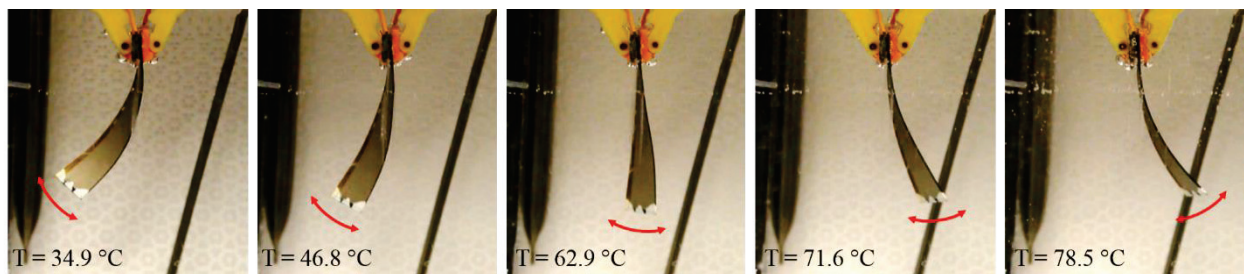


Figure 3.4 A MSM-IPMC actuator with multiple degree-of-freedom deformation.

The sample was under a sinusoid AC voltage of 3.7 V initial amplitude and 1 Hz frequency. The water was heated from 22 °C (room temperature) to 90 °C.

During the experiments, oscillation of the actuator was noticed under the applied voltage. The MSM-IPMC gradually bent from the left side to the right side, as observed from the front view, and twisted in the clockwise direction, as observed from the top view. To measure the 3D deformation of the actuator, two cameras were used for recording, and image analysis was conducted. The tip of the MSM-IPMC was painted white to facilitate image analysis. Three points were tracked at two corners and the middle of the actuator tip. In general, the MSM-IPMC actuator performed twisting, bending, and oscillating motions simultaneously.

Figure 3.5a shows the 3D track of MSM-IPMC in the middle of the tip. It was readily observable that the actuator deformed in a twisting and bending motion, resulting in a spiral motion of the tip. This was because the oscillation motion of the MSM-IPMC was perpendicular to the surface. Since the actuator was twisted and bended, it oscillated in 3D directions along its length, which resulted in the spiral motion of the tip. Figure 3.5b shows the 3D motion of the MSM-IPMC tip position, including the bending and twisting motion.

Based on the results shown in Figure 3.5, the bending motion and twisting motion were analyzed separately. Figure 3.6a shows the corresponding bending displacement of the MSM-IPMC. The bending displacement was obtained by calculating the displacement of the middle tip line point in the orthogonal direction. It can be seen that the MSM-IPMC performed a gradual but large bending motion, which resulted from thermal actuation via the thermo-mechanical actuation. This motion was combined with a higher-frequency, lower-displacement sinusoidal oscillation, which resulted from electro-mechanical actuation. From the thermal actuation aspect, a total bending displacement of 16.6 mm was measured with the temperature increasing from 34.9 °C to 84.3 °C. The time of the total bending is 268.6 s; From the electrical actuation aspect,

the oscillation amplitude is approximately 0.13 mm in the orthogonal direction and the oscillation frequency is 1 Hz.

Along with the bending motion, a twisting motion was performed by the MSM-IPMC. Figure 3.6b shows the twisting deformation of MSM-IPMC. The twisting angle was obtained by calculating the angle difference between the two end lines of the MSM-IPMC. As the temperature increased from 34.9°C to 84.3°C, the MSM-IPMC twisted by 36.6° due to the thermo-mechanical actuation. As the MSM-IPMC twisted, the electro-mechanical actuation effect resulted in an oscillation.

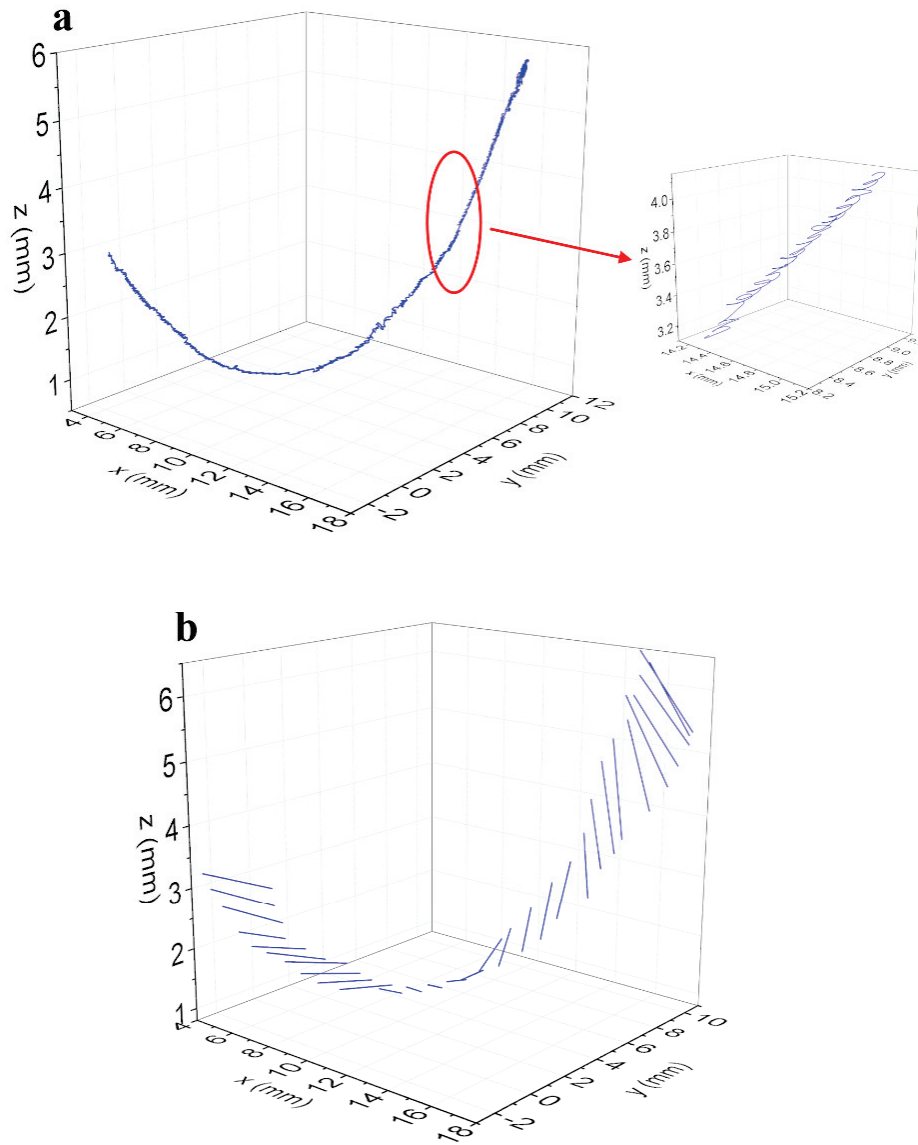


Figure 3.5 MSM-IPMC 3D motion trajectory.

(a) 3D position track of MSM-IPMC actuator. The applied sinusoid AC voltage has 3.7 V initial amplitude and 1 Hz frequency. The measured temperature increased from 34.9°C to 84.3°C. (b) 3D motion of the MSM-IPMC tip line.

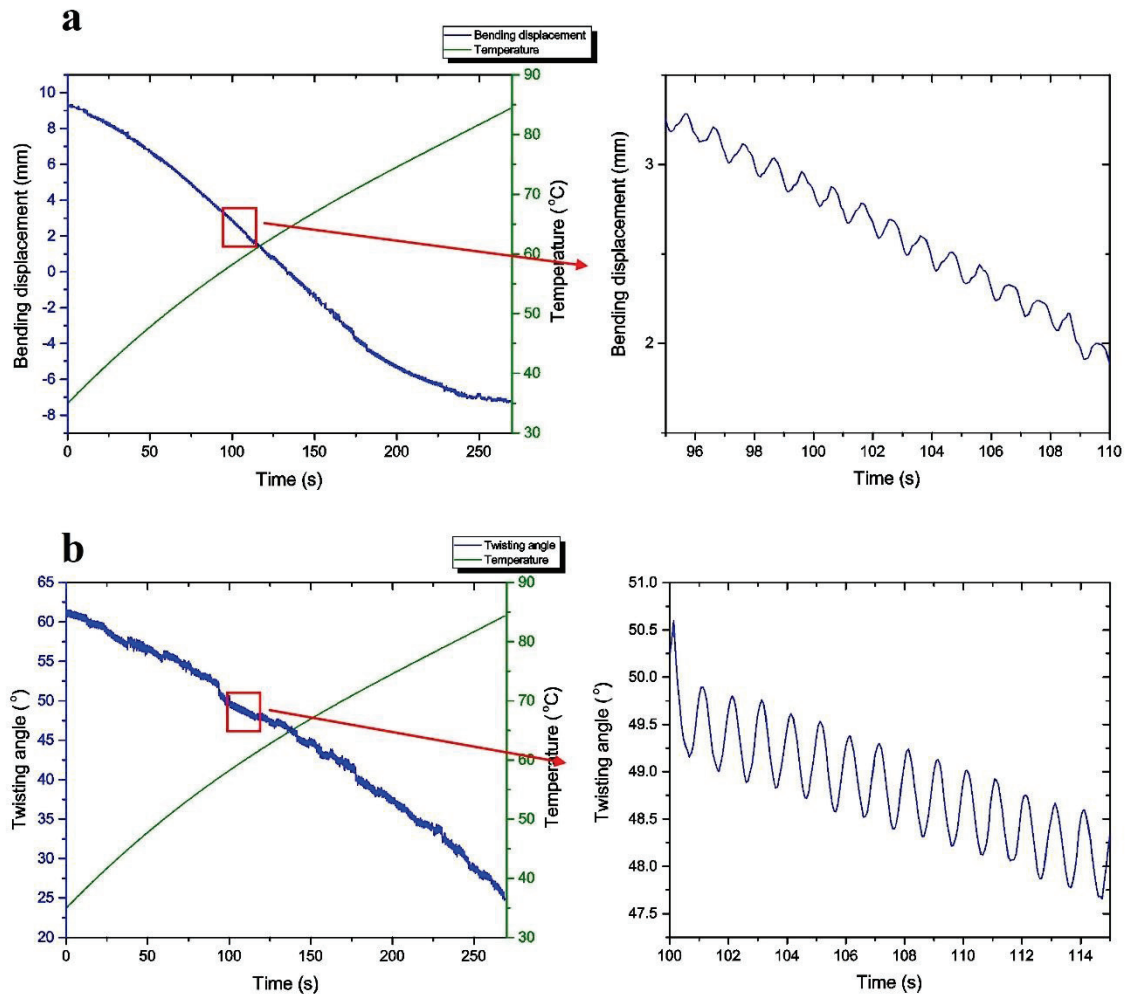


Figure 3.6 Deformation of MSM-IPMC.

(a) Bending displacement and temperature of MSM-IPMC versus time under an external electrical input of 3.7 V initial amplitude and 1 Hz frequency and thermal input from 34.9°C to 84.3°C. (b) Twisting angle and temperature of MSM-IPMC versus time under external electrical and thermal input.

3.2.3. Electrical analysis of MSM-IPMC.

Figure 3.7a and 3.7b show the applied voltage and output current of the MSM-IPMC during the experiments. A sinusoid voltage signal with an amplitude of 3.7 V and frequency of 1 Hz was applied to the MSM-IPMC. The MSM-IPMC was connected in series with a resistor in

the circuit. It is interesting to note that as the temperature increased, the measured voltage response of the MSM-IPMC decreased from 3.7 V amplitude to 3.3 V amplitude. The voltage amplitude decreased by 10.8%. Meanwhile, the current increased from 217 mA amplitude to 374 mA amplitude. The current amplitude increased by 72%. One possible reason is that with the increasing temperature of the MSM-IPMC (see Fig. 3.6), the resistance of the surface electrode decreased and the movement of the ion in the polymer increased. As a result, the total electrical impedance of the MSM-IPMC decreased and the total electrical resistance of the circuit decreased. The current of the circuit increased and the voltage on the MSM-IPMC decreased. Figure 3.7c show the electrical impedance of MSM-IPMC. It can be seen that the electrical impedance shows an overall decrease from 16.3 Ω to 8.7 Ω as the temperature increases. The mechanical impedance change of MSM-IPMC has yet to be studied.

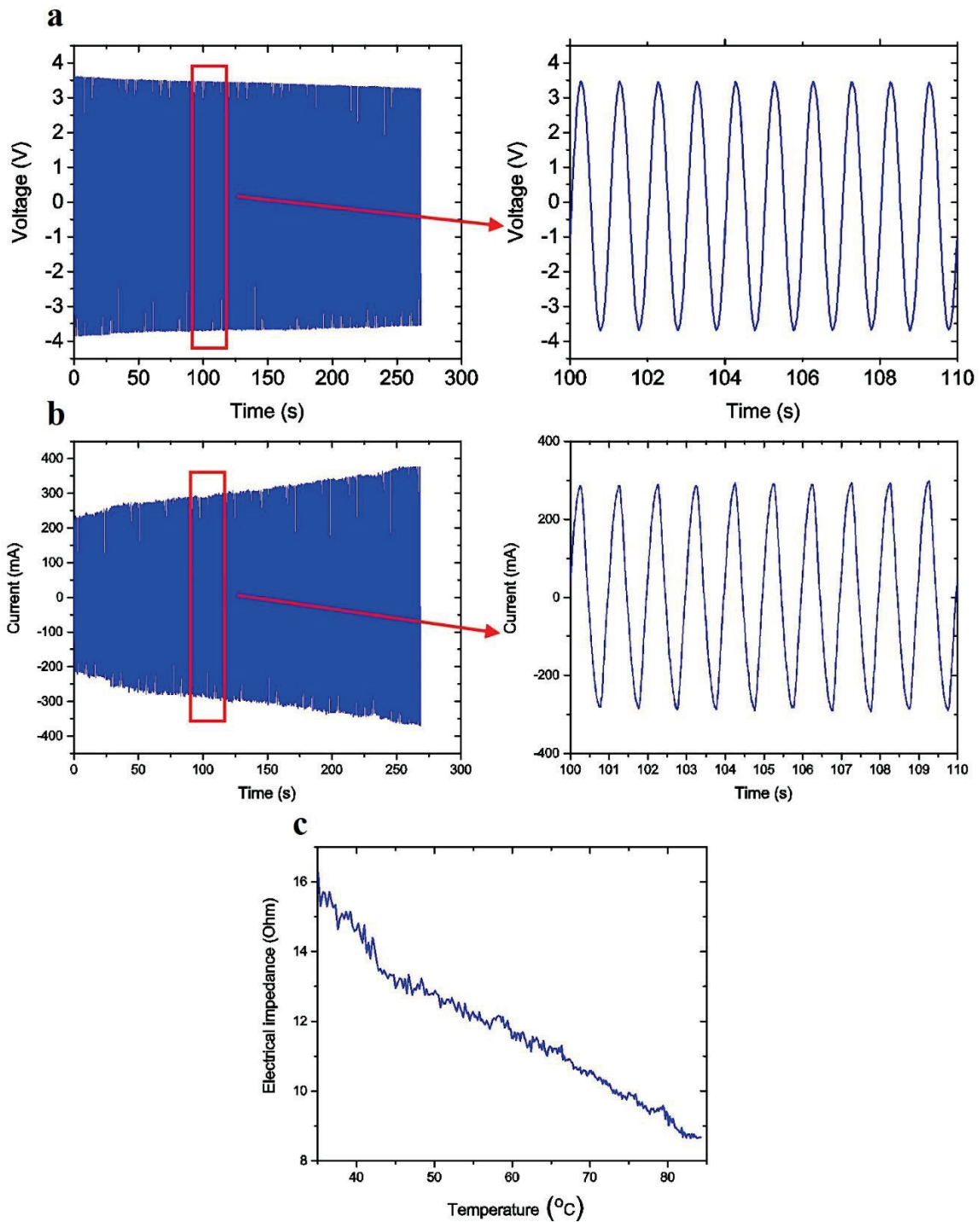


Figure 3.7 Impedance response of MSM-IPMC.

(a) Measured voltage response of MSM-IPMC versus time. The initial amplitude of sinusoid voltage input was 3.7 V and the frequency was 1 Hz. (b) Measured current response of MSM-IPMC versus time. (c) Electrical impedance of MSM-IPMC versus temperature.

In addition, experiments were conducted to obtain the fixity and recovery rates of the MSM-IPMC. The MSM-IPMC was bended by wrapping around a cylinder, namely the fixed shape. The programming process is the same as previous. The first programmed shape S_1 was programmed by heating to 85 °C and cooling to 70 °C. The second programmed shape S_2 was programmed by heating to 60 °C and cooling to 22 °C. The MSM-IPMC recovered from S_2 to S_1 upon reheating above 70 °C. The deformation of the MSM-IPMC was measured through image analysis and the strain was derived based on the deformation. By comparing the strains of fixed shape and programmed shape, the fixity of S_1 and S_2 are obtained as 96.86 % and 80.19 % respectively. Through comparing the strains of programmed shape and recovered shape, the recovery rate of S_1 is obtained as 89.83 %.

3.3. Discussion

This study successfully demonstrates for the first time that electro-mechanical and thermo-mechanical actuation can be separately performed on a single actuator, simultaneously. These multiple inputs, which is electrical and thermal inputs, allows for more complex control than before. The underlying physics of these two actuation properties of MSM-IPMC have been explored. It has a sandwich structure of a thin ion-exchange membrane with noble metal chemically plated on the surface as electrodes. With a voltage applied to the surface, the free cations and water molecules migrate from the anionic binding sites to the surface cathode electrode within the membrane [116]. The electrostatic interaction results in local swelling, which leads to the bending motion, and hence, the electro-mechanical actuation. The thermo-

mechanical actuation of Nafion™ results from the destabilization of electrostatic interactions between ions; meanwhile, the temporary shapes are held by the crystalline segments of Nafion™ as physical crosslinks [16].

Based on Figure 3.7, it was found that temperature had an influence on the electro-mechanical actuation effect of the MSM-IPMC. The resistance of the MSM-IPMC decreased as the temperature increased. This property could be applied on the thermal feedback of the MSM-IPMC. By measuring the input voltage and output current of the MSM-IPMC, the resistance could be derived. Based on the resistance change, the temperature of the MSM-IPMC actuator could be obtained.

The actuator presented above demonstrated complex 3D deformation. The bending, twisting, and oscillating motions of the actuator could be controlled simultaneously or separately by means of thermal-mechanical and electro-mechanical actuations. These two separate actuations are significant properties of the presented actuator. Based on previous work, the Nafion™ has multiple shape-memory properties and can be programmed into multiple shapes [18] and then programmed by thermal or electric inputs [33]. One assumption is that the broad glass transition temperature could be regarded as the consecutive distribution of a series of glass transitions [17]. Within the range of the broad glass transition temperature, ~55°C to ~130°C, the Nafion™ could be programmed with multiple unique shapes, and recovered under different temperatures. By programming the actuator, complex shape change of the actuator could be achieved with thermal control, and the thermo-mechanical actuation could be used for overall structural deformation. Meanwhile, the MSM-IPMC could perform an oscillation motion by applying voltage on the surface electrodes. The actuation amplitude and frequency of the

oscillation could be adjusted by changing the amplitude and frequency of input voltage. Thus, the electro-mechanical actuation of the MSM-IPMC could be utilized for locomotion.

In conclusion, an MSM-IPMC actuator with complex deformation capabilities was developed. The MSM-IPMC could be controlled separately by means of thermal and electrical inputs. It had the advantages of resilience and inherent softness; moreover, the electrical characteristics of the MSM-IPMC changed as the temperature changed. Potentially, it could be applied to medical devices and biomimetic robotics.

One potential application of MSM-IPMC is in underwater biomimetics, which has been studied for many years. The fish fins undergo considerable deformation, which enables the fish to generate propulsive forces and control body position. Robotic flapping foil devices were developed in order to understand the significance of flexible propulsive surfaces for locomotor performance [117]. A biomimetic fin was developed based on the monolithic fabrication of IPMC actuators [15]. Complex deformation modes can be produced. However, most of the devices contain complicated systems. MSM-IPMC can be used as a single actuator that performs similar deformations as does a fish fin. By programming MSM-IPMC to different desired shapes, and by controlling the thermal and electrical inputs, multiple degrees-of-freedom deformation of the actuator can be performed. There are three methods that can possibly be used to heat the actuator. The first method is adding another soft heating film on the surface of MSM-IPMC, such as PCT (Positive Temperature Coefficient) heating element. By controlling the input voltage on the heating film, the heating of the actuator can be controlled. The second method is induction heating. An additional layer of iron oxide nanoparticles will be plated on the surface of the actuator. Localized heating on the actuator can be generated by applying an alternating

electromagnetic field. The third method is heating the water directly. An immersion heater with temperature feedback control will be used to heat and control the water temperature. Another potential application is the vessel catheter. Lei et al. [118] developed a tube-shaped IPMC; however, bending of the tube-shaped IPMC was limited due to the stiffness of the tube. With the MSM-IPMC, new catheters can be fabricated with large deformations of multiple degrees of freedom, a capability that can be utilized in complex vessel networks. A flexible heating wire will be inserted inside the catheter for thermal controlling. A layer of thermal insulation film will be covered on the surface of the catheter to insulate the heat conduction between the body and the catheter.

3.4. Methods

3.4.1. Sample preparation.

MSM-IPMC samples were prepared for the experiments. First, after roughening the surface of the Nafion™ -117 membrane sheet, the membrane was immersed in 3% hydrogen peroxide (H_2O_2) to eliminate organic impurities and in 1 M sulfuric acid (H_2SO_4) to remove the metallic impurities. Second, by immersing in a platinum complex solution ($Pt(NH_3)_4Cl_2 \cdot H_2O$) and then in a sodium borohydride solution ($NaBH_4$), the membrane sheet was plated with the platinum metal (Pt) particles. To lower the surface resistance, the composite sheet was suspended in the Pt complex solution. Hydroxylamine hydrochloride ($H_2NOH \cdot HCl$) and hydrazine ($NH_2NH_2 \cdot H_2O$) were added to the solution periodically. Finally, after the plating process, the sheet was soaked in a solution of lithium chloride for ion exchange. A more detailed procedure is presented by Kim et al. [8].

3.4.2. Experiments.

Figure 3.8 shows the schematic of the experimental setup. The MSM-IPMC was submerged in deionized water of 22°C. One end of the MSM-IPMC was fixed by a clamp. Voltages were applied on the MSM-IPMC through the clamp contacts. The voltages were provided by a signal generator (FG-7002C, EZ Digital Co., Ltd) and amplified by a power amplifier (LVC-608, AE Techron, Inc.). An immersion heater (3656K169, McMaster-Carr) was used for heating the water. A thermal resistor (PRTF-11-2-100-1/8-6-E, Omega®) was used to measure the water temperature. The signals were measured through DAQ (NI SCB-68, National Instruments). The input voltage, current, and temperature were recorded simultaneously, using LabVIEW 8 Software. The MSM-IPMC was reheated from 22°C to 90°C.

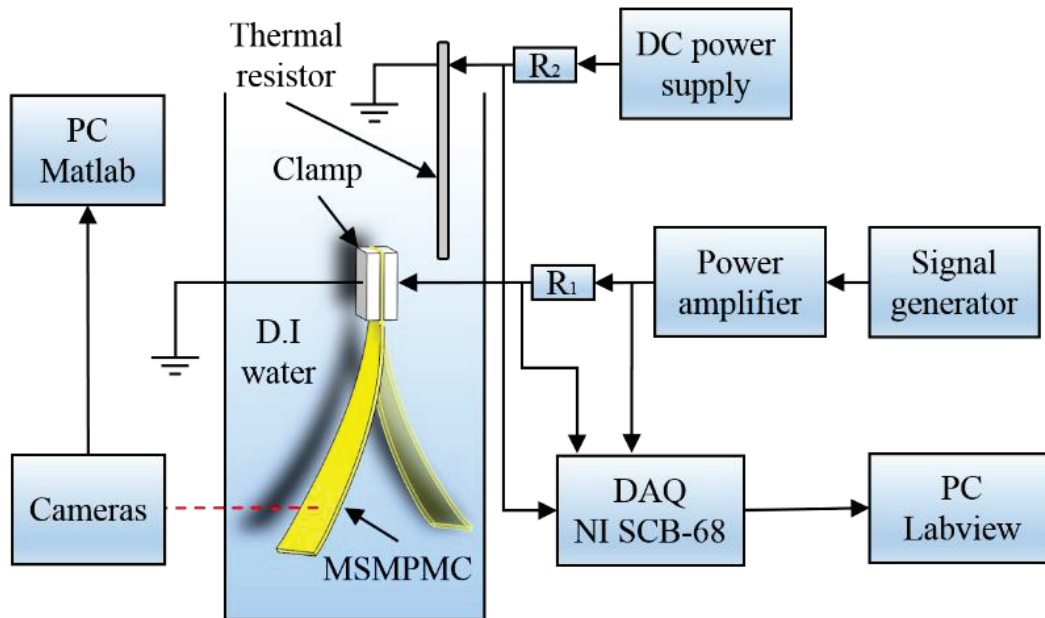


Figure 3.8 Experimental setup. The experimental setup used for measuring thermal and electromechanical responses of the MSM-IPMC actuator.

The radius of the curvature ρ_r of the MSM-IPMC can be denoted as [119]

$$\rho_r \cong \frac{L^2 + \delta^2}{2\delta} \quad (3.1)$$

where L is the length and δ is the tip deformation of the MSM-IPMC. By relating the radius of the curvature ρ_r to strain ε , one can obtain

$$\varepsilon \cong \frac{h}{2\rho_r} \quad (3.2)$$

where h is the thickness of the MSM-IPMC. The fixity can be obtained by comparing the strains of fixed shape ε_f and programmed shape ε_p

$$R_f = 100\% \times \frac{\varepsilon_p}{\varepsilon_f}. \quad (3.3)$$

The recovery rate can be obtained by comparing the strains of programmed shape ε_p and recovered shape ε_r

$$R_r = 100\% \times \frac{\varepsilon_r}{\varepsilon_p}. \quad (3.4)$$

3.4.3. Image analysis.

To measure the 3D deformation of the MSM-IPMC, image analysis was used. Two cameras were set at different positions and recorded the deformation of MSM-IPMC during the experiments. Using an open source MATLAB[®] program developed by Hedrick [120], the videos from the two cameras were analyzed to measure the twisting angle and the bending deformation of the MSM-IPMC. Prior to imaging actuator deformation, the image analysis program was calibrated to a set coordinate frame. This was done by creating a coordinate frame specifically

for the volume of space that the tank of water occupied. The videos were analyzed in the program along with the calibration coefficients file. Three points at the free end tip were tracked in the videos to determine the deformation and twist of the MSM-IPMC.

To calculate the bending deformation of the MSM-IPMC, the coordinates of the two corners X_u, Y_u of the MSM-IPMC fixed end were measured as (x_{u1}, x_{u2}, x_{u3}) and (y_{u1}, y_{u2}, y_{u3}) . Another point Z_u , which was in the same horizontal platform of X_u, Y_u and not on the line $X_u Y_u$, was measured; the coordinate was (z_{u1}, z_{u2}, z_{u3}) . Assuming the projective point of Z_u on line $X_u Y_u$ is A_u , A_u 's coordinate, (a_{u1}, a_{u2}, a_{u3}) can be obtained by solving the following equations

$$(a_{u1} - x_{u1})(a_{u1} - z_{u1}) + (a_{u2} - x_{u2})(a_{u2} - z_{u2}) + (a_{u3} - x_{u3})(a_{u3} - z_{u3}) = 0 \quad (3.5)$$

$$(a_{u1} - x_{u1})/(y_{u1} - x_{u1}) - (a_{u2} - x_{u2})/(y_{u2} - x_{u2}) = 0 \quad (3.6)$$

$$(a_{u1} - x_{u1})/(y_{u1} - x_{u1}) - (a_{u3} - x_{u3})/(y_{u3} - x_{u3}) = 0 \quad (3.7)$$

Line $X_u Y_u$ and line $Z_u A_u$ were orthogonal to each other, and line $Z_u A_u$ was in the thickness direction of the MSM-IPMC in a neutral position. By calculating the projective point of the MSM-IPMC tip point on line $Z_u A_u$, the bending displacement of the MSM-IPMC could be obtained. Assuming the coordinate of tip point Z_d was (z_{d1}, z_{d2}, z_{d3}) , the coordinate projective point A_d on line $Z_u A_u$ could be obtained by using the following equations

$$(a_{d1} - a_{u1})(a_{d1} - z_{d1}) + (a_{d2} - a_{u2})(a_{d2} - z_{d2}) + (a_{d3} - a_{u3})(a_{d3} - z_{d3}) = 0 \quad (3.8)$$

$$(a_{d1} - a_{u1})/(z_{u1} - a_{u1}) - (a_{d2} - a_{u2})/(z_{u2} - a_{u2}) = 0 \quad (3.9)$$

$$(a_{d1} - a_{u1})/(z_{u1} - a_{u1}) - (a_{d3} - a_{u3})/(z_{u3} - a_{u3}) = 0. \quad (3.10)$$

The coordinates of the two corners X_u, Y_u of the tip were measured as (x_{d1}, x_{d2}, x_{d3}) and

(y_{d1}, y_{d2}, y_{d3}) . The twisting angle θ could be obtained by calculating the angle difference

between vector $X_u Y_u$ and vector $X_d Y_d$

$$\theta = \cos^{-1} \frac{(x_{d1}x_{u1} + x_{d2}x_{u2} + x_{d3}x_{u3})}{\sqrt{x_{d1}^2 + x_{d2}^2 + x_{d3}^2} \sqrt{x_{u1}^2 + x_{u2}^2 + x_{u3}^2}}. \quad (3.11)$$

Chapter 4. Theoretical and experimental investigation of shape memory properties of ionic polymer-metal composite

In this chapter, a research paper published in Smart Materials and Structures is included. The authors are Qi Shen, Viljar Palmre, Kwang J. Kim, and Il-Kwon Oh in order of appearance on the article. In this article we laid out a theoretical framework in terms of finite element based free-energy density to describe the shape memory effect of the IPMC. This chapter was reprinted from Smart Materials and Structures, Shen, Qi, Viljar Palmre, Kwang J. Kim, and Il-Kwon Oh. "Theoretical and experimental investigation of the shape memory properties of an ionic polymer–metal composite." Smart Materials and Structures 26, no. 4 (2017): 045020, with the permission of IOP Publishing.

KJK conceived the idea and designed the project. The primary contributions to analytical physics based modeling and model coupling are from QS. The experimental work was done by QS and VP. The data analysis, simulations, conclusions, and discussion were a combined effort from the whole research team.

4.1.1. Introduction

The ionic polymer-metal composite (IPMC) is one kind of electroactive polymers [40], [46], [109]. It is composed of an ionic polymer membrane with two layers of electrodes chemically plated on both sides [4], [25], [28], [29], [48], [121]. Its most significant characteristics are the electro-mechanical and mechano-electrical transactions. The free cations will begin to migrate inside the polymer induced by an applied electric field. The ions distributions will cause the IPMC to generate a large bending deformation. Meanwhile, the mobile cations will distribute if the IPMC has a mechanical deformation. As a result, a detectable

electrical signal can be produced at both electrodes. With the capabilities of resilience, inherent softness and biocompatibility, the IPMC has a potential on underwater actuator/sensor.

Applications on biomimetic robotics, biomedical devices and energy harvesters have been demonstrated [11], [13], [14], [21], [49], [122]–[124], [9]. Shape memory polymers are materials that can memorize a permanent shape and then later return to their original shape under specific conditions of external thermal, electrical or other stimulations [125]–[127]. They have the advantages of high elastic deformation, low cost, low density and potential biocompatibility and biodegradability. Their ability to remember multiple shapes has attracted significant attention from scientists and engineers for the application of actuators, sensors and smart devices [128].

The shape memory properties of IPMC has recently been studied. Xie reported that annealed dry Nafion can be programmed to memorize four different shapes [18]. The permanent shapes were deformed at different temperatures and fixed at lower temperatures. By reheating the Nafion subsequently, the programmed shapes were obtained respectively. With the broad glass transition range, the Nafion can be potentially programmed at plenty of unique shapes, which can be recovered at different temperatures respectively. Rossiter et al. presented the shape memory properties of Nafion-based IPMC [33]. The IPMC was programmed at the deformation induced by either external force or by electrical actuation. Slow decay was also observed along with the shape memory effect. However, to date, while experimental investigations on the shape memory properties of Nafion-based IPMC have been done, few work have been done concerning the theoretical investigation of the shape memory effect of the IPMC. As a result, a poor understanding exists on the physics of the shape memory properties of IPMC. A faithful model is desirable to explain the thermo-mechanical transaction phenomenon of IPMC.

In this paper, a demonstration of the shape memory effect of Nafion fiber was firstly developed. Multi-shape programming of the Nafion fiber was conducted and the Nafion fiber was shown to be able to achieve a series of complex shapes. Secondly, a physics-based model of the IPMC was presented. The finite element approach was used to model the mechanical portion of the IPMC. The free energy density theory was used to analyze the shape memory properties of the IPMC. Finally, IPMC strip samples were prepared. Experiments were conducted to test the IPMC strip. Simulation of the model was performed and the results were compared with the experimental data.

4.2. Results

4.2.1. Multiple shape memory properties of cylindrical Nafion

Xie has reported the quadruple shape memory properties of Nafion strip [18]. Compared with the strip, the Nafion cylinder with two dimensions can achieve more complex locomotion. In the current paper, we presented the multiple shape memory properties of Nafion cylinder. Nafion pellets were heated to above fusion temperature. By extruding the molten Nafion through a brass extruder dye, the cylinder shape of the Nafion was obtained. A Nafion cylinder with the length of 99.87 mm and diameter of 0.95 mm was fabricated and used for the test. The Nafion cylinder was wrapped around a metal rod and fixed. Triple shapes were programmed with different loops of the Nafion wrapping around the rod in an oven. The cylinder with original shape S0 was wrapped and programmed at 130°C and fixed at 100°C to achieve the first programmed shape S1. The second shape S2 was programmed at 100°C and fixed at 70°C. By programming the third shape S3 at 100°C and fixed at 20°C, the triple shape programming of the Nafion cylinder was completed.

Then the Nafion cylinder was reheated. The Nafion cylinder recovered to S2', S1' and S0' upon reheating to 70°C, 100°C and 130°C respectively. Figure 4.1 shows the Nafion cylinder demonstrating quadruple shape memory cycles. Figure 4.2 shows the shape memory cycle of the Nafion cylinder in accordance with Figure 4.1. The spiral of the cylindrical Nafion was programmed to increase during the programming period and decreased as the reheating temperature increased during the recovering period. Figure 4.3 shows the recovering ratio of Nafion cylinder at different programming temperatures. It can be seen that with the programming temperature increasing, the recovering ratio decreases. Rossiter presented the spiral deformation of the IPMC strip in the shape memory cycle [33]. The Nafion-based IPMC shows to have a thermo-mechanical shape memory effects but the recovery is not complete. The reasons may be as follows: 1) the IPMC in [33] is based on the thin Nafion membrane. Comparing with the cylinder shape of current paper, the strip is relatively difficult to recover in a spiral deformation. 2) The cylinder in the current study was programmed at the temperature of 130°C, 100°C, 70°C respectively in the dehydrated status, which is higher than the programming temperature of 60°C in the hydrated status for the IPMC in [33]. 3) Electrodes were plated on the surface of the IPMC in [33], which will have some plastic effects on the deformation of the strip.

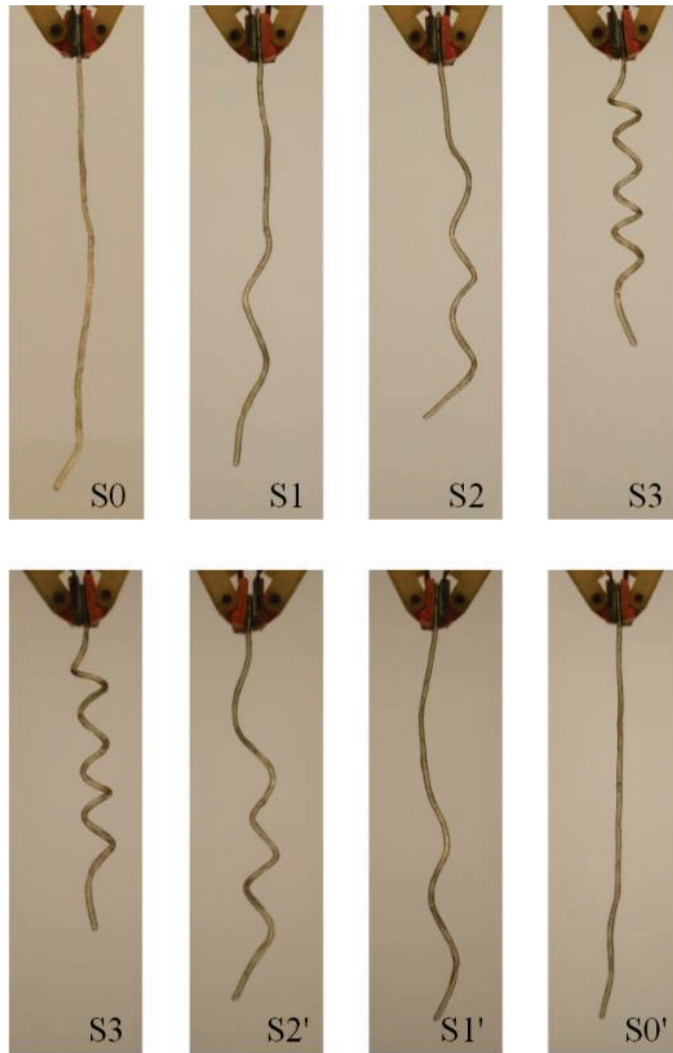


Figure 4.1 Multiple shape memory properties of Nafion cylinder.

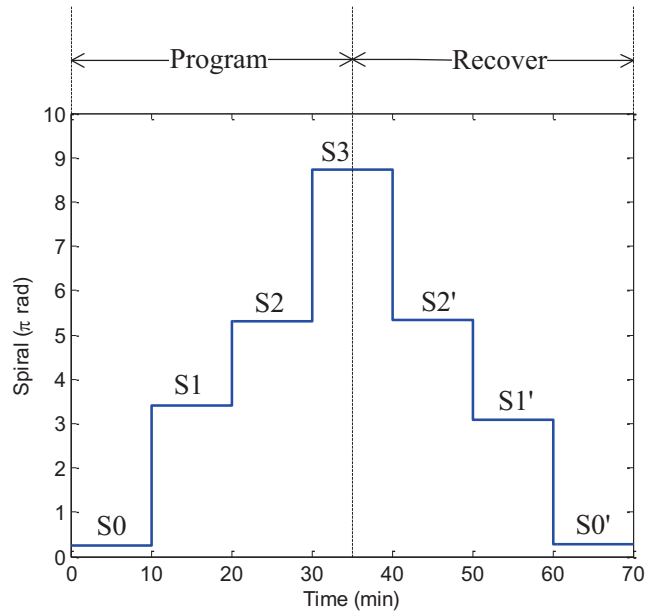


Figure 4.2 Shape memory cycle of Nafion cylinder.

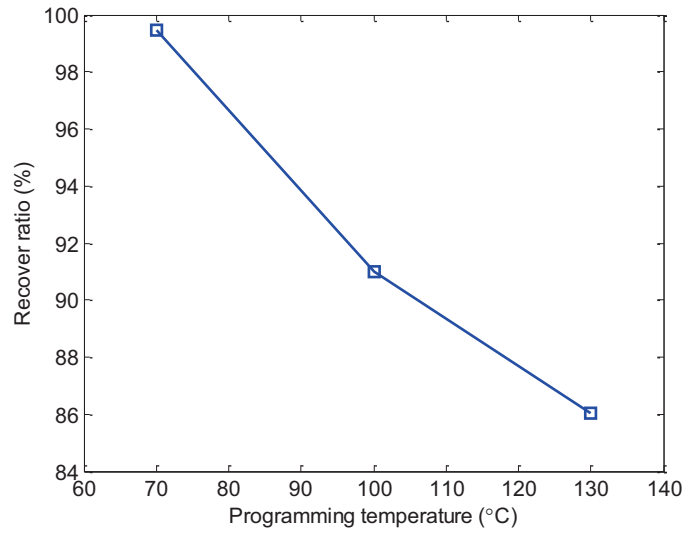


Figure 4.3 Recovering ratio of Nafion cylinder at different programming temperatures.

4.2.2. Modeling of the IPMC

The model of the IPMC is presented. The dynamics of the IPMC strip is described based on the finite element method. The IPMC strip is assumed to satisfy the following restrictions: 1) the IPMC is divided by a series of elements along the direction of thickness, as shown in Figure 4.4. Each element was analyzed and modeled individually. 2) The strain along the length direction λ_l is dominate compared with the strains λ_w, λ_h in the width and thickness directions respectively, and $\lambda_w = \lambda_h$. The strain λ_l of each element is also the main reason that causes the bending of the IPMC strip. 3) The length of the midline of the strip is constant. Thus, as the strip bends, the elements on the inner side are compressed and the elements on the outer side are stretched. The size of original IPMC strip element is L, W, dH . In the current study, we only consider the single shape memory effect. The IPMC was programmed at temperature T_1 and cooled in room temperature water. When the IPMC emerged in the water at temperature T , which is above the programming temperature $T > T_1$, the high-temperature water molecule was absorbed into the Nafion, and the IPMC strip recovered to its original shape. As a result, the size of the element changes from L, W, dH to l, w, dh . The strain along the z, y, x direction can be expressed as

$$\lambda_l = \frac{l}{L}, \lambda_w = \frac{w}{W}, \lambda_h = \frac{dh}{dH}. \quad (4.1)$$

By relating the length of the element to the deformation of the strip, the length can be rewritten as

$$l = (r - t) \frac{\omega(z)}{l} \quad (4.2)$$

where t is the position of the element in the x direction, $\omega(z)$ is the deformation of the element, r is the radius of the curved IPMC midline and is expressed as

$$r = \frac{l}{\gamma} \quad (4.3)$$

where γ is the angle of the curved beam and is denoted as

$$\tan \gamma = \frac{\omega(z)}{l}. \quad (4.4)$$

The nominal stress on the z, y, x direction is denoted as

$$S_l = \frac{F_l}{wdh} = \sigma_l \lambda_w \lambda_h, \quad S_w = \frac{F_w}{ldh} = \sigma_w \lambda_l \lambda_h, \quad S_h = \frac{F_h}{lw} = \sigma_h \lambda_l \lambda_w \quad (4.5)$$

where $\sigma_l, \sigma_w, \sigma_h$ are the actual stress and F_l, F_w, F_h are the nominal force acting on the z, y, x directions. Based on (4.5), one can obtain [129], [130]

$$\lambda_l \lambda_w \lambda_h = 1 + \nu C \quad (4.6)$$

where ν is the volume per water molecule, and C is the nominal concentration of the solvent in the polymer matrix. Gibbs first developed the theory of free-energy density for describing the behavior of swelling gel [131]. Flory presented the free-energy function for polymeric gels [132]. The Flory theory was later extended to polyelectrolyte gels [133]–[135]. The free energy density E of the element can be expressed as [132]

$$E = E_s + E_m + E_p + E_{ion} \quad (4.7)$$

where E_s is the stretching free-energy, E_m is the mix free-energy, E_p is the polarizing free-energy, and E_{ion} is the ions transporting free-energy. Since no ions in the water move inside the matrix of

the polymer, the mix free-energy is $E_{ion} = 0$. Assuming the dielectric constants of the nonpolar polymer and nonpolar water are equivalent, the free energy of polarizing the polymer is $W_p = 0$.

Based on Flory's theory, (4.7) can be rewritten as [132]

$$E = \frac{1}{2} NkT(\lambda_l^2 + \lambda_w^2 + \lambda_h^2 - 3 - 2 \log \lambda_l \lambda_w \lambda_h) - \frac{kT}{v} \left[vC \log \left(1 + \frac{1}{vC} \right) + \frac{\chi}{1 + vC} \right] \quad (4.8)$$

where N is the number of polymer chains divided by the volume of the polymer element, $k = 1.38 \times 10^{-23} J / K$ is the Boltzmann constant, T is the absolute temperature, and χ is the enthalpy constant during the mixture of the polymer matrix and the solvent. The differentiation of (8) can be written as [130]

$$\frac{\partial E}{\partial \lambda_l} = \frac{kT}{v} \left(Nv \left(\lambda_l \left(1 + \frac{2}{D^2} \right) - \frac{3}{\lambda_l} \right) \right) + \left(\frac{3\lambda_l^2}{D^2} \log \left(1 - \frac{D^2}{\lambda_l^3} \right) + \frac{3}{\lambda_l} + \frac{3\chi D^2}{\lambda_l^4} \right) \quad (4.9)$$

where D is the ratio between the strain in the z direction and the strain in the x and y direction respectively, and is expressed as

$$D = \frac{\lambda_l}{\lambda_w} = \frac{\lambda_l}{\lambda_h} \geq 1. \quad (4.10)$$

After the deformation of the element in the water, the mixture system free energy density of the polymer and the water is expressed as

$$G = E(\lambda_l, \lambda_w, \lambda_h) l w d h - F_l(l - L) - F_w(w - W) - F_h(dh - dH). \quad (4.11)$$

The free energy combines the enthalpy and entropy. The mixture system tends to be stable as the polymer and the solvent are mixed. When the whole system reaches the steady status, a key assumption is that the system free energy achieves the minimum. The differentiation of the free energy G reaches the minimum. With small variation, the strain $\lambda_l, \lambda_w, \lambda_h$ can be expanded to $\lambda_l + \delta\lambda_l, \lambda_w + \delta\lambda_w, \lambda_h + \delta\lambda_h$. The mixture system free energy density is rewritten as [130]

$$\begin{aligned} \frac{\partial G}{lwdh} = & \left[\frac{\partial E}{\partial \lambda_l} - S_l \right] \delta\lambda_l + \left[\frac{\partial E}{\partial \lambda_w} - S_w \right] \delta\lambda_w + \left[\frac{\partial E}{\partial \lambda_h} - S_h \right] \delta\lambda_h + \frac{\partial^2 E}{\partial \lambda_l^2} \partial \lambda_l^2 + \frac{\partial^2 E}{\partial \lambda_w^2} \partial \lambda_w^2 + \frac{\partial^2 E}{\partial \lambda_h^2} \partial \lambda_h^2 \\ & + \frac{\partial^2 E}{\partial \lambda_l \partial \lambda_w} \partial \lambda_l \partial \lambda_w + \frac{\partial^2 E}{\partial \lambda_w \partial \lambda_h} \partial \lambda_w \partial \lambda_h + \frac{\partial^2 E}{\partial \lambda_l \partial \lambda_h} \partial \lambda_l \partial \lambda_h \end{aligned} \quad (4.12)$$

To achieve the minimum of (4.12), the first-order differential functions of (4.12) are assigned zero. One can obtain

$$S_l = \frac{\partial E}{\partial \lambda_l}, \quad S_w = \frac{\partial E}{\partial \lambda_w}, \quad S_h = \frac{\partial E}{\partial \lambda_h}. \quad (4.13)$$

Through integrating the length direction stress of the element, the total length direction stress on the IPMC strip can be expressed as

$$\sigma = \int_{-h}^h \sigma_l dt = \int_{-h}^h \frac{S_l}{\lambda_w \lambda_h} dt. \quad (4.14)$$

By relating the bending moment on the IPMC strip to the induced stress, one can obtain

$$\sigma = \frac{Mh}{I} \quad (4.15)$$

where I is the moment of inertia of the strip and $I = 2/3 wh^3$. Based on the linear beam theory, the relation between the displacement ω of the strip and the bending moment M can be denoted as [119]

$$\frac{\partial^2 \omega(z)}{\partial z^2} = \frac{M}{YI} \quad (4.16)$$

where Y is the Young's Modulus. By combining (4.14), (4.15) and (4.16), an ordinary differential equation (ODE) of $\omega(z)$ is obtained. The boundary conditions of the ODE are $\omega(0) = 0$ and $\partial\omega(0)/\partial z = 0$. By solving the ODE, the deformation $\omega(z)$ of IPMC can be obtained. The MATLAB was used to solve for $\omega(z)$.

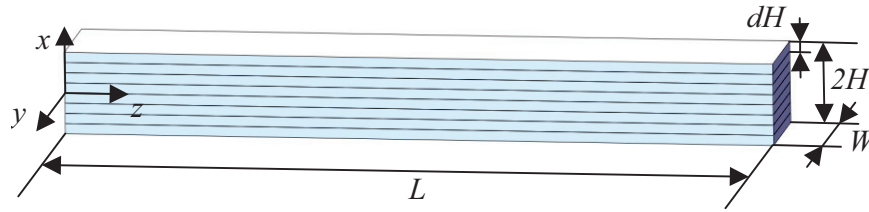


Figure 4.4 Schematic illustration of IPMC beam.

4.2.3. Experimental verification

Experiments were conducted to study the shape memory effect of the IPMC. Three IPMC samples were utilized for the experiments. The dimensions were shown in Table 4.1. The definition of L , W and $2h$ were shown in Figure 4.4. The sample was curved in a fixture and held in place during the programming period. The first step was to immerse the IPMC strip in a hot water bath with the programming temperature T_p ranging from 50°C to 70°C. Then it was cooled in room temperature water at the fixing temperature T_f of 20°C. Finally the fixture was removed

and the IPMC sample at the curved shape was fixed. A back-relaxation of the IPMC sample was noticed after the fixture was removed and the back-relaxation deformation was different at different programming temperatures. Figure 4.5 shows the experimental set up for the shape memory study. The sample was clamped vertically at one end and immersed in a water tank at different temperatures T_i from 20°C to 80°C. The tank can be filled with hot water and cold water to the desired temperature. A thermometer was used to measure the temperature of the water during the experiments. The tip displacement of the sample was measured with the grid paper attached to the water tank. The IPMC was measured every 10 minutes after the water was reheated to the next temperature. The experiments were repeated three times.

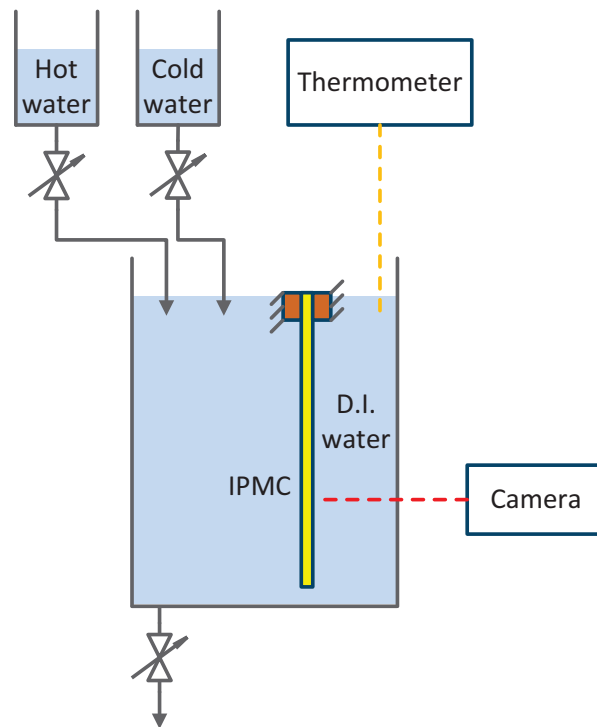


Figure 4.5 Experimental set up for the shape memory properties.

Table 4.1 Dimensions of the IPMC samples.

Item	L (mm)	W (mm)	$2h$ (mm)
IPMC 1	51.07	9.94	0.57
IPMC 2	37.05	9.94	0.57
IPMC 3	22.16	9.94	0.57

Figure 4.6 shows the deformation of IPMC strip at different temperatures under the programming temperature T_p of 60°C. The thermo-mechanical shape memory effect was presented. It can be seen that with the reheating temperature increasing, the programmed IPMC gradually relaxed back to its original shape. Shahinpoor presented the radius of the curvature ρ_r of IPMC beam as [78]

$$\rho_r \cong \frac{l^2 + \omega^2}{2\omega}. \quad (4.17)$$

The radius of the curvature ρ_r is in turn related to the maximum tensile (positive) or compressive (negative) strains, which can be expressed as

$$\varepsilon \cong \frac{h}{\rho_r}. \quad (4.18)$$

The shape recovery ratio of the IPMC sample can be expressed as

$$r_s \cong \frac{\varepsilon_t - \varepsilon_p}{\varepsilon_r - \varepsilon_p} \times 100\% \quad (4.19)$$

where ε_t is the strain under current temperature, ε_p is the strain at the fixing temperature of 20°C and ε_r is the strain at the final reheat temperature of 80°C. Similar definitions were presented in [18], [136].

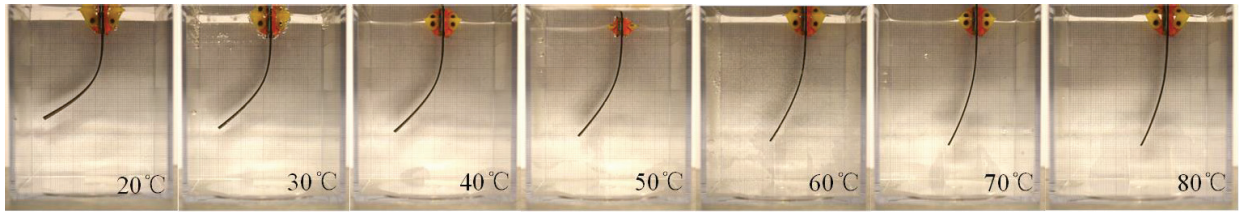
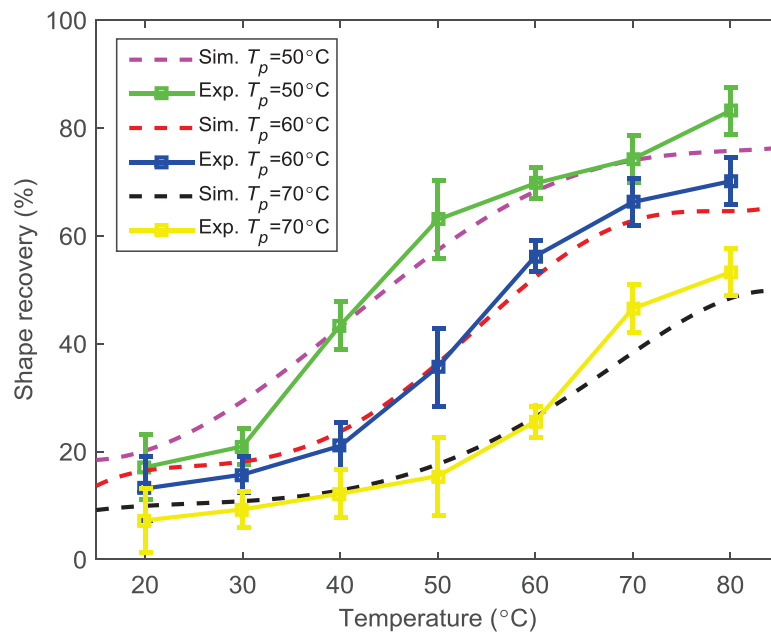


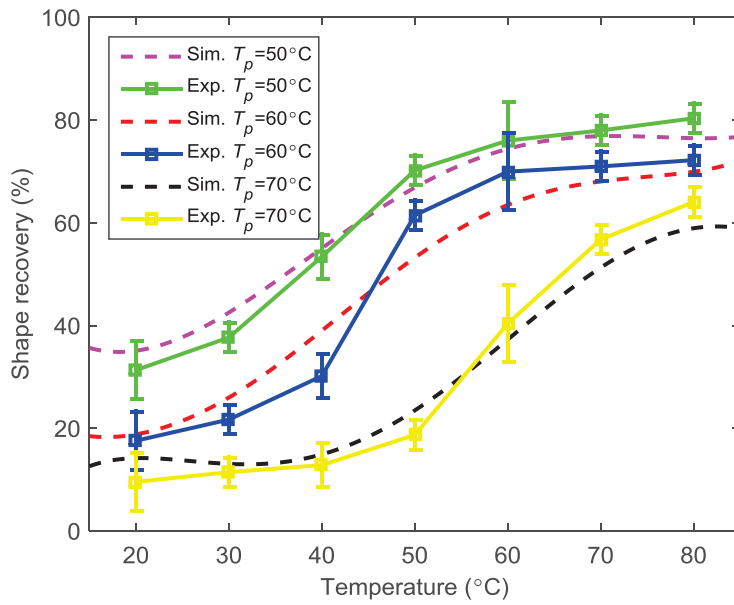
Figure 4.6 Thermo-mechanically shape of IPMC at different temperatures.

Figure 4.7 shows the comparison of the experimental results and simulation results of shape recovery of different IPMC samples. The temperature varies from 20 °C to 80 °C. It is found that the model can well describe the experimental data. Based on Figure 4.7, it can be seen that as the temperature constantly increases, initially the shape recovery increases gradually and then it rises rapidly. Finally, the sample slowly recovers to its original shape. The shape recovery decreases as the programming temperature increases, which has a good agreement with Figure 4.3. It was also noted that the reheat temperature of glass transition is lower than the programming temperature. Compared with the shape recovery ratio of Nafion cylinder shown in Figure 4.3, it can be seen that the shape recovery ratio of the IPMC strip is generally lower than that of the Nafion cylinder. One explanation is that the plastic deformation of the metal electrodes plated on the surface of the IPMC strip during the programming phase relatively holds the IPMC from recovering.

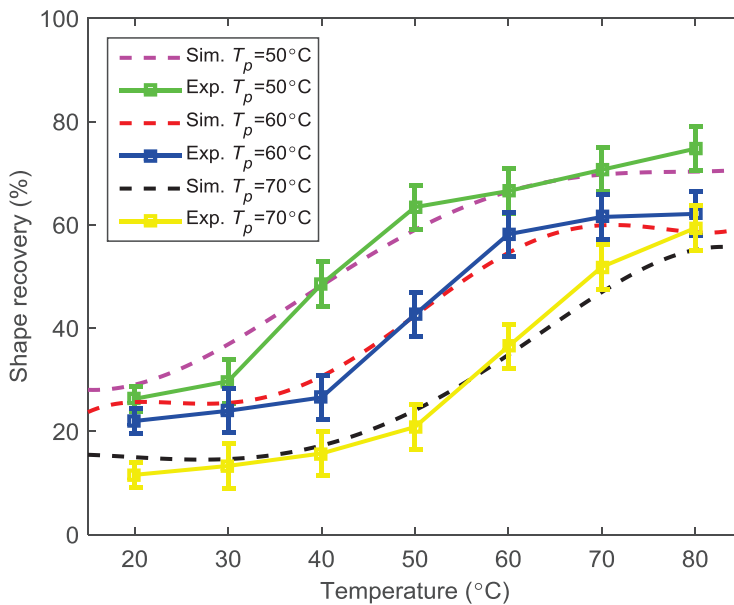
Figure 4.8 shows the back-relaxation deformation of the IPMC samples at different programming temperatures. When the fixture was removed from the IPMC sample, back-relaxation occurred and there is the difference between the desired shape with the fixture and actually programmed shape without the fixture. It was found that with the programming temperature increasing, the IPMC samples has a decreasing back-relaxation. Considering the results of Figure 4.6, it is indicated that by increasing the programming temperature, the fixed shape of the IPMC is more close to the desired shape, and less close to its original shape when the IPMC recovered.



(a)



(b)



(c)

Figure 4.7 Comparison of the simulation and experimental results of the IPMC shape recovery at different programming temperatures: (a) IPMC 1; (b) IPMC 2; (c) IPMC 3.

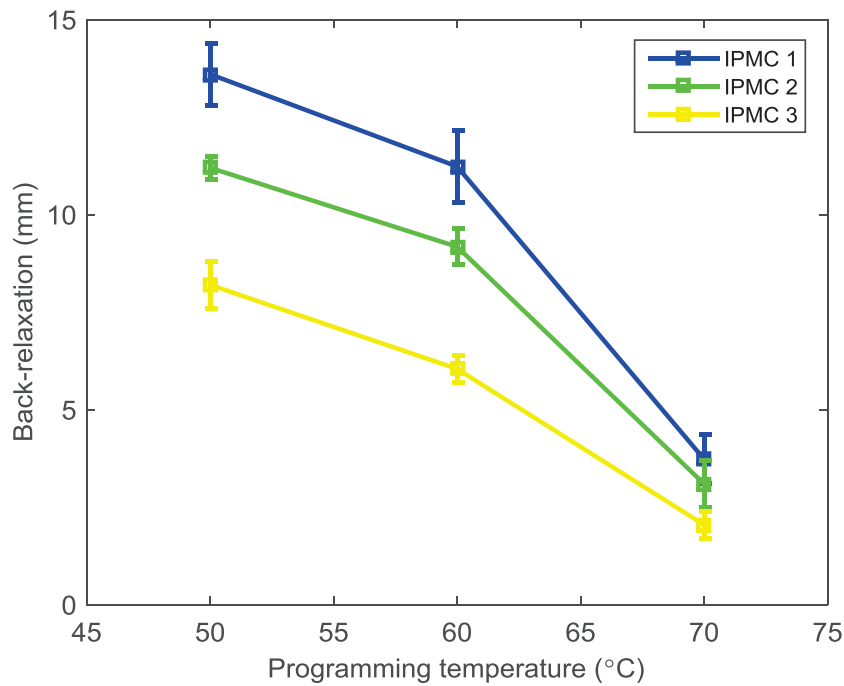


Figure 4.8 Back-relaxation deformation of the IPMC at different programming temperatures.

4.3. Discussion

4.3.1. Application of thermo-mechanical transaction

IPMCs have received significant interests as soft biomimetic actuators/sensors[137], [138]. Tremendous works have been done on its application in the fields of biomimetic robotics, biomedical devices and human affinity applications, such as underwater robots, active catheters and underwater soft sensors [13], [106]. Although the shape memory properties of the Nafion-based IPMC have been experimentally investigated, few work has been done on its potential applications or demonstrations. In this paper, a demonstration that uses the thermo-mechanical shape memory properties of Nafion fiber was presented. The demonstration has shown the Nafion fiber's capabilities of achieving a series of complex shapes with multiple shape

programming. These results indicated that the thermo-mechanical transaction phenomenon of the Nafion can be potentially applied in the field of biomedical and human affinity devices, including active cannulas, and soft catheters. Previous works have demonstrated the thermo-electrical shape memory properties of the IPMCs [33], [139]. Thermo-electrical shape memory programming was performed. By plating electrodes on the surface of the Nafion, the electro-mechanical/mechano-electrical properties and the thermo-mechanical properties of IPMC can be coupled. More interesting actuating/sensing demonstrations can be presented in the near future. It was also noticed that in both current paper and previous work, to achieve the shape recovery, the temperature of IPMC was changed by changing the liquid surrounding it, which is not applicable in the real world. To solve this problem, the thermoelectric cooler will be utilized for the fast programming heating and fixing cooling during the actuation responses of IPMC.

4.3.2. Model of the shape memory properties

Considerable efforts have been made to describe the electro-mechanical transaction of IPMC [54], [140]–[142], such as the swelling theory that the migration of the hydrated water results in the deformation of the IPMC [143]–[146], the influence of the electrode conductivity on the transduction behavior of IPMC [56], the cations redistribution which results in the electrostatic stress [27], [61], [147], [148], the effect of the electrodes on the charge dynamics of IPMC [62], and the interference between the IPMC surface electrode and the membrane [63], [64]. The mechano-electrical transaction of IPMC has also been studied [73], for instance, underwater object tracking [149], [150], energy harvesting [20], [151], surface electrode sensing [152], [153] and parametric effects [154]. Most of the models are based on the ionic immigration induced by the electric field for actuating and concentration variations of ions results from

Nafion deformation for sensing. Regarding the thermo-mechanical transactions of IPMC, the ion migration is not the major factor which results in the deformation of the IPMC. To explain this phenomenon, the free energy density theory was utilized. The volume swelling/shrinking of the Nafion membrane and the temperature variation results in the shape recovery. Through experiments, the results show that the proposed model can well describe the thermo-mechanical transactions of Nafion-based IPMC. The current study is beneficial for identifying the mechanism behind the shape memory feature of IPMC.

4.4. Methods

4.4.1. Sample preparation

IPMC strip samples were prepared for the experimental validation. The surface of the Nafion™-117 membrane sheet was polished and the membrane was immersed in 3% hydrogen peroxide (H_2O_2) to eliminate organic impurities and in 1 M sulfuric acid (H_2SO_4) to remove the metallic impurities. Then the membrane sheet was plated with the platinum metal particles by being immersed in a platinum complex solution ($Pt(NH_3)_4Cl_2 \cdot H_2O$) and after that it was immersed in a sodium borohydride solution ($NaBH_4$). To lower the surface resistance, the sheet was suspended in the solution with hydrazine ($NH_2NH_2 \cdot H_2O$) and hydroxylamine hydrochloride ($H_2NOH \cdot HCl$) being added to the solution. After the plating process, the sheet was soaked in a solution of lithium chloride for the ion exchange.

4.4.2. Parameter identification

To perform the simulation of the theoretical model, the parameters need to be identified. Some parameters can be measured directly, such as the dimensions of the IPMC sample and the temperature. Some are physical constant, such as the Boltzmann constant. The rest need to be

identified, such as the enthalpy constant. In the current study, the parameters of the model were identified based on the experimental results using the least-square method in MATLAB. For each programming temperature, the parameters were identified separately.

Chapter 5. Multiphysics modeling and experimental investigation of a soft multiple-shape-memory ionic polymer-metal composite actuator

5.1. Introduction

The Ionic Polymer-Metal Composite (IPMC) has been studied for decades due to its unique mechano-electrical and electro-mechanical transaction mechanisms [140], [155]–[157]. It is based on the ionic polymer materials such as Nafion, Aquivion and GEFC. On both sides, a layer of metal is chemically plated, which act as the electrodes. Chemically stable metals, such as gold and platinum, are usually used for this purpose. Recently, palladium and graphene have also been used to plate the surface of the polymer [121], [138], [156], [158]. When a voltage is applied on both sides of the IPMC, the mobile ions inside the polymer migrate to the cathode and accumulate at the boundary of the polymer, causing the IPMC to bend. If the IPMC is mechanically bent, a detectable voltage is generated on the surface of IPMC. Many physical models have been developed to describe the transaction [61], [140], [159]–[161]. The most interesting characteristics are its inherent softness, resilience and biocompatibility. A large number of scientist and engineers have developed many robotic systems using IPMCs as sensors and actuators [13], [106], [150], [162]–[164].

Recently, it was found that Nafion, which is the intermediate layer of IPMC, has multiple shape memory effects [18]. The original shape of the Nafion is named S0. To program the first shape, the IPMC is formed into shape S1, heated to temperature T_1 , then cooled to a lower temperature T_1' , such that $T_1' < T_1$. The programming process of S1 is then completed. The shape S1 is ‘memorized’ within the range from T_1' to T_1 . The process can be repeated multiple times. Different shapes S2 and S3 can be programmed within the temperature range $T_2' \sim T_2$,

$T3' \sim T3$. Meanwhile, it should be noted that $T3' < T3 < T2' < T2 < T1' < T1$. As the polymer is reheated from $T3'$ to $T1$, the polymer recovers to programmed shapes from $S3$ to $S0$ at each corresponding temperature $T3$, $T2$ and $T1$. Figure 5.1 shows the illustration of the multiple shape memory effect. These recoveries result from the broad glass transition ranges over the recovery temperatures. Nafion with the ability to remember multiple shapes has promising potential applications in actuators, sensors and smart devices if such a feature is effectively needed.

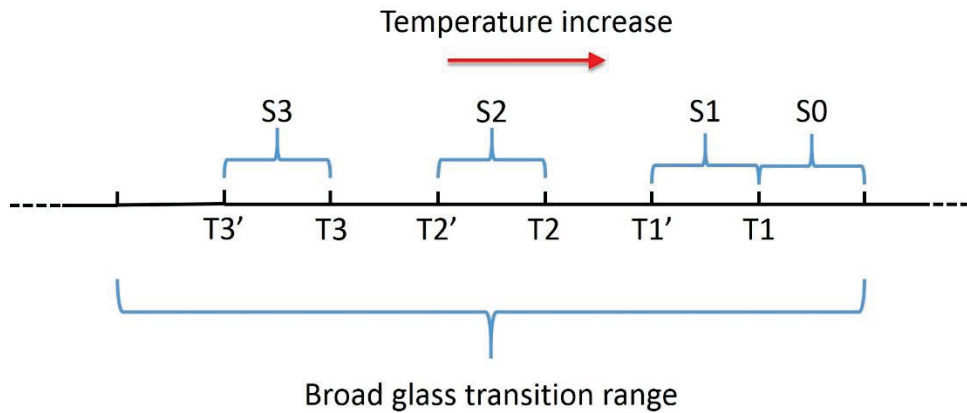


Figure 5.1 Illustration of the multiple shape memory effect.

Based on these two effects, which are the electro-mechanical transaction and multiple shape memory effect, we introduce a new actuator, multiple-shape-memory ionic polymer-metal composite (MSM-IPMC) [139]. This actuator can perform deformations of multiple degrees of freedom.

The shape memory properties of Nafion have recently been studied. Xie reported that annealed dry Nafion sample can be programmed to memorize up to four different shapes [18]. Compared with the strip, the Nafion fiber sample with two dimensions can achieve more

complex locomotion. The permanent shapes were deformed at different temperatures and fixed at lower temperatures. By reheating the Nafion subsequently, the programmed shapes were obtained respectively. With the broad glass transition range, the Nafion can be potentially programmed at plenty of unique shapes, which can be recovered at different temperatures respectively [139]. Rossiter et al. presented the shape memory properties of Nafion-based IPMC [33]. The IPMC was programmed at the deformation induced by either external force or by electrical actuation. Slow decay was also observed along with the shape memory effect. Xiao et al. applied a finite deformation, nonlinear viscoelastic model with a discrete spectrum of relaxation times to describe the shape memory behavior of the Nafion [34]. A theory was also proposed to explain this behavior [1]. The critical point for this theory is that a single broad thermal transition can be regarded as the collective contribution of numerous infinitely sharp transitions continuously distributed in the broad temperature range. Previously we laid out a theoretical framework in terms of finite element based free-energy density to describe the shape memory effect of the IPMC [165].

To date, while some experimental tests on the shape memory properties of Nafion have been conducted, limited work has been done concerning the theoretical investigation of the multiple shape memory effect of the Nafion. Poor understanding exists on the physics of the shape memory properties of the Nafion. A model is desirable to explain the thermo-mechanical transaction phenomenon.

The first goal of this study is to develop a multiphysics model of the MSM-IPMC. New physical principles were proposed to explain the multiple shape memory effect of MSM-IPMC. A theoretical model of the multiple shape memory effect, based upon thermal stress analysis,

was developed. It is based on the assumption that the multiple shape memory effect is caused by the thermal stress and each individual Young's modulus is 'memorized' during the previous programming process. As the MSM-IPMC was reheated to each temperature, the corresponding thermal stress was applied on the MSM-IPMC, and Young's modulus was recovered, which results in the shape recovery of the MSM-IPMC. This model was coupled with the electrical actuation model of IPMC, which was reported in our previous work [119], [166]. The multiphysics model of the MSM-IPMC was obtained based on the coupled model. Experiments of the MSM-IPMC was conducted. The Dynamic Mechanical Analyzer (DMA) was used to test the multiple shape memory effect. The electrical actuation and the multiple shape memory effect of the MSM-IPMC were demonstrated simultaneously. The simulation results and experimental results were compared. This work may be beneficial in exploring the underlying physics of multiple shape memory effect.

The second goal of our study is to characterize the multiple shape memory effect of the MSM-IPMC. Three different ionic exchange membranes, which are Nafion, Aquivion and GEFC, with three different ions, namely Hydrogen (H^+), Lithium (Li^+) and Sodium (Na^+), which are totally nine different kinds of MSM-IPMC samples, were fabricated and used for the test. The multiple shape recovery and the reversibility of the samples were qualitatively tested. New theories based on enthalpy and free energy were proposed to describe the multiple shape memory performance of the samples. The current method can also be used to study the multiple shape memory effect of other shape memory polymers.

The rest of the paper is organized as follows. Section 2 presents the modeling of the MSM-IPMC actuator. Section 3 introduces the experimental verification and results. The results were discussed in Section 4. Section 5 is left for the conclusion.

5.2. Mathematic model

5.2.1. Modeling of the multiple shape memory effect

Several works have been reported on the modeling of the shape memory behavior of Nafion. One theory is that by modeling the glass transition, the shape memory process can be modeled [34]. A temperature-dependent relaxation time or viscosity was assumed in the model. During the glass transition, the relaxation time changes significantly. This allows the materials to store a temporary shape and recover a permanent shape.

In this study, I proposed an alternative physics-based principle to explain the shape memory behavior. The fundamental concept is that each glass transition is independent of each other. Based on previous work, Nafion has multiple shape-memory properties. It can be programmed into multiple shapes and controlled by thermal or electric inputs. We assumed that the broad glass transition temperature could be regarded as the consecutive distribution of a series of glass transitions. Within the range of the broad glass transition temperature, $\sim 55^{\circ}\text{C}$ to $\sim 140^{\circ}\text{C}$, Nafion could be programmed with multiple unique shapes and recovered under different temperatures. A theoretical model of the multiple shape memory effect of Nafion will be developed. It is based on the assumption that the multiple shape memory effect is caused by the internal stress where Young's modulus is 'memorized' during the previous programming process. As the MSM-IPMC is reheated to each temperature, the internal stress is released on the

MSM-IPMC, and Young's modulus is recovered, which results in the shape recovery of the MSM-IPMC.

Assuming the length, width and thickness of the MSM-IPMC sample are L , W and $2h$ respectively. The internal stress, which is caused by the deformation of polymer chain at the glass transition temperature, is released on the MSM-IPMC during each shape recovering process. The expression of the internal stress can be expressed as [167]

$$\sigma(t) = \sum_i^N \frac{\rho_n RT(t)}{M_C} \left(\alpha_i - \frac{1}{\alpha_i^2} \right) \quad (5.1)$$

where i refers to each individual shape memory process, N is the total number of the shape memory process, $T(t)$ is the temperature, ρ_n is the density of the polymer, R is the gas constant, M_C is the molecule weight of the polymer and α_i is the extension ratio. The α_i can be denoted as

$$\alpha_i = 1 + \varepsilon_i \quad (5.2)$$

where ε_i is the programmed strain of the polymer at each shape memory process. As the MSM-IPMC is reheated to previously programming temperature, the previously stored Young's modulus is released accordingly. The Young's modulus can be expressed as

$$Y(t) = Y^{eq} + \sum_i^N Y_i^{neg} \exp \left(a \left(\frac{T(t)}{T_i} - 1 \right) \right) \quad (5.3)$$

where Y^{eq} is the equilibrium Young's modulus, Y_i^{neg} is the nonequilibrium Young's modulus, a is the coefficient related with the shape memory process, T_i is the reference temperature corresponds to the programming temperature at each shape memory process. Using the linear

beam deflection theory, the tip displacement w_s of the IPMC beam element relating to the z can be denoted as

$$\frac{d^2 w_s(z, t)}{dz^2} = \frac{M(z, t)}{YI} \quad (5.4)$$

where I is the moment of inertia of the IPMC actuator and $I = 2/3Wh^3$. By relating the induced stress $\sigma(\pm h, z, t)$ to the bending moment, one can obtain

$$\sigma(\pm h, z, t) = \frac{\pm hM(z, t)}{I} \quad (5.5)$$

Combing Eqs (5.3), (5.4) and (5.5), the tip displacement w_s induced by the multiple shape memory effect can be expressed as

$$w_s(L, t) = \frac{\sum_i^N \frac{\rho_n RT(t)}{M_c} \left(\alpha_e - \frac{1}{\alpha_e^2} \right) L^2}{2h \left(Y^{eq} + \sum_i^N Y_i^{neq} \exp \left(a \left(\frac{T(t)}{T_i} - 1 \right) \right) \right)}. \quad (5.6)$$

5.2.2. Modeling of the MSM-IPMC

A physics-based model of the IPMC that combines the resistance change effect of the surface electrode and the charge dynamics of the ionic polymer has been previously proposed [119]. A microstructure model of the surface electrode was developed. The arrangement of particles used in this model was inspired by the primary metallic crystal structures. Based on the volume change of the electrode caused by the IPMC beam bending, the variation of the resistance of the IPMC was obtained. Furthermore, a physics-based model of the polymer membrane was developed. The model is based on the Poisson-Nernst-Planck equations. The

Ramo-Shockley theorem was used to calculate the current in the continuous electrodes of the IPMC. The finite element approach is used to describe the dynamics of the segmented IPMC strip, which considers as the composition of finite elements that can be used to represent a mechanical deflection of the IPMC. By combining the model of the surface electrode and the polymer membrane, the actuation model of the IPMC was obtained. The deformation $w_a(L,s)$ caused by the actuation effect under the voltage $V(s)$ can be obtained by solving the following equation in the frequency domain

$$w_a(L,s) = \frac{\alpha L}{hY(s)} \frac{(-\exp(J(s)) + J(s) + 2) \left(1 + \frac{1}{J(s)}\right)}{J(s)K(s)} \sinh(A(s)h)V(s) \quad (5.7)$$

with

$$J(s) = -\frac{DW_e h_e R_e}{h} \frac{\left(\frac{2 \sinh(A(s)h)}{A(s)} + 2h \cosh(A(s)h)\right) \left(\frac{A(s)}{F} - \frac{FC_0}{RT \hat{\epsilon} A(s)}\right)}{K(s)}$$

$$K(s) = \frac{2 \sinh(A(s)h)}{\hat{\epsilon} A^2(s)} + 2h \cosh(A(s)h) \left(\frac{RTA(s)}{F^2 C_0} - \frac{1}{\hat{\epsilon} A(s)}\right)$$

$$A(s) = \sqrt{\frac{B+s}{D}}$$

$$B = \frac{\hat{z} \mu F^2 C_0}{\hat{\epsilon}}$$

where α is the proportional coefficient that relates the charge density at the boundary of polymer to the induced stress [27], Y is the Young's modulus, s is the Laplace variable, D is the diffusion constant, F is the Faraday constant, C_0 is the constant anion concentration, R is the gas constant, $\hat{\epsilon}$ is the absolute dielectric constant, W_e is the width of the surface electrode, h_e is the thickness of

the surface electrode, \hat{z} is the charge number, μ is the mobility of cations, R_e is the resistance of the surface electrode.

By solving Eq. (5.16), the deformation $w_a(L,s)$ of the IPMC under the voltage can be obtained. MATLAB was used to obtain the numerical solution for $w_a(L,s)$. Then $w_a(L,s)$, which is in the frequency domain, was converted to the time domain $w_a(L,t)$.

Based on the $w_s(L,s)$ induced by the multiple shape memory effect and $w_a(L,s)$ induced by the actuation effect, the total tip displacement $w_t(L,s)$ of MSM-IPMC can be obtained

$$w_t(L,t) = w_s(L,t) + w_a(L,t). \quad (5.8)$$

5.3. Experimental investigation

5.3.1. Multiple shape memory effect model validations

The multiple shape memory effect was tested by Dynamic Mechanical Analysis (DMA). An MSM-IPMC sample of 20 mm in length, 4.95 mm in width and 0.18 mm in thickness was used for the test. The ionic exchange membrane was Nafion. Figure 5.2 shows the quadruple shape memory properties of the MSM-IPMC. The original shape of the sample was considered as S0. During the programming period, the sample was stretched under different external stress at different temperature ranges, which were the programming temperatures. Three different shapes S1, S2 and S3 were programmed at the temperature range 130 ~ 85 °C, 85 ~ 55 °C and 55 ~ 20 °C respectively by applying the stress in the DMA. The deformation of the sample was measured in terms of the strain, which can be expressed as

$$\varepsilon = \frac{\Delta L}{L} \quad (5.9)$$

where ε is the strain, ΔL is the relative deformation of the sample, and L is the original length of the sample. During the recover process, the sample was reheated. As the temperature increases, the sample recovered to the programmed shapes S2', S1' and S0' at corresponding temperatures 55°C, 85 °C and 130 °C. It can be seen that the recovered shapes S2', S1' and S0' have a good match with the programmed shapes S2, S1 and S0. This indicates that the sample shows a good multiple shape memory effect. Quantitative analysis of the shape recovery was also performed in the next sections.

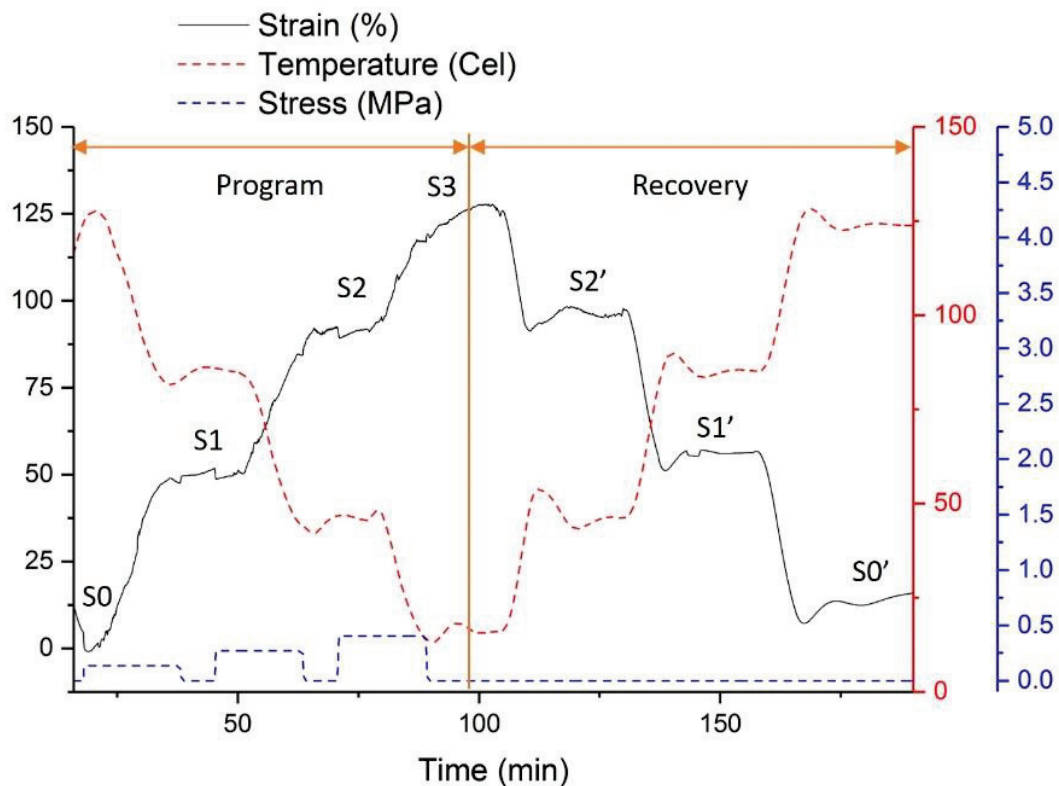


Figure 5.2 Quadruple shape memory properties of the MSM-IPMC.

The model presented in Section 5.2 was simulated in Matlab. Except for the parameters of physical constant and dimensions, parameters such as the nonequilibrium Young's modulus were identified through least-square method. Table 5.1 shows the parameters of the multiple shape memory model. It can be found that the nonequilibrium Young's modulus is relatively small compared with the equilibrium Young's modulus. It can be concluded that the internal stress mainly contribute to the shape recover of the actuator. Figure 5.3 shows the comparison between the simulation and experimental results of the multiple shape memory effect. The simulated and experimental results are in good agreement. The model describes well the multiple shape memory process of the MSM-IPMC. One of the reasons that both results match well is that the least squares fit was used and the parameters such as molecule weight M_c , nonequilibrium Young's modulus Y_i^{neg} , and shape memory coefficient a were identified based on the experimental results.

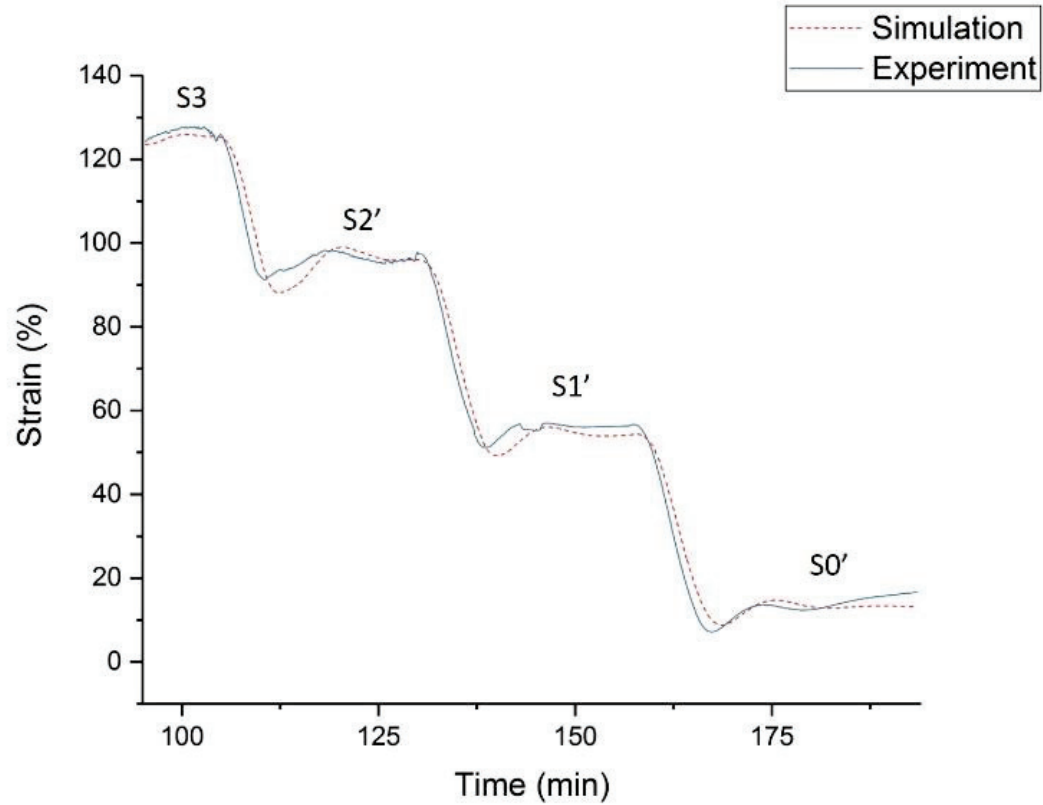


Figure 5.3 Comparison between the simulation and experimental results of the multiple shape memory effect.

Table 5.1 Parameters of the multiple shape memory model.

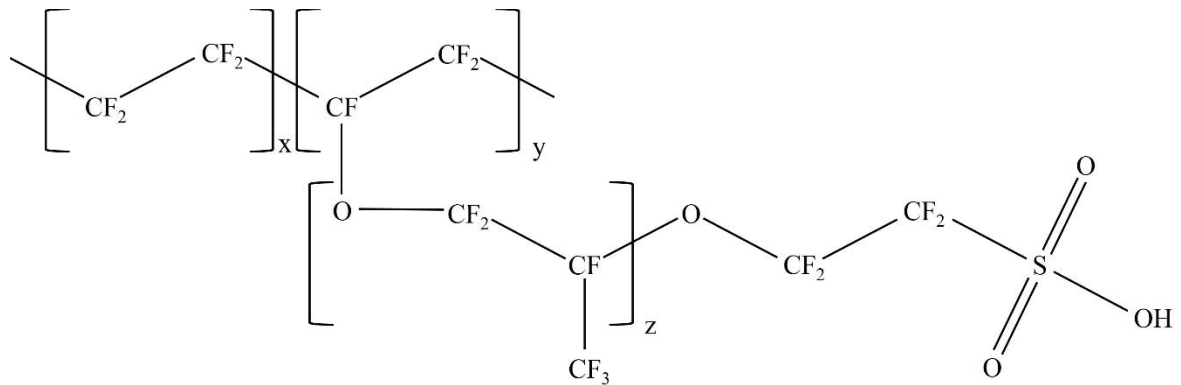
Model parameter	Value
Density of the polymer, ρ_n	874 kg/m ³
Gas constant, R	8.31 J/mol·K
Molecule weight, Mc	3.07×10^5 g/mol
Equilibrium Young's modulus, Y^{eq}	200 MPa
Nonequilibrium Young's modulus, Y_i^{neg}	1.19 kPa
Shape memory coefficient, a	1.32

5.3.2. Validation of the MSM-IPMC model

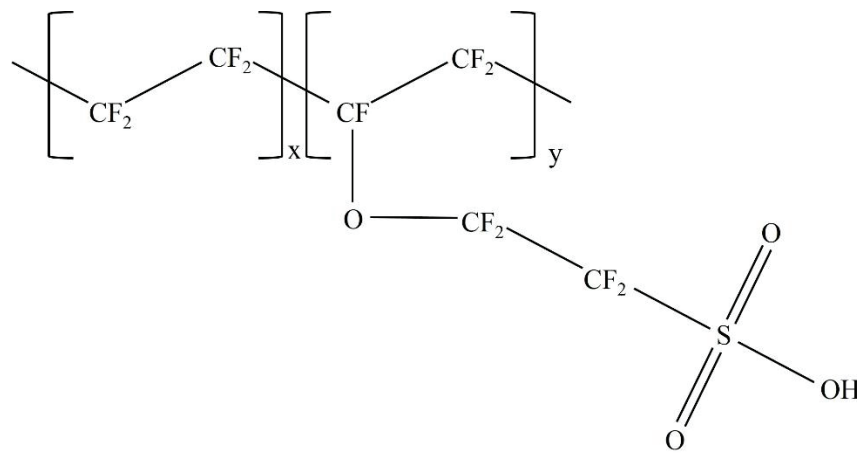
To validate the MSM-IPMC model in Equation (5.6), the MSM-IPMC samples were tested. Three MSM-IPMC samples with different ionomer membranes, namely Nafion, Aquivion, and GEFC, were used. The properties of the membranes are presented in Table 5.2 [168], [169]. The Nafion contains perfluoro vinyl ether groups terminated with sulfonate groups onto a tetrafluoroethylene backbone. The Aquivion is based on the Short Side Chain (SSC) copolymer of Tetrafluoroethylene (TFE) and Sulfonyl Fluoride Vinyl Ether (SFVE). The GEFC membrane has a perfluorinated backbone and sulfonate side chains similar to Nafion [109], [170]. The polymer structures of the membranes are shown in Figure 5.4. It can be noticed that the Aquivion has a shorter side chain compared with Nafion and GEFC. The sizes of the MSM-IPMC samples were measured. The results are presented in Table 5.3.

Table 5.2 Properties of Nafion, Aquivion and GEFC membranes.

Membrane	Manufacturer	Structure	Equivalent weight (g/eq)
Nafion	DuPont	Perfluorovinyl ether groups terminated with sulfonate groups onto a tetrafluoroethylene backbone	1100
Aquivion	Solvay	Short Side Chain (SSC) copolymer of Tetrafluoroethylene (TFE) and Sulfonyl Fluoride Vinyl Ether (SFVE)	840
GEFC	GEFC	Perfluorinated backbone and sulfonate side chains	1000



(a)



(b)

Figure 5.4 Polymer structures of different membranes: (a) Nafion and GEFC; (b) Aquivion.

Table 5.3 Dimensions of the MSM-IPMC membrane samples.

Item	W (mm)	L (mm)	$2h$ (mm)
Nafion	10.39	34.87	0.18
Aquivion	10.01	41.15	0.18
GEFC	9.92	36.12	0.29

Before the test, the samples are all programmed to several shapes. The original shape of the sample is assumed S0. The first shape S1 is programmed by folding the strip lengthwise around a rod, which was programmed at 85 °C and fixed at 70 °C. The second shape S2 is programmed by folding the strip lengthwise around the rod in the opposite direction, where the programming temperature is 55 °C and the fixing temperature is 22 °C. Finally, the shape of the sample is at S2. Figure 5.5 shows the experimental setup for the shape recovery process. The MSM-IPMC sample is submerged in deionized water. A clamp is used to fix one end of the sample. A signal generator (SDG1025, Siglent) is used to generate a sinusoid wave, which is amplified by a power amplifier (LVC-608, AE Techtron, Inc.). Through the clamp contacts, a voltage input of 2 V amplitude and 1 Hz frequency is applied to the sample. An immersion heater (3656K169, McMaster-Carr) is used to heat the water from room temperature (22 °C) to 90 °C. A circuit is developed based on a thermal resistor (PRTF-11-2-100-1/8-6-E, Omega®) to measure the water temperature. A laser sensor (optoNCDT-1401, Micro-Epsilon) is used to measure the displacement of the sample. The voltage, current, displacement and temperature were measured simultaneously through the DAQ (NI SCB-68, National Instruments) and were recorded using the LabVIEW 8 Software.

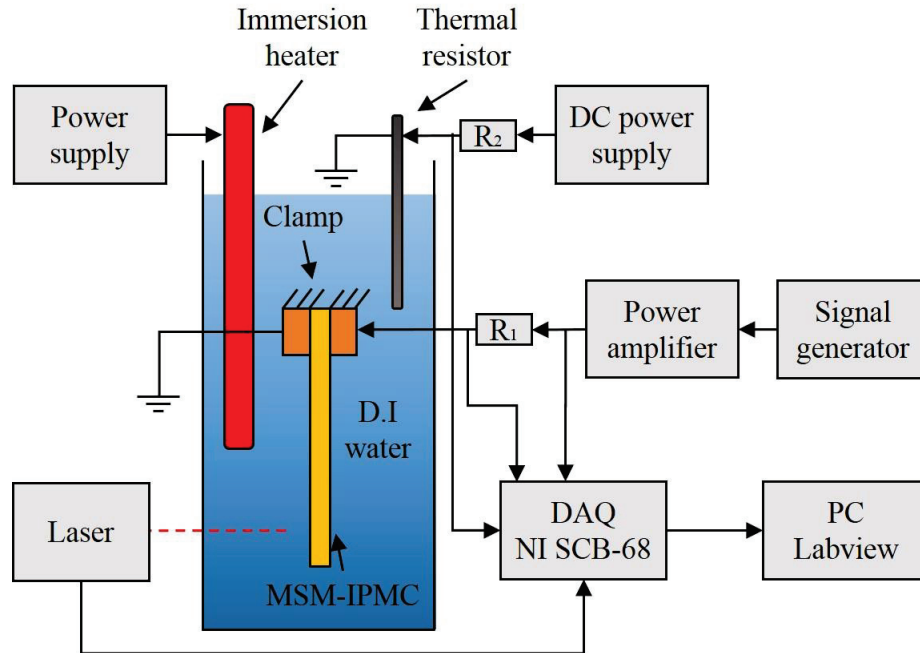


Figure 5.5 Experimental set up of the MSM-IPMC test.

Figure 5.6 shows the experimental results of the GEFC sample. It can be seen that in general, as the temperature increases, the voltage decreases and the current increases. Based on the results, it can be concluded that the electrical impedance of the MSM-IPMC decreases as the temperature of current study increases. This property can be potentially used for the thermal feedback control. Similar results were also found in our previous study [139]. According to the displacement result, the sample shows the multiple shape memory effect and the electrical actuation effect simultaneously. The general bending of the sample resulted from the multiple shape memory effect. As the temperature increases initially, the sample recovered from S2 to S1', where the sample bent toward one side. With the temperature continuing to increase, the sample finally recovered to its original shape S0', where the sample bent toward another side. Meanwhile, the sample has an oscillation motion induced by the electrical actuation.

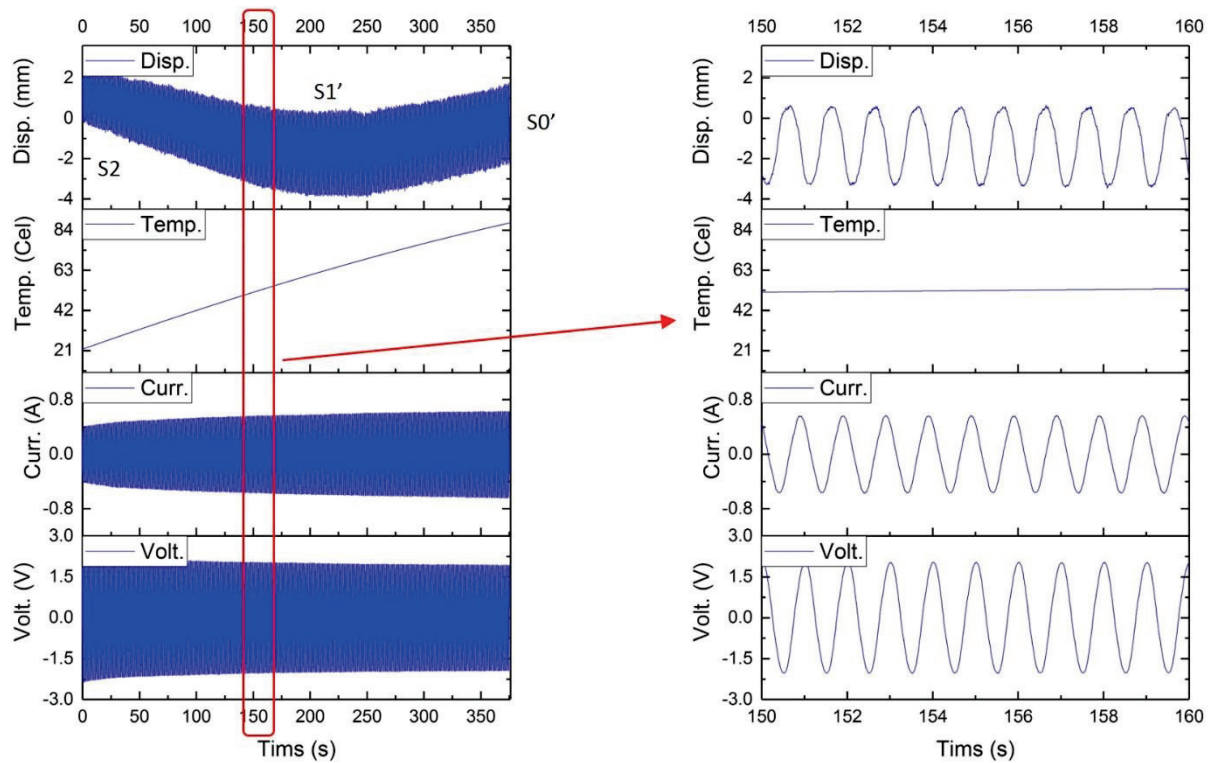


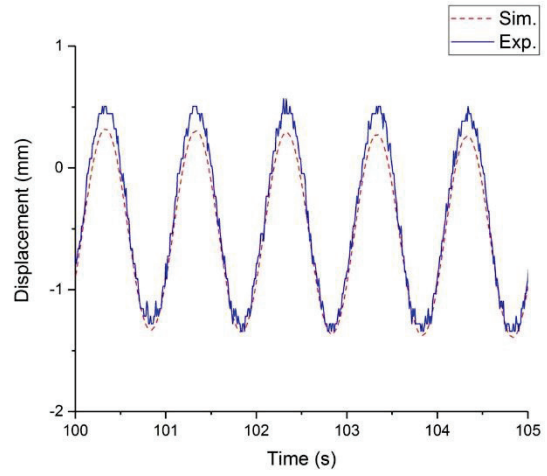
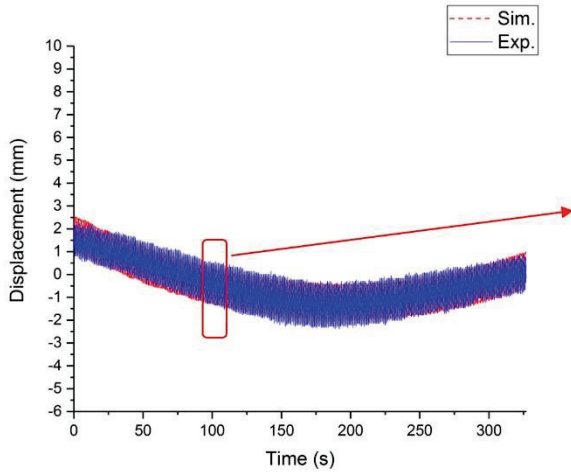
Figure 5.6 Measured displacement, temperature, current and voltage of GEFC sample.

Figure 5.7 shows the comparison between the experimental results and theoretical results of the displacements of the MSM-IPMCs, which are based on Nafion, Aquivion and GEFC membranes in Li^+ -form. The results show that the model describes well the actual displacement of the different MSM-IPMCs. In general, all three samples demonstrated the capabilities of multiple shape memory effect. It was also found that the sample of Aquivion has the largest displacement, which is ~ 8 mm; the sample of Nafion and GEFC have relatively small displacements, which are ~ 2 mm and ~ 3 mm respectively. The Aquivion membrane has a larger displacement than the other two samples. One of the reasons that cause the difference between the sample displacements is the length of the samples, where the Aquivion is longer than the

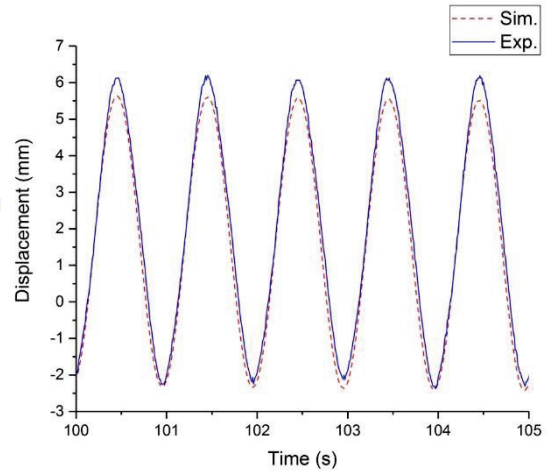
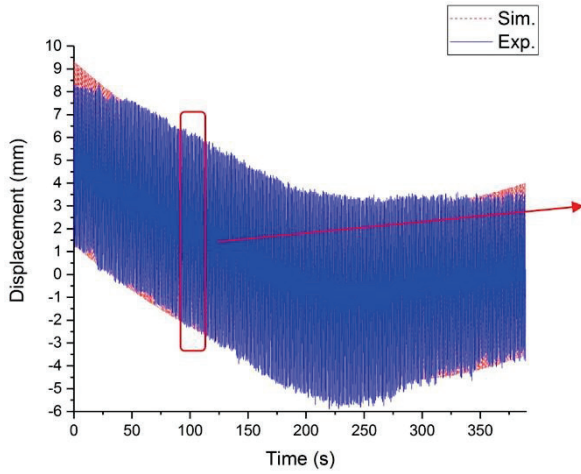
Nafion and the GEFC. Another possible explanation is that Nafion and GEFC have a perfluorovinyl ether side group and a sulfonate end group. Aquivion has the sulfonyl fluoride vinyl ether as the side group, whose molecule chain is shorter. This short side chain enables the polymer to have a lower equivalent weight, which potentially causes a higher conductivity [168]. Furthermore, the Ion Exchange Capacity (IEC) of Aquivion is higher than the other two membranes, as shown in Table 5.4. This also indicates the potential that the Aquivion has better electromechanical performance than Nafion and GEFC.

Table 5.4 The ion exchange capacity of each membrane.

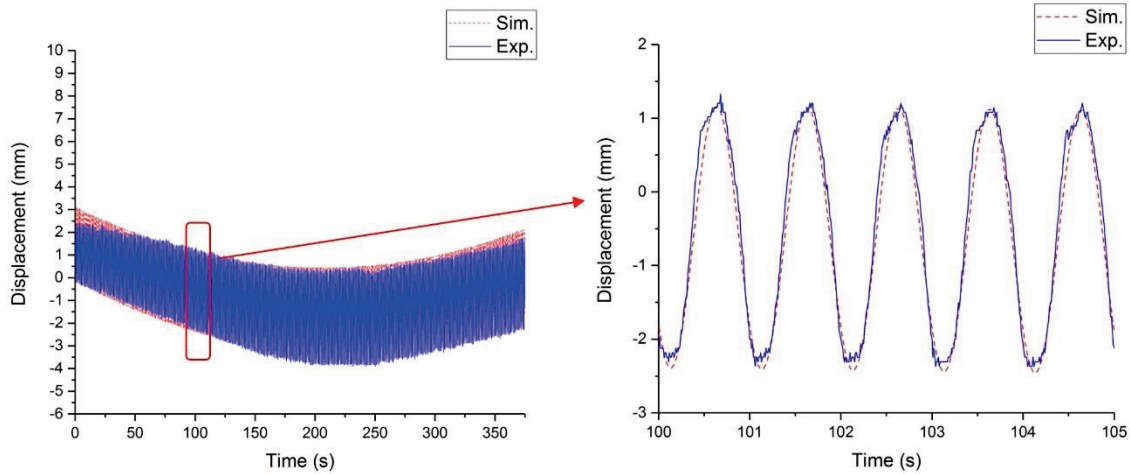
Membrane	Ion Exchange Capacity (meg/g)
Nafion	0.97 (± 0.01) [170]
Aquivion	1.25 (± 0.01) [168]
GEFC	0.95 (± 0.01) [170]



(a)



(b)



(c)

Figure 5.7 Comparison of theoretical and experimental results of different membrane based IPMCs: (a) Nafion; (b) Aquivion; (c) GEFC.

5.3.3. Glass transition

The glass transitions of different membranes with different ions were studied. In our study, we used three different ionic exchange membranes, which were Nafion, Aquivion and GEFC. Each membrane has three different ion forms, which were hydrogen (H^+), Lithium (Li^+) and Sodium (Na^+). Nine different samples in total were utilized for the test. By soaking the membranes in hydrogen chloride (HCl), Lithium chloride (LiCl) and Sodium chloride (NaCl) for the ionic exchange, the membranes in H^+ form, Li^+ form and Na^+ form were obtained respectively. Before the test, the samples were annealed in an oven at $150\text{ }^\circ\text{C}$ for 4 hours to remove the residual stress/strain from the polymer processing step. The glass transition range of each sample is first measured separately. The mechanical properties of the samples were tested in DMA. The tangent of δ which is the ratio between the loss modulus E'' and the storage

modulus E' , is obtained. By measuring the start and end temperature of the the tangent of δ curve peak, the broad glass transition can be derived. The details can be found in [18].

The glass transition ranges of the samples were obtained. Based on the experimental results, it was found that the membranes with the same ions have similar glass transition range. Figure 5.8 shows the broad glass transition range of the samples in different ions. From the view of the ions, the membranes in H^+ -form have the shortest glass transition range, which is from $\sim 50^\circ C$ to $\sim 90^\circ C$; the glass transition range of the membranes in Na^+ -form is the longest, which is from $\sim 55^\circ C$ to $\sim 160^\circ C$; the Li^+ -form membranes are between them, which is from $\sim 55^\circ C$ to $\sim 140^\circ C$. It was also found that the H^+ -form membranes have the lowest second glass transition temperature. The second glass transition temperature of the Na^+ -form membrane is the highest. The Li^+ -form membranes are in the middle. To explain this, the enthalpy and free energy of each ion were considered. This is analyzed in the discussion section.

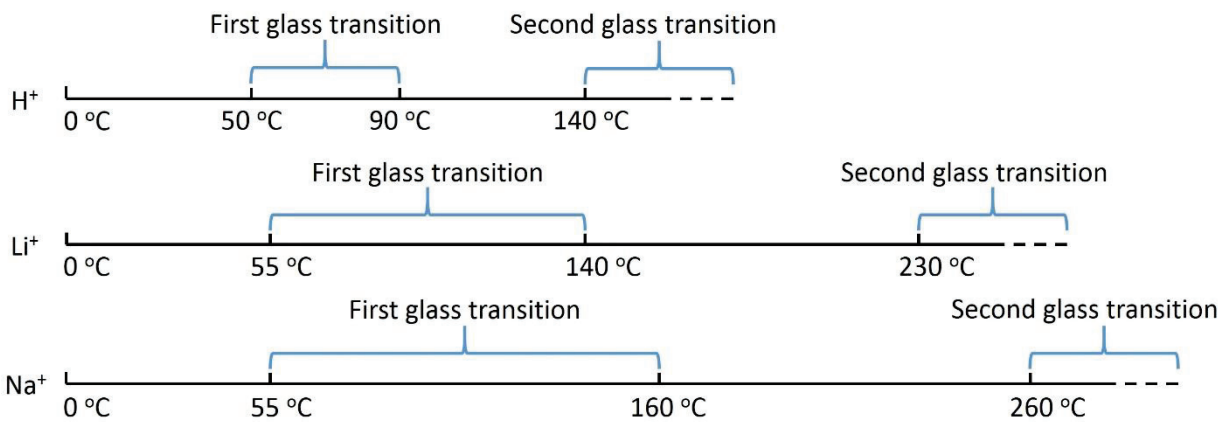


Figure 5.8 First and second glass transition ranges of membranes with different cations.

5.3.4. Shape recovery

The multiple shape memory effect of the samples was tested. Based on the obtained glass transition range of different membranes (Figure 5.8), the triple shape memory effect of the H⁺-form IPMCs was tested, the Li⁺-form MSM-IPMCs were tested with the quadruple shape memory effect, and the quintuple shape memory effect of the Na⁺-form MSM-IPMCs was also tested. Figure 5.9 shows the quintuple shape memory process of the Na⁺-form MSM-GEFC. The results show that the sample has a recoverable multiple shape memory effect. To quantitatively analyze the multiple shape memory effect, the shape recovery rate of each sample during the shape memory process was calculated. Assuming the sample recovers from shape *y* to shape *x*, The shape recover ratio $R_{f,x}$ of shape *x* can be calculated by the following equation

$$R_{f,x} = 100\% \times \frac{S_y - S_x'}{S_y - S_x} \quad (5.10)$$

where S_x , S_y are the strain at *x* and *y* shape during the shape programming process, S_x' is the strain after recovery.

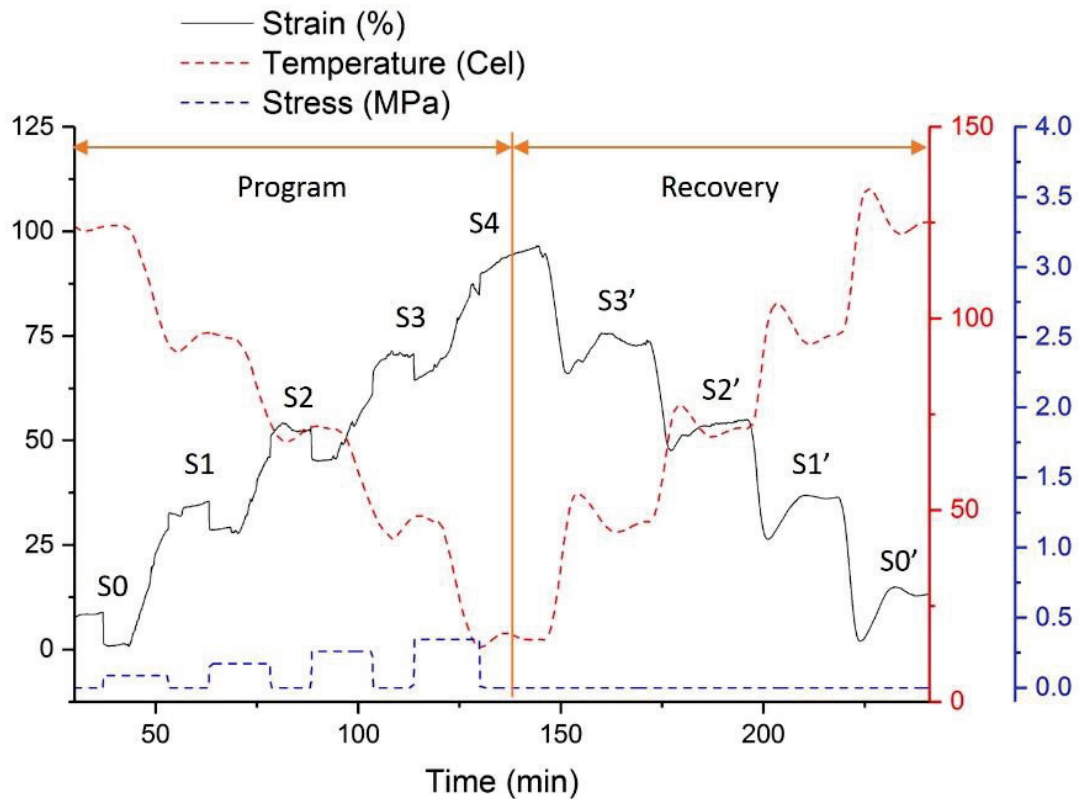
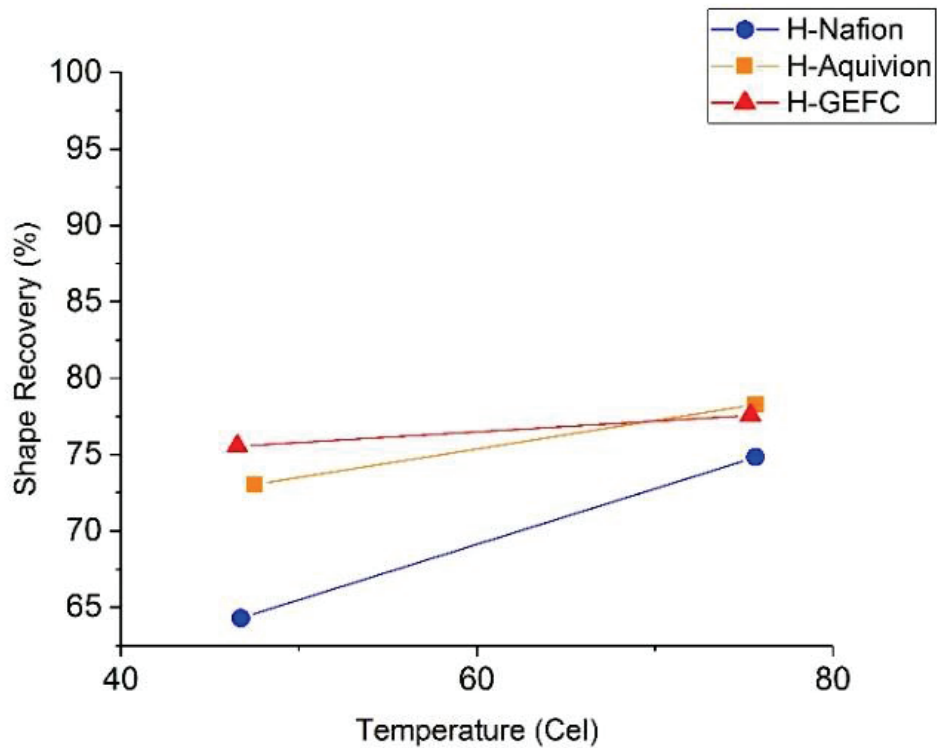


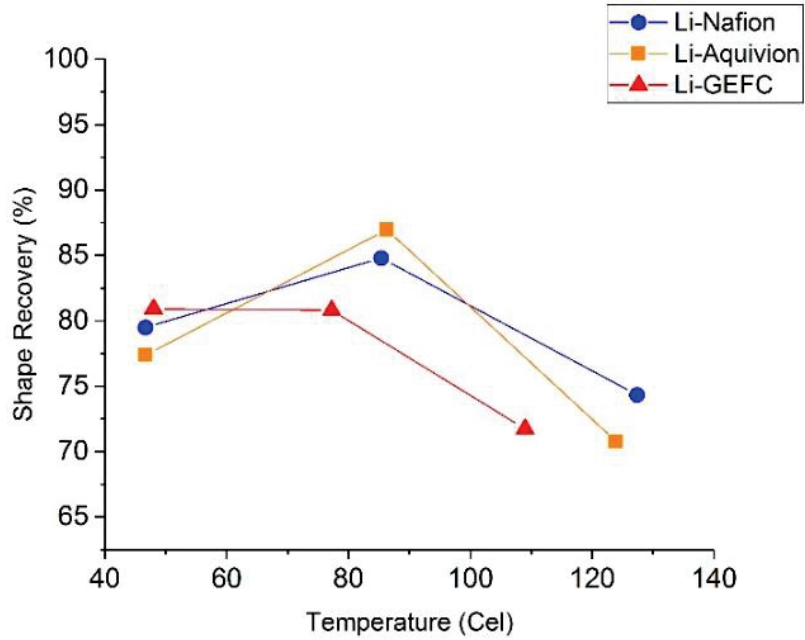
Figure 5.9 Quintuple shape memory process of the Na⁺-form GEFC.

Figure 5.10 shows the shape recovery of different samples. Based on figure 5.10 (a), the shape recovery of the H⁺-form MSM-IPMCs was within the range of 60 ~ 80 %. The triple shape memory programming temperatures of the H⁺-form samples were ~45 °C and ~75 °C respectively. According to figure 5.10 (b), the shape recovery of the Li⁺-form MSM-IPMCs was from 70 % to 90 %. The quadruple shapes of the Li⁺-form samples were programmed at ~45 °C, ~ 80 °C and ~115 °C respectively. As shown in figure 5.10 (c), the shape recovery of the Na⁺-form MSM-IPMCs was within the scope of 80 % to 100 %. The quintuple shape memory effect of the Na⁺-form samples was demonstrated with the programming temperatures of ~45 °C, ~ 70

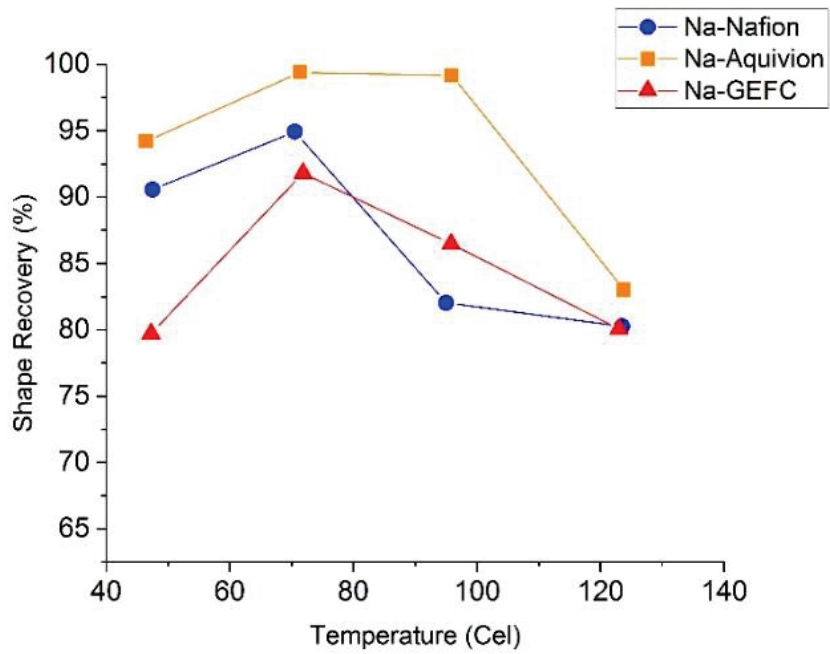
°C, ~ 95 °C and ~125 °C respectively. Based on the results, it was found that the Na⁺-form membrane based IPMCs have the highest shape recovery, the shape recovery of the Li⁺-form membrane based IPMCs is in the middle and the H⁺-form membrane based IPMCs have the lowest shape recovery. Furthermore, it is interesting the note that initially, the shape recovery increases as the temperature increases. The shape recovery reaches the peak when the temperature is approximately 80 °C. As the temperature continues to increase, the shape recovery decreases. To explain this, a detailed discussion is presented in the discussion section.



(a)



(b)



(c)

Figure 5.10 Shape recovery of different samples: (a) H⁺-form membrane based IPMCs; (b) Li⁺-form membrane based IPMCs; (c) Na⁺-form membrane based IPMCs.

5.3.5. Reversibility

In previous work, it was found that the multiple shape memory effect of the Nafion was reversible [18]. However, limited work was done regarding the reversibility of the membranes. In our study, the reversibility of all the nine samples was tested. The DMA was used for the test. Figure 5.11 shows the reversible test of the Na⁺-form Aquivion. During the programming process, the sample with its original shape S0, was programmed at the temperature of 95 °C for shape S1 and 60 °C for shape S2. Then during the recovery process, the sample shows its reversibility between S0, S1 and S2 based on the temperature variation. The recovery sequence is from 1 to 9. It can be seen that the sample has good reversibility.

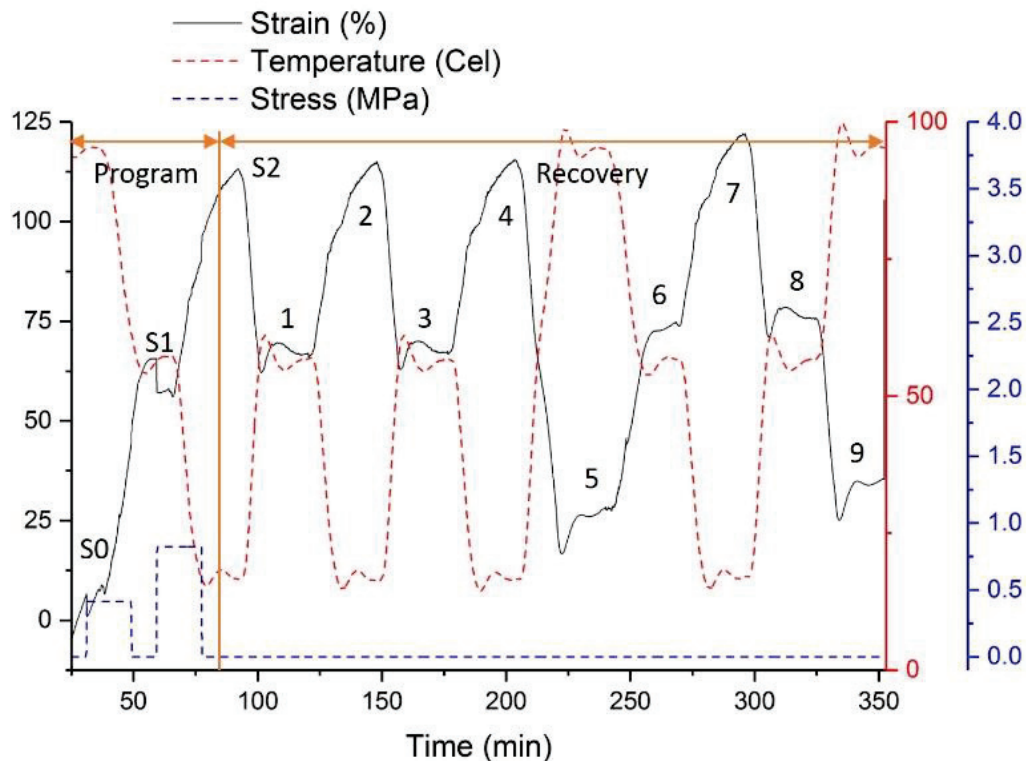
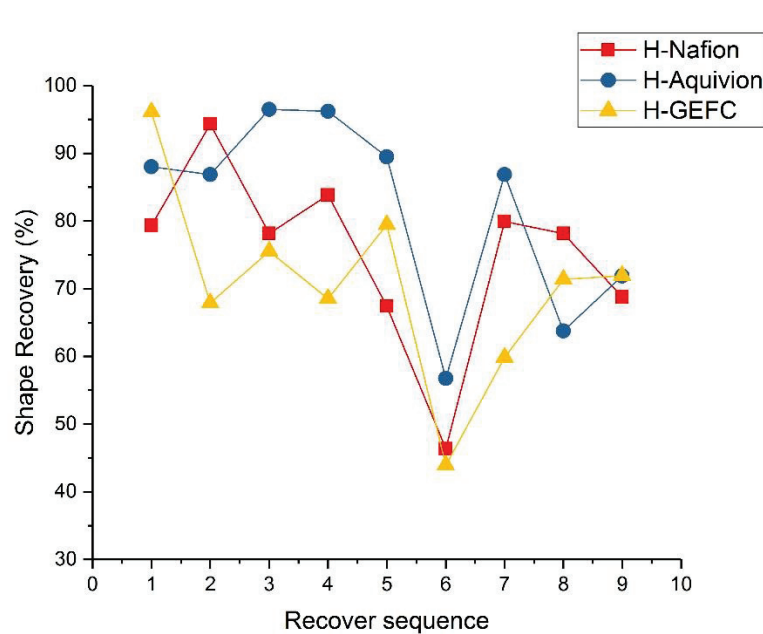
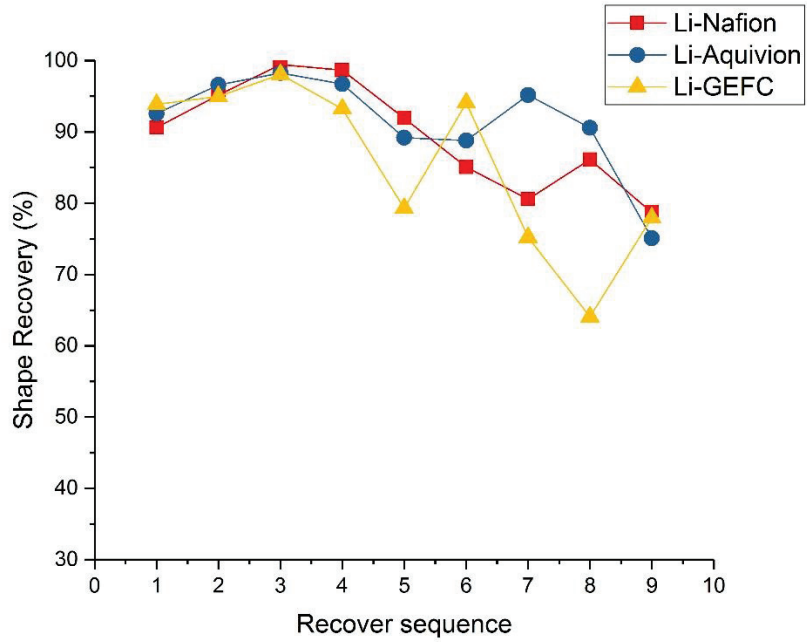


Figure 5.11 Multiple shape memory reverse process of Na⁺-form Aquivion.

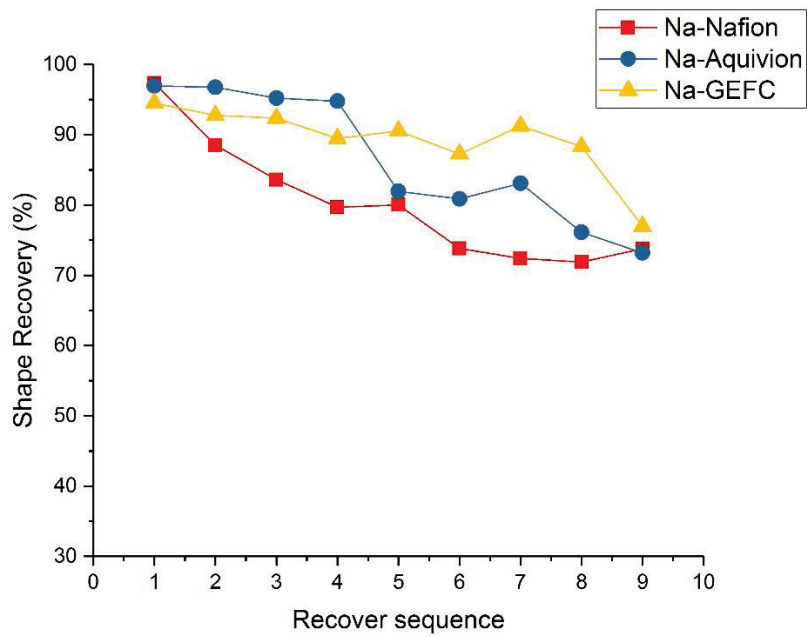
Figure 5.12 shows the shape recovery versus the recover sequence of different samples. The shape recovery was calculated based on Equation (5.9). It can be found that initially, all the samples have a maximum shape recovery. As the samples continue to recover to different shapes, the shape recovery decreases. In general, the Na⁺-form membrane based IPMCs have the highest shape recovery, which starts at ~ 95 % and ends at ~ 75 %; the H⁺-form membrane based IPMCs have the lowest shape recovery. The shape recovery range is from ~ 90 % to ~ 50 %; the shape recovery of the Li⁺-form membrane based IPMCs was between them, which is from ~ 95 % to ~ 75 %. Based on figure 5.12 (a), it was also noticed that the shape recovery has a significant decrease at recover sequence 6. One possible explanation is that the sample was reheated to recover to S2 at ~ 95 °C at sequence 5. Part of the shape memory was removed during the process, which results in the low shape recovery at recover sequence 6.



(a)



(b)



(c)

Figure 5.12 Reversibility of different samples: (a) H⁺-form membrane based IPMCs; (b) Li⁺-form membrane based IPMCs; (c) Na⁺-form membrane based IPMCs.

5.4. Discussion

5.4.1. Ionic effects on the membrane

The ionic membranes used in our study are commercial thermoplastic polymers with mobile ions and immobile anions fixed on the backbones. It can perform as the actuator and sensor when electrodes are chemically plated on the surface. The mobile cations migrate to the boundary when an electrical field is applied across the thickness direction of the membrane. The accumulation of the ions at the boundary causes the deformation of the membrane, along with the surface electrodes. When a mechanical deformation is applied on the membrane, the imbalance of the internal ionic concentration results in the migration of the cations inside the membrane. From a macro perspective, a detectable voltage is generated at the surface of the membrane. To sum up, the transport of the free cations cause the electrical actuation effect.

Meanwhile, the multiple shape memory effect results from the molecule chain motion of the membrane. The ionic exchange membraned used in this paper typically have two kinds of different glass transitions. The first glass transition corresponds to the short-range segmental motions within a static electrostatic network. The multiple shape memory effect takes places in this range. The second glass transition corresponds to the long-range molecular mobility due to the destabilization of the electrostatic network. The temperature range of the first and second glass transition is shown in Figure 5.8. It was noticed that the H^+ -form membranes have the lowest glass transition temperature. The glass transition temperature of the Na^+ -form membrane is the highest. The Li^+ -form membranes are in the middle and are relatively close to the Na^+ -form membranes. In our study, we noticed that the membranes with different ions, namely H^+ ,

Li^+ , Na^+ , have different glass transition ranges. To explain this phenomenon, a theory was proposed.

Figure 5.13 shows the enthalpy (ΔH) and the free energy (ΔG) of different ions [171]. The H^+ has the highest enthalpy and the free energy which are ~ 1500 kJ/mol. The enthalpy and the free energy of Li^+ and Na^+ are similar, where the Li^+ is ~ 685 kJ/mol and the Na^+ is ~ 500 kJ/mol. The Li^+ is relatively higher than the Na^+ . When the membrane was heated, the enthalpy and the free energy of the membrane increased. The enthalpy and free energy ions contribute to the total enthalpy and the free energy of the membrane. As the enthalpy and the free energy increase, the electrostatic network of the membranes starts to destabilize when the temperature is above the first glass transition range. Thus, the membranes with H^+ ions, whose enthalpy and free energy is the highest, are the first to have the destabilized electrostatic network and have the lowest glass transition temperatures compared with the other two ionic form membranes. The glass transition temperatures of Li^+ -form and Na^+ -form membranes are higher, where the Na^+ -form membrane is relatively higher than the Li^+ -form membrane. This has a good agreement with the enthalpy and free energy of Li^+ and Na^+ ions, where the Li^+ is relatively higher than the Na^+ . This can also be used to explain that the shape recovery of H^+ -form membrane is lower than the other two membranes, which are shown in Figure 5.13.

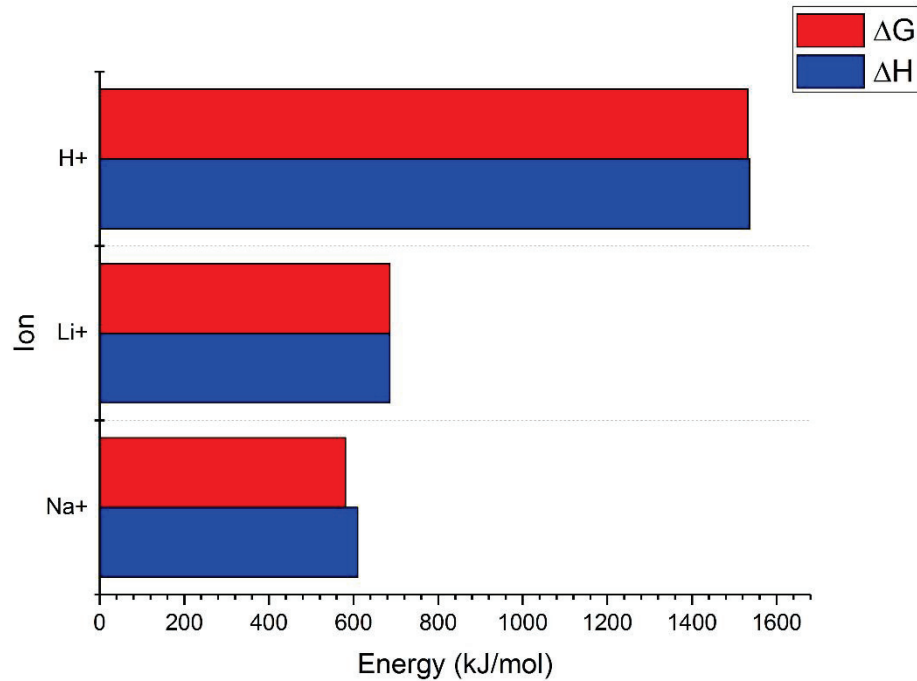


Figure 5.13 Enthalpy and free energy of different ions.

5.4.2. Shape memory distribution

The multiple shape memory effects of the membrane stem from its broad glass transition ranges. According to previous work, the broad transition can be viewed as the collective contribution of an infinite number of transitions. Each of the transitions corresponds to the sharp transition temperatures continuously distributed across the broad transition [18]. Thus, the membrane can be seen as the sum of numerous molecule segments. Each molecule segment has its individual sharp transition, which contributes to the shape memory effect at its sharp transition temperature. The incorporation of the segments demonstrates the multiple shape memory effect of the membrane.

The results of the shape recovery shown in figure 5.10 may shed some light on the distribution of the sharp transition temperatures of the molecule segments. It can be seen from the figure that the shape recovery reaches its peak at the programming temperature of ~ 80 °C. The shape recovery decreases when the programming temperature is away from ~ 80 °C towards both sides. The programming temperature can be also seen as the transition temperature. For example, the shape memory effect at ~ 80 °C results from the shape recovery of the molecule segments with the shape transition temperature of ~ 80 °C. Thus, it can be considered that the sharp transition temperature of the molecule segments mainly located at ~ 80 °C. With the sharp transition temperature being directed away from ~ 80 °C towards both sides, the amount of the molecule segments at the sharp transition temperature decreases. This method can be also used to study the shape memory effects of other ionic membranes with broad glass transitions.

5.5. Conclusion

In this study, we theoretically modeled and experimentally investigated the MSM-IPMC. A theoretical model was proposed to describe the multiple shape memory effect of the MSM-IPMC. Experiments were performed. The multiple shape memory properties of the MSM-IPMC was successfully demonstrated. By comparing the simulation results of the model and the experimental results, it is found that the model can well describe the shape memory effect. This work is useful for understanding the physical principles of the multiple shape memory effect of MSM-IPMC.

The multiple shape memory effect of different membranes with different ions were tested. The results of glass transition temperature, shape recovery and reversibility were presented. All the samples show good multiple shape memory effect and reversibility. It was

found that the membranes with the H^+ ions have the lowest glass transition temperature and shape recovery. The glass transition temperature and the shape recovery of the membranes with Na^+ ions are the highest. The membranes with the Li^+ ions are between them. A theory based on the enthalpy and free energy is proposed to explain this phenomenon. Furthermore, the shape recovery can be used to study the distribution of the sharp transition temperature of the membranes. The method is also beneficial for the study of other shape memory polymers.

With the electro-mechanical and thermo-mechanical actuation, the MSM-IPMC actuator is capable of deformability and maneuverability of multiple degrees of freedom - the complex twisting, bending, and oscillating motions – with thermal and electrical control simultaneously and separately [139]. In the future, a biomimetic soft robotic system will be developed based on the MSM-IPMC actuator.

Chapter 6. Development of a robotic fish actuated by MSM-IPMC

In this chapter, a preliminary work was published in the International Journal of Intelligent Robotics and Applications. The authors, in order of appearance on the article, are Tyler Stalbaum, Taeseon Hwang, Sarah Trabia, Qi Shen, Robert Hunt, Zakai Olsen, and Kwang J. Kim. This paper focuses on the development of an IPMC actuated soft fin that generates a travelling wave. This chapter is partially reprinted from “Tyler Stalbaum, Taeseon Hwang, Sarah Trabia, Qi Shen, Robert Hunt, Zakai Olsen, and Kwang J. Kim. Bioinspired traveling wave generation in soft-robotics using ionic polymer-metal composites. International Journal of Intelligent Robotics and Applications 1, no. 2 (2017): 167-179.” with the permission of Springer Publishing. The readers are referred to this article for a more in-depth description of the IPMC traveling wave fin fabrication.

6.1. Introduction

The IPMC has the advantages of large deformation, resilience and low actuation voltage [25], [29]. The water molecules contribute to the migration of the cations under the applied electric field, which causes the bending deformation of the IPMC actuator. Meanwhile, when the IPMC is mechanically deformed, the cations move along with the water molecules due to the imbalance of the electrical network within the polymer of the IPMC sensor. As a result, a detectable voltage is generated on the surface of the IPMC. Furthermore, the IPMC can be scaled down to less than 1 mm. Thus the IPMC is very suitable to work in water as micro actuators and sensors.

Scientists and engineers all over the world have developed many robotic systems based on the IPMC actuator. Biomimetic underwater robots such as robotic fish, robotic snake, and

robotic jellyfish have been developed [13], [164], [172]–[174]. Takagi et. al developed a rajiform swimming robot that mimics the swimming mode of ray fish [175]. Sixteen IPMCs were used for the two fins and on-board electrical devices were designed. The speed of the single fin was measured. Chen et. al developed a biomimetic robotic manta ray actuated by its pectoral fins [176]. The fins were designed based on the shape of real manta ray fin. Four IPMC strips with different sizes were attached to each fin for the actuation. Later Chen and his group members presented an IPMC actuated underwater robot that mimics the swimming motion of the manta ray [177]. The robot consists of two pectoral fins and each fin has an IPMC actuator of the polygonal shape and a passive soft film. The on-board control unit was developed. The robot was tested and the speed and power consumption was measured. A bioinspired bending/twisting fin enabled by IPMC was developed by Palmre et. al [113]. The IPMC actuators were integrated into a soft material and the fin performed complex deformation such as bending and twisting. Joel et. al presented a monolithic IPMC fin that is capable of complex deformation. The surface electrodes were patterned through the surface machining process [178]. Complex locomotion can be achieved by selectively actuating different surface regions.

Recently, Nafion, which is the intermediate layer of the IPMC, is reported to have the multiple shape memory effect [18]. It has a broad glass transition temperature, from ~ 55 °C to ~ 130 °C [33]. Multiple shapes can be programmed at random temperatures within the glass transition temperature. Upon reheating to those temperatures, the corresponding programmed shapes can be recovered. The crystalline segments, which work as physical crosslinks, hold the programmed shapes during each glass transition. In our previous work, we proposed a soft Multiple Shape Memory Ionic Polymer-Metal Composite (MSM-IPMC) actuator with multiple

degrees of freedom. By controlling two external inputs – electrical input and thermal input – the MSM-IPMC is able to perform the complex twisting, bending, and oscillating motions that are frequently observed in nature-made systems [139]. Potentially, it could be applied to medical devices and biomimetic robotics. To date, most of the robots reported before actuated by IPMCs is based on the electrical actuation effect.

In this work, I presented a biomimetic underwater robot, that was actuated by the MSM-IPMC. Compared with the previous robot, the robot in our study can not only propel itself based on the electrical actuation effect but also change its swimming modes based on the multiple shape memory effect. The design of the robot was inspired by the pectoral fish swimming modes, such as stingrays, knifefish and cuttlefish. Compared with caudal fish swimming modes, such as eel, mackerel and tuna, the pectoral fish based on the wave-like propulsion has the advantage of great maneuverability and good propulsive efficiency at low speeds [179]–[181]. The robot was actuated by two fins. Each fin consisted of six MSM-IPMC samples. A travelling wave was generated on the fin by actuating the MSM-IPMCs separately. Experiments were performed to test the robot. The displacement and the blocking force of the fin were measured. A flow channel with a force measurement system was implemented for the test of the robot. The thrusts under different frequencies and traveling wave numbers were recorded. The multiple shape memory effect was successfully demonstrated on the robot. The robot was capable of switching between Gymnotiform and Mobuliform swimming modes, which gives the robot high deformability, maneuverability and agility.

The organization of this chapter is as follows. Section 2 presents the materials and methods of our study. Section 3 shows the results. Section 4 concluded the study of this chapter.

6.2. Materials and Methods

6.2.1. Fabrication of MSM-IPMCs

The MSM-IPMCs used for this project were all fabricated in-house. The process can be broken down into five major steps: roughening the surface, cleaning process to remove impurities, impregnation of the platinum, primary plating, and secondary plating. The surface roughening step evens out the thickness of the Nafion membrane, while increasing the surface area for the platinum to impregnate. DuPont™ Nafion membranes were used. The membrane is cleaned with two baths: 3% hydrogen peroxide (H_2O_2) for removing organic impurities, and 1 M of sulfuric acid (H_2SO_4) for removing metallic impurities. Two deionized water (DI water) baths ensure that the membranes have been completely rinsed. The impregnation step uses a platinum salt solution ($Pt(NH_3)_4Cl_2 \cdot H_2O$) and the membrane is left in the solution for 3.5 hours, where it is flipped every half hour to ensure even impregnation. The primary plating process is a sodium borohydride bath, which plates the platinum onto the membrane. This is repeated three times with a cleaning process following each. The secondary plating process is a platinum solution bath and hydroxylamine hydrochloride ($H_2NOH \cdot HCl$) and hydrazine ($NH_2NH_2 \cdot H_2O$) are added every half hour. The electrode surface resistance is measured following each secondary plating, where the conductivity is considered high enough for good performance at resistance values of less than 10 ohms. The MSM-IPMC is then placed in a LiCl bath for 24 hours to reintroduce mobile cations, in this case Li^+ ions. The final plated MSM-IPMCs were of 0.36 mm thickness, 16.15 mm length and 2.65 mm width. A complete procedure is presented by Kim et al.[182].

6.2.2. Biomimetic underwater robot prototype

Figure 6.1 shows the robot prototype. The robot consists of three parts, which are the rigid robot shell, soft fins and off-board control circuit. The rigid body was designed in Solidworks and printed in a 3D printer (Form 2). Two soft fins were attached to the rigid body. From the biology view, many fish use undulating fins for auxiliary propulsions, as well as for stabilization and maneuvering. In median fins, each fin ray usually has a set of six muscles, which enable the fish to have the capability of locomotion in two degrees of freedom [179]. Six MSM-IPMC samples were used for each fin and were arranged in an array. Twelve MSM-IPMC samples in total were used. In Figure 6.1 the sequences of the MSM-IPMCs in the fin were labeled. A flexible substrate was adhered to create a surface along the structure. Based on this structure, lifting and drag forces can be generated when the waveform is excited. Silver pastes were pasted between the MSM-IPMCs and the electrodes to increase the conductivity.

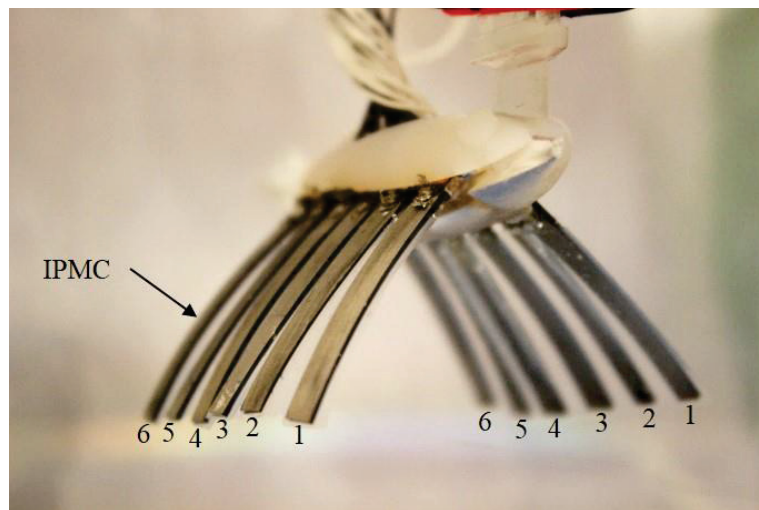


Figure 6.1 Prototype of the biomimetic robot.

An off-board control circuit was developed. Figure 6.2 shows the schematic of the control circuit. The Arduino MEGA microcontroller (ATmega2560) was used. By adjusting the potentiometer, the microcontroller can read the input signal and determine the corresponding output frequency. Six dual motor drivers (DRV8835 Dual Motor Driver Carrier, ROHM) were used to actuate the MSM-IPMC samples. The actuation voltages were supplied to the MSM-IPMCs through the flexible wires (Calmont). Each MSM-IPMC was connected by two wires. Twenty-four wires were connected to the robot in total. Through the microcontroller, the robot can perform the travelling wave on the fins. Meanwhile, by controlling the bias voltages on the IPMCs, twisting motions were generated on the fin. The control codes for the travelling wave motion and twisting motion are provided in Appendix E.

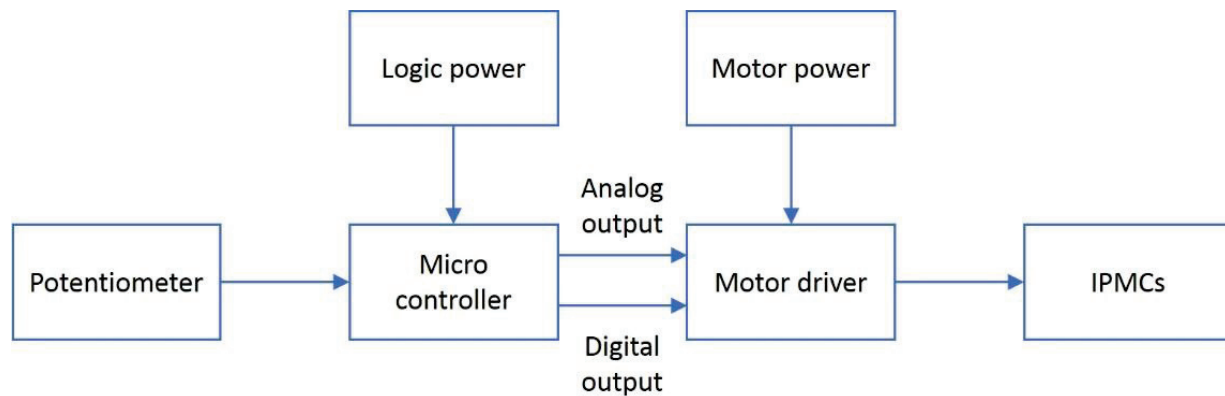


Figure 6.2 Schematic of the control circuit.

6.2.3. Displacement and blocking force

A sinusoid wave input voltage is utilized for driving the individual MSM-IPMCs. The control scheme is coded into the microcontroller for generating a traveling wave motion in an array of MSM-IPMCs. The input voltage to each MSM-IPMC can be expressed by:

$$V_i = A \sin \left[\omega t + \frac{2m\pi(i-1)}{N+1} \right] \quad (6.1)$$

where A is the amplitude of the input voltage, ω is the angular frequency and $\omega = 2\pi f$, f is the operating frequency, m is the number of waves, $N = 6$ is the total number of MSM-IPMCs in the fin, i is the order of the MSM-IPMC and $i = 1, 2, \dots, N$. The phase delay per sample is given as the fraction, $2m\pi(i-1)/(N+1)$, where the denominator can be adjusted for a different total phase shift between first and last MSM-IPMCs.

Performance testing and visualization experiments were done using the developed hardware with an external power supply (Agilent Technologies N5771A DC Power Supply) for running the motor drivers. The input voltage of the MSM-IPMCs was 5 V and the operating frequency was 0.5 Hz. Performance testing was carried out with a traveling wave microcontroller program to mimic similar motion to those used in biomimetic underwater robot design. Testing was performed in DI water.

MATLAB was used to track the position of the MSM-IPMC array. A specified mark is identified by being of regular shape, circular or rectangular, and of pronounced color. In this case a rectangular black marker is being tracked, that is, the tip of the individual MSM-IPMCs. The MATLAB code cross-references the previous frame to the new frame identifying the same marker. It uses an array of pixels to compare the array or matrix values between the two frames.

Additionally, a signal-to-noise cross-correlation between frames 1 and 2 are being used. Signal-to-noise ratio works best when the mark is half the size of the array of pixels and is dependent on initial frame signal-to-noise. Tracking of the rectangular shape and its centroid is being used. The centroid is obtained by computing a threshold, converting to binary and from there on calculated with such values.

The video is entered into the MATLAB code and decomposed into individual frames. The marker on the MSM-IPMC is chosen and frame-by-frame, the MATLAB program predicts the position of the marker in the next frame. This continues for all frames. The data is exported into excel and pixel-to-length and frame-to-time conversions are used to obtain correct position and time [120]. An offset is applied to the array by setting the initial positions of the individual MSM-IPMC's to zero. This is calculated by subtracting all values of an MSM-IPMC's vertical data by its initial value. The initial offset is due to two parts: (1) the offset in the selected zero position for the video analysis, and (2) the discrepancy between individual actuator performance and static resting positions. The data is then plotted, position versus time.

6.2.4. Thrust

The thrust force of the biomimetic underwater robot was measured. A horizontal low-velocity towing system was implemented. Figure 6.3 shows the illustration of the experimental apparatus. Driven by the motor, the carriage can move horizontally on the guide rail with the peak speed of 53.3 mm/s. The water tank was set under the guide rail and was filled with DI water. The robot and its affiliated components are fixed vertically under the towing system. A load cell with the measuring range of 1 N and a sensitivity of 0.01 N in the axial direction was mounted under the carriage. A 3D printed shaft was used to connect the robot and the load cell.

Based on the lever principle, the force on the robot was amplified by 70 times when it was transferred to the load cell. The robot was submerged under the water and was located at mid-depth in the tank. It has sufficient space in the tank to move without being affected by the free surface, boundaries on both sides and bottom of the tank. The control circuit was mounted above the water. Figure 6.3 shows the snapshot of the force measurement system.

The drag force of the robot was measured first. The robot was towed under the system with different speeds varying from 5 mm/s to 53 mm/s. Different drag forces of the robot were measured for different towing speeds. The force measured by the load cell is the drag force of the robot. The drag force can be expressed as [183]

$$F_d = \frac{1}{2} \rho_w A_c C_d v^2 \quad (6.2)$$

where ρ_w is the water density, A_c is the cross-section reference area of the robot, C_d is the form force coefficient, v is the towing velocity of the robot, A_c can be obtained from the 3D model of the robot, C_d is relevant to the robot shape and the Reynolds number and needs to be identified.

Then the thrust was measured. As shown in figure 6.4, the thrust force of the robot was measured at static state. The robot was actuated at different frequencies and wave numbers. The load cell measured the thrust force generated by the robot. LabVIEW was used to record the force signal from the load cell.

For comparison, an alternate method that measures the thrust of the robot was presented. Figure 6.5 shows the second method, where the robotic fish was towed at the prescribed speed. The force measured by the load cell is the resultant force $F_a = F_d - F_t$ applied on the robot, where the thrust force F_t and the drag force F_d acting on the robot simultaneously. Based on the

previously measured drag force F_d at the towing speed, the thrust force F_t can be obtained by $F_t = F_d - F_a$.

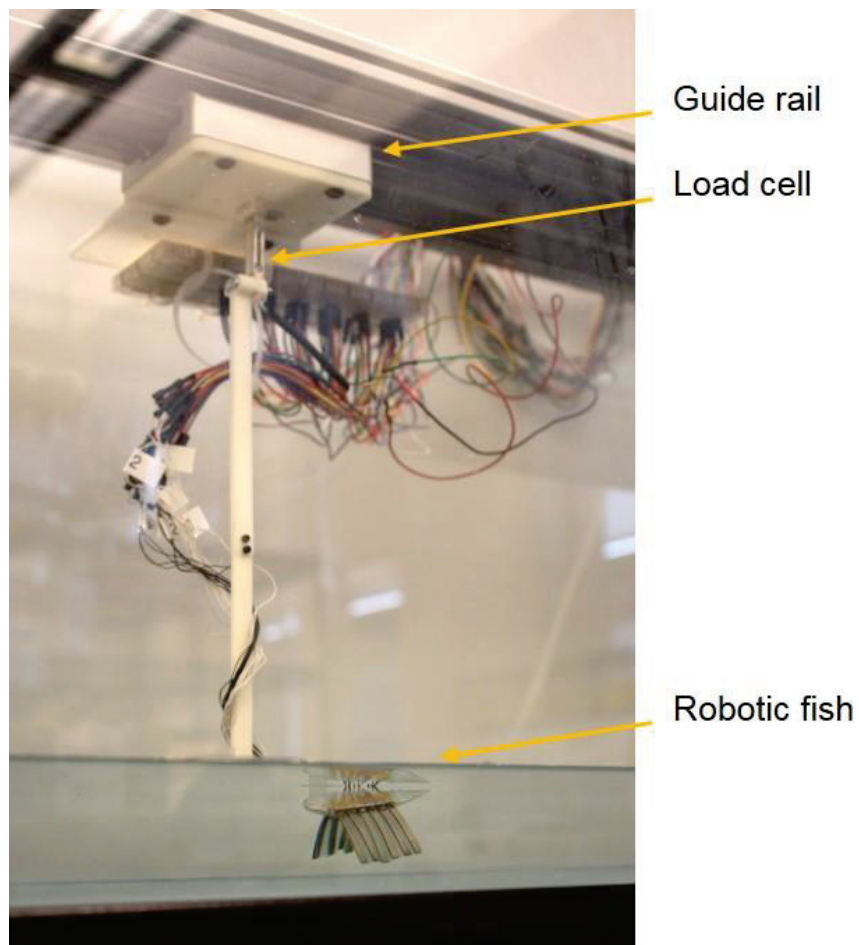


Figure 6.3 Snapshot of the thrust measurement system.

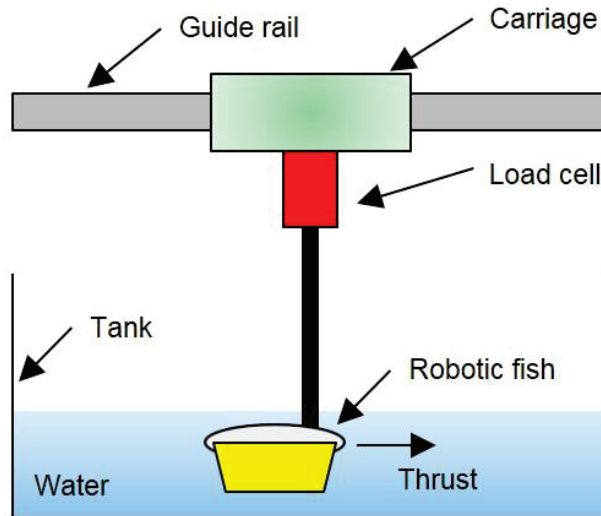


Figure 6.4 Illustration of the robot force measurement at static state.

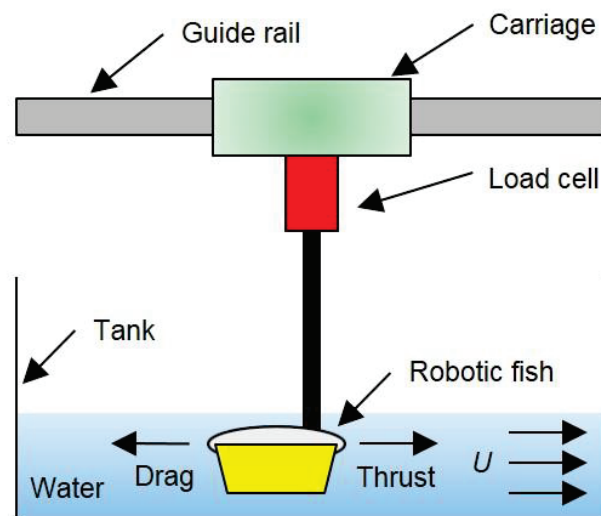


Figure 6.5 Illustration of the robot force measurement at prescribed speed.

6.2.5. Multiple shape memory effect

The multiple shape memory effect enables the MSM-IPMC to have a stable deformation.

This deformation shape is based on the programming shape and can be controlled through the

thermal input. In our study, the multiple shape memory effect was demonstrated on the biomimetic underwater robot, which allows the robot to have more maneuverability and agility. Figure 6.5 shows the illustration of the robot with different pectoral swimming modes. Based on the multiple shape memory effect, the robot can switch the swimming modes between the mobuliform and the gymnotiform, which was shown in figure 6.5 (a) and figure 6.5 (b) separately. The robot is capable of forward and backward motion based on the traveling waves generated on the fins.

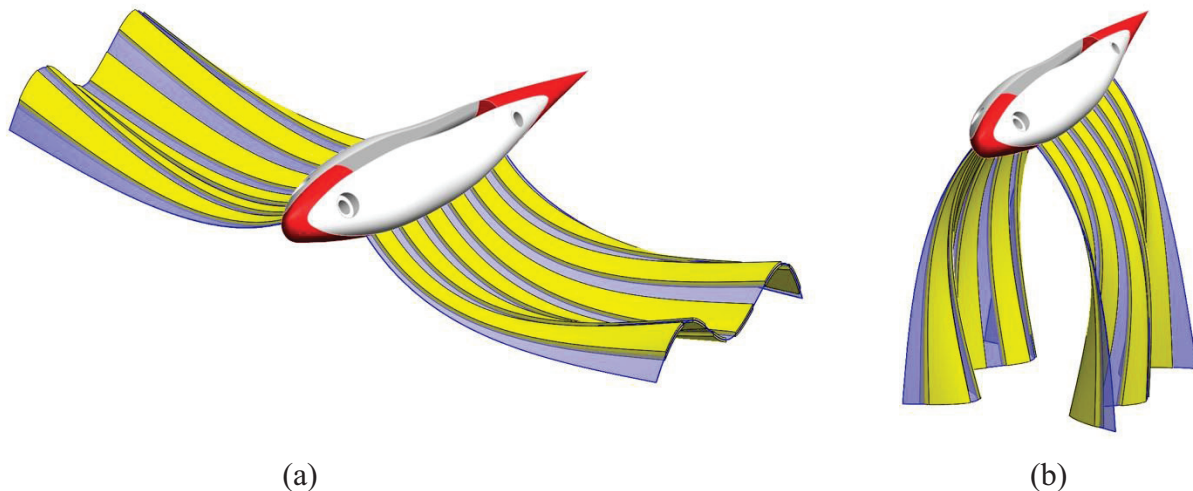


Figure 6.6 Biomimetic underwater robot with different pectoral swimming modes: (a) Mobuliform; (b) Gymnotiform.

Furthermore, by controlling the MSM-IPMCs on the fins separately, the fins on the robot can perform twisting motions. Figure 6.6 shows the twisting fins of the robot with different swimming modes. Combining with the twisting motion of the fins, the swimming modes of mobuliform allows the robot to have the motion in the pitch direction, while the robot in the gymnotiform can have the 2 degrees of the freedom movement in the horizontal direction.

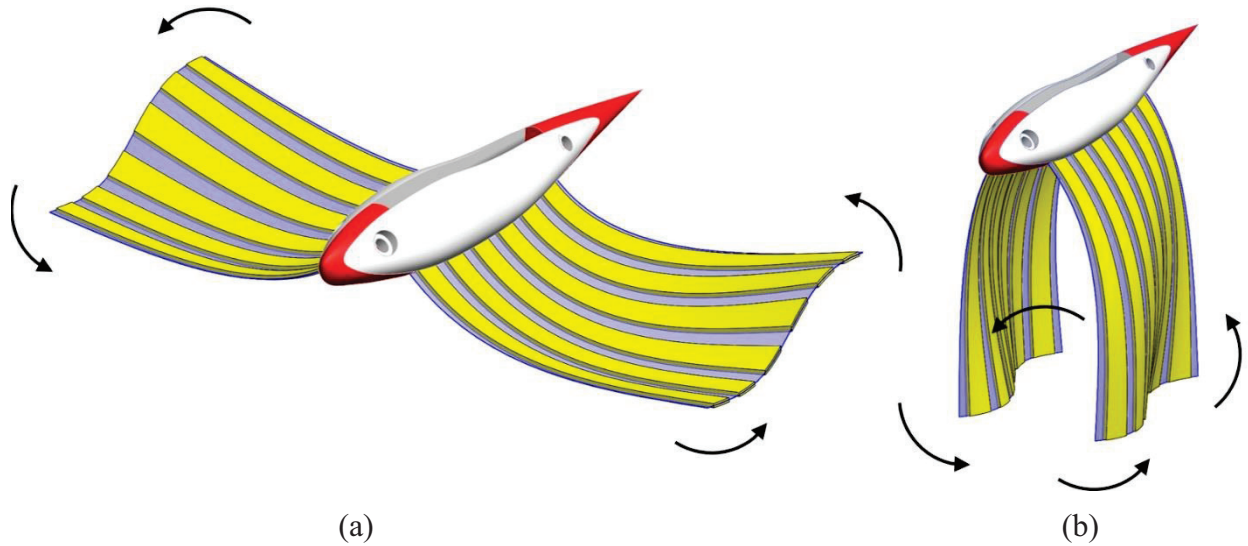
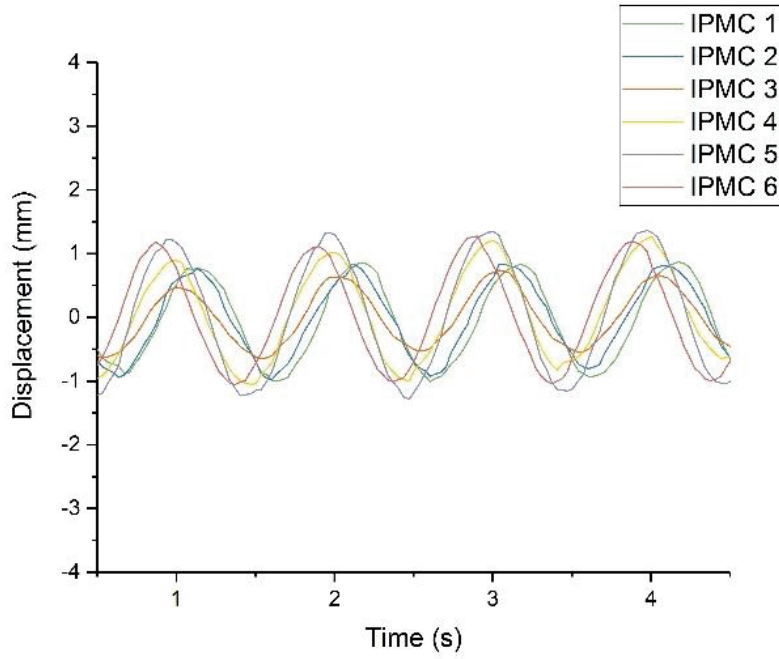


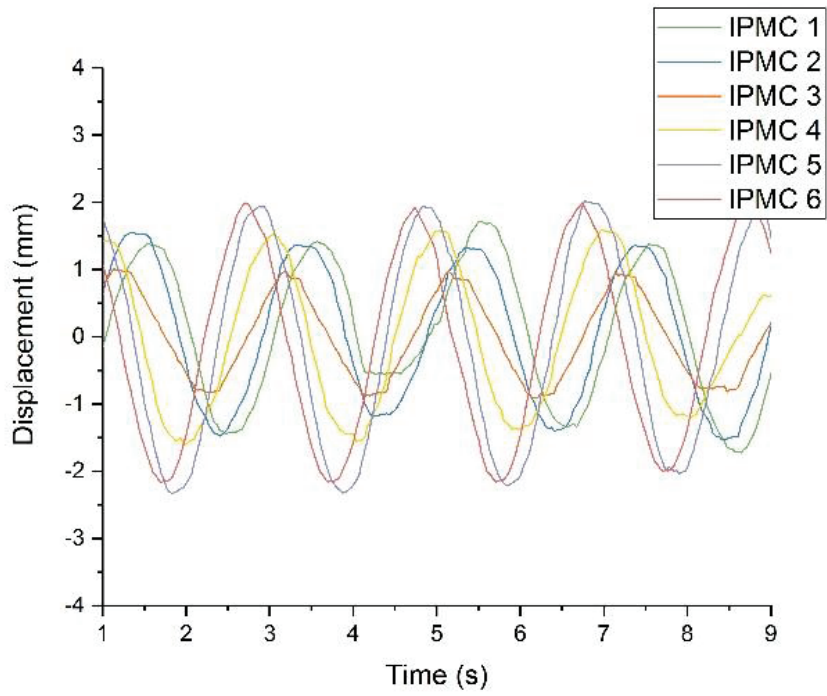
Figure 6.7 Twisting fins of the biomimetic underwater robot with different pectoral swimming modes: (a) Mobuliform; (b) Gymnotiform.

6.3. Results

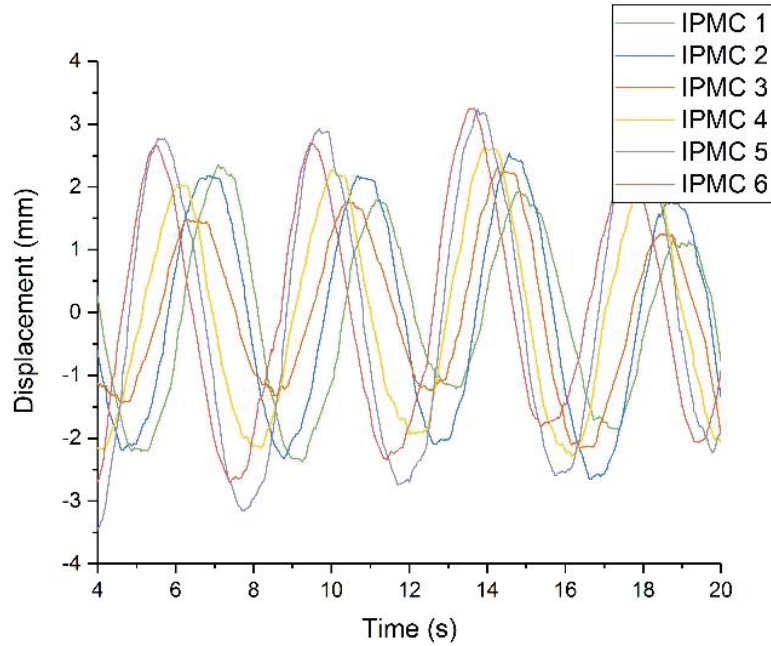
The deformation of each MSM-IPMC actuator in the robot's fin was measured. The experimental results were processed in MATLAB. Sinusoid electrical signals with phase differences were applied to each MSM-IPMC separately. Figure 6.7 shows the displacement of the traveling wave of one fin with $A = 5$ V, $m = 1$ and frequency $f = 1$ Hz, 0.5 Hz, 0.25 Hz. In general, the MSM-IPMCs have the sinusoid displacement with the amplitude from 2 mm to 6 mm. It can be noted that as the frequency decreases, the amplitudes of the MSM-IPMCs increases.



(a)



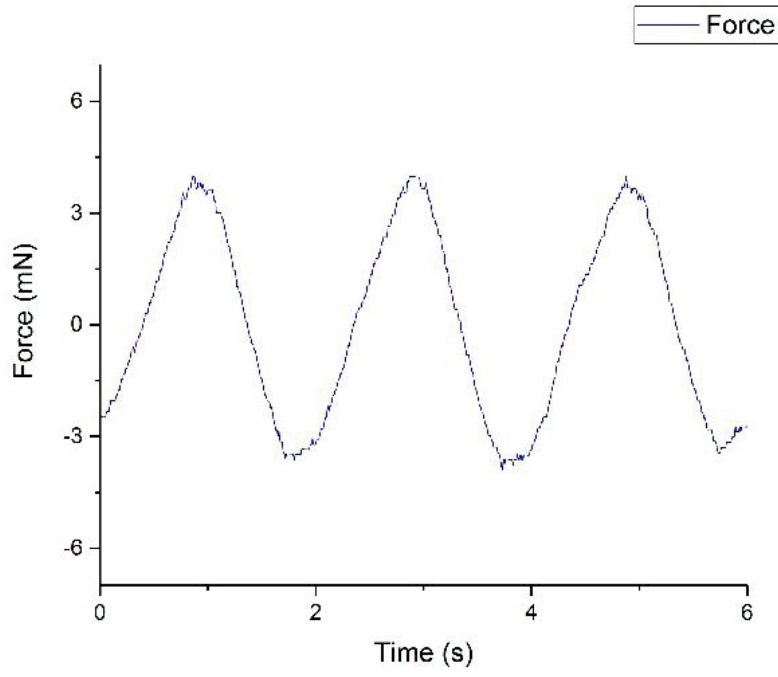
(b)



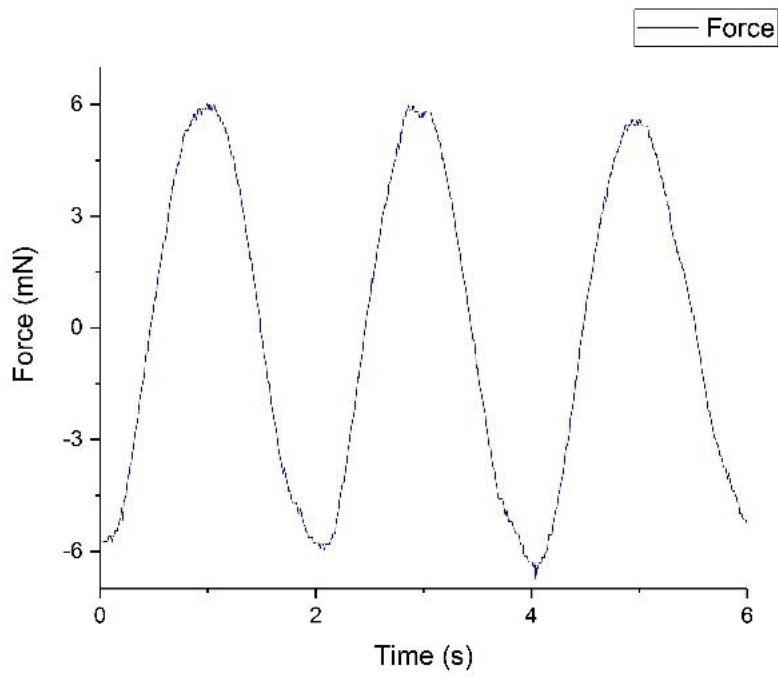
(c)

Figure 6.8 Deformation of the MSM-IPMCs in the soft fin at different frequencies: (a) 1 Hz; (b) 0.5 Hz; (c) 0.25 Hz.

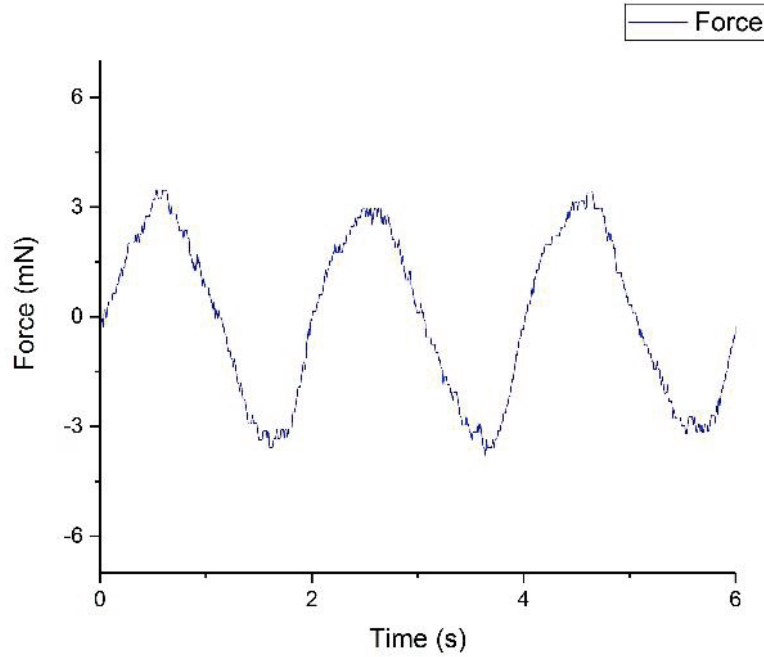
The blocking force of the fin was measured using the load cell. Figure 6.8 shows the blocking forces of different MSM-IPMCs in the fin. The MSM-IPMCs were actuated under the condition of $A = 5$ V, $m = 1$ and frequency $f = 0.5$ Hz. The blocking force of IPMC 1, IPMC 3 and IPMC 6 were presented respectively. Based on the results, a sinusoid variation of blocking force was noticed. The peak to peak force range of different MSM-IPMCs varies from 8 mN to 12 mN.



(a)



(b)



(c)

Figure 6.9 Blocking force of the MSM-IPMCs in the soft fin: (a) IPMC 1; (b) IPMC 3; (c) IPMC 6.

The drag force of the robot was measured. The robot was towed under the system with the speed varying from 5 mm/s to 53 mm/s. The MSM-IPMCs were not activated. Based on equation (6.2), the towing velocity v and the measured drag force F_d , the form force coefficient C_d was derived using the least-square method. Table 6.1 shows the parameters of the towing experiment. Figure 6.10 shows the experimental data and the theoretical prediction based on the identified C_d . It can be found that both the experimental and simulation results match well.

Table 6.1 Parameters of the towing experiment.

Parameter (Unit)	Value
A_c (m ²)	9.28×10^{-5}
C_d	0.0295
ρ_w (kg/m ³)	1000

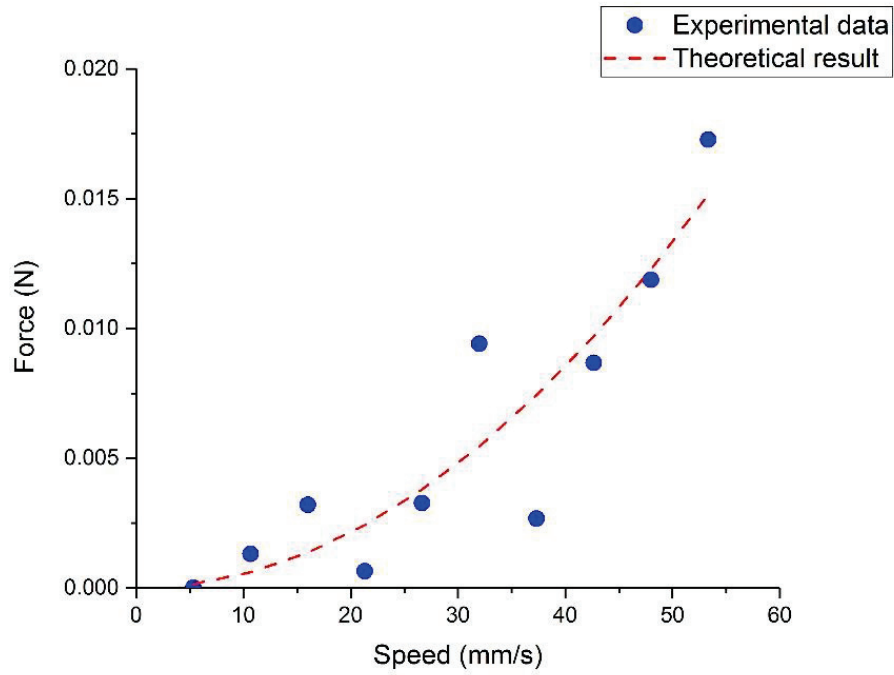


Figure 6.10 Experimental and theoretical results of the towing experiments.

The thrust force of the robot was measured under the towing system. The robot was activated at frequencies from 0.25 Hz to 2.5 Hz and wave numbers from 0.5 to 1.5. Figure 6.10 shows the thrust force of the robot at static state. It is noticed that the thrust force at wave

number $m = 1$ is higher than the thrust force at other wave numbers. Initially, the thrust force increases as the actuation frequency increase. The thrust reaches the peak at the frequency of 0.5 Hz. With the frequency continuing to increase, the thrust force decreases. The peak thrust force of the robot under static state is ~ 12 mN at the frequency of 0.5 Hz and wave number of 1.

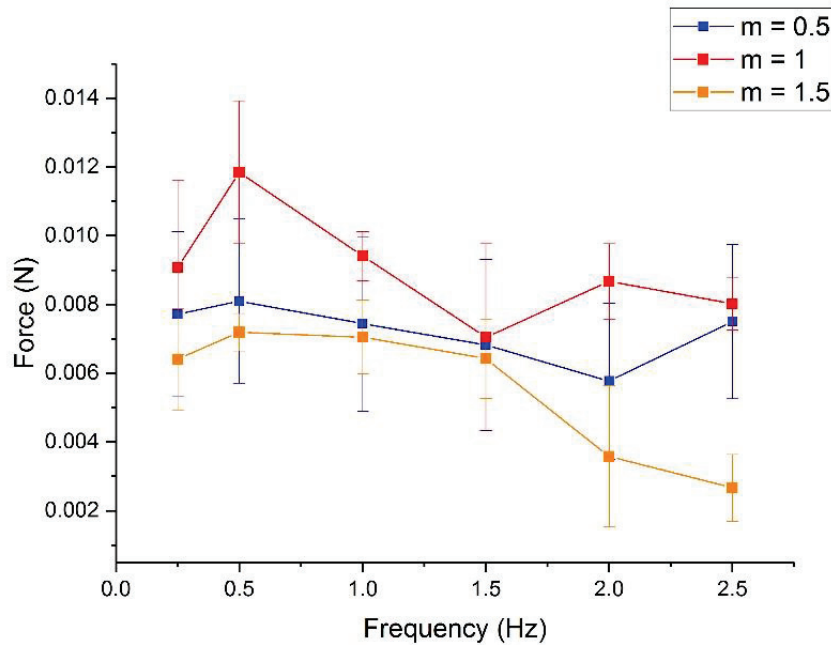


Figure 6.11 Experimental results of thrust force at static state.

Figure 6.12 shows the thrust force of the robot at prescribed velocity $U = 32$ mm/s. Compared with the thrust force at static state, a similar trend was found for both results. It can be also found that the thrust measured at static state is approximately 6% higher than the thrust at the prescribed velocity. The peak thrust force under the prescribed velocity is ~ 11 mN at the frequency of 0.5 Hz and wave number of 1, which is the same condition of the static state. One possible explanation of the thrust force at static state being higher than that at prescribed velocity

is that the traveling wave was generated when the robot was towed, which caused additional drag force on the robot. As a result, the thrust force was reduced due to the additional force.

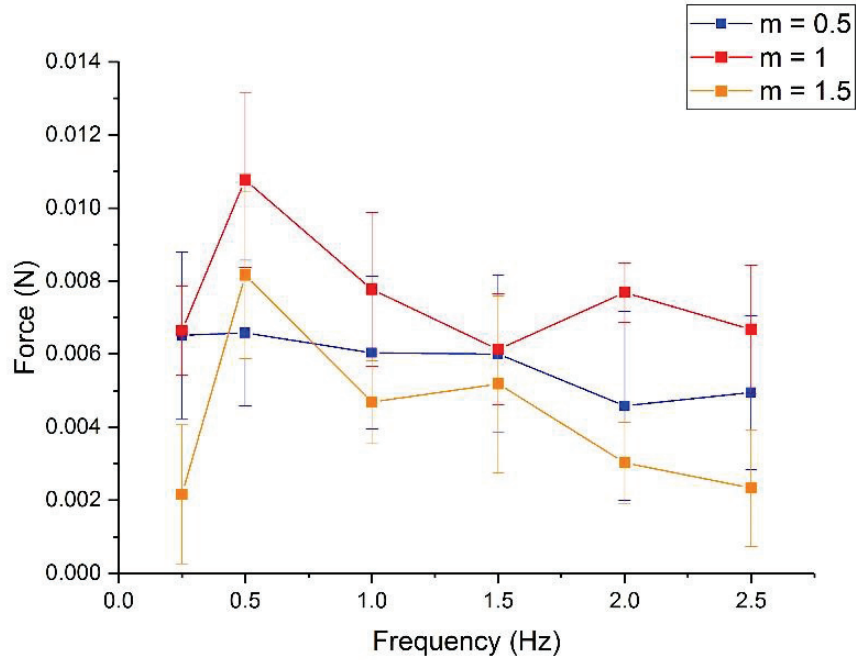


Figure 6.12 Experimental results of thrust force at prescribed towing velocity.

By controlling the MSM-IPMCs separately, the twisting deformation of the soft fin was achieved. Meanwhile, to achieve the propulsion, travelling waves were generated on the fins. Bias voltages were applied to the MSM-IPMCs. Based on Equation (6.1), the input voltages of the MSM-IPMCs from 1 to N can be rewritten as

$$V_i = A \sin \left[\omega t + \frac{2m\pi(i-1)}{N+1} \right] + 2.1 - 0.6i \quad (6.3)$$

where A is the amplitude of the voltage and $A = 2.5$ V. The rest are the same as before. Thus, forward or backward thrust can be obtained along the direction of the soft fins. Figure 6.13

shows the deformation of the soft fin. A maximum 30° of twisting was obtained. The displacement of each individual MSM-IPMC was measured using the image analysis. Figure 6.14 shows the displacements of the MSM-IPMCs during the twisting deformation. It can be seen that each MSM-IPMC has a general bending and oscillating motion with phase delay, which combined together to result in the twisting deformation of the soft fin with travelling wave on it.

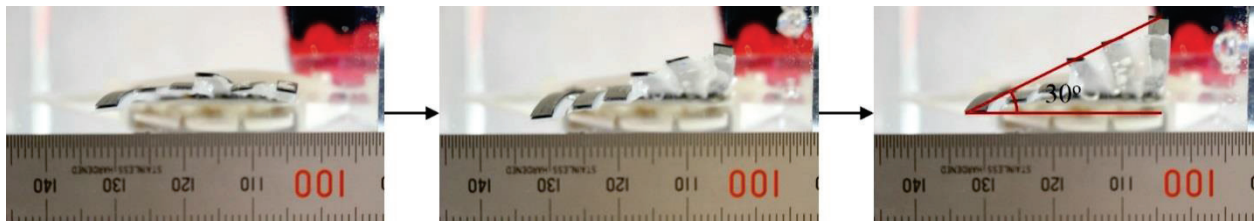


Figure 6.13 Twisting deformation of the soft fin.

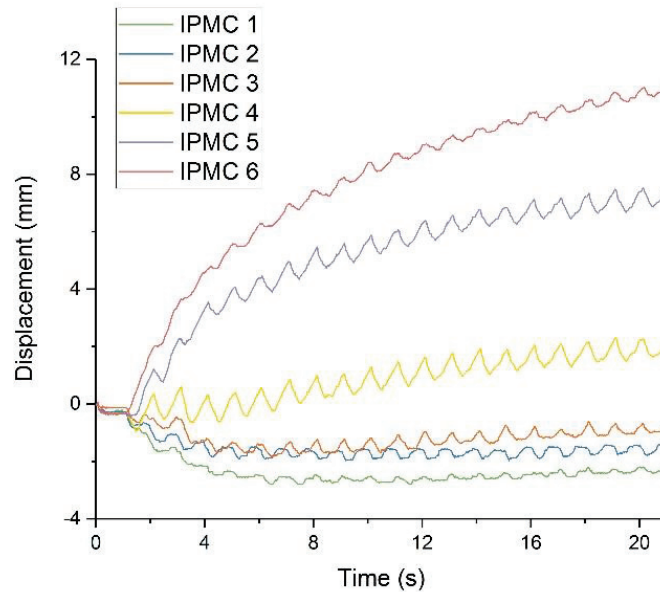
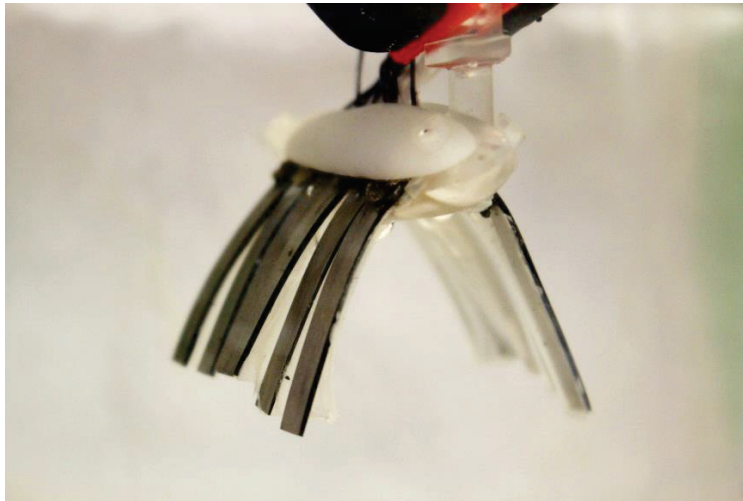


Figure 6.14 Displacement of the MSM-IPMCs during the twisting deformation.

The multiple shape memory effect was successfully demonstrated on the robot. To program the shape, the fins of the robot were fixed by the external components, which were 3D printed. Then the fixed fins were heated at 75 °C for 15 minutes and cooled at 60 °C for 5 minutes in water. Upon removing the external components, the shape of the fins was programmed. Two swimming mode shapes, which are the Mobuliform swimming mode and Gymnotiform swimming mode, were programmed separately. Figure 6.15 shows the biomimetic underwater robot with different programmed shapes. Figure 6.15 (a) shows the robot with Mobuliform swimming mode and Figure 6.15 (b) shows the Gymnotiform swimming mode of the robot. Combining with the twisting deformation of its soft fins, the robot has the potential capability of multiple-degrees-of-freedom locomotion in the water.



(a)



(b)

Figure 6.15 Programmed biomimetic underwater robot with different swimming modes: (a) Mobuliform; (b) Gymnotiform.

6.4. Conclusion

In this chapter, we presented a biomimetic underwater robot that is based on the MSM-IPMC. Inspired by the pectoral fish swimming modes, the robot was actuated by two soft fins. MSM-IPMCs were used as the skeleton on the fins. Travelling waves were generated on

the fins based on the electrical actuation effect of the MSM-IPMCs. The displacement and blocking force of the MSM-IPMCs on the fins were measured. A flow channel with force measurement system was implemented to test the robot. The drag force and thrust force of the robot were measured under the system. The maximum thrust force of 12 mN was measured at the frequency of 0.5 Hz and wave number of 1. The fins of robot show twisting deformation of 30°. Multiple shape memory effect was successfully demonstrated on the robot. The robot is capable of switching between the mobuliform and gymnotiform swimming modes based on the multiple shape memory effect, which give the robot various maneuvering capabilities.

In the current study, due to the restriction of the external wires, the robot was not able to swim freely in the water. Thus, the robot did not demonstrate its capability of motion in the 2 degrees of freedom horizontal and pitch direction. In the future, we will develop a robot which has the on-board control circuit and can swim freely in the water. Then the robot can show the electrical actuation and multiple shape memory effect simultaneously.

Chapter 7. Conclusion

In our work, we theoretically and experimentally investigated the MSM-IPMC. The electrical actuation and multiple shape memory effect of the MSM-IPMC actuators were studied separately. A physical model that considers the surface electrodes variation during the deformation of IPMC actuation was developed. The comparison of theoretical and experimental results indicates that the model can predict IPMC actuator behavior well. Furthermore, we proposed a soft MSM-IPMC actuator having multiple degrees-of-freedom and high maneuverability that can be thermally and electrically controlled. These multiple inputs allow for complex motions that are routine in nature, but that would be otherwise difficult to be achieved with a single actuator. Prior to the development of this novel actuator, this capability only could be realized with existing actuator technologies by using multiple actuators or another robotic system. To the best of our knowledge, this MSM-IPMC actuator is the first solitary actuator capable of multiple-input control and the resulting deformability and maneuverability. This technology can be applied to medical devices and biomimetic robotics. The underlying physics of the multiple shape memory effect was investigated. A physical model based on the free energy theory was developed to describe the shape memory behavior of MSM-IPMC. The multiple shape memory effect was theoretically investigated and a physics-based model that couples the electrical actuation effect and the multiple shape memory effect was presented. The simulation results show good agreement with experimental results. The multiple shape memory effect of the MSM-IPMC were characterized. A biomimetic underwater robot that is actuated by the MSM-IPMC was developed. The robot was experimentally tested under a flow channel and the thrust force was measured.

Chapter 8. Future work

The MSM-IPMC can perform high-frequency oscillation under the electrical input and stable multiple degrees of freedom deformation under the thermal input. These two deformations can be performed simultaneously and separately on a single actuator. New biomedical devices, microfluidics and soft robotic systems can be developed based on the MSM-IPMC actuator. As was mentioned above, different methods can be used to thermally control the actuator. For example, positive temperature coefficient heating film can be plated on the surface for the heating of the actuator. Figure 8.1 shows the process of screen printing.

Additionally, the physics of the multiple shape memory effect can be further explored. One method to solve this problem is to physically describe the motion of the molecule segments during the shape memory process. When the multiple shape memory effect and electrical actuation effect were performed simultaneously, the motion of the molecule segments induced by the heat may also have interactions with the migrating cations induced by the electrical field. The mobility of the cations may also be affected by the increasing temperature.

Finally, the biomimetic underwater robot developed in our study is based on the off-board control circuit. External wires connected to the robot affect the motion of the robot. In the future, we aim to develop a biomimetic underwater robot that is based on the on-board control circuit. Actuated by the MSM-IPMC actuator, the robot is propelled by the traveling wave. With the multiple shape memory effect and the electrical actuation effect, the robot is capable of high maneuverability, such as the motion in the pitch, left-right, forward and backward directions.

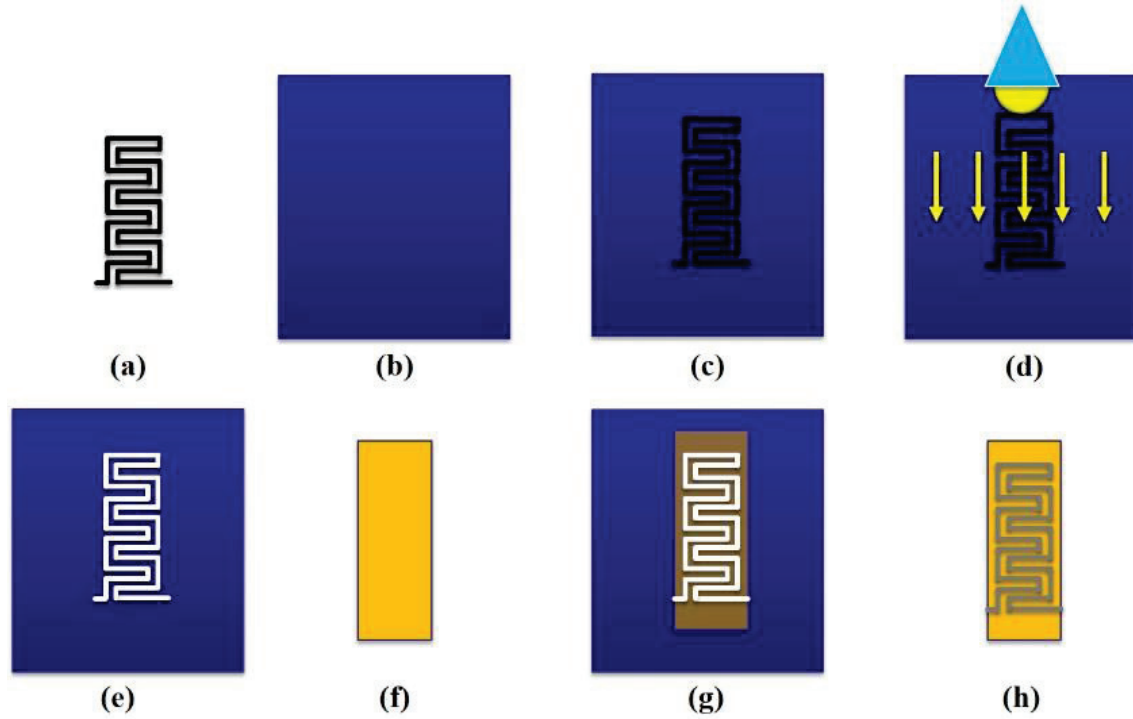


Figure 8.1 Screen printing process of MSM-IPMC.

(a) Prepare the mask for the screen printing. (b) Coat the screen. (c) Attach the mask to the screen. (d) Expose the screen to light. (e) Remove the mask and wash away the part covered by the mask. (f) Spray an isolating layer on the surface of IPMC. (g) Put the screen on top of the IPMC and print with PCT. (h) Remove the screen from IPMC.

Appendix A: Derivation of charge density

From Eq. (2.11), the expression of the local current density at an electrode boundary is

$$\begin{aligned} j(z, s) &= \frac{1}{h} \int_{-h/2}^{h/2} f(x, z, s) dx \\ &= -\frac{DC(z, s)}{h} \left(\frac{2 \sinh(A(s)h)}{A(s)} + 2h \cosh(A(s)h) \right) \left(\frac{A(s)}{F} - \frac{FC_0}{RT\hat{\epsilon}A(s)} \right). \end{aligned} \quad (\text{A.1})$$

Combing Eqs. (2.7), (2.8) and (2.10), one can obtain [74]

$$\phi(x, z, s) = -2 \frac{C(z, s) \sinh(A(s)x)}{\hat{\epsilon}A^2(s)} - 2C(z, s) \cosh(A(s)h) \left(\frac{RTA(s)}{F^2C_0} - \frac{1}{\hat{\epsilon}A(s)} \right) x. \quad (\text{A.2})$$

With Eqs. (2.12), (A.1) and (A.2), the electric potential at the boundary of IPMC element can be rewritten as

$$\begin{aligned} \frac{V(s)}{2} + \int_0^z \frac{DC(\tilde{z}, s)}{h} \left(\frac{2 \sinh(A(s)h)}{A(s)} + 2h \cosh(A(s)h) \right) \left(\frac{A(s)}{F} - \frac{FC_0}{RT\hat{\epsilon}A(s)} \right) W_e h_e R_e(w(L, s)) \frac{d\tilde{z}}{L} \\ = -2 \frac{C(z, s) \sinh(A(s)h)}{\hat{\epsilon}A^2(s)} - 2C(z, s) \cosh(A(s)h) \left(\frac{RTA(s)}{F^2C_0} - \frac{1}{\hat{\epsilon}A(s)} \right) h \end{aligned} \quad (\text{A.3})$$

Then by solving Eq. (A.3) the expression of the $C(z, s)$ is derived as

$$C(z, s) = -\frac{\exp(J(s, w(L, s))z/L)}{K(s)} V(s) \quad (\text{A.4})$$

and $\rho(x, z, s)$ can be obtained as

$$\rho(x, z, s) = -G(z, s) \sinh(A(s)x) V(s). \quad (\text{A.5})$$

Appendix B: Derivation of deformation

With the linear beam theory, the tip displacement of the IPMC beam element relating to the z can be denoted as

$$\frac{d^2 w(z, s)}{dz^2} = \frac{M(z, s)}{YI}. \quad (\text{B.1})$$

The angle of the curved beam element is denoted as

$$\tan d\varphi(z, s) = \frac{dw(z, s)}{dz}. \quad (\text{B.2})$$

Since $dw(z, s) \ll dL$, one can rewrite Eq. (B.2) as

$$d\varphi(z, s) = \frac{dw(z, s)}{dz}. \quad (\text{B.3})$$

The slope at the tip of the IPMC beam element is expressed as

$$\frac{d\varphi(z, s)}{dz} = \frac{d^2 w(z, s)}{dz^2}. \quad (\text{B.4})$$

By integrating the tip displacements of the elements, one can obtain the deformation of the IPMC as

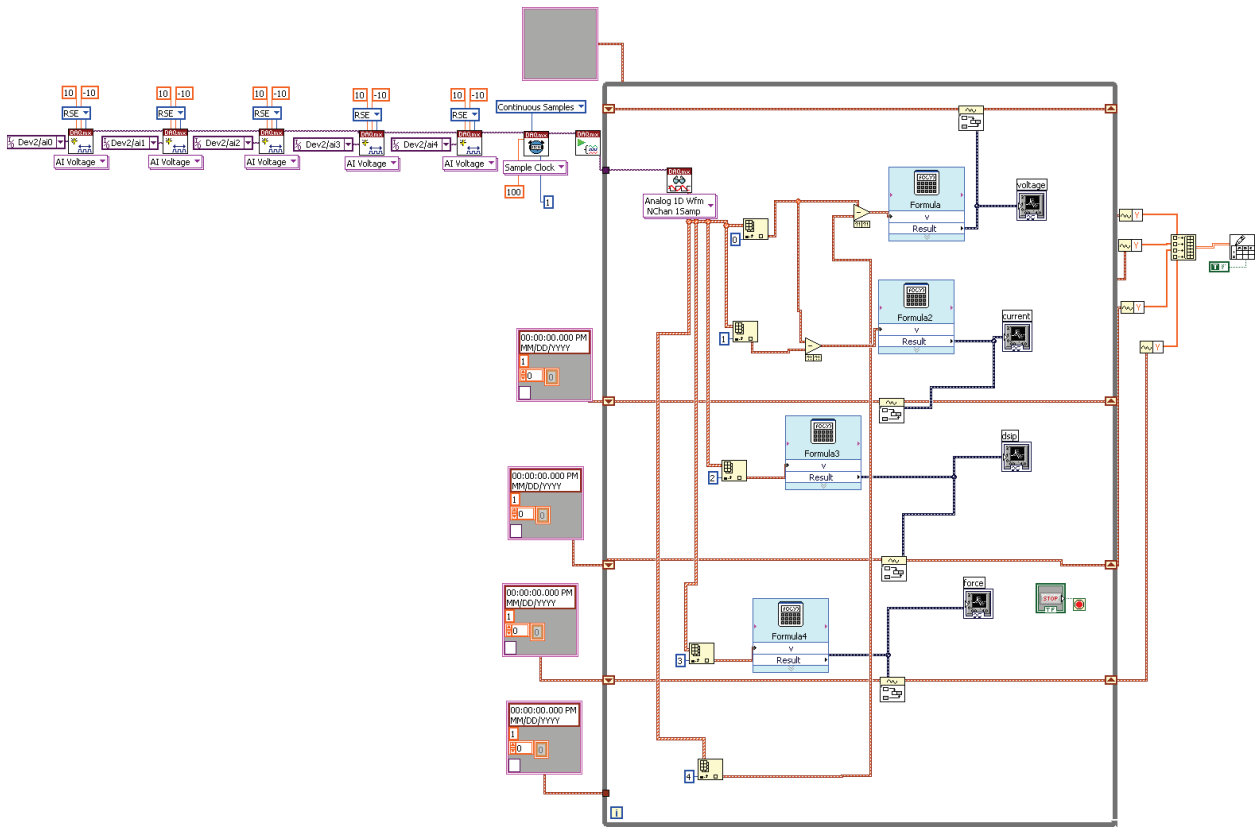
$$w(L, s) = \int_0^L dz \left(d\varphi(z, s) + \frac{d\varphi(z, s)}{dz} \right). \quad (\text{B.5})$$

Solving Eq. (B.5) with boundary conditions $w(0, s) = 0$ and $\frac{dw(0, s)}{dz} = 0$, one can obtain

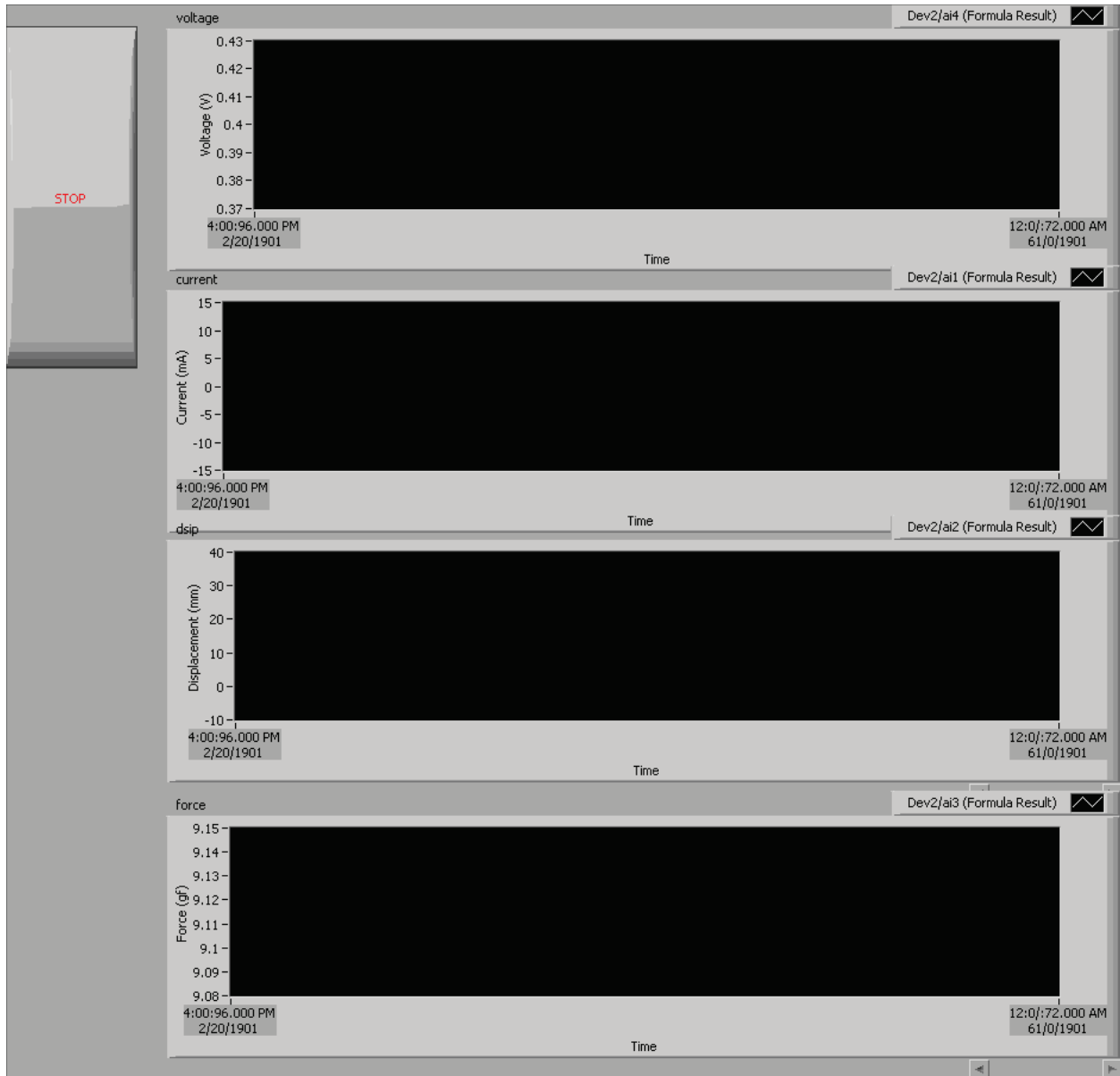
$$w(L, s) = \frac{\alpha L}{hY} \frac{(-\exp(J(s, w(L, s))) + J(s, w(L, s)) + 2)}{J(s, w(L, s))K(s)} \sinh(A(s)h) \mathcal{V}(s) \left(1 + \frac{1}{J(s, w(L, s))} \right). \quad (\text{B.6})$$

Appendix C: LabVIEW set up

The LabVIEW was set up for the experimental test of the actuator. The input voltage, current, displacement and blocking force of the actuator can be recorded simultaneously through the LabVIEW. Furthermore, the thermal couple was integrated into the measurement system. The temperature can be measured as well. All the sensors were calibrated. Figure C.1 shows the LabVIEW set up.



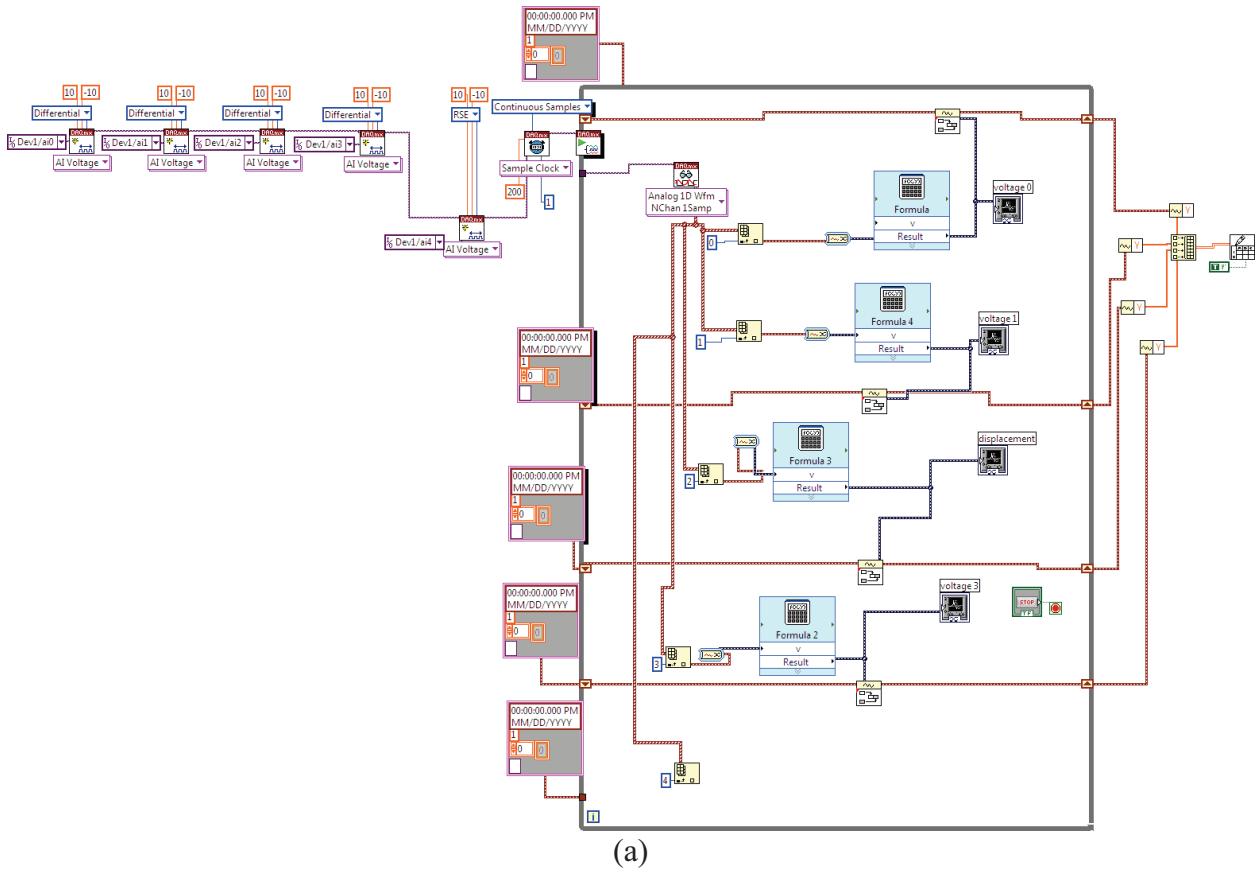
(a)



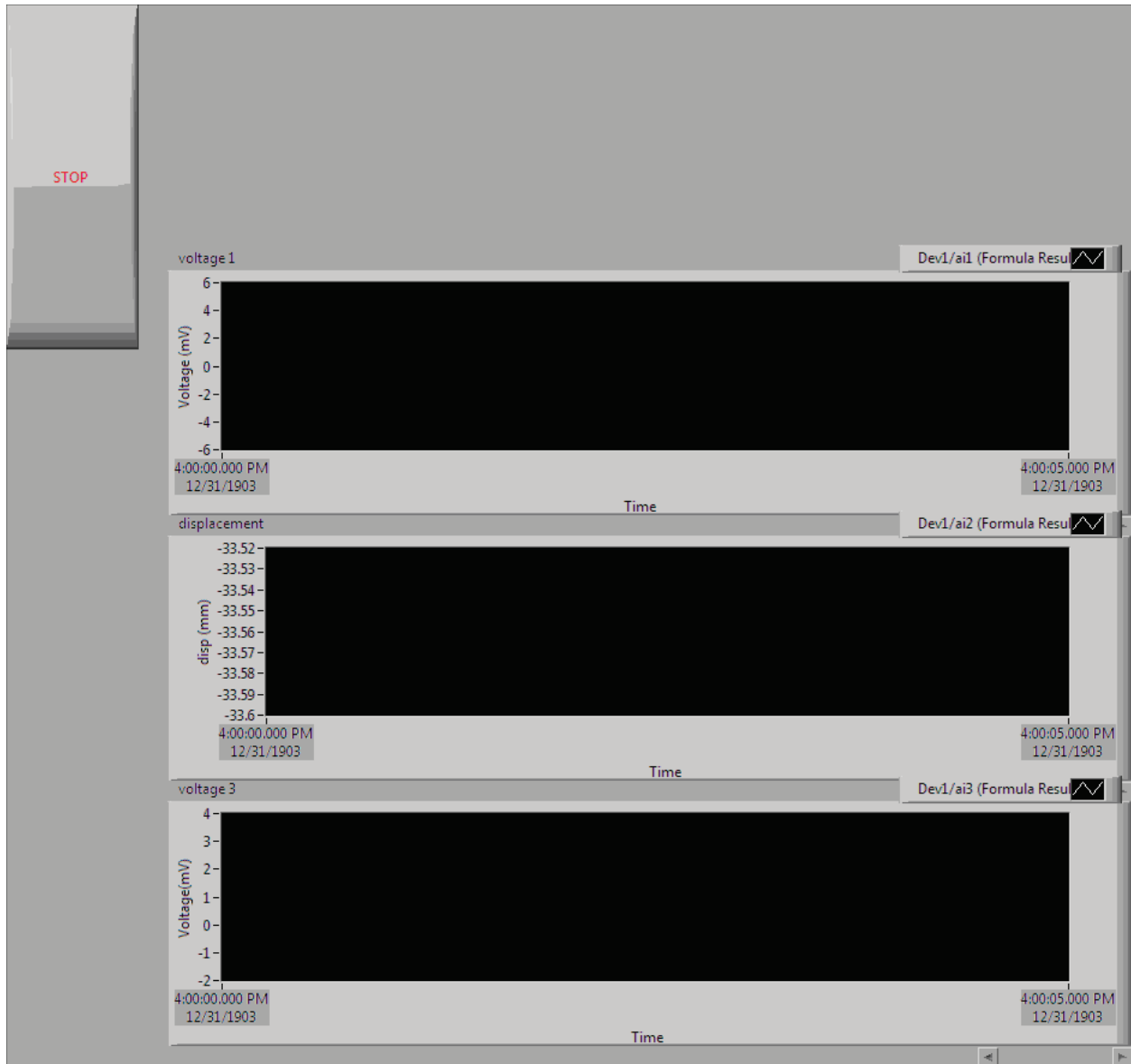
(b)

Figure C.1 LabVIEW set up for the actuator test: (a) Block diagram; (b) Front panel.

The sensing characteristics of the smart material can be tested through the LabVIEW. The output voltage, displacement and current of the actuator can be recorded simultaneously through the LabVIEW. All the sensors were calibrated. Figure C.2 shows the LabVIEW set up.



(a)

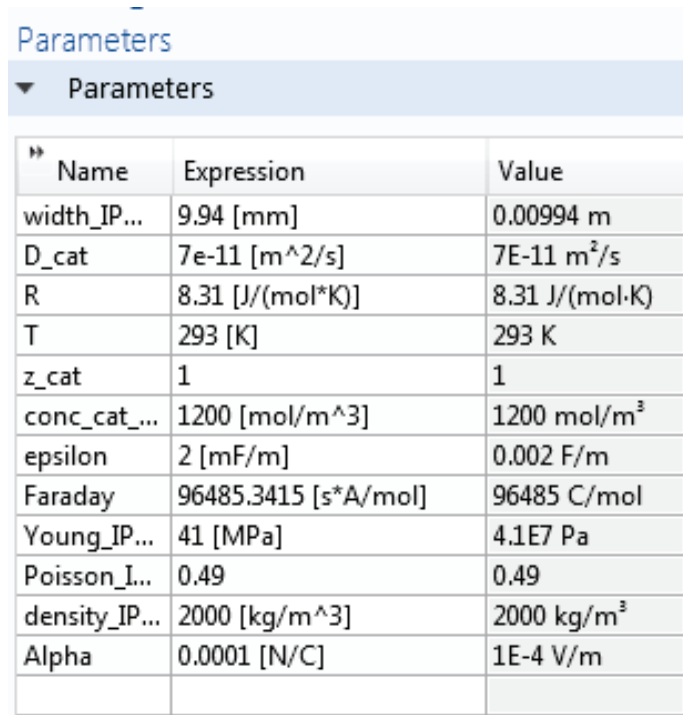


(b)

Figure C.2 LabVIEW set up for the sensor test: (a) Block diagram; (b) Front panel.

Appendix D: Modeling of the IPMC in COSMOL

This work was in cooperate with Tyler Stalbaum. The IPMC actuator was modeled in 2D utilizing COSMOL Multiphysics 4.3b software. In the Model Wizard, the first component includes Electric Current (ec), Transport of Diluted Species (tds) and General Form PDE (g), which was used to simulate the charge dynamics inside the polymer. The second component is Solid Mechanics (solid), which simulated the solid mechanics of the IPMC beam. The parameters of the model were presented in Figure D.1.



Name	Expression	Value
width_IP...	9.94 [mm]	0.00994 m
D_cat	7e-11 [m ² /s]	7E-11 m ² /s
R	8.31 [J/(mol·K)]	8.31 J/(mol·K)
T	293 [K]	293 K
z_cat	1	1
conc_cat...	1200 [mol/m ³]	1200 mol/m ³
epsilon	2 [mF/m]	0.002 F/m
Faraday	96485.3415 [s·A/mol]	96485 C/mol
Young_IP...	41 [MPa]	4.1E7 Pa
Poisson_I...	0.49	0.49
density_IP...	2000 [kg/m ³]	2000 kg/m ³
Alpha	0.0001 [N/C]	1E-4 V/m

Figure D.1 Parameters of the model.

Then the geometry and boundary conditions of the model were defined, as shown in Figure D.2. Meshes were generated separated for each component. Figure D.3 shows the Model Builder of the model. The simulations of the components were performed individually in the

study, which were all time dependent. Then the results can be obtained. The displacement of the IPMC actuator was presented in Figure D.4.

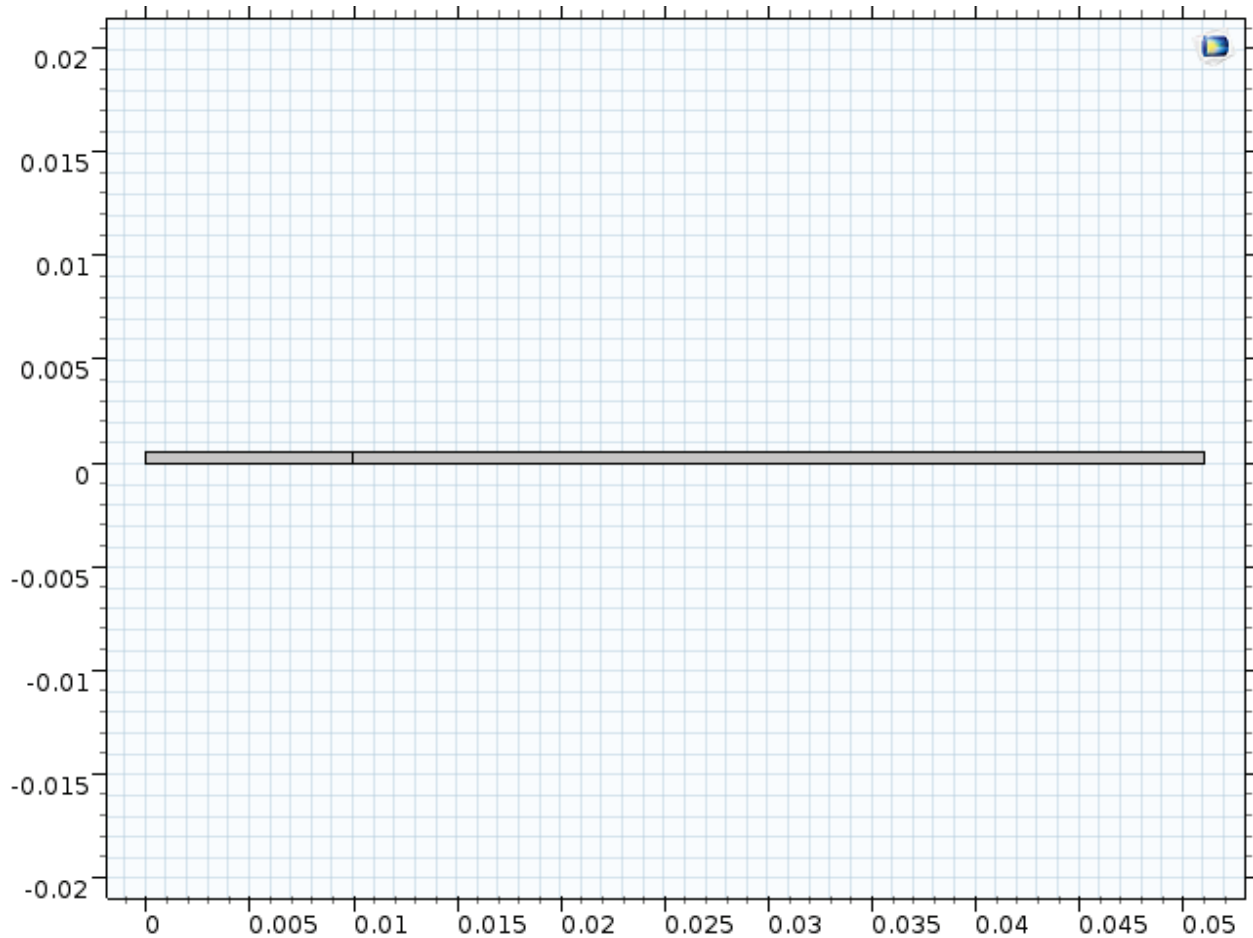


Figure D.2 Geometry of the model.

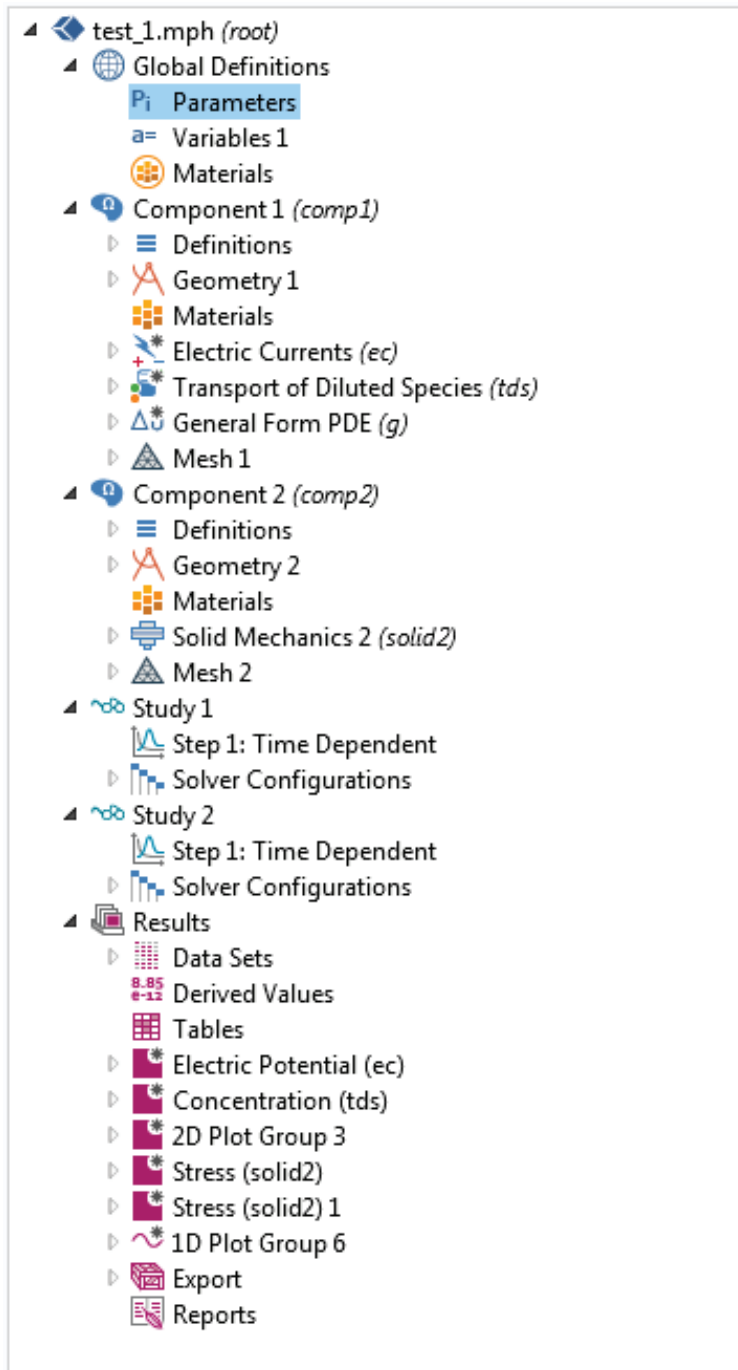


Figure D.3 The Model Builder of the model.

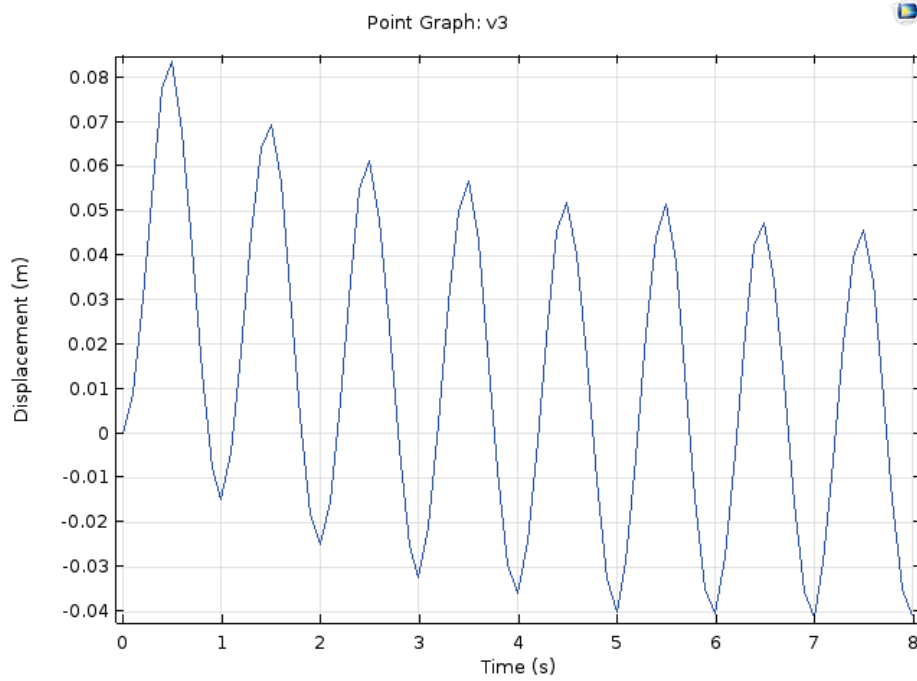


Figure D.4 Displacement of the IPMC actuator.

Appendix E: Robotic fish control code

1) Travelling wave motion control:

```
unsigned int long t0;

double v1,v2,v3,v4,v5,v6,v7,v8,v9,v10;

double v1m,v2m,v3m,v4m,v5m,v6m,v7m,v8m,v9m,v10m;

double CW,CCW,V,CW1,CW2,CW3,CW4,CW5,CW6,CW7,CW8,CW9,CW10;

double omega= 0.5*PI;

double omega1 = 0.5*PI;

double omega2 = 1*PI;

double omega3 = 2*PI;

double phatol=10;

double phase1=0;

double phase2=2*PI/phatol;

double phase3=4*PI/phatol;

double phase4=6*PI/phatol;

double phase5=8*PI/phatol;

double phase6=10*PI/phatol;

double tt=1000;

int pot = 0;

double pval = omega;
```

```

//double phase7=12*PI/phaol;

int buttonstate;

//double phase8=14*PI/phaol;

//double phase9=16*PI/phaol;

//double phase10=18*PI/phaol;

void setup() {

pinMode(2,OUTPUT); //analog motor driver 1
pinMode(3,OUTPUT); //analog motor driver 2
pinMode(4,OUTPUT); //analog motor driver 3
pinMode(5,OUTPUT); //analog motor driver 4
pinMode(6,OUTPUT); //analog motor driver 5
pinMode(7,OUTPUT); //analog motor driver 6

pinMode(A0,INPUT); //control omega

//pinMode(10,OUTPUT); //analog motor driver 7
//pinMode(11,OUTPUT); //analog motor driver 8
//pinMode(12,OUTPUT); //analog motor driver 9
//pinMode(13,OUTPUT); //analog motor driver 10
pinMode(33,OUTPUT); // digital cw motor driver 1
pinMode(35,OUTPUT); // digital cw motor driver 2

```

```

pinMode(37,OUTPUT); // digital cw motor driver 3
pinMode(39,OUTPUT); // digital cw motor driver 4
pinMode(41,OUTPUT); // digital cw motor driver 5
pinMode(43,OUTPUT); // digital cw motor driver 6
pinMode(32,OUTPUT); // digital cwr motor driver 1
pinMode(34,OUTPUT); // digital cwr motor driver 2
pinMode(36,OUTPUT); // digital cwr motor driver 3
pinMode(38,OUTPUT); // digital cwr motor driver 4
pinMode(40,OUTPUT); // digital cwr motor driver 5
pinMode(42,OUTPUT); // digital cwr motor driver 6
//pinMode(36,OUTPUT); // digital cw motor driver 7
//pinMode(38,OUTPUT); // digital cw motor driver 8
//pinMode(40,OUTPUT); // digital cw motor driver 9
//pinMode(42,OUTPUT); // digital cw motor driver 10
Serial.begin(9600);
pinMode(22,INPUT);
}
void loop() {
t0=millis();
omega = pval;
if(omega < 0.1*PI) omega = 0.1*PI;
Serial.println(omega/PI);

```

```

buttonstate = digitalRead(22);

while(millis()-t0<tt/omega*PI*2){

//while(true){

//pval = map(double(analogRead(A0)),0,1023,0.1*PI,10.0*PI);
pval = mapOmega();
if (buttonstate > 0){
v1=map(500*sin(omega*(millis()-t0)/tt+phase1),-500,500,-255,255);
v2=map(500*sin(omega*(millis()-t0)/tt+phase2),-500,500,-255,255);
v3=map(500*sin(omega*(millis()-t0)/tt+phase3),-500,500,-255,255);
v4=map(500*sin(omega*(millis()-t0)/tt+phase4),-500,500,-255,255);
v5=map(500*sin(omega*(millis()-t0)/tt+phase5),-500,500,-255,255);
v6=map(500*sin(omega*(millis()-t0)/tt+phase6),-500,500,-255,255);
//v7=map(500*sin(omega*(millis()-t0)/1000+phase7),-500,500,-255,255);
//v8=map(500*sin(omega*(millis()-t0)/1000+phase8),-500,500,-255,255);
//v9=map(500*sin(omega*(millis()-t0)/1000+phase9),-500,500,-255,255);
//v10=map(500*sin(omega*(millis()-t0)/1000+phase10),-500,500,-255,255);
v1m=detdirV(33,32,v1);

```



```

v2m=detdirV(35,34,v2);
v3m=detdirV(37,36,v3);
v4m=detdirV(39,38,v4);
v5m=detdirV(41,40,v5);
v6m=detdirV(43,42,v6);
//v7m=detdirV(36,v7);
//v8m=detdirV(38,v8);
//v9m=detdirV(40,v9);
//v10m=detdirV(42,v10);
analogWrite(2,v1m);
analogWrite (3,v2m);
analogWrite (4,v3m);
analogWrite (5,v4m);
analogWrite (6,v5m);
analogWrite (7,v6m);
//analogWrite (10,v7m);
//analogWrite (11,v8m);
//analogWrite (12,v9m);
//analogWrite (13,v10m);
}
else
{v6=map(500*sin(omega*(millis()-t0)/tt+phase1),-500,500,-255,255);

```

```

v5=map(500*sin(omega*(millis()-t0)/tt+phase2),-500,500,-255,255);
v4=map(500*sin(omega*(millis()-t0)/tt+phase3),-500,500,-255,255);
v3=map(500*sin(omega*(millis()-t0)/tt+phase4),-500,500,-255,255);
v2=map(500*sin(omega*(millis()-t0)/tt+phase5),-500,500,-255,255);
v1=map(500*sin(omega*(millis()-t0)/tt+phase6),-500,500,-255,255);
//v1=map(500*sin(omega*(millis()-t0)/1000+phase7),-500,500,-255,255);
//v8=map(500*sin(omega*(millis()-t0)/1000+phase8),-500,500,-255,255);
//v9=map(500*sin(omega*(millis()-t0)/1000+phase9),-500,500,-255,255);
//v10=map(500*sin(omega*(millis()-t0)/1000+phase10),-500,500,-255,255);
v1m=detdirV(33,32,v1);
v2m=detdirV(35,34,v2);
v3m=detdirV(37,36,v3);
v4m=detdirV(39,38,v4);
v5m=detdirV(41,40,v5);
v6m=detdirV(43,42,v6);
//v7m=detdirV(36,v7);
//v8m=detdirV(38,v8);
//v9m=detdirV(40,v9);
//v10m=detdirV(42,v10);
analogWrite(2,v1m);
analogWrite (3,v2m);
analogWrite (4,v3m);

```

```

analogWrite (5,v4m);
analogWrite (6,v5m);
analogWrite (7,v6m);
//analogWrite (10,v7m);
//analogWrite (11,v8m);
//analogWrite (12,v9m);
//analogWrite (13,v10m);}}
//Serial.println(v1m);
//Serial.print("\t");
//Serial.println(v1);
}}}

double detdirV(int CW, int CWR, double V){
    double abs(V);
    if(V<0){
        digitalWrite(CW,HIGH);
        digitalWrite(CWR,HIGH);
        // digitalWrite(CCW,LOW);
        return 255 - abs(V);
    }
    else{
        digitalWrite(CW,LOW);

```

```

digitalWrite(CWR,LOW);
// digitalWrite(CCW,HIGH);
return abs(V);
}
}

double mapOmega(){
if(analogRead(A0) < 333) return omega1;
else if(analogRead(A0) < 666) return omega2;
else return omega3;
}

```

2) Twisting motion control:

```

unsigned int long t0;
double v1,v2,v3,v4,v5,v6,v7,v8,v9,v10;
double v1m,v2m,v3m,v4m,v5m,v6m,v7m,v8m,v9m,v10m;
double CW,CCW,V,CW1,CW2,CW3,CW4,CW5,CW6,CW7,CW8,CW9,CW10;
double omega=1*PI;
double phatol=10;
double phase1=0;
double phase2=2*PI/phatol;

```

```

double phase3=4*PI/phatol;

double phase4=6*PI/phatol;

double phase5=8*PI/phatol;

double phase6=10*PI/phatol;

//double phase7=12*PI/phatol;

int buttonstate;

//double phase8=14*PI/phatol;

//double phase9=16*PI/phatol;

//double phase10=18*PI/phatol;

void setup() {

pinMode(2,OUTPUT); //analog motor driver 1

pinMode(3,OUTPUT); //analog motor driver 2

pinMode(4,OUTPUT); //analog motor driver 3

pinMode(5,OUTPUT); //analog motor driver 4

pinMode(6,OUTPUT); //analog motor driver 5

pinMode(7,OUTPUT); //analog motor driver 6

//pinMode(10,OUTPUT); //analog motor driver 7

//pinMode(11,OUTPUT); //analog motor driver 8

//pinMode(12,OUTPUT); //analog motor driver 9

//pinMode(13,OUTPUT); //analog motor driver 10

pinMode(33,OUTPUT); // digital cw motor driver 1

```

```
pinMode(35,OUTPUT); // digital cw motor driver 2
pinMode(37,OUTPUT); // digital cw motor driver 3
pinMode(39,OUTPUT); // digital cw motor driver 4
pinMode(41,OUTPUT); // digital cw motor driver 5
pinMode(43,OUTPUT); // digital cw motor driver 6
pinMode(32,OUTPUT); // digital cwr motor driver 1
pinMode(34,OUTPUT); // digital cwr motor driver 2
pinMode(36,OUTPUT); // digital cwr motor driver 3
pinMode(38,OUTPUT); // digital cwr motor driver 4
pinMode(40,OUTPUT); // digital cwr motor driver 5
pinMode(42,OUTPUT); // digital cwr motor driver 6
//pinMode(36,OUTPUT); // digital cw motor driver 7
//pinMode(38,OUTPUT); // digital cw motor driver 8
//pinMode(40,OUTPUT); // digital cw motor driver 9
//pinMode(42,OUTPUT); // digital cw motor driver 10
Serial.begin(9600);
pinMode(22,INPUT);
}
void loop() {
t0=millis();

buttonstate = digitalRead(22);
```

```

//while(millis()-t0<1000){
while(true){
  if (buttonstate > 0){
v1=map(500*sin(omega*(millis()-t0)/1000+phase1),-500,500,0,255);
v2=map(500*sin(omega*(millis()-t0)/1000+phase2),-500,500,-51,204);
v3=map(500*sin(omega*(millis()-t0)/1000+phase3),-500,500,-102,153);
v4=map(500*sin(omega*(millis()-t0)/1000+phase4),-500,500,-153,102);
v5=map(500*sin(omega*(millis()-t0)/1000+phase5),-500,500,-204,51);
v6=map(500*sin(omega*(millis()-t0)/1000+phase6),-500,500,-255,0);
//v7=map(500*sin(omega*(millis()-t0)/1000+phase7),-500,500,-255,0);
//v8=map(500*sin(omega*(millis()-t0)/1000+phase8),-500,500,-255,255);
//v9=map(500*sin(omega*(millis()-t0)/1000+phase9),-500,500,-255,255);
//v10=map(500*sin(omega*(millis()-t0)/1000+phase10),-500,500,-255,255);
v1m=detdirV(33,32,v1);
v2m=detdirV(35,34,v2);
v3m=detdirV(37,36,v3);
v4m=detdirV(39,38,v4);
v5m=detdirV(41,40,v5);
v6m=detdirV(43,42,v6);
//v7m=detdirV(36,v7);
//v8m=detdirV(38,v8);

```

```

//v9m=detdirV(40,v9);
//v10m=detdirV(42,v10);
analogWrite(2,v1m);
analogWrite (3,v2m);
analogWrite (4,v3m);
analogWrite (5,v4m);
analogWrite (6,v5m);
analogWrite (7,v6m);
//analogWrite (10,v7m);
//analogWrite (11,v8m);
//analogWrite (12,v9m);
//analogWrite (13,v10m);
}
else
{
v6=map(500*sin(omega*(millis()-t0)/1000+phase1),-500,500,0,255);
v5=map(500*sin(omega*(millis()-t0)/1000+phase2),-500,500,-51,204);
v4=map(500*sin(omega*(millis()-t0)/1000+phase3),-500,500,-102,153);
v3=map(500*sin(omega*(millis()-t0)/1000+phase4),-500,500,-153,102);
v2=map(500*sin(omega*(millis()-t0)/1000+phase5),-500,500,-204,51);
v1=map(500*sin(omega*(millis()-t0)/1000+phase6),-500,500,-255,0);
//v1=map(500*sin(omega*(millis()-t0)/1000+phase7),-500,500,-255,0);

```



```
//v8=map(500*sin(omega*(millis()-t0)/1000+phase8),-500,500,-255,255);  
//v9=map(500*sin(omega*(millis()-t0)/1000+phase9),-500,500,-255,255);  
//v10=map(500*sin(omega*(millis()-t0)/1000+phase10),-500,500,-255,255);  
v1m=detdirV(33,32,v1);  
v2m=detdirV(35,34,v2);  
v3m=detdirV(37,36,v3);  
v4m=detdirV(39,38,v4);  
v5m=detdirV(41,40,v5);  
v6m=detdirV(43,42,v6);  
//v7m=detdirV(36,v7);  
//v8m=detdirV(38,v8);  
//v9m=detdirV(40,v9);  
//v10m=detdirV(42,v10);  
analogWrite(2,v1m);  
analogWrite (3,v2m);  
analogWrite (4,v3m);  
analogWrite (5,v4m);  
analogWrite (6,v5m);  
analogWrite (7,v6m);  
//analogWrite (10,v7m);  
//analogWrite (11,v8m);  
//analogWrite (12,v9m);
```

```

//analogWrite (13,v10m);} }
//Serial.println(v1m);
//Serial.print("\t");
//Serial.println(v1);
}}}

double detdirV(int CW, int CWR, double V){
    double abs(V);
    if(V<0){
        digitalWrite(CW,HIGH);
        digitalWrite(CWR,HIGH);
        // digitalWrite(CCW,LOW);
        return 255-abs(V);
    }
    else{
        digitalWrite(CW,LOW);
        digitalWrite(CWR,LOW);
        // digitalWrite(CCW,HIGH);
        return abs(V);
    }
}
}

```

Appendix F: Copyright Permission Approvals

IOP Publishing LICENSE TERMS AND CONDITIONS

Oct 17, 2017

This is a License Agreement between University of Nevada, Las Vegas (UNLV) -- Qi Shen ("You") and IOP Publishing ("IOP Publishing") provided by Copyright Clearance Center ("CCC"). The license consists of your order details, the terms and conditions provided by IOP Publishing, and the payment terms and conditions.

All payments must be made in full to CCC. For payment instructions, please see information listed at the bottom of this form.

License Number	4200921059837
License date	Sep 27, 2017
Licensed content publisher	IOP Publishing
Licensed content title	Smart Materials and Structures
Licensed content date	Jan 1, 1992
Type of Use	Thesis/Dissertation
Requestor type	Academic institution
Format	Print, Electronic
Portion	chapter/article
Title or numeric reference of the portion(s)	Theoretical and experimental investigation of the shape memory properties of an ionic polymer-metal composite
Title of the article or chapter the portion is from	Theoretical and experimental investigation of the shape memory properties of an ionic polymer-metal composite
Editor of portion(s)	N/A
Author of portion(s)	Qi Shen
Volume of serial or monograph.	26

Issue, if republishing an article from a serial 045020

Page range of the portion

Publication date of portion 9 March 2017

Rights for Main product

Duration of use Life of current edition

Creation of copies for the disabled no

With minor editing privileges no

For distribution to Worldwide

In the following language(s) Original language of publication

With incidental promotional use no

The lifetime unit quantity of new product Up to 499

Made available in the following markets

The requesting person/organization is: Qi Shen

Order reference number

Author/Editor

Title of New Work

Publisher of New Work

Expected publication date Dec 2017

Estimated size (pages)

Total (may include CCC user fee) 0.00 USD

Terms and Conditions

TERMS AND CONDITIONS

The following terms are individual to this publisher:

These special terms and conditions are in addition to the standard terms and conditions for CCC's Reproduction Service and, together with those standard terms and conditions, govern the use of the Works.

As the User you will make all reasonable efforts to contact the author(s) of the article which the Work is to be reused from, to seek consent for your intended use. Contacting one author who is acting expressly as authorised agent for their co-author(s) is acceptable.

User will reproduce the following wording prominently alongside the Work:

- the source of the Work, including author, article title, title of journal, volume number, issue number (if relevant), page range (or first page if this is the only information available) and date of first publication. This information can be contained in a footnote or reference note; and
- a link back to the article (via DOI); and
- if practicable, and IN ALL CASES for new works published under any of the Creative Commons licences, the words “© IOP Publishing. Reproduced with permission. All rights reserved”

Without the express permission of the author(s) and the Rightsholder of the article from which the Work is to be reused, User shall not use it in any way which, in the opinion of the Rightsholder, could: (i) distort or alter the author(s)’ original intention(s) and meaning; (ii) be prejudicial to the honour or reputation of the author(s); and/or (iii) imply endorsement by the author(s) and/or the Rightsholder.

This licence does not apply to any article which is credited to another source and which does not have the copyright line ‘© IOP Publishing Ltd’. User must check the copyright line of the article from which the Work is to be reused to check that IOP Publishing Ltd has all the necessary rights to be able to grant permission. User is solely responsible for identifying and obtaining separate licences and permissions from the copyright owner for reuse of any such third party material/figures which the Rightsholder is not the copyright owner of. The Rightsholder shall not reimburse any fees which User pays for a republication license for such third party content.

This licence does not apply to any material/figure which is credited to another source in the Rightsholder’s publication or has been obtained from a third party. User must check the Version of Record of the article from which the Work is to be reused, to check whether any of the material in the Work is third party material. Third party citations and/or copyright notices and/or permissions statements may not be included in any other version of the article from which the Work is to be reused and so cannot be relied upon by the User. User is solely responsible for identifying and obtaining separate licences and permissions from the copyright owner for reuse of any such third party material/figures where the Rightsholder is not the copyright owner. The Rightsholder shall not reimburse any fees which User pays for a republication license for such third party content.

User and CCC acknowledge that the Rightsholder may, from time to time, make changes or additions to these special terms and conditions without express notification, provided that these shall not apply to permissions already secured and paid for by User prior to such change or addition.

User acknowledges that the Rightsholder (which includes companies within its group and third parties for whom it publishes its titles) may make use of personal data collected through the service in the course of their business.

If User is the author of the Work, User may automatically have the right to reuse it under the rights granted back when User transferred the copyright in the article to the Rightsholder. User should check the copyright form and the relevant author rights policy to check whether permission is required. If User is the author of the Work and does require

permission for proposed reuse of the Work, User should select ‘Author of requested content’ as the Requestor Type. The Rightsholder shall not reimburse any fees which User pays for a republication license.

If User is the author of the article which User wishes to reuse in User’s thesis or dissertation, the republication licence covers the right to include the Accepted Manuscript version (not the Version of Record) of the article. User must include citation details and, for online use, a link to the Version of Record of the article on the Rightsholder’s website. User may need to obtain separate permission for any third party content included within the article. User must check this with the copyright owner of such third party content. User may not include the article in a thesis or dissertation which is published by ProQuest. Any other commercial use of User’s thesis or dissertation containing the article would also need to be expressly notified in writing to the Rightsholder at the time of request and would require separate written permission from the Rightsholder.

User does not need to request permission for Work which has been published under a CC BY licence. User must check the Version of Record of the CC BY article from which the Work is to be reused, to check whether any of the material in the Work is third party material and so not published under the CC BY licence. User is solely responsible for identifying and obtaining separate licences and permissions from the copyright owner for reuse of any such third party material/figures. The Rightsholder shall not reimburse any fees which User pays for such licences and permissions.

As well as CCC, the Rightsholder shall have the right to bring any legal action that it deems necessary to enforce its rights should it consider that the Work infringes those rights in any way.

For STM Signatories ONLY (as agreed as part of the STM Guidelines)

Any licence granted for a particular edition of a Work will apply also to subsequent editions of it and for editions in other languages, provided such editions are for the Work as a whole in situ and do not involve the separate exploitation of the permitted illustrations or excerpts.

Other Terms and Conditions:

STANDARD TERMS AND CONDITIONS

1. Description of Service; Defined Terms. This Republication License enables the User to obtain licenses for republication of one or more copyrighted works as described in detail on the relevant Order Confirmation (the “Work(s)”). Copyright Clearance Center, Inc. (“CCC”) grants licenses through the Service on behalf of the rightsholder identified on the Order Confirmation (the “Rightsholder”). “Republication”, as used herein, generally means the inclusion of a Work, in whole or in part, in a new work or works, also as described on the Order Confirmation. “User”, as used herein, means the person or entity making such republication.

2. The terms set forth in the relevant Order Confirmation, and any terms set by the Rightsholder with respect to a particular Work, govern the terms of use of Works in connection with the Service. By using the Service, the person transacting for a republication license on behalf of the User represents and warrants that he/she/it (a) has been duly authorized by the User to accept, and hereby does accept, all such terms and conditions on behalf of User, and (b) shall inform User of all such terms and conditions. In the event such person is a “freelancer” or other third party independent of User and CCC, such party shall

be deemed jointly a “User” for purposes of these terms and conditions. In any event, User shall be deemed to have accepted and agreed to all such terms and conditions if User republishes the Work in any fashion.

3. Scope of License; Limitations and Obligations.

3.1 All Works and all rights therein, including copyright rights, remain the sole and exclusive property of the Rightsholder. The license created by the exchange of an Order Confirmation (and/or any invoice) and payment by User of the full amount set forth on that document includes only those rights expressly set forth in the Order Confirmation and in these terms and conditions, and conveys no other rights in the Work(s) to User. All rights not expressly granted are hereby reserved.

3.2 General Payment Terms: You may pay by credit card or through an account with us payable at the end of the month. If you and we agree that you may establish a standing account with CCC, then the following terms apply: Remit Payment to: Copyright Clearance Center, 29118 Network Place, Chicago, IL 60673-1291. Payments Due: Invoices are payable upon their delivery to you (or upon our notice to you that they are available to you for downloading). After 30 days, outstanding amounts will be subject to a service charge of 1-1/2% per month or, if less, the maximum rate allowed by applicable law. Unless otherwise specifically set forth in the Order Confirmation or in a separate written agreement signed by CCC, invoices are due and payable on “net 30” terms. While User may exercise the rights licensed immediately upon issuance of the Order Confirmation, the license is automatically revoked and is null and void, as if it had never been issued, if complete payment for the license is not received on a timely basis either from User directly or through a payment agent, such as a credit card company.

3.3 Unless otherwise provided in the Order Confirmation, any grant of rights to User (i) is “one-time” (including the editions and product family specified in the license), (ii) is non-exclusive and non-transferable and (iii) is subject to any and all limitations and restrictions (such as, but not limited to, limitations on duration of use or circulation) included in the Order Confirmation or invoice and/or in these terms and conditions. Upon completion of the licensed use, User shall either secure a new permission for further use of the Work(s) or immediately cease any new use of the Work(s) and shall render inaccessible (such as by deleting or by removing or severing links or other locators) any further copies of the Work (except for copies printed on paper in accordance with this license and still in User's stock at the end of such period).

3.4 In the event that the material for which a republication license is sought includes third party materials (such as photographs, illustrations, graphs, inserts and similar materials) which are identified in such material as having been used by permission, User is responsible for identifying, and seeking separate licenses (under this Service or otherwise) for, any of such third party materials; without a separate license, such third party materials may not be used.

3.5 Use of proper copyright notice for a Work is required as a condition of any license granted under the Service. Unless otherwise provided in the Order Confirmation, a proper copyright notice will read substantially as follows: “Republished with permission of [Rightsholder’s name], from [Work’s title, author, volume, edition number and year of copyright]; permission conveyed through Copyright Clearance Center, Inc. ” Such notice

must be provided in a reasonably legible font size and must be placed either immediately adjacent to the Work as used (for example, as part of a by-line or footnote but not as a separate electronic link) or in the place where substantially all other credits or notices for the new work containing the republished Work are located. Failure to include the required notice results in loss to the Rightsholder and CCC, and the User shall be liable to pay liquidated damages for each such failure equal to twice the use fee specified in the Order Confirmation, in addition to the use fee itself and any other fees and charges specified.

3.6 User may only make alterations to the Work if and as expressly set forth in the Order Confirmation. No Work may be used in any way that is defamatory, violates the rights of third parties (including such third parties' rights of copyright, privacy, publicity, or other tangible or intangible property), or is otherwise illegal, sexually explicit or obscene. In addition, User may not conjoin a Work with any other material that may result in damage to the reputation of the Rightsholder. User agrees to inform CCC if it becomes aware of any infringement of any rights in a Work and to cooperate with any reasonable request of CCC or the Rightsholder in connection therewith.

4. Indemnity. User hereby indemnifies and agrees to defend the Rightsholder and CCC, and their respective employees and directors, against all claims, liability, damages, costs and expenses, including legal fees and expenses, arising out of any use of a Work beyond the scope of the rights granted herein, or any use of a Work which has been altered in any unauthorized way by User, including claims of defamation or infringement of rights of copyright, publicity, privacy or other tangible or intangible property.

5. Limitation of Liability. UNDER NO CIRCUMSTANCES WILL CCC OR THE RIGHTSHOLDER BE LIABLE FOR ANY DIRECT, INDIRECT, CONSEQUENTIAL OR INCIDENTAL DAMAGES (INCLUDING WITHOUT LIMITATION DAMAGES FOR LOSS OF BUSINESS PROFITS OR INFORMATION, OR FOR BUSINESS INTERRUPTION) ARISING OUT OF THE USE OR INABILITY TO USE A WORK, EVEN IF ONE OF THEM HAS BEEN ADVISED OF THE POSSIBILITY OF SUCH DAMAGES. In any event, the total liability of the Rightsholder and CCC (including their respective employees and directors) shall not exceed the total amount actually paid by User for this license. User assumes full liability for the actions and omissions of its principals, employees, agents, affiliates, successors and assigns.

6. Limited Warranties. THE WORK(S) AND RIGHT(S) ARE PROVIDED "AS IS". CCC HAS THE RIGHT TO GRANT TO USER THE RIGHTS GRANTED IN THE ORDER CONFIRMATION DOCUMENT. CCC AND THE RIGHTSHOLDER DISCLAIM ALL OTHER WARRANTIES RELATING TO THE WORK(S) AND RIGHT(S), EITHER EXPRESS OR IMPLIED, INCLUDING WITHOUT LIMITATION IMPLIED WARRANTIES OF MERCHANTABILITY OR FITNESS FOR A PARTICULAR PURPOSE. ADDITIONAL RIGHTS MAY BE REQUIRED TO USE ILLUSTRATIONS, GRAPHS, PHOTOGRAPHS, ABSTRACTS, INSERTS OR OTHER PORTIONS OF THE WORK (AS OPPOSED TO THE ENTIRE WORK) IN A MANNER CONTEMPLATED BY USER; USER UNDERSTANDS AND AGREES THAT NEITHER CCC NOR THE RIGHTSHOLDER MAY HAVE SUCH ADDITIONAL RIGHTS TO GRANT.

7. Effect of Breach. Any failure by User to pay any amount when due, or any use by User of a Work beyond the scope of the license set forth in the Order Confirmation and/or these

terms and conditions, shall be a material breach of the license created by the Order Confirmation and these terms and conditions. Any breach not cured within 30 days of written notice thereof shall result in immediate termination of such license without further notice. Any unauthorized (but licensable) use of a Work that is terminated immediately upon notice thereof may be liquidated by payment of the Rightsholder's ordinary license price therefor; any unauthorized (and unlicensable) use that is not terminated immediately for any reason (including, for example, because materials containing the Work cannot reasonably be recalled) will be subject to all remedies available at law or in equity, but in no event to a payment of less than three times the Rightsholder's ordinary license price for the most closely analogous licensable use plus Rightsholder's and/or CCC's costs and expenses incurred in collecting such payment.

8. Miscellaneous.

8.1 User acknowledges that CCC may, from time to time, make changes or additions to the Service or to these terms and conditions, and CCC reserves the right to send notice to the User by electronic mail or otherwise for the purposes of notifying User of such changes or additions; provided that any such changes or additions shall not apply to permissions already secured and paid for.

8.2 Use of User-related information collected through the Service is governed by CCC's privacy policy, available online here: <http://www.copyright.com/content/cc3/en/tools/footer/privacypolicy.html>.

8.3 The licensing transaction described in the Order Confirmation is personal to User. Therefore, User may not assign or transfer to any other person (whether a natural person or an organization of any kind) the license created by the Order Confirmation and these terms and conditions or any rights granted hereunder; provided, however, that User may assign such license in its entirety on written notice to CCC in the event of a transfer of all or substantially all of User's rights in the new material which includes the Work(s) licensed under this Service.

8.4 No amendment or waiver of any terms is binding unless set forth in writing and signed by the parties. The Rightsholder and CCC hereby object to any terms contained in any writing prepared by the User or its principals, employees, agents or affiliates and purporting to govern or otherwise relate to the licensing transaction described in the Order Confirmation, which terms are in any way inconsistent with any terms set forth in the Order Confirmation and/or in these terms and conditions or CCC's standard operating procedures, whether such writing is prepared prior to, simultaneously with or subsequent to the Order Confirmation, and whether such writing appears on a copy of the Order Confirmation or in a separate instrument.

8.5 The licensing transaction described in the Order Confirmation document shall be governed by and construed under the law of the State of New York, USA, without regard to the principles thereof of conflicts of law. Any case, controversy, suit, action, or proceeding arising out of, in connection with, or related to such licensing transaction shall be brought, at CCC's sole discretion, in any federal or state court located in the County of New York, State of New York, USA, or in any federal or state court whose geographical jurisdiction covers the location of the Rightsholder set forth in the Order Confirmation. The parties expressly submit to the personal jurisdiction and venue of each such federal or state court.

you have any comments or questions about the Service or Copyright Clearance Center, please contact us at 978-750-8400 or send an e-mail to info@copyright.com.
v 1.1

Questions? customercare@copyright.com or +1-855-239-3415 (toll free in the US) or +1-978-646-2777.

AIP PUBLISHING LLC LICENSE TERMS AND CONDITIONS

Oct 17, 2017

This Agreement between University of Nevada, Las Vegas (UNLV) -- Qi Shen ("You") and AIP Publishing LLC ("AIP Publishing LLC") consists of your license details and the terms and conditions provided by AIP Publishing LLC and Copyright Clearance Center.

License Number	4197750008720
License date	Sep 28, 2017
Licensed Content Publisher	AIP Publishing LLC
Licensed Content Publication	Journal of Applied Physics
Licensed Content Title	Electrode of ionic polymer-metal composite sensors: Modeling and experimental investigation
Licensed Content Author	Qi Shen, Kwang J. Kim, Tianmiao Wang
Licensed Content Date	May 21, 2014
Licensed Content Volume	115
Licensed Content Issue	19
Type of Use	Thesis/Dissertation
Requestor type	Author (original article)
Format	Print and electronic
Portion	Excerpt (> 800 words)
Will you be translating?	No
Title of your thesis / dissertation	Theoretical and Experimental Investigation on the Multiple Shape Memory Ionic Polymer-Metal Composite
Expected completion date	Dec 2017
Estimated size (number of pages)	90
Requestor Location	University of Nevada, Las Vegas (UNLV) 4505 S. Maryland Pkwy. Las Vegas, NV 89154

Las Vegas, NV 89121

188

United States
Attn: University of Nevada, Las Vegas (UNLV)

Billing Type Invoice

Billing Address University of Nevada, Las Vegas (UNLV)
4505 S. Maryland Pkwy. Las Vegas, NV 89154

Las Vegas, NV 89121
United States
Attn: Qi Shen

Total 0.00 USD

Terms and Conditions

AIP Publishing LLC -- Terms and Conditions: Permissions Uses

AIP Publishing hereby grants to you the non-exclusive right and license to use and/or distribute the Material according to the use specified in your order, on a one-time basis, for the specified term, with a maximum distribution equal to the number that you have ordered. Any links or other content accompanying the Material are not the subject of this license.

1. You agree to include the following copyright and permission notice with the reproduction of the Material: "Reprinted from [FULL CITATION], with the permission of AIP Publishing." For an article, the credit line and permission notice must be printed on the first page of the article or book chapter. For photographs, covers, or tables, the notice may appear with the Material, in a footnote, or in the reference list.
2. If you have licensed reuse of a figure, photograph, cover, or table, it is your responsibility to ensure that the material is original to AIP Publishing and does not contain the copyright of another entity, and that the copyright notice of the figure, photograph, cover, or table does not indicate that it was reprinted by AIP Publishing, with permission, from another source. Under no circumstances does AIP Publishing purport or intend to grant permission to reuse material to which it does not hold appropriate rights.
You may not alter or modify the Material in any manner. You may translate the Material into another language only if you have licensed translation rights. You may not use the Material for promotional purposes.
3. The foregoing license shall not take effect unless and until AIP Publishing or its agent, Copyright Clearance Center, receives the Payment in accordance with Copyright Clearance Center Billing and Payment Terms and Conditions, which are incorporated herein by reference.
4. AIP Publishing or Copyright Clearance Center may, within two business days of granting this license, revoke the license for any reason whatsoever, with a full refund payable to you. Should you violate the terms of this license at any time, AIP Publishing, or Copyright Clearance Center may revoke the license with no refund to you. Notice of such revocation will be made using the contact information provided by you. Failure to receive such notice will not nullify the revocation.
5. AIP Publishing makes no representations or warranties with respect to the Material. You agree to indemnify and hold harmless AIP Publishing, and their officers, directors, employees or agents from and against any and all claims arising out of your use of the Material other than as specifically authorized herein.
6. The permission granted herein is personal to you and is not transferable or assignable without the prior written permission of AIP Publishing. This license may not be amended except in a writing signed by the party to be charged.

7. If purchase orders, acknowledgments or check endorsements are issued on any forms containing terms and conditions which are inconsistent with these provisions, such inconsistent terms and conditions shall be of no force and effect. This document, including the CCC Billing and Payment Terms and Conditions, shall be the entire agreement between the parties relating to the subject matter hereof.

This Agreement shall be governed by and construed in accordance with the laws of the State of New York. Both parties hereby submit to the jurisdiction of the courts of New York County for purposes of resolving any disputes that may arise hereunder.

V1.1

Questions? customercare@copyright.com or +1-855-239-3415 (toll free in the US) or +1-978-646-2777.

AIP PUBLISHING LLC LICENSE TERMS AND CONDITIONS

Oct 17, 2017

This Agreement between University of Nevada, Las Vegas (UNLV) -- Qi Shen ("You") and AIP Publishing LLC ("AIP Publishing LLC") consists of your license details and the terms and conditions provided by AIP Publishing LLC and Copyright Clearance Center.

License Number	4197190262556
License date	Sep 27, 2017
Licensed Content Publisher	AIP Publishing LLC
Licensed Content Publication	Journal of Applied Physics
Licensed Content Title	A comprehensive physics-based model encompassing variable surface resistance and underlying physics of ionic polymer-metal composite actuators
Licensed Content Author	Qi Shen, Viljar Palmre, Tyler Stalbaum, et al
Licensed Content Date	Sep 28, 2015
Licensed Content Volume	118
Licensed Content Issue	12
Type of Use	Thesis/Dissertation
Requestor type	Author (original article)
Format	Print and electronic
Portion	Excerpt (> 800 words)
Will you be translating?	No
Title of your thesis / dissertation	Theoretical and Experimental Investigation on the Multiple Shape Memory Ionic Polymer-Metal Composite
Expected completion date	Dec 2017
Estimated size (number of pages)	90
Requestor Location	University of Nevada, Las Vegas (UNLV) 4505 S. Maryland Pkwy. Las Vegas, NV 89154

Las Vegas, NV 89121
United States
Attn: University of Nevada, Las Vegas (UNLV)

Billing Type

Invoice

Billing Address

University of Nevada, Las Vegas (UNLV)
4505 S. Maryland Pkwy. Las Vegas, NV 89154

Las Vegas, NV 89121
United States
Attn: Qi Shen

Total

0.00 USD

Terms and Conditions

AIP Publishing LLC -- Terms and Conditions: Permissions Uses

AIP Publishing hereby grants to you the non-exclusive right and license to use and/or distribute the Material according to the use specified in your order, on a one-time basis, for the specified term, with a maximum distribution equal to the number that you have ordered. Any links or other content accompanying the Material are not the subject of this license.

1. You agree to include the following copyright and permission notice with the reproduction of the Material: "Reprinted from [FULL CITATION], with the permission of AIP Publishing." For an article, the credit line and permission notice must be printed on the first page of the article or book chapter. For photographs, covers, or tables, the notice may appear with the Material, in a footnote, or in the reference list.
2. If you have licensed reuse of a figure, photograph, cover, or table, it is your responsibility to ensure that the material is original to AIP Publishing and does not contain the copyright of another entity, and that the copyright notice of the figure, photograph, cover, or table does not indicate that it was reprinted by AIP Publishing, with permission, from another source. Under no circumstances does AIP Publishing purport or intend to grant permission to reuse material to which it does not hold appropriate rights.
You may not alter or modify the Material in any manner. You may translate the Material into another language only if you have licensed translation rights. You may not use the Material for promotional purposes.
3. The foregoing license shall not take effect unless and until AIP Publishing or its agent, Copyright Clearance Center, receives the Payment in accordance with Copyright Clearance Center Billing and Payment Terms and Conditions, which are incorporated herein by reference.
4. AIP Publishing or Copyright Clearance Center may, within two business days of granting this license, revoke the license for any reason whatsoever, with a full refund payable to you. Should you violate the terms of this license at any time, AIP Publishing, or Copyright Clearance Center may revoke the license with no refund to you. Notice of such revocation will be made using the contact information provided by you. Failure to receive such notice will not nullify the revocation.
5. AIP Publishing makes no representations or warranties with respect to the Material. You agree to indemnify and hold harmless AIP Publishing, and their officers, directors, employees or agents from and against any and all claims arising out of your use of the Material other than as specifically authorized herein.
6. The permission granted herein is personal to you and is not transferable or assignable without the prior written permission of AIP Publishing. This license may not be amended except in a writing signed by the party to be charged.

7. If purchase orders, acknowledgments or check endorsements are issued on any forms containing terms and conditions which are inconsistent with these provisions, such inconsistent terms and conditions shall be of no force and effect. This document, including the CCC Billing and Payment Terms and Conditions, shall be the entire agreement between the parties relating to the subject matter hereof.

This Agreement shall be governed by and construed in accordance with the laws of the State of New York. Both parties hereby submit to the jurisdiction of the courts of New York County for purposes of resolving any disputes that may arise hereunder.

V1.1

Questions? customercare@copyright.com or +1-855-239-3415 (toll free in the US) or +1-978-646-2777.

**SPRINGER LICENSE
TERMS AND CONDITIONS**

Oct 17, 2017

This Agreement between University of Nevada, Las Vegas (UNLV) -- Qi Shen ("You") and Springer ("Springer") consists of your license details and the terms and conditions provided by Springer and Copyright Clearance Center.

License Number	4197311277659
License date	Sep 27, 2017
Licensed Content Publisher	Springer
Licensed Content Publication	International Journal of Intelligent Robotics and Applications
Licensed Content Title	Bioinspired travelling wave generation in soft-robotics using ionic polymer-metal composites
Licensed Content Author	Tyler Stalbaum, Taeseon Hwang, Sarah Trabia et al
Licensed Content Date	Jan 1, 2017
Licensed Content Volume	1
Licensed Content Issue	2
Type of Use	Thesis/Dissertation
Portion	Full text
Number of copies	1
Author of this Springer article	Yes and you are a contributor of the new work
Order reference number	
Title of your thesis / dissertation	Theoretical and Experimental Investigation on the Multiple Shape Memory Ionic Polymer-Metal Composite
Expected completion date	Dec 2017
Estimated size(pages)	90
Requestor Location	University of Nevada, Las Vegas (UNLV) 4505 S. Maryland Pkwy. Las Vegas, NV 89154

Las Vegas, NV 89121

United States
Attn: University of Nevada, Las Vegas (UNLV)

Billing Type Invoice

Billing Address University of Nevada, Las Vegas (UNLV)
4505 S. Maryland Pkwy. Las Vegas, NV 89154

Las Vegas, NV 89121
United States
Attn: Qi Shen

Total 0.00 USD

Terms and Conditions

Introduction

The publisher for this copyrighted material is Springer. By clicking "accept" in connection with completing this licensing transaction, you agree that the following terms and conditions apply to this transaction (along with the Billing and Payment terms and conditions established by Copyright Clearance Center, Inc. ("CCC"), at the time that you opened your Rightslink account and that are available at any time at <http://myaccount.copyright.com>).

Limited License

With reference to your request to reuse material on which Springer controls the copyright, permission is granted for the use indicated in your enquiry under the following conditions:

- Licenses are for one-time use only with a maximum distribution equal to the number stated in your request.
- Springer material represents original material which does not carry references to other sources. If the material in question appears with a credit to another source, this permission is not valid and authorization has to be obtained from the original copyright holder.
- This permission
 - is non-exclusive
 - is only valid if no personal rights, trademarks, or competitive products are infringed.
 - explicitly excludes the right for derivatives.
- Springer does not supply original artwork or content.
- According to the format which you have selected, the following conditions apply accordingly:
 - **Print and Electronic:** This License include use in electronic form provided it is password protected, on intranet, or CD-Rom/DVD or E-book/E-journal. It may not be republished in electronic open access.
 - **Print:** This License excludes use in electronic form.
 - **Electronic:** This License only pertains to use in electronic form provided it is password protected, on intranet, or CD-Rom/DVD or E-book/E-journal. It may not be republished in electronic open access.

For any electronic use not mentioned, please contact Springer at permissions.springer@spiglobal.com.

- Although Springer controls the copyright to the material and is entitled to negotiate on rights, this license is only valid subject to courtesy information to the author (address is given in the article/chapter).
- If you are an STM Signatory or your work will be published by an STM Signatory and you are requesting to reuse figures/tables/illustrations or single text extracts, permission is granted according to STM Permissions Guidelines: <http://www.stm-assoc.org/permissions-guidelines/>

For any electronic use not mentioned in the Guidelines, please contact Springer at permissions.springer@spi-global.com. If you request to reuse more content than stipulated in the STM Permissions Guidelines, you will be charged a permission fee for the excess content.

Permission is valid upon payment of the fee as indicated in the licensing process. If permission is granted free of charge on this occasion, that does not prejudice any rights we might have to charge for reproduction of our copyrighted material in the future.

-If your request is for reuse in a Thesis, permission is granted free of charge under the following conditions:

This license is valid for one-time use only for the purpose of defending your thesis and with a maximum of 100 extra copies in paper. If the thesis is going to be published, permission needs to be reobtained.

- includes use in an electronic form, provided it is an author-created version of the thesis on his/her own website and his/her university's repository, including UMI (according to the definition on the Sherpa website: <http://www.sherpa.ac.uk/romeo/>);

- is subject to courtesy information to the co-author or corresponding author.

Geographic Rights: Scope

Licenses may be exercised anywhere in the world.

Altering/Modifying Material: Not Permitted

Figures, tables, and illustrations may be altered minimally to serve your work. You may not alter or modify text in any manner. Abbreviations, additions, deletions and/or any other alterations shall be made only with prior written authorization of the author(s).

Reservation of Rights

Springer reserves all rights not specifically granted in the combination of (i) the license details provided by you and accepted in the course of this licensing transaction and (ii) these terms and conditions and (iii) CCC's Billing and Payment terms and conditions.

License Contingent on Payment

While you may exercise the rights licensed immediately upon issuance of the license at the end of the licensing process for the transaction, provided that you have disclosed complete and accurate details of your proposed use, no license is finally effective unless and until full payment is received from you (either by Springer or by CCC) as provided in CCC's Billing and Payment terms and conditions. If full payment is not received by the date due, then any license preliminarily granted shall be deemed automatically revoked and shall be void as if never granted. Further, in the event that you breach any of these terms and conditions or any of CCC's Billing and Payment terms and conditions, the license is automatically revoked and shall be void as if never granted. Use of materials as described in a revoked license, as well as any use of the materials beyond the scope of an unrevoked license, may

constitute copyright infringement and Springer reserves the right to take any and all action to protect its copyright in the materials.

Copyright Notice: Disclaimer

You must include the following copyright and permission notice in connection with any reproduction of the licensed material:

"Springer book/journal title, chapter/article title, volume, year of publication, page, name(s) of author(s), (original copyright notice as given in the publication in which the material was originally published) "With permission of Springer"

In case of use of a graph or illustration, the caption of the graph or illustration must be included, as it is indicated in the original publication.

Warranties: None

Springer makes no representations or warranties with respect to the licensed material and adopts on its own behalf the limitations and disclaimers established by CCC on its behalf in its Billing and Payment terms and conditions for this licensing transaction.

Indemnity

You hereby indemnify and agree to hold harmless Springer and CCC, and their respective officers, directors, employees and agents, from and against any and all claims arising out of your use of the licensed material other than as specifically authorized pursuant to this license.

No Transfer of License

This license is personal to you and may not be sublicensed, assigned, or transferred by you without Springer's written permission.

No Amendment Except in Writing

This license may not be amended except in a writing signed by both parties (or, in the case of Springer, by CCC on Springer's behalf).

Objection to Contrary Terms

Springer hereby objects to any terms contained in any purchase order, acknowledgment, check endorsement or other writing prepared by you, which terms are inconsistent with these terms and conditions or CCC's Billing and Payment terms and conditions. These terms and conditions, together with CCC's Billing and Payment terms and conditions (which are incorporated herein), comprise the entire agreement between you and Springer (and CCC) concerning this licensing transaction. In the event of any conflict between your obligations established by these terms and conditions and those established by CCC's Billing and Payment terms and conditions, these terms and conditions shall control.

Jurisdiction

All disputes that may arise in connection with this present License, or the breach thereof, shall be settled exclusively by arbitration, to be held in the Federal Republic of Germany, in accordance with German law.

Other conditions:

V 12AUG2015

Questions? customercare@copyright.com or +1-855-239-3415 (toll free in the US) or +1-978-646-2777.

**ROYAL SOCIETY OF CHEMISTRY LICENSE
TERMS AND CONDITIONS**

Oct 31, 2017

This Agreement between University of Nevada, Las Vegas (UNLV) -- Qi Shen ("You") and Royal Society of Chemistry ("Royal Society of Chemistry") consists of your license details and the terms and conditions provided by Royal Society of Chemistry and Copyright Clearance Center.

License Number	4219471043326
License date	Oct 31, 2017
Licensed Content Publisher	Royal Society of Chemistry
Licensed Content Publication	Soft Matter
Licensed Content Title	Dielectric elastomers as next-generation polymeric actuators
Licensed Content Author	Ravi Shankar, Tushar K. Ghosh, Richard J. Spontak
Licensed Content Date	Jul 18, 2007
Licensed Content Volume	3
Licensed Content Issue	9
Type of Use	Thesis/Dissertation
Requestor type	academic/educational
Portion	figures/tables/images
Number of figures/tables/images	1
Format	print and electronic
Distribution quantity	100
Will you be translating?	no
Order reference number	
Title of the thesis/dissertation	Theoretical and Experimental Investigation on the Multiple Shape Memory Ionic Polymer-Metal Composite
Expected completion date	Dec 2017
Estimated size	90
Requestor Location	University of Nevada, Las Vegas (UNLV) 4505 S. Maryland Pkwy. Las Vegas, NV 89154

Las Vegas, NV 89121
United States
Attn: University of Nevada, Las Vegas (UNLV)

Billing Type

Invoice

Billing Address

University of Nevada, Las Vegas (UNLV)
4505 S. Maryland Pkwy. Las Vegas, NV 89154

Las Vegas, NV 89121
United States
Attn: Qi Shen

Total

0.00 USD

Terms and Conditions

This License Agreement is between {Requestor Name} ("You") and The Royal Society of Chemistry ("RSC") provided by the Copyright Clearance Center ("CCC"). The license consists of your order details, the terms and conditions provided by the Royal Society of Chemistry, and the payment terms and conditions.

RSC / TERMS AND CONDITIONS

INTRODUCTION

The publisher for this copyrighted material is The Royal Society of Chemistry. By clicking "accept" in connection with completing this licensing transaction, you agree that the following terms and conditions apply to this transaction (along with the Billing and Payment terms and conditions established by CCC, at the time that you opened your RightsLink account and that are available at any time at .

LICENSE GRANTED

The RSC hereby grants you a non-exclusive license to use the aforementioned material anywhere in the world subject to the terms and conditions indicated herein. Reproduction of the material is confined to the purpose and/or media for which permission is hereby given.

RESERVATION OF RIGHTS

The RSC reserves all rights not specifically granted in the combination of (i) the license details provided by you and accepted in the course of this licensing transaction; (ii) these terms and conditions; and (iii) CCC's Billing and Payment terms and conditions.

REVOCATION

The RSC reserves the right to revoke this license for any reason, including, but not limited to, advertising and promotional uses of RSC content, third party usage, and incorrect source figure attribution.

THIRD-PARTY MATERIAL DISCLAIMER

If part of the material to be used (for example, a figure) has appeared in the RSC publication with credit to another source, permission must also be sought from that source. If the other source is another RSC publication these details should be included in your RightsLink request. If the other source is a third party, permission must be obtained from the third party. The RSC disclaims any responsibility for the reproduction you make of items owned by a third party.

PAYMENT OF FEE

ELSEVIER LICENSE TERMS AND CONDITIONS

Oct 31, 2017

This Agreement between University of Nevada, Las Vegas (UNLV) -- Qi Shen ("You") and Elsevier ("Elsevier") consists of your license details and the terms and conditions provided by Elsevier and Copyright Clearance Center.

License Number	4219471354238
License date	Oct 31, 2017
Licensed Content Publisher	Elsevier
Licensed Content Publication	Polymer
Licensed Content Title	Recent advances in polymer shape memory
Licensed Content Author	Tao Xie
Licensed Content Date	Oct 13, 2011
Licensed Content Volume	52
Licensed Content Issue	22
Licensed Content Pages	16
Start Page	4985
End Page	5000
Type of Use	reuse in a thesis/dissertation
Intended publisher of new work	other
Portion	figures/tables/illustrations
Number of figures/tables/illustrations	1
Format	both print and electronic
Are you the author of this Elsevier article?	No
Will you be translating?	No
Original figure numbers	Figure 3

Title of your thesis/dissertation	Theoretical and Experimental Investigation on the Multiple Shape Memory Ionic Polymer-Metal Composite
Publisher of new work	University of Nevada, Las Vegas (UNLV)
Author of new work	Dr. Kwang J. Kim
Expected completion date	Dec 2017
Estimated size (number of pages)	90
Requestor Location	University of Nevada, Las Vegas (UNLV) 4505 S. Maryland Pkwy. Las Vegas, NV 89154
	Las Vegas, NV 89121 United States Attn: University of Nevada, Las Vegas (UNLV)
Publisher Tax ID	98-0397604
Total	0.00 USD
Terms and Conditions	

INTRODUCTION

1. The publisher for this copyrighted material is Elsevier. By clicking "accept" in connection with completing this licensing transaction, you agree that the following terms and conditions apply to this transaction (along with the Billing and Payment terms and conditions established by Copyright Clearance Center, Inc. ("CCC"), at the time that you opened your Rightslink account and that are available at any time at <http://myaccount.copyright.com>).

GENERAL TERMS

2. Elsevier hereby grants you permission to reproduce the aforementioned material subject to the terms and conditions indicated.
3. Acknowledgement: If any part of the material to be used (for example, figures) has appeared in our publication with credit or acknowledgement to another source, permission must also be sought from that source. If such permission is not obtained then that material may not be included in your publication/copies. Suitable acknowledgement to the source must be made, either as a footnote or in a reference list at the end of your publication, as follows:
"Reprinted from Publication title, Vol /edition number, Author(s), Title of article / title of chapter, Pages No., Copyright (Year), with permission from Elsevier [OR APPLICABLE SOCIETY COPYRIGHT OWNER]." Also Lancet special credit - "Reprinted from The Lancet, Vol. number, Author(s), Title of article, Pages No., Copyright (Year), with permission from Elsevier."
4. Reproduction of this material is confined to the purpose and/or media for which permission is hereby given.
5. Altering/Modifying Material: Not Permitted. However figures and illustrations may be altered/adapted minimally to serve your work. Any other abbreviations, additions, deletions and/or any other alterations shall be made only with prior written authorization

of Elsevier Ltd. (Please contact Elsevier at permissions@elsevier.com). No modifications can be made to any Lancet figures/tables and they must be reproduced in full.

6. If the permission fee for the requested use of our material is waived in this instance, please be advised that your future requests for Elsevier materials may attract a fee.

7. Reservation of Rights: Publisher reserves all rights not specifically granted in the combination of (i) the license details provided by you and accepted in the course of this licensing transaction, (ii) these terms and conditions and (iii) CCC's Billing and Payment terms and conditions.

8. License Contingent Upon Payment: While you may exercise the rights licensed immediately upon issuance of the license at the end of the licensing process for the transaction, provided that you have disclosed complete and accurate details of your proposed use, no license is finally effective unless and until full payment is received from you (either by publisher or by CCC) as provided in CCC's Billing and Payment terms and conditions. If full payment is not received on a timely basis, then any license preliminarily granted shall be deemed automatically revoked and shall be void as if never granted. Further, in the event that you breach any of these terms and conditions or any of CCC's Billing and Payment terms and conditions, the license is automatically revoked and shall be void as if never granted. Use of materials as described in a revoked license, as well as any use of the materials beyond the scope of an unrevoked license, may constitute copyright infringement and publisher reserves the right to take any and all action to protect its copyright in the materials.

9. Warranties: Publisher makes no representations or warranties with respect to the licensed material.

10. Indemnity: You hereby indemnify and agree to hold harmless publisher and CCC, and their respective officers, directors, employees and agents, from and against any and all claims arising out of your use of the licensed material other than as specifically authorized pursuant to this license.

11. No Transfer of License: This license is personal to you and may not be sublicensed, assigned, or transferred by you to any other person without publisher's written permission.

12. No Amendment Except in Writing: This license may not be amended except in a writing signed by both parties (or, in the case of publisher, by CCC on publisher's behalf).

13. Objection to Contrary Terms: Publisher hereby objects to any terms contained in any purchase order, acknowledgment, check endorsement or other writing prepared by you, which terms are inconsistent with these terms and conditions or CCC's Billing and Payment terms and conditions. These terms and conditions, together with CCC's Billing and Payment terms and conditions (which are incorporated herein), comprise the entire agreement between you and publisher (and CCC) concerning this licensing transaction. In the event of any conflict between your obligations established by these terms and conditions and those established by CCC's Billing and Payment terms and conditions, these terms and conditions shall control.

14. Revocation: Elsevier or Copyright Clearance Center may deny the permissions described in this License at their sole discretion, for any reason or no reason, with a full refund payable to you. Notice of such denial will be made using the contact information provided by you. Failure to receive such notice will not alter or invalidate the denial. In

no event will Elsevier or Copyright Clearance Center be responsible or liable for any costs, expenses or damage incurred by you as a result of a denial of your permission request, other than a refund of the amount(s) paid by you to Elsevier and/or Copyright Clearance Center for denied permissions.

LIMITED LICENSE

The following terms and conditions apply only to specific license types:

15. Translation: This permission is granted for non-exclusive world **English** rights only unless your license was granted for translation rights. If you licensed translation rights you may only translate this content into the languages you requested. A professional translator must perform all translations and reproduce the content word for word preserving the integrity of the article.

16. Posting licensed content on any Website: The following terms and conditions apply as follows: Licensing material from an Elsevier journal: All content posted to the web site must maintain the copyright information line on the bottom of each image; A hyper-text must be included to the Homepage of the journal from which you are licensing at <http://www.sciencedirect.com/science/journal/xxxxx> or the Elsevier homepage for books at <http://www.elsevier.com>; Central Storage: This license does not include permission for a scanned version of the material to be stored in a central repository such as that provided by Heron/XanEdu.

Licensing material from an Elsevier book: A hyper-text link must be included to the Elsevier homepage at <http://www.elsevier.com>. All content posted to the web site must maintain the copyright information line on the bottom of each image.

Posting licensed content on Electronic reserve: In addition to the above the following clauses are applicable: The web site must be password-protected and made available only to bona fide students registered on a relevant course. This permission is granted for 1 year only. You may obtain a new license for future website posting.

17. For journal authors: the following clauses are applicable in addition to the above:

Preprints:

A preprint is an author's own write-up of research results and analysis, it has not been peer-reviewed, nor has it had any other value added to it by a publisher (such as formatting, copyright, technical enhancement etc.).

Authors can share their preprints anywhere at any time. Preprints should not be added to or enhanced in any way in order to appear more like, or to substitute for, the final versions of articles however authors can update their preprints on arXiv or RePEc with their Accepted Author Manuscript (see below).

If accepted for publication, we encourage authors to link from the preprint to their formal publication via its DOI. Millions of researchers have access to the formal publications on ScienceDirect, and so links will help users to find, access, cite and use the best available version. Please note that Cell Press, The Lancet and some society-owned have different preprint policies. Information on these policies is available on the journal homepage.

Accepted Author Manuscripts: An accepted author manuscript is the manuscript of an article that has been accepted for publication and which typically includes author-

incorporated changes suggested during submission, peer review and editor-author communications.

Authors can share their accepted author manuscript:

- immediately
 - via their non-commercial person homepage or blog
 - by updating a preprint in arXiv or RePEc with the accepted manuscript
 - via their research institute or institutional repository for internal institutional uses or as part of an invitation-only research collaboration work-group
 - directly by providing copies to their students or to research collaborators for their personal use
 - for private scholarly sharing as part of an invitation-only work group on commercial sites with which Elsevier has an agreement
- After the embargo period
 - via non-commercial hosting platforms such as their institutional repository
 - via commercial sites with which Elsevier has an agreement

In all cases accepted manuscripts should:

- link to the formal publication via its DOI
- bear a CC-BY-NC-ND license - this is easy to do
- if aggregated with other manuscripts, for example in a repository or other site, be shared in alignment with our hosting policy not be added to or enhanced in any way to appear more like, or to substitute for, the published journal article.

Published journal article (JPA): A published journal article (PJA) is the definitive final record of published research that appears or will appear in the journal and embodies all value-adding publishing activities including peer review co-ordination, copy-editing, formatting, (if relevant) pagination and online enrichment.

Policies for sharing publishing journal articles differ for subscription and gold open access articles:

Subscription Articles: If you are an author, please share a link to your article rather than the full-text. Millions of researchers have access to the formal publications on ScienceDirect, and so links will help your users to find, access, cite, and use the best available version.

Theses and dissertations which contain embedded PJAs as part of the formal submission can be posted publicly by the awarding institution with DOI links back to the formal publications on ScienceDirect.

If you are affiliated with a library that subscribes to ScienceDirect you have additional private sharing rights for others' research accessed under that agreement. This includes use for classroom teaching and internal training at the institution (including use in course packs and courseware programs), and inclusion of the article for grant funding purposes.

Gold Open Access Articles: May be shared according to the author-selected end-user license and should contain a [CrossMark logo](#), the end user license, and a DOI link to the formal publication on ScienceDirect.

Please refer to Elsevier's [posting policy](#) for further information.

18. **For book authors** the following clauses are applicable in addition to the above: Authors are permitted to place a brief summary of their work online only. You are not allowed to download and post the published electronic version of your chapter, nor may you scan the printed edition to create an electronic version. **Posting to a repository:** Authors are permitted to post a summary of their chapter only in their institution's repository.

19. **Thesis/Dissertation:** If your license is for use in a thesis/dissertation your thesis may be submitted to your institution in either print or electronic form. Should your thesis be published commercially, please reapply for permission. These requirements include permission for the Library and Archives of Canada to supply single copies, on demand, of the complete thesis and include permission for Proquest/UMI to supply single copies, on demand, of the complete thesis. Should your thesis be published commercially, please reapply for permission. Theses and dissertations which contain embedded PJAs as part of the formal submission can be posted publicly by the awarding institution with DOI links back to the formal publications on ScienceDirect.

Elsevier Open Access Terms and Conditions

You can publish open access with Elsevier in hundreds of open access journals or in nearly 2000 established subscription journals that support open access publishing. Permitted third party re-use of these open access articles is defined by the author's choice of Creative Commons user license. See our [open access license policy](#) for more information.

Terms & Conditions applicable to all Open Access articles published with Elsevier:

Any reuse of the article must not represent the author as endorsing the adaptation of the article nor should the article be modified in such a way as to damage the author's honour or reputation. If any changes have been made, such changes must be clearly indicated. The author(s) must be appropriately credited and we ask that you include the end user license and a DOI link to the formal publication on ScienceDirect.

If any part of the material to be used (for example, figures) has appeared in our publication with credit or acknowledgement to another source it is the responsibility of the user to ensure their reuse complies with the terms and conditions determined by the rights holder.

Additional Terms & Conditions applicable to each Creative Commons user license:

CC BY: The CC-BY license allows users to copy, to create extracts, abstracts and new works from the Article, to alter and revise the Article and to make commercial use of the Article (including reuse and/or resale of the Article by commercial entities), provided the user gives appropriate credit (with a link to the formal publication through the relevant DOI), provides a link to the license, indicates if changes were made and the licensor is not represented as endorsing the use made of the work. The full details of the license are available at <http://creativecommons.org/licenses/by/4.0>.

CC BY NC SA: The CC BY-NC-SA license allows users to copy, to create extracts, abstracts and new works from the Article, to alter and revise the Article, provided this is not done for commercial purposes, and that the user gives appropriate credit (with a link to the formal publication through the relevant DOI), provides a link to the license, indicates if changes were made and the licensor is not represented as endorsing the use made of the work. Further, any new works must be made available on the same conditions. The full details of the license are available at <http://creativecommons.org/licenses/by-nc-sa/4.0>.

CC BY NC ND: The CC BY-NC-ND license allows users to copy and distribute the Article, provided this is not done for commercial purposes and further does not permit distribution of the Article if it is changed or edited in any way, and provided the user gives appropriate credit (with a link to the formal publication through the relevant DOI), provides a link to the license, and that the licensor is not represented as endorsing the use made of the work. The full details of the license are available at <http://creativecommons.org/licenses/by-nc-nd/4.0>. Any commercial reuse of Open Access articles published with a CC BY NC SA or CC BY NC ND license requires permission from Elsevier and will be subject to a fee.

Commercial reuse includes:

- Associating advertising with the full text of the Article
- Charging fees for document delivery or access
- Article aggregation
- Systematic distribution via e-mail lists or share buttons

Posting or linking by commercial companies for use by customers of those companies.

20. Other Conditions:

v1.9

Questions? customercare@copyright.com or +1-855-239-3415 (toll free in the US) or +1-978-646-2777.



Bibliography

- [1] Q. Zhao, H. J. Qi, and T. Xie, "Recent progress in shape memory polymer: New behavior, enabling materials, and mechanistic understanding," *Prog. Polym. Sci.*, vol. 49–50, pp. 79–120, 2014.
- [2] Y. Wang, X. Yang, Y. Chen, D. K. Wainwright, C. P. Kenaley, Z. Gong, Z. Liu, H. Liu, J. Guan, T. Wang, and others, "A biorobotic adhesive disc for underwater hitchhiking inspired by the remora suckerfish," *Sci. Robot.*, vol. 2, no. 10, p. eaan8072, 2017.
- [3] Z. Ren, X. Yang, T. Wang, and L. Wen, "Hydrodynamics of a robotic fish tail: effects of the caudal peduncle, fin ray motions and the flow speed," *Bioinspir. Biomim.*, vol. 11, no. 1, p. 16008, 2016.
- [4] C. Jo, D. Pugal, I.-K. Oh, K. J. Kim, and K. Asaka, "Recent advances in ionic polymer–metal composite actuators and their modeling and applications," *Prog. Polym. Sci.*, vol. 38, no. 7, pp. 1037–1066, 2013.
- [5] L. Wen, J. C. Weaver, P. J. M. Thornycroft, and G. V. Lauder, "Hydrodynamic function of biomimetic shark skin: effect of denticle pattern and spacing," *Bioinspir. Biomim.*, vol. 10, no. 6, p. 66010, 2015.
- [6] L. Wen, D. Vogt, Z. Shi, and Q. Shen, "Advanced Materials for Soft Robotics," *Des. Fabr. Prop. Appl. Smart Adv. Mater.*, p. 342, 2016.
- [7] K. J. Kim and M. Shahinpoor, "A novel method of manufacturing three-dimensional ionic polymer-metal composites (IPMCs) biomimetic sensors, actuators and artificial muscles," *Polymer (Guildf.)*, vol. 43, no. 3, pp. 797–802, 2001.
- [8] K. J. Kim and M. Shahinpoor, "Ionic polymer metal composites: II. Manufacturing techniques," *Smart Mater. Struct.*, vol. 12, no. 1, pp. 65–79, 2003.
- [9] K. J. Kim, V. Palmre, T. Stalbaum, T. Hwang, Q. Shen, and S. Trabia, "Promising Developments in Marine Applications With Artificial Muscles : Electrodeless Artificial Cilia Microfibers," *Mar. Technol. Soc. J.*, vol. 50, no. 5, pp. 24–34, 2016.
- [10] Q. Shen, K. J. Kim, and T. Wang, "Electrode of ionic polymer-metal composite sensors: Modeling and experimental investigation," *J. Appl. Phys.*, vol. 115, no. 19, p. 194902, 2014.
- [11] T. Wang, Q. Shen, L. Wen, and J. Liang, "On the thrust performance of an ionic polymer-metal composite actuated robotic fish: Modeling and experimental investigation," *Sci. China Technol. Sci.*, vol. 55, no. 12, pp. 3359–3369, 2012.
- [12] L. Wen, J. Liang, Q. Shen, L. Bao, and Q. Zhang, "Hydrodynamic performance of an undulatory robot: Functional roles of the body and caudal fin locomotion," *Int. J. Adv. Robot. Syst.*, vol. 10, 2013.
- [13] Q. Shen, T. Wang, J. Liang, and L. Wen, "Hydrodynamic performance of a biomimetic robotic swimmer actuated by ionic polymer–metal composite," *Smart Mater. Struct.*, vol. 22, no. 7, p. 75035, 2013.
- [14] Q. Shen, T. Wang, L. Wen, J. Liang, and Y. Chen, "On the thrust efficiency of an IPMC actuated robotic swimmer: dynamic modeling and experimental investigation," in *The Twenty-second International Offshore and Polar Engineering Conference*, 2012.
- [15] Z. Chen and X. Tan, "Monolithic fabrication of ionic polymer-metal composite actuators capable of complex deformation," *Sensors Actuators, A Phys.*, vol. 157, no. 2, pp. 246–

- 257, 2010.
- [16] G. J. Berg, M. K. McBride, C. Wang, and C. N. Bowman, “New directions in the chemistry of shape memory polymers,” *Polymer (Guildf)*, vol. 55, no. 23, pp. 5849–5872, 2014.
- [17] H. Meng and G. Li, “A review of stimuli-responsive shape memory polymer composites,” *Polymer (Guildf)*, vol. 54, no. 9, pp. 2199–2221, 2013.
- [18] T. Xie, “Tunable polymer multi-shape memory effect,” *Nature*, vol. 464, no. 7286, pp. 267–270, 2010.
- [19] Z. Chen, S. Shatara, and X. Tan, “Modeling of Biomimetic Robotic Fish Propelled by An Ionic Polymer – Metal Composite Caudal Fin,” *IEEE/ASME Trans. Mechatronics*, 2009.
- [20] Q. Shen, T. Wang, and K. J. Kim, “A biomimetic underwater vehicle actuated by waves with ionic polymer–metal composite soft sensors,” *Bioinspir. Biomim.*, vol. 10, no. 5, p. 55007, 2015.
- [21] Q. Shen, T. Wang, L. Wen, J. Liang, X. Yang, and G. Yao, “A novel method for investigating the kinematic effect on the hydrodynamics of robotic fish,” in *Robotics and Biomimetics (ROBIO), 2013 IEEE International Conference on*, 2013, pp. 1306–1311.
- [22] T. Stalbaum, S. Trabia, Q. Shen, and K. J. Kim, “Fluid flow sensing with ionic polymer-metal composites,” in *SPIE Smart Structures and Materials+ Nondestructive Evaluation and Health Monitoring*, 2016, p. 97982E--97982E.
- [23] S. Trabia, Q. Shen, T. Stalbaum, R. Hunt, T. Hwang, and K. Kim, “Numerical and experimental investigation of a biomimetic robotic jellyfish actuated by Ionic Polymer-Metal Composite,” in *Ubiquitous Robots and Ambient Intelligence (URAI), 2016 13th International Conference on*, 2016, pp. 204–205.
- [24] Q. Shen, V. Palmre, J. Lee, and K. J. Kim, “A physics model of the multi-degree freedom ionic polymer-metal composite cylinder actuator,” in *Behavior and Mechanics of Multifunctional Materials and Composites 2016*, 2016, vol. 9800, p. 98001B.
- [25] M. Shahinpoor and K. J. Kim, “Ionic polymer – metal composites : I . Fundamentals,” *Smart Mater. Struct.*, vol. 819, no. 4, p. 819, 2001.
- [26] R. Shankar, K. Ghosh, R. J. Spontak, and S. R. D. Gilbert, “Dielectric elastomers as next-generation polymeric actuators,” *Soft Matter*, vol. 3, no. 9, pp. 1116--1129, 2007.
- [27] S. Nemat-Nasser and J. Y. Li, “Electromechanical response of ionic polymer-metal composites,” *J. Appl. Phys.*, vol. 87, no. 7, p. 3321, 2000.
- [28] M. Shahinpoor, Y. Bar-Cohen, J. O. Simpson, and J. Smith, “Ionic polymer-metal composites (IPMCs) as biomimetic sensors, actuators and artificial muscles - a review,” *Smart Mater. Struct.*, vol. 7, no. 6, pp. R15–R30, 1998.
- [29] M. Shahinpoor and K. J. Kim, “Ionic polymer–metal composites: III. Modeling and simulation as biomimetic sensors, actuators, transducers, and artificial muscles,” *Smart Mater. Struct.*, vol. 13, no. 6, pp. 1362–1388, 2004.
- [30] T. Stalbaum, Q. Shen, and K. J. Kim, “A model framework for actuation and sensing of ionic polymer-metal composites: prospective on frequency and shear response through simulation tools,” in *Electroactive Polymer Actuators and Devices (EAPAD) 2017*, 2017, vol. 10163, p. 101630L.
- [31] J. Hu, Y. Zhu, H. Huang, and J. Lu, “Progress in Polymer Science Recent advances in shape – memory polymers : Structure , mechanism , functionality , modeling and

- applications,” *Prog. Polym. Sci.*, vol. 37, no. 12, pp. 1720–1763, 2012.
- [32] Q. Shen, T. Stalbaum, S. Trabia, T. Hwang, R. Hunt, and K. Kim, “Modeling of a soft multiple-shape-memory ionic polymer-metal composite actuator,” in *Behavior and Mechanics of Multifunctional Materials and Composites 2017*, 2017, vol. 10165, p. 101650C.
- [33] J. Rossiter, K. Takashima, and T. Mukai, “Shape memory properties of ionic polymer – metal composites,” *Smart Mater. Struct.*, vol. 21, p. 112002, 2012.
- [34] R. Xiao, J. Guo, and T. D. Nguyen, “Modeling the multiple shape memory effect and temperature memory effect in amorphous polymers,” *RSC Adv.*, vol. 5, no. 1, pp. 416–23, 2015.
- [35] Z. Chen, D. R. Hedgepeth, and X. Tan, “A nonlinear, control-oriented model for ionic polymer–metal composite actuators,” *Smart Mater. Struct.*, vol. 18, no. 5, p. 55008, 2009.
- [36] T. Xie, “Recent advances in polymer shape memory,” *Polymer (Guildf.)*, vol. 52, no. 22, pp. 4985–5000, 2011.
- [37] G. V. Lauder, E. J. Anderson, J. Tangorra, and P. G. a. Madden, “Fish biorobotics: kinematics and hydrodynamics of self-propulsion,” *J. Exp. Biol.*, vol. 210, no. 16, pp. 2767–2780, 2007.
- [38] D. Zhao, Y. Wang, J. Liu, M. Luo, D. Li, and H. Chen, “A multi-segment soft actuator for biomedical applications based on IPMCs,” *Proc. SPIE - Int. Soc. Opt. Eng.*, vol. 9430, no. January, p. 94302Z, 2015.
- [39] K. Cho, J. Koh, S. Kim, W. Chu, Y. Hong, and S. Ahn, “Review of Manufacturing Processes for Soft Biomimetic Robots,” *Int. J. Precis. Eng. Manuf.*, vol. 10, no. 3, pp. 171–181, 2009.
- [40] D. Pugal, K. J. Kim, A. Punning, H. Kasemägi, M. Kruusmaa, and A. Aabloo, “A self-oscillating ionic polymer-metal composite bending actuator,” *J. Appl. Phys.*, vol. 103, no. 8, p. 84908, 2008.
- [41] J. Jayender, R. V Patel, S. Nikumb, and M. Ostojic, “Modeling and Control of Shape Memory Alloy Actuators,” *IEEE Trans. Control Syst. Technol.*, vol. 16, no. 2, pp. 279–287, 2008.
- [42] Z. Wang, G. Hang, Y. Wang, and J. Li, “Embedded SMA wire actuated biomimetic fin : a module for biomimetic underwater propulsion,” *Smart Mater. Struct.*, vol. 17, no. 2, p. 25039, 2008.
- [43] A. D. Marchese, C. D. Onal, and D. Rus, “Autonomous Soft Robotic Fish Capable of Escape Maneuvers Using Fluidic Elastomer Actuators,” *Soft Robot.*, vol. 1, no. 1, pp. 75–87, 2014.
- [44] S. Ahn, K. Lee, H. Kim, R. Wu, J. Kim, and S. Song, “Smart Soft Composite : An Integrated 3D Soft Morphing Structure Using Bend – Twist Coupling of Anisotropic Materials,” *Int. J. Precis. Eng. Manuf.*, vol. 13, no. 4, pp. 631–634, 2012.
- [45] A. Villanueva, C. Smith, and S. Priya, “A biomimetic robotic jellyfish (Robojelly) actuated by shape memory alloy,” *Bioinspir. Biomim.*, vol. 6, no. 3, p. 36004, 2011.
- [46] B. Bhandari, G. Y. Lee, and S. H. Ahn, “A review on IPMC material as actuators and sensors: Fabrications, characteristics and applications,” *Int. J. Precis. Eng. Manuf.*, vol. 13, no. 1, pp. 141–163, 2012.
- [47] M. Shahinpoor, K. J. Kim, B. K. Henderson, and D. J. Leo, “Sensing capabilities of ionic

- polymer-metal composites,” in *SPIE’s 8th Annual International Symposium on Smart Structures and Materials*, 2001, pp. 267–274.
- [48] M. Shahinpoor and K. J. Kim, “Ionic polymer–metal composites: IV. Industrial and medical applications,” *Smart Mater. Struct.*, vol. 14, no. 1, pp. 197–214, 2005.
- [49] Q. Shen, T. Wang, L. Wen, and J. Liang, “Modelling and fuzzy control of an efficient swimming ionic polymer-metal composite actuated robot,” *Int. J. Adv. Robot. Syst.*, vol. 10, pp. 1–13, 2013.
- [50] Z. Chen and X. Tan, “Monolithic fabrication of ionic polymer – metal composite actuators capable of complex deformation,” *Sensors Actuators A Phys.*, vol. 157, pp. 246–257, 2010.
- [51] J. W. L. Zhou, H. Y. Chan, T. K. H. To, K. W. C. Lai, and W. J. Li, “Polymer MEMS actuators for underwater micromanipulation,” *IEEE/ASME Trans. Mechatronics*, vol. 9, no. 2, pp. 334–342, 2004.
- [52] F. Guo-Hua and C. Ri-Hong, “Improved cost-effective fabrication of arbitrarily shaped μ IPMC transducers,” *J. Micromechanics Microengineering*, vol. 18, no. 1, p. 15016, 2008.
- [53] S. Cho and D. Lee, “Microelectronic Engineering A biomimetic micro-collector based on an ionic polymer metal composite,” *Microelectron. Eng.*, vol. 86, no. 4–6, pp. 916–919, 2009.
- [54] R. Kanno, S. Tadokoro, T. Takamori, M. Hattori, and K. Oguro, “Linear approximate dynamic model of ICPF (ionic conducting polymer gel film) actuator,” in *Robotics and Automation, 1996. Proceedings., 1996 IEEE International Conference on*, 1996, vol. 1, pp. 219–225.
- [55] P. G. De Gennes, K. Okumura, M. Shahinpoor, and K. J. Kim, “Mechanoelectric effects in ionic gels,” *Europhys. Lett.*, vol. 50, pp. 513–518, 2000.
- [56] M. Shahinpoor and K. J. Kim, “The effect of surface-electrode resistance on the performance of ionic polymer-metal composite (IPMC) artificial muscles,” *Smart Mater. Struct.*, vol. 9, no. 4, pp. 543–551, 2000.
- [57] K. M. Farinholt, “Modeling and characterization of ionic polymer transducers for sensing and actuation,” 2005.
- [58] K. M. Newbury and D. J. Leo, “Linear Electromechanical Model of Ionic Polymer Transducers – Part I : Model Development,” *J. Intell. Mater. Syst. Struct.*, vol. 14, no. June 2003, pp. 333–342, 2003.
- [59] C. Bonomo, L. Fortuna, P. Giannone, S. Graziani, and S. Strazzeri, “A nonlinear model for ionic polymer metal composites as actuators,” *Smart Mater. Struct.*, vol. 16, no. 1, p. 1, 2006.
- [60] P. Brunetto, L. Fortuna, S. Graziani, and S. Strazzeri, “A model of ionic polymer – metal composite actuators in underwater operations,” *Smart Mater. Struct.*, vol. 17, no. 2, p. 25029, 2008.
- [61] Z. Chen and X. Tan, “A Control-Oriented and Physics-Based Model for Ionic Polymer – Metal Composite Actuators,” *IEEE/ASME Trans. Mechatronics*, vol. 13, no. 5, pp. 519–529, 2008.
- [62] M. Porfiri, “Influence of electrode surface roughness and steric effects on the nonlinear electromechanical behavior of ionic polymer metal composites,” *Phys. Rev. E - Stat.*

- Nonlinear, Soft Matter Phys.*, vol. 79, no. 4, pp. 1–13, 2009.
- [63] D. Pugal, K. J. Kim, and A. Aabloo, “An explicit physics-based model of ionic polymer-metal composite actuators,” *J. Appl. Phys.*, vol. 110, no. 8, p. 84904, 2011.
- [64] S. J. Kim, S.-M. Kim, K. J. Kim, and Y. H. Kim, “An electrode model for ionic polymer-metal composites,” *Smart Mater. Struct.*, vol. 16, no. 6, pp. 2286–2295, 2007.
- [65] S. Ramo, “Currents induced by electron motion,” *Proc. Ire*, vol. 27, no. 9, pp. 584–585, 1939.
- [66] H. H. Barrett, J. D. Eskin, and H. B. Barber, “Charge transport in arrays of semiconductor gamma-ray detectors,” *Phys. Rev. Lett.*, vol. 75, no. 1, p. 156, 1995.
- [67] S. Dannefaer, P. Mascher, and D. Kerr, “Monovacancy formation enthalpy in silicon,” *Phys. Rev. Lett.*, vol. 56, no. 20, p. 2195, 1986.
- [68] R. C. Richardson, M. C. Levesley, M. D. Brown, J. A. Hawkes, K. Watterson, and P. G. Walker, “Control of ionic polymer metal composites,” *IEEE/ASME Trans. Mechatronics*, vol. 8, no. 2, pp. 245–253, 2003.
- [69] M. Levesque and E. Mart, “Simple concentration-dependent pair interaction model for large-scale simulations of Fe-Cr alloys,” *Phys. Rev. B*, vol. 184205, pp. 1–10, 2011.
- [70] D. J. Backlund and S. K. Estreicher, “Ti, Fe, and Ni in Si and their interactions with the vacancy and the A center: A theoretical study,” *Phys. Rev. B - Condens. Matter Mater. Phys.*, vol. 81, no. 23, pp. 1–8, 2010.
- [71] L. Ismer, M. S. Park, A. Janotti, and C. G. Van de Walle, “Erratum: Interactions between hydrogen impurities and vacancies in Mg and Al: A comparative analysis based on density functional theory,” *Phys. Rev. B*, vol. 81, no. 13, p. 184110, 2010.
- [72] K. Asaka, K. Oguro, Y. Nishimura, M. Mizuhata, and H. Takenaka, “Bending of polyelectrolyte membrane-platinum composites by electric stimuli I. Response characteristics to various waveforms,” *Polym. J.*, vol. 27, no. 4, pp. 436–440, 1995.
- [73] Z. Chen, X. Tan, A. Will, and C. Ziel, “A dynamic model for ionic polymer-metal composite sensors,” *Smart Mater. Struct.*, vol. 16, no. 4, pp. 1477–1488, 2007.
- [74] M. Porfiri, “Charge dynamics in ionic polymer metal composites,” *J. Appl. Phys.*, vol. 104, no. 10, p. 104915, 2008.
- [75] P. Liu, C. Liu, and Z. Xu, “Generalized Shockley-Ramo theorem in electrolytes,” *Commun. Math. Sci.*, vol. 15, no. 2, pp. 555–564, 2017.
- [76] M. A. Wahab, *Dynamics and Vibration: An Introduction*. John Wiley & Sons Ltd., Hoboken, NJ, USA, 2008.
- [77] Y. Cha, H. Kim, and M. Porfiri, “Influence of temperature on the impedance of ionic polymer metal composites,” *Mater. Lett.*, vol. 133, pp. 179–182, 2014.
- [78] M. Shahinpoor, “Ionic polymer-conductor composites as biomimetic sensors, robotic actuators and artificial muscles - A review,” *Electrochim. Acta*, vol. 48, no. 14–16 SPEC., pp. 2343–2353, 2003.
- [79] D. Weihs, “Hydromechanics of Fish Schooling,” *Nature*, vol. 241, p. 290, 1973.
- [80] J. Engelmann, W. Hanke, J. Mogdans, and H. Bleckmann, “Hydrodynamic stimuli and the fish lateral line,” *Nature*, vol. 408, no. November, pp. 51–52, 2000.
- [81] C. D. Wilga and G. V. Lauder, “Hydrodynamic function of the shark’s tail,” *Nature*, vol. 430, no. August, p. 2004, 2004.
- [82] K. Singer, “Engineered ‘jellyfish,’” *Nature*, vol. 487, no. July, p. 408, 2012.

- [83] N. Huebsch and D. J. Mooney, "Inspiration and application in the evolution of biomaterials.," *Nature*, vol. 462, no. 7272, pp. 426–432, 2009.
- [84] A. Hashidzume, H. Yamaguchi, and A. Harada, "Expansion–contraction of photoresponsive artificial muscle regulated by host–guest interactions," *Nat. Commun.*, vol. 3, pp. 1–8, 2012.
- [85] M. Madeleine, G. Guille, M. Curie, E. Pratique, C. National, and D. Recherche, "Biomimetism and bioinspiration as tools for the design of innovative materials and systems," *Nat. Mater.*, vol. 4, pp. 277–288, 2005.
- [86] D. Rus and M. T. Tolley, "Design, fabrication and control of soft robots," *Nature*, vol. 521, no. 7553, pp. 467–475, 2015.
- [87] L. Wen, J. C. Weaver, and G. V. Lauder, "Biomimetic shark skin: design, fabrication and hydrodynamic function," *J. Exp. Biol.*, vol. 217, no. 10, pp. 1656–1666, 2014.
- [88] P. Egan, R. Sinko, P. R. LeDuc, and S. Keten, "The role of mechanics in biological and bio-inspired systems," *Nat. Commun.*, vol. 6, no. May, p. 7418, 2015.
- [89] B. Kim, M. G. Lee, Y. P. Lee, Y. Kim, and G. Lee, "An earthworm-like micro robot using shape memory alloy actuator," *Sensors Actuators, A Phys.*, vol. 125, no. 2, pp. 429–437, 2006.
- [90] K. Takashima, J. Rossiter, and T. Mukai, "McKibben artificial muscle using shape-memory polymer," *Sensors Actuators, A Phys.*, vol. 164, no. 1–2, pp. 116–124, 2010.
- [91] M. T. Tolley, R. F. Shepherd, B. Mosadegh, K. C. Galloway, M. Wehner, M. Karpelson, R. J. Wood, and G. M. Whitesides, "A Resilient, Untethered Soft Robot," *Soft Robot.*, vol. 1, no. 3, pp. 213–223, Aug. 2014.
- [92] M. Rolf and J. J. Steil, "Efficient exploratory learning of inverse kinematics on a bionic elephant trunk," *IEEE Trans. Neural Networks Learn. Syst.*, vol. 25, no. 6, pp. 1147–1160, 2014.
- [93] S. Kurbanhusen Mustafa, G. Yang, S. Huat Yeo, W. Lin, and M. Chen, "Self-calibration of a biologically inspired 7 DOF cable-driven robotic arm," *Mechatronics, IEEE/ASME Trans.*, vol. 13, no. 1, pp. 66–75, 2008.
- [94] G. Sen Gupta, S. C. Mukhopadhyay, C. H. Messom, and S. N. Demidenko, "Master--slave control of a teleoperated anthropomorphic robotic arm with gripping force sensing," *Instrum. Meas. IEEE Trans.*, vol. 55, no. 6, pp. 2136–2145, 2006.
- [95] H. Irschik, "A review on static and dynamic shape control of structures by piezoelectric actuation," *Eng. Struct.*, vol. 24, no. 1, pp. 5–11, 2002.
- [96] D. Pugal, K. Jung, A. Aabloo, and K. J. Kim, "Ionic polymer-metal composite mechano-electrical transduction: Review and perspectives," *Polym. Int.*, vol. 59, no. 3, pp. 279–289, 2010.
- [97] J. Foroughi, G. M. Spinks, G. G. Wallace, J. Oh, M. E. Kozlov, S. Fang, T. Mirfakhrai, J. D. W. Madden, M. K. Shin, S. J. Kim, and R. H. Baughman, "Torsional Carbon Nanotube Artificial Muscles," *Science*, vol. 334, no. 6055, pp. 494–497, 2011.
- [98] I. Chopra, "Review of state of art of smart structures and integrated systems," *AIAA J.*, vol. 40, no. 11, pp. 2145–2187, 2002.
- [99] C. Jo, D. Pugal, I. K. Oh, K. J. Kim, and K. Asaka, "Recent advances in ionic polymer-metal composite actuators and their modeling and applications," *Prog. Polym. Sci.*, vol. 38, no. 7, pp. 1037–1066, 2013.

- [100] O. Kim, T. J. Shin, and M. J. Park, “Fast low-voltage electroactive actuators using nanostructured polymer electrolytes,” *Nat. Commun.*, vol. 4, p. 2208, 2013.
- [101] Y. Liu, C. Lu, S. Twigg, M. Ghaffari, J. Lin, N. Winograd, and Q. M. Zhang, “Direct observation of ion distributions near electrodes in ionic polymer actuators containing ionic liquids,” *Sci. Rep.*, vol. 3, no. Mim, p. 973, 2013.
- [102] Q. Shen, K. J. Kim, T. Wang, Q. Shen, K. J. Kim, and T. Wang, “Electrode of ionic polymer-metal composite sensors: Modeling and experimental investigation,” *J. Appl. Phys.*, vol. 115, no. 194902, pp. 1–14, 2014.
- [103] E. a Peraza-Hernandez, D. J. Hartl, R. J. Malak Jr, and D. C. Lagoudas, “Origami-inspired active structures: a synthesis and review,” *Smart Mater. Struct.*, vol. 23, no. 9, p. 94001, 2014.
- [104] Y. Tanaka, Y. Himuro, R. Kainuma, Y. Sutou, T. Omori, and K. Ishida, “Ferrous polycrystalline shape-memory alloy showing huge superelasticity,” *Science*, vol. 327, no. 5972, pp. 1488–1490, 2010.
- [105] S. Felton, M. Tolley, E. Demaine, D. Rus, and R. Wood, “A method for building self-folding machines,” *Science (80-.)*, vol. 345, no. 6197, pp. 644–646, 2014.
- [106] W. Chae, Y. Cha, S. D. Peterson, and M. Porfiri, “Flow measurement and thrust estimation of a vibrating ionic polymer metal composite,” *Smart Mater. Struct.*, vol. 24, no. 9, p. 95018, 2015.
- [107] M. Shahinpoor, “Biomimetic robotic Venus flytrap (*Dionaea muscipula* Ellis) made with ionic polymer metal composites,” *Bioinspir. Biomim.*, vol. 6, no. 4, p. 46004, Dec. 2011.
- [108] L. DeVries, F. D. Lagor, H. Lei, X. Tan, and D. a Paley, “Distributed flow estimation and closed-loop control of an underwater vehicle with a multi-modal artificial lateral line,” *Bioinspir. Biomim.*, vol. 10, no. 2, p. 25002, 2015.
- [109] V. Palmre, D. Pugal, K. J. Kim, K. K. Leang, K. Asaka, and A. Aabloo, “Nanoothorn electrodes for ionic polymer-metal composite artificial muscles,” *Sci. Rep.*, vol. 4, p. 6176, 2014.
- [110] A. Punning, K. J. Kim, V. Palmre, F. Vidal, C. Plesse, N. Festin, A. Maziz, K. Asaka, T. Sugino, G. Alici, G. Spinks, G. Wallace, I. Must, I. Põldsalu, V. Vunder, R. Temmer, K. Kruusamäe, J. Torop, F. Kaasik, P. Rinne, U. Johanson, A.-L. Peikola, T. Tamm, and A. Aabloo, “Ionic electroactive polymer artificial muscles in space applications,” *Sci. Rep.*, vol. 4, p. 6913, 2014.
- [111] G. Wu, Y. Hu, Y. Liu, J. Zhao, X. Chen, V. Whoehling, C. Plesse, G. T. M. Nguyen, F. Vidal, and W. Chen, “Graphitic carbon nitride nanosheet electrode-based high-performance ionic actuator,” *Nat. Commun.*, vol. 6, p. 7258, 2015.
- [112] G.-H. Feng and S.-Y. Hou, “Double-section curvature tunable functional actuator with micromachined buckle and grid wire for electricity delivery,” *Smart Mater. Struct.*, vol. 24, no. 9, p. 95010, 2015.
- [113] V. Palmre, J. J. Hubbard, M. Fleming, D. Pugal, S. Kim, K. J. Kim, and K. K. Leang, “An IPMC-enabled bio-inspired bending/twisting fin for underwater applications,” *Smart Mater. Struct.*, vol. 22, no. 1, p. 14003, 2013.
- [114] X. Xiao, D. Kong, X. Qiu, W. Zhang, Y. Liu, S. Zhang, F. Zhang, Y. Hu, and J. Leng, “Shape memory polymers with high and low temperature resistant properties,” *Sci. Rep.*, vol. 5, no. 2, p. 14137, Sep. 2015.

- [115] Q. Meng and J. Hu, "A review of shape memory polymer composites and blends," *Compos. Part A Appl. Sci. Manuf.*, vol. 40, no. 11, pp. 1661–1672, 2009.
- [116] M. Shahinpoor and K. J. Kim, "Ionic polymer metal composites: I. Fundamentals," *Smart Mater. Struct.*, vol. 819, no. 833, pp. 819–833, 2001.
- [117] G. V. Lauder, E. J. Anderson, J. L. Tangorra, and P. G. A. Madden, "Fish biorobotics: kinematics and hydrodynamics of self-propulsion," *J. Exp. Biol.*, vol. 210, no. Pt 16, pp. 2767–2780, 2007.
- [118] H. Lei, M. Sharif, and X. Tan, "Dynamics of Omnidirectional IPMC Sensor: Experimental Characterization and Physical Modeling," *IEEE/ASME Trans. Mechatronics*, vol. 21, no. 2, pp. 601–612, 2016.
- [119] Q. Shen, V. Palmre, T. Stalbaum, and K. J. Kim, "A comprehensive physics-based model encompassing variable surface resistance and underlying physics of ionic polymer-metal composite actuators," *J. Appl. Phys.*, vol. 118, no. 12, p. 124904, 2015.
- [120] T. L. Hedrick, "Software techniques for two- and three-dimensional kinematic measurements of biological and biomimetic systems," *Bioinspir. Biomim.*, vol. 3, no. 3, pp. 1–6, 2008.
- [121] Y. Wang, H. Chen, Y. Wang, Z. Zhu, and D. Li, "Effect of Dehydration on the Mechanical and Physicochemical Properties of Gold- and Palladium -Ionomeric Polymer-Metal Composite (IPMC) Actuators," *Electrochim. Acta*, vol. 129, pp. 450–458, 2014.
- [122] B. K. Fang, M. S. Ju, and C. C. K. Lin, "A new approach to develop ionic polymer-metal composites (IPMC) actuator: Fabrication and control for active catheter systems," *Sensors Actuators, A Phys.*, vol. 137, no. 2, pp. 321–329, 2007.
- [123] A. Giacomello and M. Porfiri, "Underwater energy harvesting from a heavy flag hosting ionic polymer metal composites," *J. Appl. Phys.*, vol. 109, no. 8, p. 84903, 2011.
- [124] Y. Cha, M. Verotti, H. Walcott, S. D. Peterson, and M. Porfiri, "Energy harvesting from the tail beating of a carangiform swimmer using ionic polymer-metal composites," *Bioinspir. Biomim.*, vol. 8, p. 36003, 2013.
- [125] A. Lendlein, H. Jiang, O. Junger, and R. Langer, "Light-induced shape-memory polymers," *Nature*, vol. 434, no. 7035, pp. 879–882, 2005.
- [126] H. Koerner, G. Price, N. A. Pearce, M. Alexander, and R. A. Vaia, "Remotely actuated polymer nanocomposites - stress-recovery of carbon-nanotube-filled thermoplastic elastomers," *Nat. Mater.*, vol. 3, no. 2, pp. 115–20, 2004.
- [127] C. Liu, H. Qin, and P. T. Mather, "Review of progress in shape-memory polymers," *J. Mater. Chem.*, vol. 17, no. 16, pp. 1543–1558, 2007.
- [128] C. Liu, S. B. Chun, P. T. Mather, L. Zheng, E. H. Haley, and E. B. Coughlin, "Chemically cross-linked polycyclooctene: Synthesis, characterization, and shape memory behavior," *Macromolecules*, vol. 35, no. 27, pp. 9868–9874, 2002.
- [129] H. Lv, J. Leng, Y. Liu, and S. Du, "Shape-memory polymer in response to solution," *Adv. Eng. Mater.*, vol. 10, no. 6, pp. 592–595, 2008.
- [130] H. Lu, Y. Liu, J. Leng, and S. Du, "Qualitative separation of the effect of the solubility parameter on the recovery behavior of shape-memory polymer," *Smart Mater. Struct.*, vol. 18, no. 8, p. 85003, 2009.
- [131] J. W. Gibbs, *The scientific papers of J. Willard Gibbs*, vol. 1. Longmans, Green and Company, 1906.

- [132] P. J. Flory, *Principles of Polymer Chemistry*. Cornell University Press, 1953.
- [133] J. Ricka and T. Tanaka, "Swelling of ionic gels: quantitative performance of the Donnan theory," *Macromolecules*, vol. 17, no. 12, pp. 2916–2921, 1984.
- [134] H. H. Hooper, J. P. Baker, H. W. Blanch, and J. M. Prausnitz, "Swelling equilibria for positively ionized polyacrylamide hydrogels," *Macromolecules*, vol. 23, no. 4, pp. 1096–1104, 1990.
- [135] L. Brannon-Peppas and N. A. Peppas, "Equilibrium swelling behavior of pH-sensitive hydrogels," *Chem. Eng. Sci.*, vol. 46, no. 3, pp. 715–722, 1991.
- [136] J. Li, J. A. Viveros, M. H. Wrue, and M. Anthamatten, "Shape-memory effects in polymer networks containing reversibly associating side-groups," *Adv. Mater.*, vol. 19, no. 19, pp. 2851–2855, 2007.
- [137] S. Trabia, T. Hwang, and K. J. Kim, "A fabrication method of unique Nafion® shapes by painting for ionic polymer–metal composites," *Smart Mater. Struct.*, vol. 25, no. 8, p. 85006, 2016.
- [138] D. Zhao, D. Li, Y. Wang, and H. Chen, "Improved manufacturing technology for producing porous Nafion for high-performance ionic polymer--metal composite actuators," *Smart Mater. Struct.*, vol. 25, no. 7, p. 75043, 2016.
- [139] Q. Shen, S. Trabia, T. Stalbaum, V. Palmre, K. Kim, and I. Oh, "A multiple-shape memory polymer-metal composite actuator capable of programmable control, creating complex 3D motion of bending, twisting, and oscillation," *Sci. Rep.*, vol. 6, no. April, p. 24462, 2016.
- [140] Z. Zhu, Y. Wang, Y. Liu, K. Asaka, X. Sun, L. Chang, and P. Lu, "Application-oriented simplification of actuation mechanism and physical model for ionic polymer-metal composites," *J. Appl. Phys.*, vol. 120, no. 3, p. 34901, 2016.
- [141] L. Chang, K. Asaka, Z. Zhu, Y. Wang, H. Chen, and D. Li, "Effects of surface roughening on the mass transport and mechanical properties of ionic polymer-metal composite," *J. Appl. Phys.*, vol. 115, no. 24, p. 244901, 2014.
- [142] Q. He, M. Yu, X. Zhang, and Z. Dai, "Electromechanical performance of an ionic polymer–metal composite actuator with hierarchical surface texture," *Smart Mater. Struct.*, vol. 22, no. 5, p. 55001, 2013.
- [143] S. Tadokoro, S. Yamagami, T. Takamori, and K. Oguro, "Modeling of Nafion-Pt composite actuators (ICPF) by ionic motion," in *SPIE's 7th Annual International Symposium on Smart Structures and Materials*, 2000, vol. 3987, pp. 92–102.
- [144] Y. Gong, C. Tang, C. Tsui, and J. Fan, "Modelling of ionic polymer--metal composites by a multi-field finite element method," *Int. J. Mech. Sci.*, vol. 51, no. 11, pp. 741–751, 2009.
- [145] Y. Toi and S.-S. Kang, "Finite element analysis of two-dimensional electrochemical--mechanical response of ionic conducting polymer--metal composite beams," *Comput. Struct.*, vol. 83, no. 31, pp. 2573–2583, 2005.
- [146] T. Yamaue, H. Mukai, K. Asaka, and M. Doi, "Electrostress diffusion coupling model for polyelectrolyte gels," *Macromolecules*, vol. 38, no. 4, pp. 1349–1356, 2005.
- [147] M. Porfiri, "An electromechanical model for sensing and actuation of ionic polymer metal composites," *Smart Mater. Struct.*, vol. 18, no. 1, p. 15016, 2008.
- [148] G. Feng, "Numerical study on dynamic characteristics of micromachined ionic polymer metal composite devices based on molecular-scale modeling," *Comput. Mater. Sci.*, vol.

- 50, no. 1, pp. 158–166, 2010.
- [149] A. T. Abdulsadda and X. Tan, “An artificial lateral line system using IPMC sensor arrays,” *Int. J. Smart Nano Mater.*, vol. 3, no. 3, pp. 226–242, 2012.
- [150] A. T. Abdulsadda and X. Tan, “Underwater tracking of a moving dipole source using an artificial lateral line: algorithm and experimental validation with ionic polymer–metal composite flow sensors,” *Smart Mater. Struct.*, vol. 22, no. 4, p. 45010, 2013.
- [151] M. Aureli, C. Prince, M. Porfiri, and S. D. Peterson, “Energy harvesting from base excitation of ionic polymer metal composites in fluid environments,” *Smart Mater. Struct.*, vol. 19, no. 1, p. 15003, 2009.
- [152] Q. Shen, K. J. Kim, and T. Wang, “Electrode of ionic polymer-metal composite sensors: Modeling and experimental investigation,” *J. Appl. Phys.*, vol. 115, no. 19, p. 194902, 2014.
- [153] Q. Shen, K. J. Kim, and T. Wang, “Electrode of ionic polymer-metal composite sensors: Modeling and experimental investigation,” in *Proceedings of SPIE - The International Society for Optical Engineering*, 2014, p. 9056.
- [154] R. Tiwari and K. J. Kim, “IPMC as a piezoelectric energy harvester: tailored properties,” *Smart Mater. Struct.*, vol. 22, no. 1, p. 15017, 2013.
- [155] J. Nam, T. Hwang, K. J. Kim, and D. Lee, “A new high-performance ionic polymer–metal composite based on Nafion/polyimide blends,” *Smart Mater. Struct.*, vol. 26, no. 3, p. 35015, 2017.
- [156] Q. He, M. Yu, X. Yang, K. J. Kim, and Z. Dai, “An ionic electro-active actuator made with graphene film electrode, chitosan and ionic liquid,” *Smart Mater. Struct.*, vol. 24, no. 6, p. 65026, 2015.
- [157] A. D. Drozdov, “Modeling the response of polymer–ionic liquid electromechanical actuators,” *Acta Mech.*, vol. 227, no. 2, pp. 437–465, 2016.
- [158] Y. Wang, Z. Zhu, J. Liu, L. Chang, and H. Chen, “Effects of surface roughening of Nafion 117 on the mechanical and physicochemical properties of ionic polymer–metal composite (IPMC) actuators,” *Smart Mater. Struct.*, vol. 25, no. 8, p. 85012, 2016.
- [159] Y. Cha and M. Porfiri, “Bias-dependent model of the electrical impedance of ionic polymer-metal composites,” *Phys. Rev. E*, vol. 87, no. 2, p. 22403, 2013.
- [160] M. Aureli, V. Kopman, and M. Porfiri, “Control-oriented modeling of ionic polymer metal composites for biomimetic underwater propulsion,” in *American Control Conference (ACC), 2010*, 2010, pp. 6016–6021.
- [161] S. Nemat-Nasser, “Micromechanics of actuation of ionic polymer-metal composites,” *J. Appl. Phys.*, vol. 92, no. 5, pp. 2899–2915, 2002.
- [162] H. Lei, M. A. Sharif, and X. Tan, “Dynamics of omnidirectional IPMC sensor: Experimental characterization and physical modeling,” *IEEE/ASME Trans. Mechatronics*, vol. 21, no. 2, pp. 601–612, 2016.
- [163] Z. Chen, S. Shatara, and X. Tan, “Modeling of biomimetic robotic fish propelled by an ionic polymer-metal composite caudal fin,” *IEEE/ASME Trans. Mechatronics*, vol. 15, no. 3, pp. 448–459, 2010.
- [164] M. Aureli, S. Member, V. Kopman, S. Member, and M. Porfiri, “Free-locomotion of underwater vehicles actuated by ionic polymer metal composites,” *IEEE/ASME Trans. Mechatronics*, vol. 15, no. 4, pp. 603–614, 2010.

- [165] Q. Shen, V. Palmre, K. J. Kim, and I.-K. Oh, "Theoretical and experimental investigation of the shape memory properties of an ionic polymer--metal composite," *Smart Mater. Struct.*, vol. 26, no. 4, p. 45020, 2017.
- [166] Q. Shen, V. Palmre, T. Stalbaum, and K. J. Kim, "Comprehensive modeling of ionic polymer-metal composite actuators based upon variable surface resistance and underlying physics of the polymer membrane," *SPIE Smart Struct. Mater. Nondestruct. Eval. Heal. Monit.*, p. 94302J--94302J, 2015.
- [167] F. Tanaka, *Polymer Physics: Applications to Molecular Association and Thermoreversible Gelation*. Cambridge University Press, 2011.
- [168] S. Trabia, Z. Olsen, and K. J. Kim, "Searching for a new ionomer for 3D printable ionic polymer-metal composites: Aquivion® as a candidate," *Smart Mater. Struct.*, vol. 26, no. 11, p. 115029, 2017.
- [169] J. Park, V. Palmre, T. Hwang, K. Kim, W. Yim, and C. Bae, "Electromechanical performance and other characteristics of IPMCs fabricated with various commercially available ion exchange membranes," *Smart Mater. Struct.*, vol. 23, no. 7, p. 74001, 2014.
- [170] J. Park, V. Palmre, T. Hwang, K. Kim, W. Yim, and C. Bae, "Electromechanical performance and other characteristics of IPMCs fabricated with various commercially available ion exchange membranes," *Smart Mater. Struct.*, vol. 23, no. 7, p. 74001, 2014.
- [171] A. Ciferri and A. Perico, *Ionic interactions in natural and synthetic macromolecules*. John Wiley & Sons, 2012.
- [172] M. Yamakita, N. Kamamichi, T. Kozuki, K. Asaka, and Z. W. Luo, "A snake-like swimming robot using IPMC actuator and verification of doping effect," in *2005 IEEE/RSJ International Conference on Intelligent Robots and Systems, IROS, 2005*, pp. 3333--3338.
- [173] S.-W. Yeom and I.-K. Oh, "A biomimetic jellyfish robot based on ionic polymer metal composite actuators," *Smart Mater. Struct.*, vol. 18, no. 8, p. 85002, 2009.
- [174] J. Najem, S. a Sarles, B. Akle, and D. J. Leo, "Biomimetic jellyfish-inspired underwater vehicle actuated by ionic polymer metal composite actuators," *Smart Mater. Struct.*, vol. 21, p. 94026, 2012.
- [175] K. Takagi, M. Yamamura, Z. W. Luo, M. Onishi, S. Hirano, K. Asaka, and Y. Hayakawa, "Development of a rajiform swimming robot using ionic polymer artificial muscles," in *IEEE International Conference on Intelligent Robots and Systems, 2006*, pp. 1861--1866.
- [176] Z. Chen, T. I. Um, and H. Bart-Smith, "Bio-inspired robotic manta ray powered by ionic polymer-metal composite artificial muscles," *Int. J. Smart Nano Mater.*, vol. 3, no. 4, pp. 296--308, 2012.
- [177] Z. Chen, T. I. Um, and H. Bart-smith, "Ionic Polymer-Metal Composite Enabled Robotic Manta Ray," in *Proc. SPIE, 2011*, vol. 7976, p. 797637.
- [178] J. J. Hubbard, M. Fleming, V. Palmre, D. Pugal, K. J. Kim, and K. K. Leang, "Monolithic IPMC fins for propulsion and maneuvering in bioinspired underwater robotics," *IEEE J. Ocean. Eng.*, vol. 39, no. 3, pp. 540--551, 2014.
- [179] M. Sfakiotakis, D. M. Lane, and J. B. C. Davies, "Review of fish swimming modes for aquatic locomotion," *IEEE J. Ocean. Eng.*, vol. 24, no. 2, pp. 237--252, 1999.
- [180] R. W. Blake, "The mechanics of labriform locomotion I. Labriform locomotion in the angelfish (*Pterophyllum eimekei*): an analysis of the power stroke," *J. Exp. Biol.*, vol. 82,

- no. 1, pp. 255–271, 1979.
- [181] P. J. Geerlink, “Pectoral fin kinematics of *Coris formosa* (Teleostei, Labridae),” *Netherlands J. Zool.*, vol. 33, no. 4, pp. 515–531, 1982.
- [182] K. J. Kim and M. Shahinpoor, “Ionic polymer – metal composites : II . Manufacturing techniques,” vol. 65, 2003.
- [183] M. J. Lighthill, “Note on the swimming of slender fish,” *J. Fluid Mech.*, vol. 9, no. 2, pp. 305–317, 1960.

Curriculum Vitae

Qi Shen

Graduate Research and Teaching Assistant

University of Nevada-Las Vegas (UNLV)

Email: qi.shen@unlv.edu

Google Scholar Citations:

https://scholar.google.com/citations?hl=en&user=te33TuUAAAAJ&view_op=list_works

A. Primary areas of research interest:

- 1) **Soft Robotics:** Mechanical and Electronic System Design, Dynamic Programming, Intelligent Control, Experimental Apparatus Development, Data Collection and Analysis, Kinematic and Dynamic modeling, Development of Soft Actuators/Sensors using Smart Materials
- 2) **Electroactive Polymer:** Materials Analysis, Fabrication, Synthesis, Processing, Characterization, Properties/Performance, 3D Printing, Physical Modeling, and Finite Element Analysis

B. Education

- 1/2015-12/2017 **Doctor of Mechanical Engineering**, University of Nevada, Las Vegas, U.S.
Mechanical Engineering
Advisor: Prof. Kwang J. Kim
Dissertation: *Theoretical and Experimental Investigation on the Multiple Shape Memory Ionic Polymer-Metal Composite Actuator*
- 09/2010-06/2016 **Doctor of Mechatronic Engineering**, Beihang University, P. R. China
Mechatronic Engineering
Advisor: Prof. Tianmiao Wang
Dissertation: *On the Actuating/Sensing Capabilities and Applications of Ionic Polymer-Metal Composites: Modeling and Experimental Investigation*
- 09/2006-07/2010 **Bachelor of Mechanical Engineering**, Beihang University (Beijing University of Aeronautics and Astronautics), P. R. China
Mechanical Engineering
Thesis: *Modeling and Analysis of the Locust Robot and the Design of Its Leg*

C. Experience

- 10/2013-10/2014 **Visiting Scholar**, University of Nevada, Las Vegas, U.S.
12/2012-02/2013 **Visiting Scholar**, University of Nevada, Las Vegas, U.S.

D. Research

(a) Teaching and Research Assistant

Department of Mechanical Engineering, University of Nevada, Las Vegas 10/2013-present

- Doctoral research under supervision of Prof. Kwang J. Kim at the Active Materials and Smart Living (AMSL) Laboratory, UNLV
- Designed and implemented experimental platform to test the electroactive materials
- Worked on characterization (using instruments such as DMA, DSC et.al), synthesis, processing, and fabrication (including 3D printing) of new smart materials
- Developed soft actuators/sensors, soft robotic systems (mechanical and electronic system) based on the electroactive materials
- Physically modeled the electroactive materials and performed simulation
- Performed finite element analysis of electroactive materials
- Wrote research proposals of soft robotic systems

(b) Research Assistant

Department of Mechanical Engineering and Automation, Beihang University 07/2007-10/2013

- Undergraduate and Doctoral research under supervision of Prof. Tianmiao Wang at the Intelligent Technology and Robotics (ITR) Laboratory, Beihang University
- Developed several robotic systems (mechanical and electronic system) including underwater robot, submersible unmanned aerial vehicle, and mobile-hopping robot
- Designed a force feedback system for the self-propulsion experimental test of biomimetic underwater robot
- Worked on the development of intelligent controller for the robotic system
- Modeled the robotic systems kinematically and dynamically

E. Honors

- 1) Summer Doctoral Research Fellowship (UNLV) 2017
- 2) **2016-2017 Outstanding Teaching Assistant of Mechanical Engineering Department (UNLV)** 2017
- 3) Nominee of the College of Engineering for the 2017 UNLV Outstanding Graduate Student Teaching Award 2017
- 4) **UNLV Graduate Differential Fees Scholarships** 2016
- 5) **Outstanding Graduate of Beijing Metropolitan** 2016
- 6) Beihang Huaheng Scholarship 2016
- 7) UNLV Rebel Grad Slam 2015, Semi-Finalist (UNLV) 2015
- 8) Beihang Huaheng Scholarship, First-grade Prize (Top 1 in ME Department) 2015
- 9) Best Paper Award of Beihang Finalist of Graduate Student in Top 10 2015
- 10) Best Paper Award of Beihang Finalist of Graduate Student in Top 10 2014
- 11) Best Poster Award in Mini-Symposium on Biotechnology, Energy, and Materials (BEM), Utah State University (USU) – University of Nevada, Las Vegas (UNLV) 2014
- 12) **National Scholarship of China (Top 2 in ME Department of Beihang)** 2013

13) National Doctoral Consortium, First-grade Prize (16/100) (Beihang)	2012
14) Beihang Excellent Graduate Student (4/51)	2011
15) Beihang Excellent Graduate Student (4/51)	2010
16) Beihang Qixian Scholarship, First-grade Prize	2009
17) Feng-Ru Cup Science And Technology Contest, First-grade Prize (1/193)	2009
18) Beihang ITR Lab Excellent Student	2009
19) Beihang Merit Scholarship	2009
20) Beihang Merit Scholarship	2008
21) Beihang Social Work Scholarship	2008
22) Department Social Work Scholarship (Beihang)	2007
23) Beihang Merit Scholarship	2007

F. Publications (H-index: 8, Total Citation > 150, date: 8-30-2017)

Google Scholar:

https://scholar.google.com/citations?hl=en&user=te33TuUAAA&view_op=list_works

(c) Journal Paper

- 1) **Qi Shen**, Viljar Palmre, Kwang Kim, and Il-Kwon Oh, "Theoretical and Experimental Investigation of Shape Memory Properties of Ionic Polymer-Metal Composite." *Smart Materials and Structures*, vol. 26, no. 4, pp. 045020, 2017.
- 2) Tyler Stalbaum, Taeseon Hwang, Sarah Trabia, **Qi Shen**, Robert Hunt, Zakai Olsen, and Kwang Kim, "Bioinspired Travelling Wave Generation in Soft-Robotics using Ionic Polymer-Metal Composites," *Intelligent Journal of Intelligent Robotics and Applications*, vol. 1, no. 2, pp. 167-179, 2017.
- 3) **Qi Shen**, Sarah Trabia, Tyler Stalbaum, Viljar Palmre, Kwang Kim, and Il-Kwon Oh, "A multiple-shape memory polymer-metal composite actuator capable of programmable control, creating complex 3D motion of bending, twisting, and oscillation." *Scientific Reports*, vol. 6, 2016.
- 4) Kim, Kwang J., Viljar Palmre, Tyler Stalbaum, Taeseon Hwang, **Qi Shen**, and Sarah Trabia, "Promising Developments in Marine Applications With Artificial Muscles: Electrodeless Artificial Cilia Microfibers", *Marine Technology Society Journal*, vol. 50, no. 5, pp. 24-34, 2016.
- 5) **Qi Shen**, Tianmiao Wang, and Kwang J. Kim, "A biomimetic underwater vehicle actuated by waves with ionic polymer-metal composite soft sensors", *Bioinspiration & biomimetics*, vol. 10, no. 5, pp. 055007, 2015.
- 6) **Qi Shen**, Viljar Palmre, Tyler Stalbaum, Kwang J. Kim, "A comprehensive physics-based model encompassing variable surface resistance and underlying physics of ionic polymer-metal composite actuators", *Journal of Applied Physics*, vol. 118, no. 12, pp. 124904, 2015.
- 7) **Qi Shen**, Miao Liu, Chenhao Han, Jianhong Liang, Tianmiao Wang, "Theoretical and experimental study of a novel power generating device based on IPMC", *Journal of Shenyang Aerospace University*, vol. 32, no. 3, pp. 42-46, 2015.
- 8) **Qi Shen**, Kwang J. Kim, Tianmiao Wang, "Electrode of ionic polymer-metal composite sensors: Modeling and experimental investigation", *Journal of Applied Physics*, vol. 115, pp. 194902, 2014.

- 9) **Qi Shen**, Chenhao Han, Tianmiao Wang, Jianhong Liang, “Experimental Investigation of a Biomimetic Robotic Fish Actuated by IPMC”, *Journal of Beijing University of Aeronautics and Astronautics*, vol. 12, pp. 016, 2014.
- 10) **Qi Shen**, Tianmiao Wang, Jianhong Liang, Li Wen, “Hydrodynamic Performance of a Biomimetic Robotic Swimmer Actuated by Ionic Polymer-Metal Composite”, *Smart Materials and Structures*, vol. 22, no. 7, pp. 075035, 2013.
- 11) **Qi Shen**, Tianmiao Wang, Li Wen, Jianhong Liang, “Modeling and Fuzzy Control of an Efficient-Swimming Ionic Polymer-Metal Composite Actuated Robot”, *International Journal of Advanced Robotic Systems*, vol. 10, no. 5, pp. 1-10, 2013.
- 12) Junmao Yin, Diansheng Chen, **Qi Shen**, “Design and analysis of the locust-like jumping mechanism”, *Journal of Beijing University of Aeronautics and Astronautics*, vol. 39, no. 10, pp. 1348-1353, 2013.
- 13) Tianmiao Wang, **Qi Shen**, Li Wen, Jianhong Liang, “On the thrust performance of an ionic polymer-metal composite actuated robotic fish: modeling and experimental investigation”, *Science China Technological Sciences*, vol. 55, no. 12, pp. 3359–3369, 2012. (Tianmiao Wang and Qi Shen contributed equally to the work. Qi Shen is the corresponding author.)
- 14) Li Wen, Jianhong Liang, **Qi Shen**, Lei Bao, and Qian Zhang, “Hydrodynamic Performance of an Undulatory Robot: Functional Roles of the Body and Caudal Fin Locomotion”, *International Journal of Advanced Robotic Systems*, vol. 9, pp. 1-10, 2012.
- 15) Diansheng Chen, Wanjun Zheng, Yu Huang, **Qi Shen**, Tianmiao Wang, “The design and optimization of a hopping robot’ tipping mechanism”, *Chinese Journal of Mechanical Engineering*, vol. 1, pp. 004, 2011.

(d) Conference and Proceedings Paper

- 1) **Qi Shen**, Tyler Stalbaum, Sarah Trabia, Taeseon Hwang, Robert Hunt, and Kwang Kim, "Modeling of a Soft Multiple-Shape-Memory Ionic Polymer-Metal Composite Actuator," *In SPIE Smart Structures and Materials+ Nondestructive Evaluation and Health Monitoring*, pp. 101650C-101650C, 2017.
- 2) Tyler Stalbaum, **Qi Shen**, and Kwang J. Kim. "A model framework for actuation and sensing of ionic polymer-metal composites: prospective on frequency and shear response through simulation tools." *In Electroactive Polymer Actuators and Devices (EAPAD)*, vol. 10163, p. 101630L, 2017.
- 3) **Qi Shen**, Viljar Palmre, Jameson Lee, and Kwang J. Kim, “A physics model of the multi-degree freedom ionic polymer-metal composite cylinder actuator”, (Conference paper and poster) *In SPIE Smart Structures and Materials+ Nondestructive Evaluation and Health Monitoring*, pp.98001B-98001B, 2016.
- 4) Sarah Trabia, **Qi Shen**, Tyler Stalbaum, Robert Hunt, Taeseon Hwang, and Kwang Kim, "Numerical and experimental investigation of a biomimetic robotic jellyfish actuated by Ionic Polymer-Metal Composite", *In 2016 13th International Conference on Ubiquitous Robots and Ambient Intelligence (URAI)*, pp. 204-205, 2016.
- 5) Tyler Stalbaum, Sarah Trabia, **Qi Shen**, and Kwang J. Kim, “Fluid flow sensing and control with ionic polymer-metal composites”, *In SPIE Smart Structures and Materials+ Nondestructive Evaluation and Health Monitoring*, pp. 97982E-97982E, 2016.

- 6) **Qi Shen**, Viljar Palmre, Tyler Stalbaum, Kwang J. Kim, “Comprehensive modeling of ionic polymer-metal composite actuators based upon variable surface resistance and underlying physics of the polymer membrane”, (Conference paper and poster) *Proc. SPIE 9430, Electroactive Polymer Actuators and Devices (EAPAD)*, pp. 94302J, 2015.
- 7) **Qi Shen**, Kwang J. Kim, Tianmiao Wang, “Electrode of ionic polymer-metal composite sensors: modeling and experimental investigation”, (Conference paper and poster) *Proc. SPIE 9056, Electroactive Polymer Actuators and Devices (EAPAD)*, pp. 90563M, 2014.
- 8) **Qi Shen**, Tianmiao Wang, Li Wen, Jianhong Liang, Xingbang Yang, Guocai Yao, “A novel method for investigating the kinematic effect on the hydrodynamics of robotic fish”, (Conference paper and presentation) *IEEE International Conference on Robotics and Biomimetics*, pp. 1306-1311, 2013.
- 9) Guocai Yao, Jianhong Liang, Tianmiao Wang, Xingbang Yang, **Qi Shen**, Yucheng Zhang, Hailiang Wu, Weicheng Tian, “Development of a turtle-like underwater vehicle using central pattern generator”, *IEEE International Conference on Robotics and Biomimetics*, pp. 44-49, 2013.
- 10) Yang, Xingbang, Jianhong Liang, Tianmiao Wang, Guocai Yao, Wendi Zhao, and **Qi Shen**, "Submersible Unmanned Aerial Vehicle Concept Design Study." *Aviation Technology, Integration, and Operations Conference*, pp. 4422, 2013.
- 11) **Qi Shen**, Tianmiao Wang, Li Wen, Jianhong Liang, and Yang Chen, “On the thrust efficiency of an IPMC actuated robotic swimmer: dynamic modeling and experimental investigation”, *International Offshore and Polar Engineering Conference*, pp. 556-562, 2012.
- 12) Li Wen, Guan hao Wu, **Qi Shen**, Tianmiao Wang, and Jianhong Liang, “The Use of Robotic Apparatus for Studying Propulsion Performance and Fluid Mechanism Of Undulatory Fish Locomotion”, *International Offshore and Polar Engineering Conference*, pp. 548-555, 2012.
- 13) Xingbang Yang, Tianmiao Wang, Jianhong Liang, Guocai Yao, Yang Chen, **Qi Shen**, “Numerical Analysis of Biomimetic Gannet Impacting with Water during Plunge-diving”, *IEEE International Conference on Robotics and Biomimetics*, pp. 569-574, 2012.

(e) Book Chapter

- 1) Kwang J. Kim, Tyler Stalbaum, Sarah Trabia, Taeseon Hwang, Zakai Olsen, Shelby Nelson, **Qi Shen**, Dong-Chan Lee, James Carrico, Kam K. Leang, Viljar Palmre, Jungsoo Nam, Ilseok Park, Rashi Tiwari, Doyeon Kim, and Sungjun Kim. Guidelines for making Ionic Polymer-Metal Composite (IPMC) materials as artificial muscles by advanced manufacturing methods: State-of-the-Art. In *Advances in manufacturing and processing of materials and structures*. Submitted for review, 2017.
- 2) Li Wen, Daniel Vogot, Zhenyun Shi, **Qi Shen** and Ziyu Ren, Chapter "Advanced material for soft robotics", in book “Design, Fabrication, Properties and Applications of Smart and Advanced Materials”. *SCIENCE PUBLISHERS, Imprint of CRC Press/ Taylor & Francis Group*. pp. 342-375, 2015.

G. Patent

- 1) Jianhong Liang, Sicheng Liang, Hang Xiao, Shengxi Li, Xingbang Yang, Ziyu Ren, and **Qi Shen**, “A self-adaption finger mechanism with one-way flexible knuckles”, State Intellectual Property Office of the People’s Republic of China (ID# CN103552086A), 2013.
- 2) Jianhong Liang, Hailiang Wu, Chenhao Han, Yicheng Zhang, **Qi Shen**, Xingbang Yang, Yao Wu, and Han Gao, “A hybrid duct and propellers robot for aerial reconnaissance”, State Intellectual Property Office of the People’s Republic of China (ID# CN103552686A), 2013.
- 3) Tianmiao Wang, **Qi Shen**, Jianhong Liang, Lei Bao, and Xiaotian Yu, “Bionic water surface moving device”, State Intellectual Property Office of the People’s Republic of China (ID# CN103144754A), 2013.
- 4) Tianmiao Wang, **Qi Shen**, Jianhong Liang, and Zhongyu Wang, “A biomimetic robotic manna ray based on ionic polymer-metal composite”, State Intellectual Property Office of the People’s Republic of China (ID# CN102923286A), 2012.
- 5) Tianmiao Wang, **Qi Shen**, Jianhong Liang, and Zhongyu Wang, “A micro power generator based on ionic polymer-metal composite”, State Intellectual Property Office of the People’s Republic of China (ID# CN 102931876A), 2012.
- 6) Diansheng Chen, Yu Huang, **Qi Shen**, Wanjun Zheng, and Tianmiao Wang, “The design of a locust-based hopping tipping robot”, State Intellectual Property Office of the People’s Republic of China (ID# CN101716962B), 2010.

H. Invited Talk

- 1) “Ionic Polymer-Metal Composite Based Soft Robots.” University of California, Los Angeles, April, 2017.

I. Selected Professional Activity

- 1) **Qi Shen**, Sarah Trabia, Tyler Stalbaum, Taeseon Hwang, Robert Hunt, Zakai Olsen, Kwang Kim, “Development of an origami soft robot using multiple shape memory ionic polymer-metal composite”, 19th Annual EAP-in-Action Session and Demonstrations on SPIE Smart Structures/NDE 2017.
- 2) **Qi Shen**, Sarah Trabia, Tyler Stalbaum, Choonhan Lee, Robert Hunt, and Kwang Kim, “Shape memory programmable and electrically controllable IPMC”, 18th Annual EAP-in-Action Session and Demonstrations on SPIE Smart Structures/NDE 2016.
- 3) **Qi Shen**, Tyler Stalbaum, Shelby E. Nelson, Sara Trabia, Jameson Lee, Viljar Palmre, and Kwang J. Kim, “Advanced IPMC actuators and sensors”, 17th Annual EAP-in-Action Session and Demonstrations on SPIE Smart Structures/NDE 2015.

J. Professional Service

(a) Active Reviewer for the following Journals

- 1) Scientific Reports (2015 IF = 5.228)
- 2) IEEE Transactions on Industrial Electronics (2015 IF = 6.393);
- 3) IEEE Transactions on Systems, Man and Cybernetics: Systems (2016 IF = 2.350);
- 4) Smart Materials and Structures (2015 IF = 2.769);
- 5) Journal of Intelligent Material Systems and Structures (2015 IF = 1.975);
- 6) Smart Structures and Systems (2015 IF = 1.138);
- 7) Computer Modeling in Engineering and Sciences (2015 IF = 1.06);
- 8) Engineering.

(b) Editorship

- 1) Guest Editor (with Drs. Qingsong He and David Vokoun), Applied Bionics and Biomechanics Biomimetic, special issue on Actuation and Artificial Muscle (June 2017 issue).
- 2) Guest Editor (with Drs. Junshi Zhang, Gianluca Rizzello, Jianwen Zhao and Yanjie Wang), International Journal of Polymer Science, special issue on Stimuli-Responsive Smart Polymers and Structures: Characteristics and Applications (Jul 2017 issue).

K. Teaching

(a) As Instructor

- 1) Analysis Dynamic System (ME 330), Mechanical Engineering, University of Nevada, Las Vegas, Summer 2017
- 2) Analysis Dynamic System (ME 330), Mechanical Engineering, University of Nevada, Las Vegas, Summer 2016
- 3) Analysis Dynamic System (ME 330), Mechanical Engineering, University of Nevada, Las Vegas, Summer 2015

(b) As Teaching Assistant

- 1) Fluid Dynamics (ME 380L), Mechanical Engineering, University of Nevada, Las Vegas, Fall 2017
- 2) Fluid Dynamics (ME 380L), Mechanical Engineering, University of Nevada, Las Vegas, Spring 2017
- 3) Fluid Dynamics (ME 380L), Mechanical Engineering, University of Nevada, Las Vegas, Fall 2016
- 4) Fluid Dynamics (ME 380L), Mechanical Engineering, University of Nevada, Las Vegas, Spring 2016
- 5) Automatic controls (ME 421L), Mechanical Engineering, University of Nevada, Las Vegas, Fall 2015
- 6) Analysis Dynamic System (ME 330), Mechanical Engineering, University of Nevada, Las Vegas, Spring 2015

(c) As Guest Lecturer

- 1) Fluid Dynamics (ME 380), Mechanical Engineering, University of Nevada, Las Vegas, Spring 2017
- 2) Analysis Dynamic System (ME 330), Mechanical Engineering, University of Nevada, Las Vegas, Summer 2015

Vegas, Spring 2016

- 3) Fluid Dynamics (ME 380), Mechanical Engineering, University of Nevada, Las Vegas, Fall 2015

L. Proficiency

Experiment: Contact Angle Analyzer (CAA), Differential Scanning Calorimetry (DSC), Dynamic Mechanical Analysis (DMA), Fourier Transform Infrared Spectroscopy (FT-IR), Optical Microscope, Scanning Electrochemical Microscope (SEM), Energy Dispersive X-Ray Analysis (EDX), Thermal Conductivity Meter, Thermogravimetric Analysis (TGA), 3D printer.

Software: Solidworks CAD, Matlab, COMSOL Multiphysics, Labview, Altium Designer, Origin Graphing & Analysis, Microsoft Office Suite